CO_2 and Ion Transport via Plant Aquaporins

Zhao Manchun

School of Agriculture, Food and Wine

The University of Adelaide

This thesis is submitted to the University of Adelaide in accordance with the requirements of the degree of PhD

September 2013

Table of Contents

ABSTRACT

CO_2 diffusion across membranes is one of the rate limiting steps during photosynthesis, therefore understanding the process of CO_2 permeation across membranes is important. The question of whether CO_2 transport across membranes can be facilitated by aquaporins is very controversial. Previous research where aquaporins were heterologously expressed in either *Xenopus* oocytes or yeast protoplasts showed that some plasma membrane intrinsic proteins (PIPs) or animal aquaporins could facilitate CO_2 transport. However, others have demonstrated using molecular simulation approaches and biophysical calculations that the unstirred layer poses the major rate limiting step for CO_2 diffusion across membranes, and that it is unlikely that CO_2 permeates via the water pathway in aquaporins, because this pathway exhibits a greater energy barrier compared to that for the lipid bilayer.

If water and CO_2 share the same pathway through aquaporins or if the presence and activity of aquaporins somehow affects CO_2 permeation, there should be a correlation between water permeability and CO_2 permeability. Therefore, by employing the stopped-flow technique and using pea plasma membrane vesicles isolated from pea leaves, this thesis explored the links between CO_2 permeability and water permeability. Plasma membrane vesicles from pea plants that were grown in different conditions showed considerable variability in water permeability. The very high and variable (between preparations) water permeability (0.06 to 0.18 m s^{-1}) plus the low activation energy (10.8 KJ mol^{-1}) of water transport indicated aquaporins dominated water flow, yet there was no significant correlation between water permeability and CO_2 permeability (1.49 x 10^{-2} cm s^{-1}). The activation energy for CO_2 permeation was 37 KJ/mol which is about double that for CO_2 diffusion in water. Also the aquaporin inhibitor silver sulfadiazine resulted in a large inhibition of water permeability but this did not affect CO_2 permeability. Similar results were obtained for plasma membrane

vesicles isolated from *Arabidopsis* leaves though the water permeability was lower. In performing these measurements care was taken to exclude artifacts caused by the concentration of carbonic anhydrase (CA) and its temperature dependence, since vesicular entrapped CA was required to measure CO_2 permeability via changes in vesicular pH.

Because there are not many aquaporins that have been identified in pea, some *Arabidopsis* aquaporins that have been suggested to be involved in CO_2 transport were expressed in *Xenopus* oocytes for further investigation. Water transport via these aquaporins was first studied. It was demonstrated that PIP2s were functional water channels when expressed alone, while PIP1s were not. However when PIP1 and PIP2 aquaporins were co-expressed in *Xenopus* oocytes a greater than additive effect on water permeation was observed for some combinations. This suggested that AtPIP1;2 and AtPIP2;1, and AtPIP1;5 and AtPIP2;1 interact. A previously identified natural mutation in the pore region of VvPIP2;5 from grapevine (G100W), which prevented water flow, was used to probe AtPIP2;1 and its interaction with AtPIP1;2. This showed that the interaction still occurred despite the lower water permeation of the combined pair when expressed in *Xenopus* oocytes.

Originally, the CO_2 permeabilities of the *Arabidopsis* aquaporins of interest were intended to be tested using the external pH micro-electrode technique which was first employed to test CO_2 transport across *Xenopus* oocyte plasma membrane. However, one of the criteria for using this technique is that the expression of the aquaporins should not induce any ion conductance, which would potentially alter external pH either directly or indirectly. Therefore, electrophysiology experiments were conducted to test whether the expressed aquaporins induced any ionic currents. It was found that AtPIP2;1 indeed induced ionic currents selective to anions including HCO_3^- when expressed in *Xenopus* oocytes. It was

demonstrated that AtPIP2;1 homotetramer was likely to function as an ion channel since when co-expressed with its interacting partner (AtPIP1;2) this abolished the anion conductance. Furthermore the G100W mutation also prevented anion conductance of the AtPIP2;1 indicating that the pathway may be via the water pore. Expression of AtPIP2;1 in *Saccharomyces cerevisiae* was undertaken to test a potential anion sensitivity induced by the expression of AtPIP2;1. The expression of AtPIP2;1 induced increased water permeability of the yeast spheroplast as it does in *Xenopus* oocytes, and gave a low growth phenotype on all media tested, however this could not be linked to increased anion transport.

This thesis has demonstrated that measurements of CO_2 permeability are extremely difficult and likely to be limited by factors not always controlled for in previous experiments. Furthermore it has been demonstrated that some plant PIP aquaporins may function as anion channels and that this could complicate the interpretation of CO_2 permeation particularly when the HCO_3^- anion can permeate as was demonstrated for AtPIP2;1.

Declaration

I certify that this work contains no material which has been accepted for the award of any other degree or diploma in any university or other tertiary institution. To the best of my knowledge and belief, this thesis contains no material previously published or written by another person, except where due reference has been made in the text.

I give consent to this copy of my thesis, when deposited in the University Library, being made available for loan and photocopying, subject to the provisions of the Copyright Act 1968.

Zhao Manchun

September 2013

Acknowledgments

I wish to thank my supervisors Prof. Steve Tyerman, Dr Carolyn Schultz and Dr Brent Kaiser for their great support and guidance throughout my PhD. In particular, I would like to express my sincere appreciation for Prof. Steve Tyerman for teaching me many physiology techniques and many encouraging discussions that extended my ideas.

A special thank you to Dr Carolyn Schultz for teaching me molecular knowledge and techniques. Your kind assistance is greatly appreciated. I am particularly grateful to Dr Sunita Ramesh for kindly teaching me some molecular techniques and answering so many of my questions about molecular experiments and her assistance with the *Xenopus* oocyte experiments. Thank you to Ms Wendy Sullivan for her excellent technical support, harvesting the oocytes and teaching me some specific techniques in the laboratory. Thank you to all the members of the Tyerman lab, Kaiser lab and Gilliham lab who have assisted in any way during my studies, in particular Danielle Mazurkiewicz for answering many of my questions concerning molecular biology and yeast.

Thank you to Prof. John Evans in Australian National University for many discussions that extended my ideas and Ms Stephanie McCaffery for excellent technical support.

Thank you to all members in Plant Research Centre, especially Skadi Lau, Zeyu Xiao, Danielle Mazurkiewicz, Johannes Scharwies, Asmini Athman and Hayden Ng Weng Wah for your friendship, endless laughs and support. A special thank you to Ms Nenah Mackenzie for her treats for lunch, spring rolls, cakes and big support.

Thank you to my friends at my conservation group – Natural History Society of South Australia Inc. and my “morning walking group” for the friendship and lovely company.

I gratefully acknowledge the International Postgraduate Research Scholarship for the financial support.

Finally, a special thank you to my husband, Vince, my parents and extended family for their continuing love and support throughout my study.

Chapter 1 General Introduction

Understanding the mechanism of CO_2 transport through the plasma membrane is very important because it is one of the rate limiting steps during photosynthesis (Evans et al., 2009). Aquaporins are water channels that belong to the major intrinsic protein family and have multiple integrated functions. Some aquaporins have been shown to facilitate small neutral molecule and gas transport in addition to water transport (Maurel, 2007; Maurel et al., 2008). Whether aquaporins can facilitate CO_2 transport across biological membranes is very controversial (de Groot and Hub, 2011). This thesis has firstly focused on investigating whether aquaporin activity in native leaf plasma membranes is correlated to CO_2 permeation using the stopped-flow technique. Then, certain *Arabidopsis* aquaporins were selected and expressed in *Xenopus* oocytes. Before attempting to measure CO_2 permeation using an external pH microelectrode technique (Geyer et al., 2013), the requirement of this technique that no ion conductance is induced by the aquaporin, was tested. It was discovered that AtPIP2;1 aquaporin induced anion channel activity. Therefore, the subsequent work mainly focused on characterizing the anion channel properties of AtPIP2;1. In the following review of the literature, I have therefore attempted to cover the research on why CO_2 transport across plant membranes is important, general features of aquaporins, and the research that relates to gas transport and ion transport via aquaporins, which also includes many studies undertaken on animal aquaporins.

1.1 CO_2 transport

1.1.1 Resistance along the CO_2 pathway inside leaves

During photosynthesis, CO_2 diffuses from the atmosphere across the boundary layers adjacent to the surface of the leaves, then through stomata to the sub-stomatal internal cavities. Subsequently, CO_2 must diffuse to the site of carboxylation inside the chloroplast stroma within mesophyll cells. From Fick's first law of diffusion, the net photosynthetic flux at steady state can be expressed as:

$$A_N = g_s (Ca - Ci) = g_m (Ci - Cc) \qquad \text{Equation 1-1}$$

where g_s and g_m are stomatal conductance and mesophyll conductance to CO_2 diffusion, respectively; Ca, Cc and Ci are CO_2 concentration in atmosphere, carboxylation site in the chloroplast stroma and sub-stomatal internal cavity, respectively (Evans et al., 2009). CO_2 is restricted by a series of resistances along the pathway mentioned above: the boundary layer resistance, the stomatal resistance, and the internal or mesophyll resistance. Mesophyll resistance (r_m) is complex and comprises both gaseous phase resistance and liquid phase resistance.

The gaseous phase, namely the intercellular airspaces resistance (r_{ias}), can be influenced by cell shape, leaf thickness *etc.* (Evans et al., 1994; Hanba et al., 1999). It is likely that the gaseous phase resistance varies between species and during different stages of plant development depending on growth conditions (*eg*. sun leaves versus shade leaves, or growth

temperature) (Nobel, 1977; Terashima et al., 2006). However, it is generally assumed that gaseous phase resistance is much smaller than liquid phase resistance (Niinemets and Reichstein, 2003; Evans et al., 2009).

The liquid pathway consists of many steps along which CO_2 diffuses to reach the enzyme Rubisco. First CO_2 must dissolve into the water-filled cell wall. As soon as it enters a water phase CO_2 will react with water, either slowly (rate constant = K_1 = $3.7*10^{-2}$ s^{-1}, 25 ℃) or more rapidly in the presence of carbonic anhydrases (CA) that catalyze the hydration/dehydration step (60 μM CA increases the rate constant by 10^5) according to equation 1-2 below (Gutknecht et al., 1977):

$$CO_2 + H_2O \underset{K_{-1}}{\overset{K_1}{\leftrightarrow}} H_2CO_3 \underset{K_{-2}}{\overset{K_2}{\leftrightarrow}} H^+ + HCO_3^- \underset{K_{-3}}{\overset{K_3}{\leftrightarrow}} 2H^+ + CO_3^{2-} \qquad \text{Equation 1-2}$$

Either CO_2, H_2CO_3 or HCO_3^- must diffuse across the cell plasma membrane to enter the cytoplasm then across the chloroplast envelope membrane to reach Rubisco within the stroma. In each cell compartment there may also be CAs. Therefore the total resistance contributed by the liquid pathway can be expressed as the sum of the separate resistance of each element (Figure 1-3) (Evans et al., 1994; Niinemets and Reichstein, 2003; Terashima et al., 2006):

$$r'_{liq} = r'_{wall} + r'_{plasma} + r'_{cytosol} + r'_{chloroplast} + r'_{stroma} \qquad \text{Equation 1-3}$$

The ranges in resistance associated with each element along the pathway were calculated by Evans *et al.* (2009) as shown in the table below (Table 1-1). Different pHs in each of the compartments arises which complicates the apparent resistances due to the effect of pH on the

reactions in Eqn 1-2, pH ranges for cell wall 5.5–6.0, cytosol 7.3–7.5, and stroma 7.6–8.0, have been used for the calculation of the resistance towards CO_2 (Evans et al., 2009). From the calculation of each resistance to CO_2, it is interesting to note that membranes, both plasma membrane and chloroplasts membranes account for most of the total resistance (above 60%).

Table 1-1 CO_2 resistance (r) generated by different element of mesophyll cells (Evans et al., 2009)

Element/compartment	r'_x (m^2_{chlor} s bar mol^{-1})
Cell wall	3-156
Plasmalemma	2.1-12500
Cytosol	0-1
Envelope	4.2-25000
Stroma	0.3-6.5
Total, r'_{liquid}	9.6-37664

1.1.2 CO_2 diffusion through biological membranes

CO_2 is considered lipophilic, hence, according to Meyer and Overton's rule where the gas permeability coefficient across membranes is proportional to its oil-water partition coefficient, then CO_2 should cross biological membranes rapidly (Gutknecht et al., 1977). However, with the discovery of the first plant aquaporins in 1993 (Maurel et al., 1993), the concept that CO_2 diffuses solely through the lipid bilayer has been challenged (Missner and Pohl, 2009). Evidence has been growing to support their role not only as water channels but also as CO_2 channels (Uehlein et al., 2003; Musa-Aziz et al., 2009; Heckwolf et al., 2011; Uehlein et al., 2012; Ding et al., 2013; Geyer et al., 2013).

CO_2 transport by aquaporins has been hotly debated in the literature over the last decade (de Groot and Hub, 2011; Heckwolf et al., 2011; Kaldenhoff, 2012; Uehlein et al., 2012; Ding et

al., 2013; Geyer et al., 2013). Research that indicates a role for aquaporins in CO_2 transport includes: 1) Decreased mesophyll conductance to CO_2 when aquaporins were inhibited in *Vicia faba* cv. Minpo (Terashima and Ono, 2002). 2) Overexpression of *Arabidopsis* PIP1b in tobacco plants significantly increased photosynthesis efficiency (Aharon et al., 2003). 3) A tobacco PIP1, NtAQP1, was indicated to facilitate CO_2 transport in *Xenopus* oocytes system and to increase leaf growth and stomatal opening (Uehlein et al., 2003). 4) With over expression of barley aquaporin (*HvPIP2;1*) in rice, the mesophyll conductance increased by 40% compared to the mesophyll conductance in wild type, increased stomatal conductance by 27%, and increased CO_2 assimilation by 14% (Hanba et al., 2004). However, there are several reasons that contribute to the difficulty to resolve this issue: Firstly, in aqueous solution, CO_2 reacts with water to form carbonic acid, and carbonic acid further dissociates, forming bicarbonate and carbonate (Eqn 1-2), this makes it difficult to measure the absolute CO_2 concentrations especially since the equilibrium concentrations of the products are pH dependent. It is also possible that carbonic acid and bicarbonate transport can be facilitated by aquaporins, since the aquaporin AtNIP2;1 transports undissociated lactic acid. Choi *et al.* (2007) heterologously expressed AtNIP2;1 in *Xenopus* oocytes and uptake experiments showed that it does not transport water or glycerol, but can facilitate transport of the protonated lactic acid (Choi and Roberts, 2007).

Previous research investigating CO_2 permeation has used intracellular or extracellular pH changes to identify changes in CO_2 concentration (Boron and Deweer, 1976; Nakhoul et al., 1998), however, this approach has also been challenged because the reaction between CO_2 and water is catalyzed by CA, and CA activity may change the kinetics of the reaction, e.g. CA is temperature dependent. One early work demonstrated that photosynthesis is

temperature dependent mainly because of CA and not Rubisco (Downton and Slatyer, 1972; Kaldenhoff, 2012). Also the CA concentration can affect the measured CO_2 permeability. The effect of CA concentration will be described in detail in Chapter 2 of this thesis. Additionally, the unstirred layer effects and the membrane permeability toward bicarbonate and carbonic acid also need to be considered (de Groot and Hub, 2011) since there is the possibility that bicarbonate and carbonic acid can be transported via anion exchanger proteins.

Two research groups, one working with animal aquaporins (group of W. Boron) and one with plant aquaporins (group of R. Kaldenhof), have independently observed clear differences on CO_2 permeability with and without aquaporins present (Cooper and Boron, 1998; Nakhoul et al., 1998; Uehlein et al., 2008; Musa-Aziz et al., 2009; de Groot and Hub, 2011; Heckwolf et al., 2011; Navarro-Ródenas et al., 2012; Uehlein et al., 2012; Geyer et al., 2013). All these results suggest a role for aquaporins in apparent CO_2 permeability across biological membranes. However, by contrast, P. Pohl's group suggest that unstirred layers rather than the lipid bilayer form the main barrier to CO_2 permeation, mainly based on pure biophysical arguments (Pohl et al., 1998; Missner et al., 2008; Missner and Pohl, 2009). This indicates that the techniques used to determine the role of aquaporins in facilitating CO_2 permeation needs close examination. Until now, there are three approaches that have been most commonly used to measure CO_2 permeability:

1) The stopped-flow spectrometer technique. This technique may minimise unstirred layer effects by virtue of being able to measure permeation into small diameter (100 nm to 1000 nm) vesicles or cells. It has been used to measure CO_2 permeability of either; reconstituted liposomes containing aquaporins that are entrapped with CA and a pH sensitive dye (Prasad et

al., 1998; Yang et al., 2000); or yeast cells expressing aquaporins and CA (Otto et al., 2010; Ding et al., 2013). However, none of these studies have addressed both the temperature effect on CA and the effect of CA concentration on the measured CO_2 permeability. In this thesis, I also used the stopped-flow spectrometry technique to measure CO_2 permeability but I also addressed effects of temperature on CA and CA concentration that may affect the measured CO_2 permeability.

2) ^{18}O-exchange measured by mass spectrometry. Recently this technique was used to demonstrate that cholesterol levels in biological membranes directly affect the CO_2 permeability (Itel et al., 2012). With analysis of increasing cholesterol in the vesicle membranes (5% - 70%), they showed that with the presence of 70% cholesterol, the CO_2 permeability decreased drastically by 2 orders of magnitude compared to phospholipid bilayer, even though with the sensitivity of the mass spectrometer they could only measure a lower limit value of 0.16 cm s^{-1} in phospholipid bilayers. Further, reconstitution of hsAQP1 into the cholesterol containing vesicles can significantly increase the CO_2 permeability (Itel et al., 2012). This result matches to molecular dynamics simulations (de Groot and Hub, 2011), which indicate that in membranes with extremely low intrinsic gas permeability or in membranes with a major fraction of aquaporin (i.e. low lipid-protein ratio), gases such as CO_2 are more likely to permeate via aquaporins (Terashima et al., 2006; Endeward and Gros, 2009; Evans et al., 2009; de Groot and Hub, 2011; Kaldenhoff, 2012; Ding et al., 2013)

3) pH transients measured by microelectrodes positioned against the cell surface. This technique has been used to measure CO_2 permeability and NH_3 permeability across *Xenopus* oocyte plasma membranes (Endeward et al., 2006). The technique involves placing a pH

sensitive microelectrode close to the surface of an oocyte, which is then exposed to changes in CO_2/HCO_3^- concentration. Based on the reaction described in Eqn 1-2, as CO_2 is transported across the plasma membrane, the chemical equilibrium of the reaction will move to the left, causing the concentration of H^+ to decrease, therefore, the external pH will increase. Using this approach the mammalian aquaporins, bAQP0, hsAQP1, rAQP4-M23, rAQP5, rAQP6, rAQP9 have been indicated to have CO_2 transport activity (Geyer et al., 2013). However, there is also one challenge towards this method: they have not tested if the expression of the aquaporins changes ion permeation through the oocyte plasma membrane which will affect the interpretation of changes in external pH.

Recent research on lipid membranes indicates that biological membranes are more "patchy" than uniformly fluid. The thickness and composition of the membrane may vary and the fluidity is affected by proteins in the membrane (Engelman, 2005; Catala, 2012). If aquaporins play an important role towards CO_2 diffusion across membranes, there have to be several mandatory criteria to be tested (Modified from Boron *et al.* 2011): 1) the unstirred layer must be relatively small; 2) the membrane (also considering all protein in the membranes except the gas channel) must have very low CO_2 permeability; 3) the CO_2 permeability of the aquaporin channel must be high (Boron et al., 2011); 4) it must be demonstrated that the expression of the particular aquaporin does not otherwise alter the function of the membrane, e.g. through altering function of other proteins or via inducing an ion conductance.

1.1.2.1 The chloroplast envelope

The chloroplast is bounded by two membranes, the inner membrane and the outer membrane. By separating the inner and outer chloroplasts membranes of spinach, it has been demonstrated that the two membranes have different features and properties. The outer envelope membrane has three times higher lipid to protein ratio compared to the inner membrane (Block et al., 1983). The inner membrane has been considered to be the actual permeability barrier, while the outer membrane has been demonstrated to be permeable to some small molecules as a result of the presence of large porins (Flugge and Benz, 1984; Pottosin, 1992; Heibert et al., 1995; Bolter and Soll, 2001). The pore-forming proteins (OEP16, OEP21 and OEP24) in the outer membrane have been well characterized. Biochemical evidence suggested that these three proteins form homo-oligomers and have ion channel properties (Pohlmeyer et al., 1997; Pohlmeyer et al., 1998; Bolter et al., 1999; Bolter and Soll, 2001). Aquaporins are more likely to be present in the inner membrane of chloroplasts (Uehlein et al., 2008; Beebo et al., 2013). Uehlein *et al.* (2008) identified that NtAQP1 was present in the chloroplast inner membrane in addition to the plasma membrane using confocal fluorescence microscopy of cells expressing NtAQP1 - GFP fusion proteins, *in-situ* immunology protein gel blotting, and protein identification in isolated membranes. They also used RNA interference (RNAi) approach to reduce the expression of NtAQP1 in *Nicotiana tabacum* plasma membrane and chloroplast envelope membrane. This resulted in an increased chloroplast membrane resistance to CO_2 diffusion of 56%. The diffusive resistance was calculated from conductance based on the measurement of photosynthetic $^{13}CO_2$ discrimination from a combined leaf gas exchange together with tunable diode laser spectroscopy (TDL). In addition, there was a reduction in the rate of photosynthesis in the

RNAi lines. Interestingly, even though the water permeability of the plasma membrane decreased, the apparent CO_2 permeability was not significantly affected (10% reduction). However, the opposite phenomenon was observed in chloroplast envelopes, which has a 90% reduction for CO_2 permeability and only slight reduction with water permeability. One explanation for this difference is the possibility that different combinations of homotetramer or heterotetramer formation of NtAQP1 with other aquaporins occurred in the different membranes. Uehlein *et al.* (2008) concluded that NtAQP1 is likely to facilitate CO_2 transport in chloroplasts. It was also shown that CO_2 permeability of plasma membrane is 5 times more than that of chloroplast envelopes, indicating that the chloroplast envelop membrane could be the major rate limiting step along the CO_2 diffusion pathway (Uehlein et al., 2008).

Using computer modelling, it has been demonstrated that lower energy barriers occur for CO_2 diffusion through the lipid bilayer than through aquaporins. Therefore aquaporin-mediated CO_2 transport is expected only in membranes with extremely low intrinsic CO_2 permeability (Hub and de Groot, 2006). The chloroplast envelope may have intrinsically low gas permeability so that CO_2 transport may be more dependent on aquaporins. One of the difficulties however, with manipulating one particular aquaporin gene is that altering the expression of one gene may result in altering the expressions of other aquaporin genes (Jang et al., 2007; Li et al., 2008), and it is also not clear what other effects over or under-expression of the aquaporin will have on permeation of other ions or molecules related to CO_2 (see Eqn 1-2)

1.1.2.2 CO_2 permeability of animal cell membranes

Human aquaporin 1 (hsAQP1) has been extensively studied for both water and gas transport properties. hsAQP1 is highly expressed in proximal tubule of kidney and erythrocytes. As described earlier, W. Boron's group first used the blunt pH microelectrode method to test hsAQP or Rh family proteins for CO_2 permeability by monitoring the change in surface pH. They first expressed hsAQP1 in *Xenopus* oocytes and monitored the intracellular pH. By increasing extracellular CO_2, they observed that the oocytes expressing hsAQP1 had 40% faster CO_2 induced intracellular acidification compared with controls. Meanwhile, ethoxzolamide (a CA inhibitor) significantly reduced the acidification rate (Nakhoul et al., 1998). Using the same method on normal human red blood cells, they demonstrated that hsAQP1 could be a major pathway for CO_2 transport in human erythrocyte membrane (Endeward et al., 2006). This method was used to assess the relative permeability of different proposed mammalian gas channels. According to their research hsAQP1, rAQP4, rAQP5, rAQP6, rAQP9, AmtB and RhAG were apparently permeable to CO_2, while rAQP3, hAQP7 and hAQP8 did not possess CO_2 transporter activity (Musa-Aziz et al., 2009; Geyer et al., 2013). The plasma membrane lipid of human red blood cells has intrinsically low gas permeability (Endeward et al., 2006), and the gas selectivity of hsAQP1 and RhAG complex would provide control over dissolved gases crossing the membrane (Musa-Aziz et al., 2009). Molecular dynamics simulations of membrane-embedded hsAQP1 in POPE bilayer suggested that CO_2 can pass through each of the four monomers, however, it has also been proposed that CO_2 could pass through the central pore between the 4 monomers as this pathway exhibits a much lower free energy barrier for CO_2 permeation (Wang et al., 2007).

1.2 General features of Aquaporins

Aquaporins are channel proteins embedded in the plasma and intracellular membranes of cells. They are small integral membrane proteins belonging to an ancient highly conserved family of major intrinsic proteins (MIPs) (Maurel et al., 2008; Hachez and Chaumont, 2010). Aquaporins facilitate the movement of water and other small molecules across cellular membranes, and a few have been shown to transport small-molecular weight solutes, such as boron (Takano et al., 2006; Schnurbusch et al., 2010; Li et al., 2011), silicon (Gregoire et al., 2012; Montpetit et al., 2012), urea (Gerbeau et al., 1999; Liu et al., 2003; Gu et al., 2012) and NH_3 (Niemietz and Tyerman, 2000; Musa-Aziz et al., 2009; Hwang et al., 2010), which are of great physiological significance (Hove and Bhave, 2011). As described earlier, even though there is also research that shows the potential role of aquaporin being a CO_2 transporter, this issue is still under debate.

The first aquaporin protein identified, human red cell AQP1 (CHIP28), was isolated from the erythrocyte membrane (Denker et al., 1988) and when expressed in *Xenopus laevis* oocytes, the osmotic water permeability increased. The protein also reduced the activation energy of water transport. The water permeability was reversibly inhibited by mercuric chloride, suggesting that the protein was the first identified water selective channel (Preston et al., 1992). An atomic model of AQP1 was established by Murata *et al.* (2000) at 3.8 Å resolution from electron crystallographic data (Murata et al., 2000). In the last decade, the function of a number of aquaporins has been identified. The bacterial protein GlpF facilitates glycerol transport, however, it does not facilitate water uptake (Sweet et al., 1990) and the crystal structure has been determined (Fu et al., 2000). Maurel *et al*. (1993) were the first to

clone and functionally characterise a plant aquaporin; the tonoplast integral membrane protein from *Arabidopsis thaliana* (γ-TIP). They demonstrated that γ-TIP does not facilitate glycerol transport and ion transport in oocytes, but functioned as a water specific channel in the vacuolar membrane (Maurel et al., 1993). MIP genes have been identified in over 30 plant species of both monocots and dicots. 35 MIP encoding genes have been identified in *Arabidopsis thaliana* (Johanson *et al*., 2001). Thirty three MIPs have been identified in rice, 36 MIPs in maize, 37 MIPs in tomato (Chaumont et al., 2001; Maurel et al., 2008; Sade et al., 2009), and at least 35 in wheat (Forrest and Bhave, 2008). Most recently, the MIPs in soybean have been identified using a bioinformatic homology search and 66 GmMIPs were identified (Zhang et al., 2013). MIPs have also been identified in woody plants such as grapevine (Vandeleur et al., 2009), walnut (Sakr et al., 2003) and olive (Secchi et al., 2007), and in an alga (Anderberg et al., 2011).

1.2.1 Aquaporin classification, and sub-cellular and tissue localization

The structure of aquaporins (AQPs) is highly conserved among plants, animals, fungi and bacteria (Fu et al., 2000). Plant AQPs can be divided into seven sub-families (Alleva et al., 2012; Luu and Maurel, 2013) (Figure 1-1), based on sequence homology and the putative sub-cellular localizations (Anderberg et al., 2011). Two of the sub-families are named based on their generalised membrane locations: plasma membrane intrinsic proteins (PIPs), and tonoplast intrinsic proteins (TIPs). However, some may occur at different membrane locations (Barkla et al., 1999; Alexandersson et al., 2004; Whiteman et al., 2008). The PIPs can be further classified into two subgroups: PIP1 and PIP2 according to their sequence identity. PIP2 proteins have a shorter N-terminal extension and a longer C-terminal end

containing putative phosphorylation sites compared with PIP1 proteins. The PIPs contain 13 family members in *Arabidopsis thaliana*; in comparison, the TIPs contain 10 family members. PIPs and TIPs are the most abundant aquaporins in the plasma membrane and vacuolar membrane of plants, respectively (Chaumont et al., 2001; Johanson et al., 2001; Quigley et al., 2002). The third family is named as NOD26-like intrinsic proteins (NIPs) (Heymann and Engel, 1999). NOD26 was the first identified member of this subfamily. It is located in the peribacteroid membrane of nitrogen-fixating symbiosomes in legume root nodules (Fortin et al., 1987). A fourth MIP subfamily in plants was named small basic intrinsic proteins (SIPs), because the proteins are relatively small (~27 kDa) (Ishikawa et al., 2005) compared to 28~31 kDa for PIPs and TIPs (Serra et al., 2013). Ishikawa *et al.* (2005) investigated the SIPs in *Arabidopsis thaliana*. When expressed in yeast, SIP1;1 and SIP 1;2 show water channel activity, however, SIP 2;1 does not. Their research also shows that SIPs are localized in the endoplasmic reticulum of plant cells and were expressed in all tissues examined except for dry seeds (Ishikawa et al., 2005). A fifth subfamily, the X intrinsic proteins (XIPs), have been discovered in the moss, *Physcomitrella patens*, poplar (Danielson and Johanson, 2008), tomato and grapevine (Danielson and Johanson, 2008; Sade et al., 2009). Quantitative real time PCR experiments showed that *PtXIP2;1* and *PtXIP3;2* were expressed in vegetative tissues, and *PtXIP2;1* was involved in response to abiotic stresses. When expressed in *Xenopus* oocytes, PtXIP2;1 and PtXIP3;3 can transport water (Lopez et al., 2012). Two additional AQP subfamilies were described in the non-vascular moss *Physcomitrella patens*: GlpF-like intrinsic proteins (GIPs) were shown to act as glycerol channels of Gram-positive bacteria (Gustavsson et al., 2005) and the hybrid intrinsic proteins (HIPs) which have only been identified in *P. patens* (Danielson and Johanson, 2008).

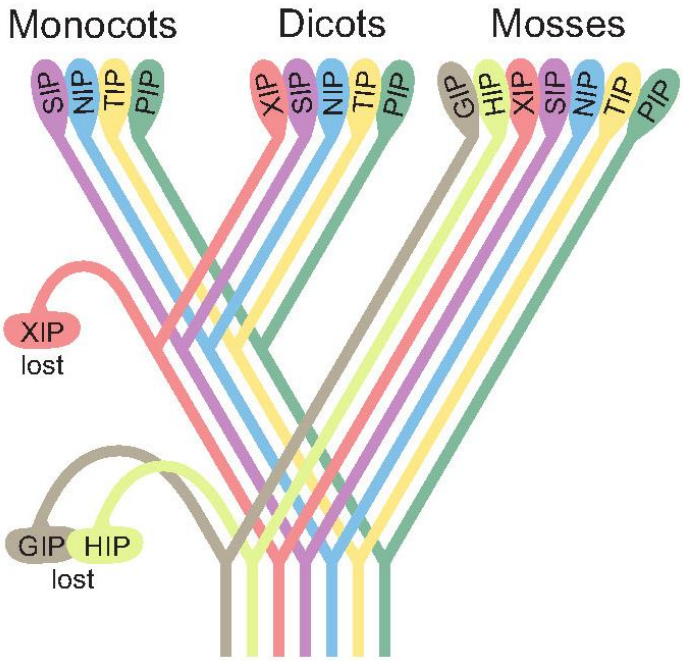

Figure 1-1 A graph of the MIP superfamily in plants. XIP, HIP and GIP have not been found in *Arabidopsis thaliana*. GIP and HIP were lost during the evolution of higher plants and XIP subfamily was lost in monocots (Danielson and Johanson, 2008).

1.2.2 Structural characteristics of aquaporins

Aquaporins are 26~30 kDa proteins that consist of six membrane-spanning alpha helices connected by five loops (A-E) (Figure 1-2) (Gonen and Walz, 2006; Fu and Lu, 2007). Both the N- and C- termini of the polypeptide are located on the cytoplasmic side of the membrane and the two halves of the polypeptide present significant sequence similarity to each other. Each half has hydrophobic loops, loop B and loop E, both of which contain the highly conserved asparagine-proline-alanine (NPA) motif that characterize most aquaporins (Reizer et al., 1993; Park and Saier, 1996; Tyerman et al., 1999; Ishibashi, 2006). Structurally, loop B and loop E overlap in the middle of the lipid bilayer to form two hemipores creating a narrow, water-filled channel (Figure 1-2) (Jung et al., 1994; Cheng et al., 1997; Tornroth-Horsefield et

al., 2006; Fujiyoshi, 2007). The two Asn residues of the NPA motif are crucial for the formation of water selectivity. The NPA motif is highly conserved among all the PIP family members in *Arabidopsis*, however, in other aquaporin subfamilies, TIPs and NIPs, this NPA motif can show minor modifications (Wallace and Roberts, 2004; Ishibashi, 2006).

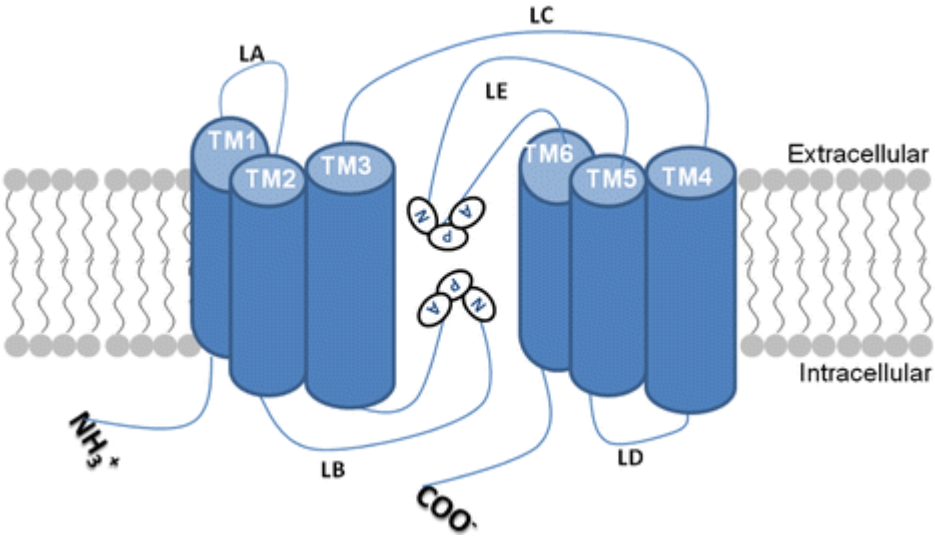

Figure 1-2 The predicted secondary structure of the AQP and the manner in which the two NPA motifs in Loop B and Loop E, respectively, fold inwards to form a water-filled pore (Hove and Bhave, 2011).

1.3 Aquaporin functions

1.3.1 Water uptake

Water use and yield are generally positively correlated in plants through the link between CO_2 uptake and water loss via stomata. During daylight hours, in most C3 and C4 plants water moves through the plant in the transpiration stream to the atmosphere via open stomata. Also

water uptake and movement of water into and out of cells is an essential feature of numerous physiological functions in plants, such as the uptake and transport of nutrients from the soil (Chrispeels and Agre, 1994). Within a tissue there are three possible pathways for water flow: the apoplastic path, the symplastic path and the cell-to-cell path. The apoplastic path encompasses water flow within the cell wall. The symplastic path involves water flow through the cytoplasm and plasmodesmata, while the cell-to-cell path involves water flow through cell membranes, mainly plasma membranes, which is mostly mediated by aquaporins in many plant tissues. It is difficult to separate the symplastic from the cell-to-cell path so these are normally taken together as the transcellular pathway (Maurel et al., 2008). The identification of aquaporins greatly changed our view about how plants may regulate water flow, since they increase the efficiency for the transcellular path (Steudle, 1992; Chrispeels and Maurel, 1994). Aquaporins are important for root water transport where they can increase osmotic water permeability by up to 20-fold (Maurel and Chrispeels, 2001). It was demonstrated that aquaporins contribute substantially (83-95%) to root water uptake in 14 to 17 days-old hydroponically grown barley plants (Knipfer et al., 2011).

PIPs and TIPs are the most abundant aquaporins in the plasma membrane and tonoplast membrane of plants, respectively. TIPs are thought to be involved in rapid osmotic equilibration between vacuole and cytosol by solute transport and recirculation of water (Barrieu et al., 1998) though there is little evidence for this. Mature living plant cells are characterized by a large single vacuole with a thin layer of cytosol between the cell plasma membrane and the vacuolar membrane. The composition of the cytosol has to be tightly controlled so as to maintain the best conditions for the various metabolic activities occurring

in the cytosol. TIPs are likely to be crucial in the regulation of the cytosolic osmolarity (Karlsson et al., 2000).

The major function of PIPs is to facilitate the diffusion of water and small molecular weight solutes into and out of the cell (Johansson et al., 2000). The presence of aquaporins gives the cell better control over water flow, which could not be readily achieved through alterations to lipid bilayer composition. Although, the amino acid sequences are similar between PIP1s and PIP2s, the functions of these two sub-families are different (Kaldenhoff and Fischer, 2006). While expressing PIP1s and PIP2s in *Xenopus* oocytes respectively, PIP2s show substantial water channel activity, whereas PIP1s show very slight activity or none (Chaumont et al., 2000).

Much research has shown that aquaporins play a significant role in roots (Vandeleur et al., 2009; Knipfer et al., 2011) and some PIPs and TIPs have been reported to be expressed at a higher level in roots than leaves such as the *Zea mays ZmPIP1;1*, *ZmPIP1;2* and *ZmPIP2;5* (Chaumont et al., 2000). However, there are also some aquaporins that have a higher expression level in leaves, for instance, the tulip *PIP2;1* (*TgPIP2;1*) and *TgPIP2;2* are highly expressed in leaves and only *TgPIP2;2* expresses at a very low level in roots (Azad et al., 2008). It has been shown that aquaporins also play key roles in leaf physiology such as leaf water stress, leaf growth and photosynthesis (Heinen et al., 2009; Pou et al., 2013). In *Arabidopsis* plants, reduced expression of some *PIPs* results in reduced hydraulic conductivity of isolated leaf protoplasts (Martre et al., 2002). Over-expression of *B. napus BnPIP1* in tobacco mesophyll cells resulted in a significantly faster swelling of leaf protoplasts in hypotonic medium (Yu et al., 2005).

1.3.2 Non-charged small neutral solute transport

In plants, many more aquaporins are found than in animals. This greater diversity of plant aquaporins could indicate a much wider range of transport functions. Heterologous expression of plant aquaporins in *Xenopus* oocytes showed that some plant aquaporins function in plant nutrient uptake in addition to water transport. Some aquaporins seem to function by facilitating the passage of solutes such as glycerol and urea (Biela et al., 1999). Nodlin26 (NOD26), a member of the aquaporin water channel family, is a major protein component of the soybean symbiosome membrane (SM) that encloses the rhizobium bacteroid. Dean *et al*. (1999) purified the protein from SMs and reconstituted it into carboxyfluorescein-loaded liposomes for transport studies using stopped-flow spectrofluorimetry. Liposomes containing NOD26 showed a high water permeability that is mercury-sensitive. NOD26 proteoliposomes also facilitate glycerol transport, showing a 43-fold higher rate of glycerol flux than control liposomes. However, NOD26 isn't permeable to urea. Some recent work has demonstrated the role of NOD26 as a NH_3 transporter (Hwang et al., 2010; Masalkar et al., 2010) and further detail will be discussed in the following gas transport section. These results indicate that NOD26 is a multifunctional AQP that conducts both water, glycerol and NH_3 across the SM, and likely plays a role in osmoregulation during legume/rhizobia symbioses (Rivers et al., 1997; Dean et al., 1999). Some studies also showed that NOD26 can function as an ion channel (Weaver et al., 1994; Hwang et al., 2010), which will be discussed in Chapter 4.

TIP transporters may play a role in equilibrating urea concentrations between different cellular compartments in addition to their role as water channels (Liu et al., 2003). They

conducted uptake studies using ^{14}C-labeled urea into AtTIP2;1-expressing *Xenopus* oocytes and showed that AtTIP2;1 facilitated urea transport in a pH-independent manner and with linear concentration dependency. The plasma membrane located NtAQP1, which is highly expressed in tobacco roots, is also permeable to urea (Eckert et al., 1999).

Takano *et al*. (2006) identified significant *NIP5;1* up-regulation in boron (B) deficient roots of *Arabidopsis*. When expressed in *Xenopus* oocytes, NIP5;1 showed boric acid transport activity in addition to water channel activity. The two T-DNA insertion lines of *NIP5;1* present lower uptake of boric acid into roots, which results in lower biomass production. These results indicated that NIP5;1 functions as a boric acid channel and is crucial for B uptake, which is essential for plant growth and development (Takano et al., 2006). A barley NIP, HvNIP2;1, is also a boric acid transporter, and when expressed in *Xenopus* oocytes and yeast, significant transport of boric acid was observed compared to the controls. By substituting the rice NIP2;1 (OsNIP2;1) ala132 to thr, lower shoot B accumulation was observed (Schnurbusch et al., 2010).

Silicon is another nutrient essential to plant growth where NIP aquaporins are involved in uptake. Silicon can help plants develop stronger resistance towards pathogen attack. Ma *et al.* (2006) identified a low silicon rice mutant (*Lsi*) and identified the mutated gene belonging to the NIP subfamily, which is mainly expressed in roots. *Lsi* expression is down-regulated by high plant silicon levels. Expression of Lsi1 in *Xenopus* oocytes resulted in Si uptake (probably silicic acid, uncharged at neutral pH) transport activity. By suppressing the expression of *Lsi* using RNA interference, silicon uptake was greatly reduced compared to the control plants. These results indicate that Lsi1 is a silicon transporter in rice (Ma et al., 2006).

A wheat NIP aquaporin, TaLsi1, when expressed in *Xenopus* oocytes also functions as a silicon transporter (Montpetit et al., 2012).

1.3.3 Gas transport

CO_2 permeability has already been discussed in the first section of this chapter, and in this section, NH_3 transport will be mainly discussed. Gas transport through membranes is one of the most fundamental and significant metabolic steps in the development of both plants and animals. It is very important for nutritive transport, photosynthesis and signaling. For the past few decades, it has generally been assumed that gas molecules permeate through membranes mainly by simple diffusion through the lipid component of the membrane (Gutknecht et al., 1977). However, some membranes have no detectable permeability to gases, for instance, apical membrane of gastric gland (Waisbren et al., 1994) and colonic crypt (Singh et al., 1995). Aquaporins may play an important role in cell membranes that have relatively low intrinsic gas permeability (Boron et al., 2011).

NH_3 is an important form of reduced nitrogen for amino acid synthesis in plants and can be transferred from endosymbiotic bacteria to the host plant across a plant derived symbiosome membrane in nitrogen fixing plants (Niemietz and Tyerman, 2000). A first link between aquaporins and N assimilation came from the observation that the expression of some aquaporin genes is dependent on N-compounds (Maurel et al., 2008). NIPs and some aquaporins in the TIP family have been reported to be involved in NH_3 transport (Niemietz and Tyerman, 2000; Zelazny et al., 2007; Hwang et al., 2010; Masalkar et al., 2010). Although aquaporins are by no means specific for the transport of water, their non-specificity

in transport of molecules other than water may have played a key role during the development of plants (Maurel and Chrispeels, 2001; Maurel et al., 2008). NOD26 was demonstrated to be involved in NH_3 movement through the peribacteroid membrane (Rivers et al., 1997; Niemietz and Tyerman, 2000). Stopped-flow measurement of NH_3 permeability properties of the carboxyfluorescein (CF) loaded NOD26 proteoloposomes demonstrated that NOD26 facilitate the transport of NH_3, and mercury can inhibit the measured NH_3 permeability (Hwang et al., 2010). The ability of plant aquaporins to facilitate gas transport has revealed an important potential role for aquaporins in nitrogen fixation that may extend to carbon fixation as well.

Because *Xenopus* oocytes have low permeability towards NH_3, it is a model system for NH_3 transport research. By using ion-selective microelectrodes to test the intracellular pH of oocytes that express hsAQP1, it was demonstrated that although oocytes membrane does have some NH_3 permeability, hsAQP1 can significantly enhanced NH_3 permeability (Nakhoul et al., 2001). It was also shown that human AQP8 and wheat aquaporin TaTIP2;1 are permeable to NH_3. When heterologously expressed in mutant yeast that is deficient in NH_3 transport, AQP8 and TaTIP2;1 can restore cell growth on low external NH_4^+. In *Xenopus* oocytes, AQP8, AQP9, AQP3 and TaTIP2;1 supported inward currents carried by NH_4^+ under voltage-clamp conditions, provided sufficient NH_3 was present in the external solution (Jahn et al., 2004; Holm et al., 2005). By expressing in yeast cells, *Arabidopsis thaliana* aquaporins AtTIP2;1 and AtTIP2;3 were also shown to transport methylammonium or ammonium at high medium pH, acting as NH_3 channel and facilitating the transport of NH_3 across membranes (Loque et al., 2005). Similarly, using stopped-flow, yeast cells that expresses TaPIP2;2 show the ability to transport NH_3. TaPIP2;2 shows mercury insensitive water transport in yeast

cells, but NH_3 transport can be severely inhibited by $HgCl_2$. This inhibition experiment suggests that NH_3 and water transport occur via different pathways in this aquaporin (Bertl and Kaldenhoff, 2007).

It is very important to note that similar techniques have been used for measurement of CO_2 permeability and NH_3 permeability: the permeability of either gas was measured indirectly. Both gases react with water and produce ions that result in changes to pH, thus, the measured gas permeability is based on the change in pH, on either side of the membrane depending on the experimental configuration (Niemietz and Tyerman, 2000; Holm et al., 2005; Bertl and Kaldenhoff, 2007; Geyer et al., 2013). However, it is much easier to demonstrate NH_3 transport than CO_2 transport. The reason for this is that NH_3 has a much lower oil/water coefficient ($Kp<<1$) compared to CO_2 ($Kp\geq1$) (Missner and Pohl, 2009). Membrane channels will only facilitate the transport of gas by decreasing the otherwise large energy barrier for diffusion across the lipid bilayer. Another problem is, the presence of ion transporters (i.e. NH_4^+ transporter or HCO_3^- transporter) in the membrane which could severely affect the measured gas permeability. If that was the case, the techniques for NH_3 and CO_2 permeability measurement will have to be challenged.

1.3.4 Ion transport via aquaporins

As indicated in Section 1.1.2, any ion transport facilitated or induced by an aquaporin that may be suspected of CO_2 transport could compromise the methods for measurement of CO_2 transport. This is because of the formation of ionic derivatives of CO_2 when it reacts with water (Eqn 1-2), and the common case where CO_2 permeability is indirectly measured as a

change in pH. Changes in pH can also occur indirectly by movement of other charged species across the membrane of interest. Initially, aquaporins were assumed to transport only water and a range of neutral molecules, and the selectivity filter formed by the NPA motifs appeared to function to exclude hydronium ions (Ilan et al., 2004; de Groot and Grubmuller, 2005; Eriksson et al., 2013). However, there is some evidence that aquaporins can sometimes function as gated ion channels in addition to water channels (Yool, 2007; Yool et al., 2010; Yool and Campbell, 2012). Even though this role for aquaporins has been controversial, it is likely to have significant physiological relevance if correct. Some detailed molecular mechanisms have been obtained to determine the crucial region of aquaporins that mediate ion transport (Campbell et al., 2012). For instance, the mammalian aquaporin 1 (AQP1) is one of the most studied aquaporins. A central pore formed in the centre of the homotetramer of AQP1 is the most likely pathway for ions (Yu et al., 2006; Yool, 2007; Campbell et al., 2012). Besides AQP1, until now, there are several aquaporins that have been shown to have ion transport activity: AQP0, AQP1, AQP6, *Drosophila* Big Brain (BIB) and plant NOD26 (Yool and Campbell, 2012). These findings are essential for understanding the multifunctional properties of aquaporin channel proteins and the regulation of membrane transport for water and ions. The detail of aquaporin ion channel activity will be further discussed in Chapter 4 and 5.

1.4 Aquaporins blockers

Here I discuss aquaporin pharmacology since various agents have been used to test aquaporin activity *in vivo* and to distinguish between pathways of permeation through the protein. In 1990, Wayne and Tazawa showed that the osmotic water permeability of *Nitellopsis* can be

inhibited by the mercurial reagent p-chloromercuribenzenesulphonate (pCMBS), which was also found to inhibit aquaporins in animal cells (Naccache and Shaafi, 1974; Wayne and Tazawa, 1990). Subsequently, mercurial reagents were tested for their effects on water permeability in different membranes, cells and tissues. In general, mercurial and sulphydryl reagents block aquaporins. However, some can be mercury-insensitive , e.g. NtAQP1 (Biela et al., 1999).

Normally, reagents that can oxidize cysteine residues associated with the pore region of the protein can act as blockers, mercurials act by covalent modification of cysteine residues within the water pore and in other regions of the protein causing either block or conformational changes leading to inhibition of water transport (Zhang and Tyerman, 1999). However, the analysis of aquaporin function is difficult because of the lack of specificity of mercurial agents. Although mercurial agents have been used as an effective aquaporin blocker, great care has to be taken because of the numerous side-effects of these types of substances (Schütz and Tyerman, 1997), for instance, they are toxic to cells and can inhibit many other proteins (Loo et al., 1996). Hence, their effect on membrane water permeability may not be direct (Daniels et al., 1994; Maurel et al., 1995; Johansson et al., 1998).

Silver and gold compounds can also block aquaporins at low concentrations *in vitro* (Niemietz and Tyerman, 2002). Silver inhibition is rapid and is not reversible with mercaptoethanol. In the peribacteroid membrane (PBM) of soybean nodules, the inhibition constant for silver is about 40 times lower than that for mercury. For human red cells the inhibition was about 200 times more potent than mercury compounds. Silver inhibition is not only restricted to the PBM; it was also effective on plant plasma membrane vesicles as well as

human red blood cells. The mechanism of silver and gold inhibition is most likely due to their ability to interact with sulfhydryl groups of proteins (Niemietz and Tyerman, 2002).

Human aquaporins are an important target for drug design and discovery in medical research. Some human diseases such as cancer and brain oedema involve tissues where aquaporins are highly expressed (Yool et al., 2010). Brooks *et al.* (2000) identified that quaternary ammonium tetraethylammonium ion (TEA^+) as the first non-mercurial AQP1 inhibitor. It blocks water permeability of AQP1 expressed in oocytes by about 30% at 10 mM concentration. By mutating certain amino acid residues in the protein, it was demonstrated that tyr186 is essential for sensitivity to TEA. Substitution of tyr186 to phe186 completely silenced TEA sensitivity but the mutant aquaporin was still permeable to water (Brooks et al., 2000; Søgaard and Zeuthen, 2008). Interestingly, the carbonic anhydrase inhibitor acetazolamide (10 μM) was also shown to inhibit the water permeability of AQP1 expressed in *Xenopus* oocytes by 80% (Bing et al., 2004).

1.5 Interaction between aquaporins

Aquaporins generally exist as tetramers. Each monomer of the tetramer functions as an independent water pore (Daniels et al., 1999; Engel et al., 2000; Fotiadis et al., 2001). The assembly of the tetramer is important for folding of the protein and for its stability and targeting to the correct cellular membrane (Barkla et al., 1999; Maurel et al., 2008; Shao et al., 2008). There is evidence that aquaporins form both homotetramers and heterotetramers (Fetter et al., 2004; Otto et al., 2010; Jozefkowicz et al., 2013). Fetter *et al.* (2004) showed that co-expression of ZmPIP1;2 and certain ZmPIP2s isoforms led to increased water

permeability depending on the quantity of *ZmPIP1;2* cRNA injected into the oocytes (Fetter et al., 2004). This suggests that PIP1 isoforms have an important role in water permeability, possibly interacting with PIP2. Nickel affinity chromatography column purification of His-ZmPIP2;1 co-eluted with ZmPIP1;2-GFP directly demonstrated that ZmPIP1;2 and ZmPIP2*s* physically interact and form heterotetramers. Zelazny *et al.* (2007) fused ZmPIP*s* to monometric yellow fluorescent protein or monomeric cyan fluorescent protein and expressed in maize mesophyll protoplasts. When expressed alone, ZmPIP2 were re-localized to the plasma membrane, whereas ZmPIP1s were retained in the endoplasmic reticulum. Interestingly, by using FRET/fluorescence lifetime imaging microscopy, they observed that when co-expressed ZmPIP1s with ZmPIP2s, ZmPIP1s were re-localized to the plasma membrane as well. These data clearly suggest that ZmPIP1s need to interact with ZmPIP2s to be targeted to the plasma membrane, and ZmPIP1s and ZmPIP2s can form heterotetramers in the plasma membrane. This provides the cells with an additional mechanism for regulating membrane permeability and that PIP1-PIP2 interaction is required in *planta*. The diversity of channel activity in the membrane could be greatly increased by the different combinations of PIP1-PIP2 heterotetramers in specific cell types, developmental stages, certain organs or in response to different environmental cues (Zelazny et al., 2007). Otto *et al.* (2010) co-expressed NtAQP1 and NtPIP2;1 in yeast cells, and using split YFP experiments, protein chromatography, and gel electrophoresis, they demonstrated that these two proteins formed heterotetramers when co-expressed in yeast. NtAQP1 is a member of the PIP1 sub-family and does not display any water transport activity when expressed in yeast. By contrast, NtPIP2;1, which belongs to the PIP2 subfamily, is a functional water channel. When coexpressed in yeast cell, the ratios of PIP1/PIP2 in the tetramer had significant effects on water transport (Otto et al., 2010).

1.6 Conclusion and project aims

Research has shown that mesophyll conductance to CO_2 is of similar magnitude to stomatal conductance to CO_2 (Flexas et al., 2012), and among all the elements that contribute to mesophyll conductance, the membrane conductance has the greatest impact. However, the nature of the pathway of CO_2 diffusion across biological membranes is controversial. Although more evidence has been accumulating showing that the diffusion process can be facilitated by aquaporins, many studies show that it does not (Missner et al., 2008; Missner and Pohl, 2009), also the real situation in an intact plant remains unknown. This is crucial, as understanding how CO_2 gets to the sites of photosynthesis is a global issue important for developing models used to predict the impact of rising CO_2 concentration on plant productivity and CO_2 sequestration (Poorter, 1993; Franks et al., 2013).

This thesis aims are to:

1. Discover the functional link between water uptake and CO_2 uptake in photosynthetic plant cells.
2. Test some of the underlying assumptions in CO_2 permeability measurements on vesicles.
3. Test criterion for CO_2 diffusion pathway through aquaporins, such as blocker sensitivity and temperature dependence.
4. Characterize and express specific aquaporins in *Xenopus* oocytes and to test the water and CO_2 permeability after it was established that ion permeation was not involved.

Initially I intended to carry out these aims on *Arabidopsis* mesophyll cells then investigate *Arabidopsis* aquaporins that are expressed in leaf mesophyll cells for CO_2 permeability using

the external pH electrode method (Endeward et al., 2006; Geyer et al., 2013). However it proved difficult to get good plasma membrane vesicles from *Arabidopsis* that had high water permeability, while it was found that pea (*Pisum sativum* L cv Massey) yielded excellent plasma membrane vesicles from leaf tissue that showed very high and variable water permeability. The variable water permeability caused by different growth conditions was reasoned to be useful to examine a potential correlation between water permeability and CO_2 permeability (Chapter 2, Aims 1, 2 & 3). Since very few of the pea aquaporin genes had been identified (Ampilogova et al., 2006; Beaudette et al., 2007). I continued the heterologous expression analysis on *Arabidopsis* aquaporins that were considered potential CO_2 channels (Aim 4). First the water transport properties of these aquaporins were investigated (Chapter 3), then before trying to carry out the external pH technique, I tested the possible ion channel properties of the aquaporins. This yielded a surprising result with one of the aquaporins, the much studied AtPIP2;1 (Verdoucq et al., 2008; Martinière et al., 2012; Luu and Maurel, 2013) which showed anion channel activity, including permeability to the bicarbonate anion, when expressed in *Xenopus* oocytes (Chapter 4). As a consequence of this discovery much of the remaining time in the PhD was spent characterising this aquaporin further and then testing anion channel function of AtPIP2;1 in yeast (Chapter 5).

Chapter 2 Water and CO_2 transport across leaf plasma membranes

2.1 Introduction

There are several steps along the pathway of CO_2 diffusion to the sites of fixation. As a result of CO_2 being consumed by Rubisco in the stroma of the chloroplasts, the partial pressure of CO_2 drops to below that in the ambient air and a diffusion gradient is created from outside the leaf to the site of fixation. CO_2 in the ambient air must first diffuse across the boundary layer, which is the air layer that adjacent to the surface of the leaves, then through the stomata, to sub-stomatal cavities. From here, CO_2 must diffuse through liquid in the cell walls and across membranes to the site of carboxylation inside the chloroplast stroma within mesophyll cells. CO_2 diffusion is restricted by a series of resistances along this pathway: the boundary layer resistance, the stomatal resistance and the mesophyll resistance. The mesophyll resistance can be represented as the sum of gaseous phase resistance and liquid phase resistance generated during the diffusion through the mesophyll cells (Evans et al., 2009). It is generally assumed that resistance through the gaseous phase is relatively small compared to that through the liquid phase (Niinemets and Reichstein, 2003). Among all the elements that contribute to the liquid phase resistance, the membrane resistance generates more than 60% of the total liquid phase resistance (Evans et al., 2009).

The transport of gaseous compounds across biological membranes is essential in all forms of life. Traditionally, it was believed that as CO_2 is lipophilic, it could freely penetrate the lipid matrix of biological membranes and the rate limiting diffusion would be more likely the unstirred layers adjacent to the membrane (Gutknecht et al., 1977). However, there are

several examples that challenged this view, since some biological membranes were found to have either very low or very high gas-permeability. Low gas permeability (either NH_3 or CO_2) have been reported for some epithelial apical membranes (Waisbren et al., 1994; Negrete et al., 1996; Endeward and Gros, 2005). On the other hand, high CO_2 permeability was measured for the cell membranes of human red blood cells and tobacco mesophyll cells which might due to these cells having high densities of aquaporins in the cell membrane, facilitating CO_2 entry into the cells (Blank and Ehmke, 2003; Uehlein et al., 2008). These observations led to the apparent identification of several membrane-embedded "gas channels", proposed to facilitate the transport of biological active gases, such as carbon dioxide, nitric oxide, and ammonia (Endeward et al., 2008). However, some of these findings are in conflict with the well-known Meyer–Overton rule, which predicts much higher membrane permeability from the molecule's water-oil partition coefficient (Missner and Pohl, 2009).

After the discovery of plant aquaporins in 1993 (Maurel et al., 1993), evidence has been accumulating to challenge the concept that CO_2 diffuses solely through the lipid bilayer. It is now believed that there are two parallel pathways through which CO_2 can enter the cell: 1) via the lipid pathway across membranes (1 layer of plasma membrane or 2 layers of chloroplast envelope membrane); 2) via aquaporins in the three membranes (Evans et al., 2009). In 1998, Cooper and Boron first demonstrated enhanced membrane permeability to CO_2 by expressing human red blood cell *AQP1* gene in *Xenopus* oocytes (Cooper and Boron, 1998). In 2002, Terashima and Ono provided the first evidence that aquaporins may enhance CO_2 permeability in *Vicia faba* leaves using mercury, an aquaporin inhibitor, that inhibited this effect (Terashima and Ono, 2002). Using *AtPIP1;2* T-DNA insertion line, Uehlein *et al.* demonstrated that cellular CO_2 transport depends on the expression of the aquaporin AtPIP1;2.

Complementation of the *AtPIP1;2* knockout restored membrane CO_2 flux levels to that of controls (Uehlein et al., 2012).

The aim of this chapter is to examine links between CO_2 permeability (P_{CO2}) and water permeability (P_{os}) taking into account some of the chemical constraints that may lead to artifacts in the measurement of CO_2 permeability. Membrane vesicles were isolated from pea leaves by a modified two phase partitioning technique (Larsson et al., 1994; Niemietz and Tyerman, 2000). A pH dependant fluorescent dye, HPTS, was entrapped within vesicles to detect changes in intravesicular pH as a result of the reaction of CO_2 with water to produce carbonic acid. This reaction was catalysed by carbonic anhydrase (CA), which was also entrapped within the vesicles. Using stopped-flow spectrofluorimetry, a sudden change in external CO_2 concentration was imposed and the kinetics of intravesicular pH was obtained and used to calculate CO_2 permeability. Temperature dependences of both water and CO_2 permeability were examined and used to infer flow/diffusion pathways across the membrane. DIDS (4, 4'-Diisothiocyano-2, 2'-stilbenedisulfonic acid) was tested because Endeward *et al.* has shown that human blood cell AQP1 is a CO_2 channel and by surface pH and CO_2 permeability measurement in *Xenopus* oocytes, which were exposed to solution containing CO_2/HCO_3^-, they demonstrated that half of the CO_2 permeability can be inhibited by DIDS, meanwhile, DIDS does not affect water permeability (Benga et al., 1992). Thus, they concluded that half of the CO_2 passes through the central cavity of the aquaporin and DIDS may affect or block the central cavity (Endeward et al., 2006). The aquaporin inhibitor, silver sulfadiazine (Ag-sul), was also tested to examine the pathway of CO_2 transfer. Pea plants were grown in different conditions to vary their leaf plasma membrane water permeabilities. Vesicles isolated from different batches of plants were used to measure water permeability as

well as CO_2 permeability in parallel. I tested the hypothesis that the permeability to CO_2 and water permeability should be correlated if CO_2 permeation was facilitated by aquaporins or in some other way positively affected by the activity of aquaporins.

2.2 Materials and Methods

2.2.1 Plant material and growth conditions

The soil for growing *Pisum sativum* L cv Massey was prepared by mixing 1 part of vermiculite perlite mix (vermiculite and perlite were mixed at a 1: 1 ratio) and 3 parts of university of California mix (UC mix) obtained from South Australian Research and Development Institute. Nutrients were supplied as mini osmocote granules (Smoult Horticultural Suppliers P/L). The seeds were sown about 4 cm deep and on a grid of 9 x 12 seeds (approx. 1 seed/cm) in trays (28 cm x 18 cm x 11 cm) with drainage holes. After sowing, approximately 1 cm of sand was spread on top of the soil to avoid black flies laying eggs in the soil. The trays were placed in a glasshouse with 12-h light/dark cycle for about 21 days and watered when required. Plants were 3 to 4 weeks old when used to isolate plasma membrane vesicles, when 20-25 leaves had emerged and were 8-10 cm high.

2.2.2 Stomatal conductance measurement

The stomatal conductance was measured by a porometer (Delt-T Device, UK) each time before harvesting the pea plants for vesicle preparation. The porometer was calibrated each time according to manufacturer's instructions.

2.2.3 Vesicle isolation

Plasma membrane vesicles from leaves were obtained by an aqueous two phase partitioning process (Larsson et al., 1987). According to Larsson and co-workers (1984), plant plasma membranes obtained from the upper phase after purification by aqueous two phase partition are mainly sealed right-side-out vesicles (Larsson et al., 1984). Lowry protein assay was done to determine the total protein level of vesicles (Lowry et al., 1951). Previous studies have demonstrated that this two-phase partitioning technique form pure plasma membrane vesicles (Larsson et al., 1987; Larsson et al., 1994; Niemietz and Tyerman, 1997).

(1) Solutions

All components of solutions and media were analytical or molecular biology grade and purchased from Sigma-Aldrich unless indicated otherwise.

Table 2-1: General solutions for vesicle preparation.

Solutions	Components
Isolation solution	0.5 M Sucrose, 50 mM HEPES-KOH, 5 mM ascorbic acid, 1 mM DTT and 0.6 % (w/v) PVP 10, 20 mM EDTA, 20 mM EGTA, 50 mM NaF, 0.5 mM PMSF, pH 7.5 (Ascorbic acid, DTT, NaF and PMSF should be added freshly on the day)
Resuspension medium	330 mM Sucrose, 3 mM KC1, 5 mM K_2HPO_4/KH_2PO_4, 0.1 mM EDTA, pH 7.8
Upper phase dilution medium	10 mM Tricine-NaOH, 0.1 mM EDTA, pH 7.6
Final resuspension medium	0.33 M Sucrose, 0.1 mM EDTA, 10 mM Tricine-NaOH, pH 7.6

Phase system	6.2% Dextran T500/6.2% PEG 6000, 330 mM Sucrose, 3 mM KC1, 5 mM K_2HPO_4/KH_2PO_4, pH 7.8, add water to a final weight of 27 g, mixed thoroughly, and stored at 4 ℃
Bulk Phase system	6.2% Dextran T500/6.2% PEG 6000, 330 mM Sucrose, 3 mM KC1, 5 mM K_2HPO_4/KH_2PO_4, pH 7.8, add water to a final weight of 300 g, mixed thoroughly, poured it into a separatory funnel and stored at 4 ℃ overnight for separation. The fresh lower phase was collected on the second day.

(2) Protocol

1) 100 g of leaves were excised and homogenized in a stainless steel blender with three 20 s pulses in about 275 ml of ice-cold isolation medium.
2) The homogenate was filtered through four layers of Miracloth (Calbiochem), and centrifuged for 10 min at 10,000 *g* (ss-34 rotor) to remove the bulk of chloroplast and mitochondria.
3) Subsequently, the supernatant was centrifuged for 40 min at 50,000 *g* (Ti 70 rotor) to obtain a microsomal pellet.
4) Microsomes were resuspended in resuspension medium and made up to 10 ml in a glass homogeniser.
5) 72 µl of 1 mM DTT-EDTA stock solution was added to the 27-g phase system in a falcon tube. DTT-EDTA is a protective reagent to retain high activity of vesicles (Pamgren et al., 1990). Then, the balance was tared and 5 ml of homogenate was added to the falcon tube and topped up to a final weight of 9 g by carefully adding resuspension solution. The falcon tube was inverted 40 times and centrifuged at 1500 *g* for 10 min. Two layers normally form after centrifugation.

6) The upper phase was carefully transferred to 10 ml of fresh lower phase (obtained from the bulk phase system) in a new falcon tube. The two phases were mixed by inverting the falcon tube 40 times. Then, the tube was centrifuged at 1500 *g* for 10 min. The upper phase obtained was washed again with fresh lower phase (repeated step 6 once more) to achieve a high purity of vesicles.
7) After three partitioning steps the membranes in the upper (UIII) phase were diluted to 100 ml with upper phase dilution medium and the membranes were pelleted for 60 min at 100,000 *g* (Ti 70 rotor).
8) After resuspension in a small volume of final resuspension medium, aliquots of 250 µl were transferred to Eppendorff tubes. These were snap-frozen in liquid nitrogen and stored for up to 4 weeks at -80 ℃ before being used in stopped flow experiments.

2.2.4 Vesicle size determination

Vesicle size was determined by dynamic laser light scattering in a NICOMP 380 particle sizer (PSS-NICOMP Particle Sizing Systems, Santa Barbara, CA, USA). The NICOMP 380 particle sizer was calibrated against latex beads of known diameter distributions. The mode was set for testing the size of vesicles. Three distribution analyses were obtained: intensity-weighted Gaussian distribution analysis, volume-weighted Gaussian distribution analysis and number-weighted Gaussian distribution analysis. The number-weighted Gaussian distribution analysis was used to obtain the diameter of vesicles.

2.2.5 Water permeability (P_{os}) determination

Water permeability (P_{os}) was determined from the kinetics of vesicle shrinkage measured by a stopped-flow spectrofluorimetry (DX.l7MV, Applied Photophysics, Leatherhead, UK) (Figure 2-1). The dead time, which is the time between the end of mixing the two solutions and the beginning of observation of the reaction, was between 1-2 ms. Light scattering (90 °) or fluorescence was recorded from the mixing chamber.

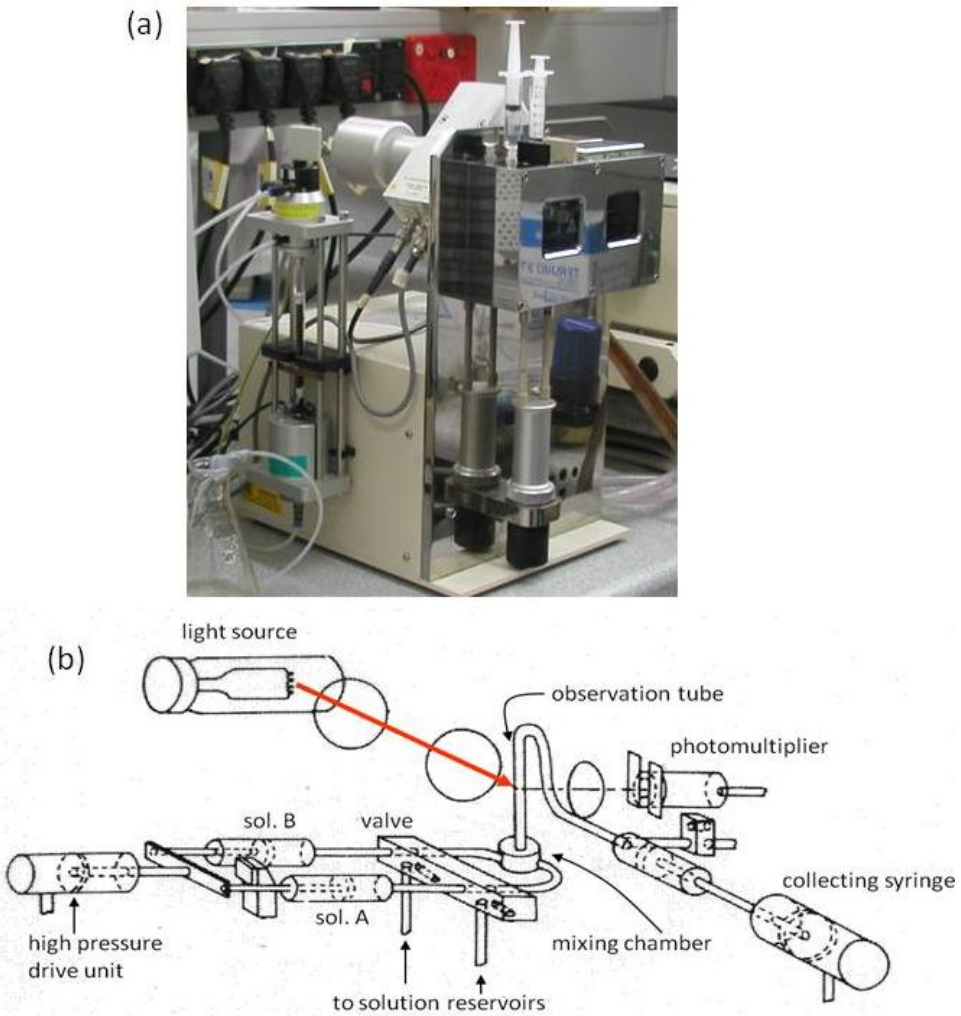

Figure 2-1. Stopped-flow spectrometer used to measure water permeability and CO_2 permeability. (a), Stopped-flow apparatus. (b), Schematic diagram of the Stopped-flow. The high pressure unit is filled with nitrogen gas.

According to Lowry protein test, purified plasma membrane vesicles (UIII) were diluted to 60-200 μg/ml of protein, and suspended in base solution (50 mM Mannitol, 5 mM EGTA, 50 mM HEPES-KOH, pH 7.6) were injected against a hyperosmotic solution (0.45 M extra Mannitol added to base solution) to create an inwardly directed 225 mosmol mannitol gradient after mixing 1:1.

The mixing chamber was surrounded by a water jacket that was connected to a water bath. The water bath regulated temperature between 13.5 ℃-22 ℃ as recorded in the mixing chamber.

The activation energy (E_a) of vesicles shrinking was calculated using the *Arrhenius* equation (Equation 2-1):

$$Ea = T * R * (Ln(A) - Ln(K_T)) \qquad \text{Equation 2-1}$$

where:

E_a is the activation energy (KJ/mol);

K_T is the reaction rate constant that depends on temperature;

A is a constant;

R is the universal gas constant (8.314 J mol^{-1} K^{-1});

T is the temperature (Kelvin).

The time course of vesicle shrinking was followed as an increase in light scattering at 550 nm excitation wavelength. The photomultiplier voltage was normally set to 500 V, with voltage

sensitivity of +/-0.1 V. Data were collected (7.5 kHz) over a time interval of 2.0 ms to 500 ms (the first 2 ms is the dead time of the machine). Shrinkage kinetics were measured on two injections at each temperature, and the average of the two was obtained. A single phase exponential function was fitted to the data using minimised least squares using ProData Viewer software provided by Applied Photophysics (Leatherhead, UK), and the rate constant (K_{os}) used to calculate P_{os}. The osmotic water permeability was calculated according to the following equation (van Heeswijk and van Os, 1986) (Equation 2-2):

$$P_{os} = \frac{V}{S} * \frac{K_{os}}{\bar{V}_w * C_o} \qquad \text{Equation 2-2}$$

Where,

P_{os} is the membrane water permeability coefficient (m/s);

V/S is the volume to surface area ratio;

K_{os} is the rate constant of the exponential kinetics of increase in scattering light;

$\bar{V}_w$ is the partial molar volume of water (given as 18 ml/mol);

C_o is the external osmolarity after mixing.

2.2.6 CO_2 uptake experiments

The kinetics of acidification in vesicles in response to CO_2 transport were performed on the same stopped-flow spectrometer as described above. Vesicles were loaded with carbonic anhydrase (CA) from Bovine at various concentrations in different experiments, and the fluorescent pH-sensitive dye HPTS (8-Hydrozy-1, 2, 6-pyrenetrisulfonate) to a final concentration of 0.15 mM. The loading of CA and HPTS was achieved by incubating

vesicles in hypoosmotic base solution (50 mM HEPES-KOH pH 7.5) containing CA and HPTS on ice for 2 hours. Loaded vesicles were then incubated in a resealing solution (300 mM Mannitol, 50 mM HEPES-KOH, pH 7.5) on ice for 20 min. Then vesicles were quickly mixed with 5 mM quencher (p-Xylene-bis-pyridinium bromide, DPX) (Daleke et al., 1990) which quenches the fluorescence outside the vesicles (Figure 2-2).

The vesicles were then injected in the stopped-flow against a CO_2 saturated resealing solution containing the same concentration of quencher. CO_2 was bubbled through resealing solution for more than 1 hour to achieve saturation. Saturation was indicated when pH reached 6.2. Kinetics of acidification were measured with an excitation wavelength of 460 nm and emission above 515 nm (OG515 long pass filter, Schott, supplied by Applied Photophysics, Leatherhead, UK). The photomultiplier voltage was normally set to 600 V, and voltage sensitivity for data acquisition of +/- 0.1 V. Data were collected (10 kHz) over a time interval from 2.0 ms to 200 ms. The fast kinetics of the decrease in fluorescence was fitted to a single exponential to obtain a rate constant K_{CO2}. $P\mathrm{co}_2$ was calculated based on the equation as follows (Fang et al., 2002) (Equation 2-3):

$$P_{CO_2} = \frac{Kco2 * V * 10^{(pH_f - pK_a)}}{S} \qquad \text{Equation 2-3}$$

Where,

P_{co_2} is the membrane CO_2 permeability coefficient (m/s);

V is vesicle volume and S is vesicle surface area;

pH_f is the final intracellular pH;

pK_a for HCO_3^- is 6.1;

K_{co_2} is the rate constant of the exponential kinetics of decrease in fluorescence.

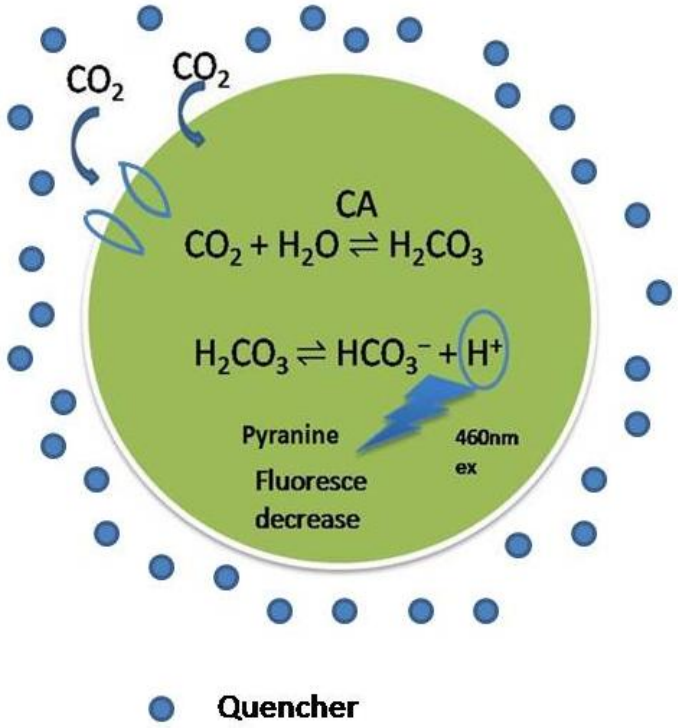

Figure 2-2 Measurement of CO_2 permeability: this cartoon indicates the principle of the experiments. With the entrance of CO_2 into the vesicles, the pH inside the vesicles will decrease due to the reaction of CO_2 and water, the change of the pH can be indicated by HPTS as it is a pH sensitive dye. The quencher outside the vesicles is to quench the fluorescence outside.

2.2.7 Final intracellular pH calculation

The fluorescence of HPTS was titrated at different pH (from pH 4.0 to pH 12.0) at two different excitation wavelengths, 400 nm and 460 nm, respectively, using the stopped-flow spectrometer. The fluorescence ratios of 400 nm/460 nm at different pH were calculated and plotted against pH to make a standard ratio-pH curve. Therefore, for each measurement, the fluorescence intensities excited by each of 460 nm and 400 nm were measured, and the final pH was calculated from the standard ratio-pH curve.

2.2.8 Inhibitors

For the vesicle shrinking experiment, vesicles (UIII) in base solution were mixed with 12 μM silver sulfadiazine (Ag-sul), which was dissolved in 0.5% dimethyl sulfoxide (DMSO) and injected against the hyperosmotic solution containing the same inhibitor concentration. Ag-sul can inhibit water flow through aquaporins (Niemietz and Tyerman, 2002). All solutions were made up fresh daily.

For the inhibition of CO_2 uptake, vesicles were loaded with CA and HPTS in hypoosmotic base solution, then, vesicles were mixed with resealing solution. After that, vesicles were mixed with inhibitor, incubated for 10 min, and then quickly mixed with 5 mM quencher to quench the fluorescence outside the vesicles, injected against CO_2 saturated resealing solution containing the same concentration of inhibitor and quencher.

Ag-sul, DIDS and the CA inhibitor, 50 μM acetazolamide (AZ) were dissolved in 10 mM DMSO. A final concentration of 100 μM for DIDS was used; DIDS was dissolved in 75 % ethanol, which (5 μl 75% ethanol) had no significant effect on the observed shrinking and acidification rate. The CA inhibitor AZ is membrane permeable (Hempleman et al., 2000).

2.2.9 *Arabidopsis* vesicles

Arabidopsis plants were grown in growth chamber with 21 ℃, 8 hours day light and 50% humidity. The leaves were harvested after 8 weeks and vesicles were isolated following a similar protocol which was described in (Alexandersson et al., 2004). The protocol is similar

to that for pea leaf vesicle preparation, and only differs in certain solutions. Using the same techniques for measuring the P_{os} and P_{CO2} for pea leaf vesicles, the *Arabidopsis* leaf plasma membrane vesicles were also tested.

2.3 Results

2.3.1 Water permeability (P_{os}) determination

Subjecting pea leaf UIII vesicles to a 225 mOsmol osmotic gradient, resulted in water flow out of the vesicles and hence, vesicle shrinking (Figure 2-3a). The traces were fitted with single exponential curves to obtain rate constants for vesicle shrinking. After the initial water efflux, a steady final value of light-scattering was observed. At 20 ℃, the rate constant for UIII vesicles was 222 s^{-1} (SEM 14 s^{-1}, n = 13 separate pea leaf vesicle preparations with at least 3 replicate injections). In the presence of the inhibitor silver sulfadiazine, the rate of shrinking decreased over 17-fold to 12.8 s^{-1} (SEM 2.1 s^{-1}, n = 7 vesicle preparations) for pea leaf UIII vesicles (Figure 2-3a dashed line).

The activation energy for pea leaf vesicle shrinking was 10.8 KJ/mol. When vesicles were incubated with 12 μM silver sulfadiazine, the activation energy increased almost 5 times to 51.3 KJ/mol (Figure 2-3b). This value is similar to the activation energy of water diffusion through lipid bilayers (Marrink and Berendsen, 1994). The average P_{os} value for pea plasma membrane (UIII) was 1478 μm s^{-1} (SEM 127 μm s^{-1}, n = 10 vesicle preparations). However, after inhibition, the P_{os} value was 92 μm s^{-1} (SEM 19 μm s^{-1}, n = 6 vesicle preparations).

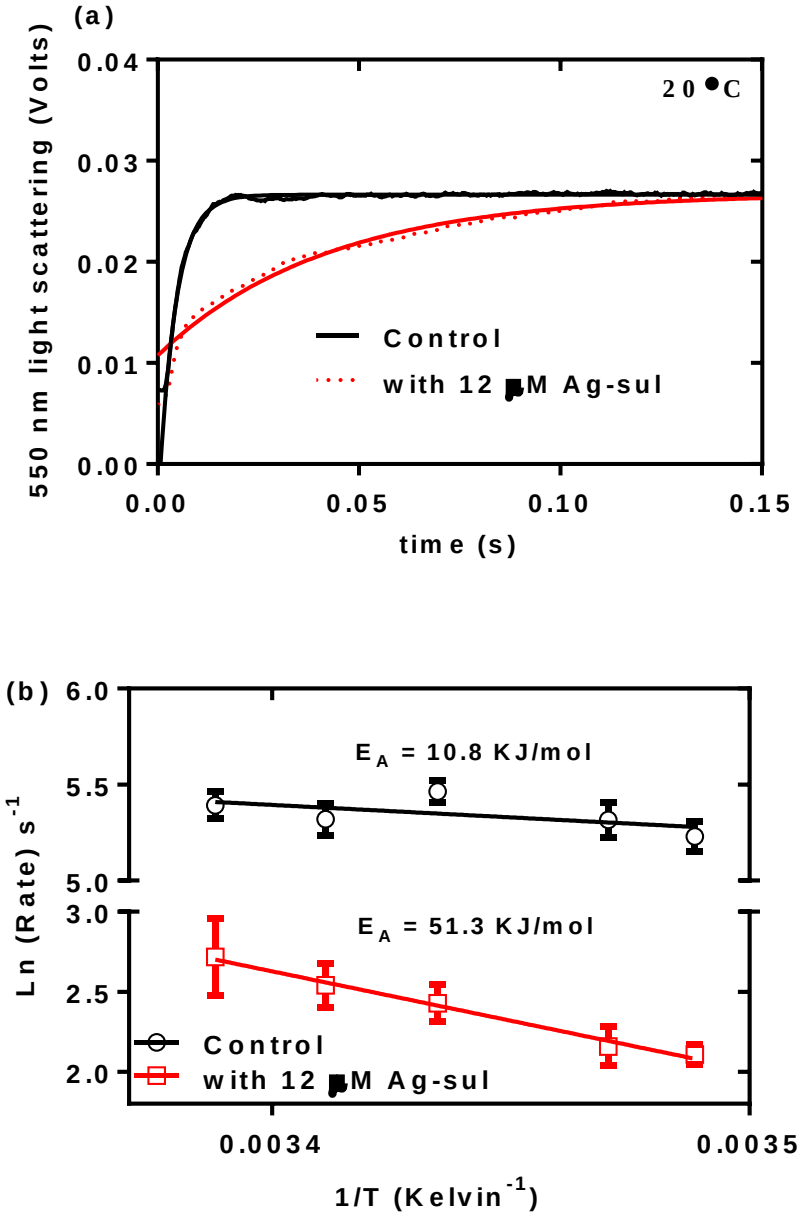

Figure 2-3. Time course of 550-nm light scattering and activation energy for pea leaf vesicles with and without Ag-sul. (a) Black continuous line: vesicles (UIII) subjected to an osmotic gradient of 225 mOsmol. Red dashed line: effect of Ag-sul (12 µM) inhibition on the shrinking rate of pea leaf vesicles. The temperature was 20 ℃. The curves were fitted with a single exponential. (b) Temperature dependence of vesicles shrinking with (□) and without (O) Ag-sul. Shrinking rates were obtained for temperatures ranging from 13.5 ℃ to 22 ℃ for vesicles (UIII). Activation energy was calculated using *Arrhenius* equation (n = 3 independent vesicle preparations).

2.3.2 CO_2 Permeability

(1) pH titration of HPTS and pH determination inside vesicles

HPTS is a hydrophilic fluorescent dye that displays pH sensitive fluorescence. The fluorescence intensity of the hydrophilic fluorescent dye is strongly dependent on the state of the 8-hydroxy group (pK_a = 7.22), which depends on the free hydrogen ion concentration of the solution. An increase in pH in the medium leads to a significant red shift in the fluorescence excitation maximum from 400 nm (pH = 6) to 460 nm (pH = 9). However, the emission maximum which is above 515 nm remains unchanged (Kano and Fendler, 1978; Clement and Gould, 1981; Damiano et al., 1984) (Figure 2-4a). Due to this characteristic, previous research has shown that HPTS is an extremely sensitive and convenient probe for measuring pH changes in unilamellar phospholipid vesicles (Clement and Gould, 1981). The fluorescence with excitation at 400 nm (F_{400}) is divided by the fluorescence with excitation at 460 nm (F_{460}) to provide a ratio that can report the pH value. For pH between 6~7, the F_{400}/F_{460} ratio can be fit with a single exponential curve (Figure 2-4b).

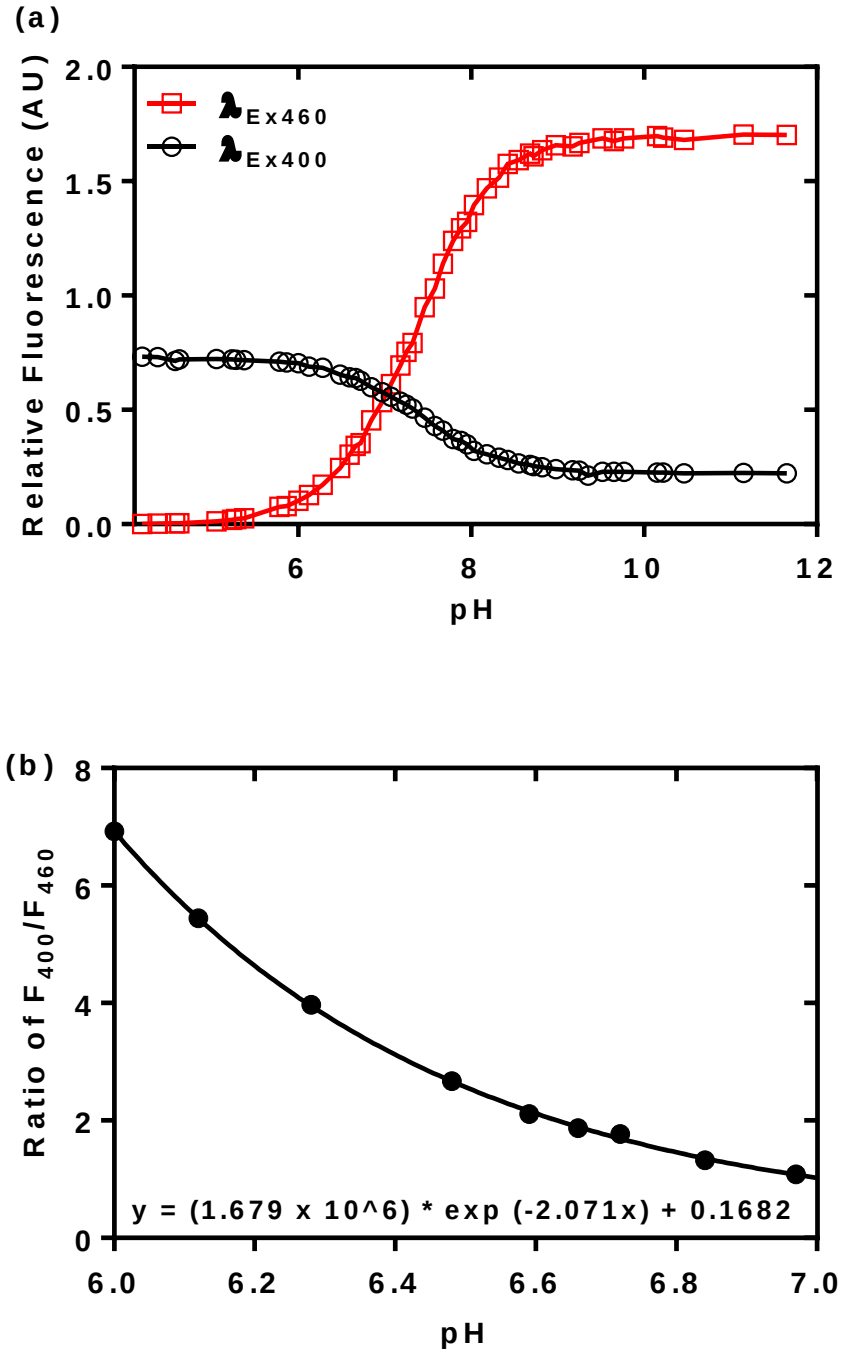

Figure 2-4. The pH-dependent fluorescent dye. (a) The pH dependence of HPTS relative fluorescence intensity at 20 ℃. Excitation wavelength was 460 nm (o) or 400 nm (□). HPTS concentration: 3 μM; buffer: 20 mM HEPES-NaOH. (b) Ratio of F_{400}/F_{460} nm emission over the range pH 6-7 was fitted with an exponential curve (•).

(2) Vesicle acidification in response to CO_2 transport

Uptake of CO_2 resulted in an intravesicular acidification and consequently a decrease in fluorescence. The internal solution of pea plasma membrane vesicles containing 6 mg/ml CA acidified following exposure to CO_2 saturated external solution at 13.5 ℃ (Figure 2-5a). The rate constant for this process was 522.7 s^{-1}. The amplitude represents the span of the fitted acidification curve extrapolated back to time zero. Neither Ag-sul nor DIDS appeared to inhibit CO_2 transport (Figure 2-5c, d). For both inhibitors, the derived rate constants were slightly greater than for the control (516.6 s^{-1}, 502.1 s^{-1} compared to 483 s^{-1}). By contrast, when the CA inhibitor acetazolamide was added to the system, there was a large decrease in the rate constant to 75.54 s^{-1} (Figure 2-5b). For control, Ag-sul experiment and DIDS experiment, the amplitudes were similar as the actual amplitude obtained from the AZ experiment (0.032, 0.032, 0.039 compared to 0.030).

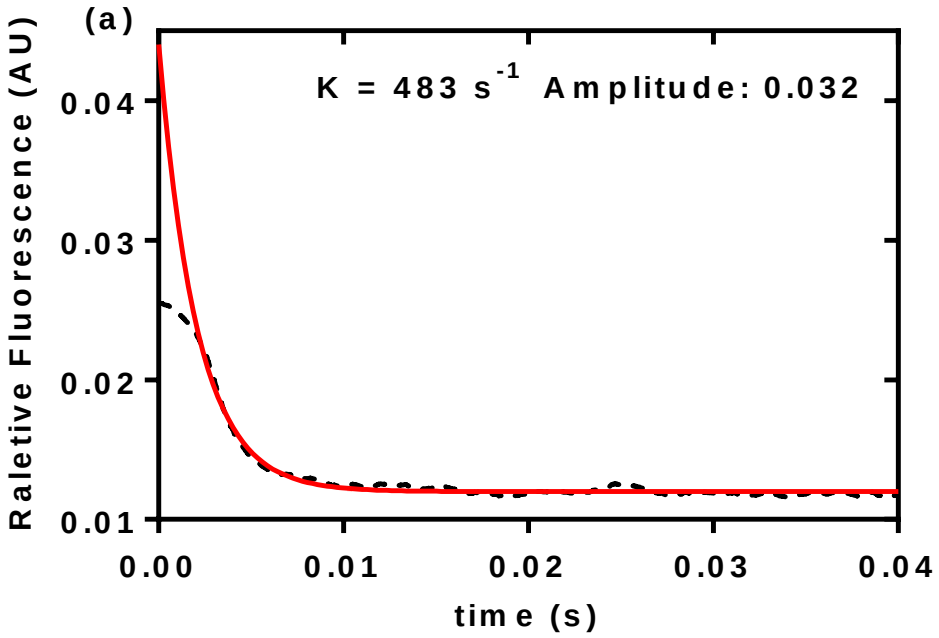
(a)
K = 483 s-1 Amplitude: 0.032
Raletive Fluorescence (AU)
0.04
0.03
0.02
0.01
0.00
0.01
0.02
0.03
0.04
time (s)

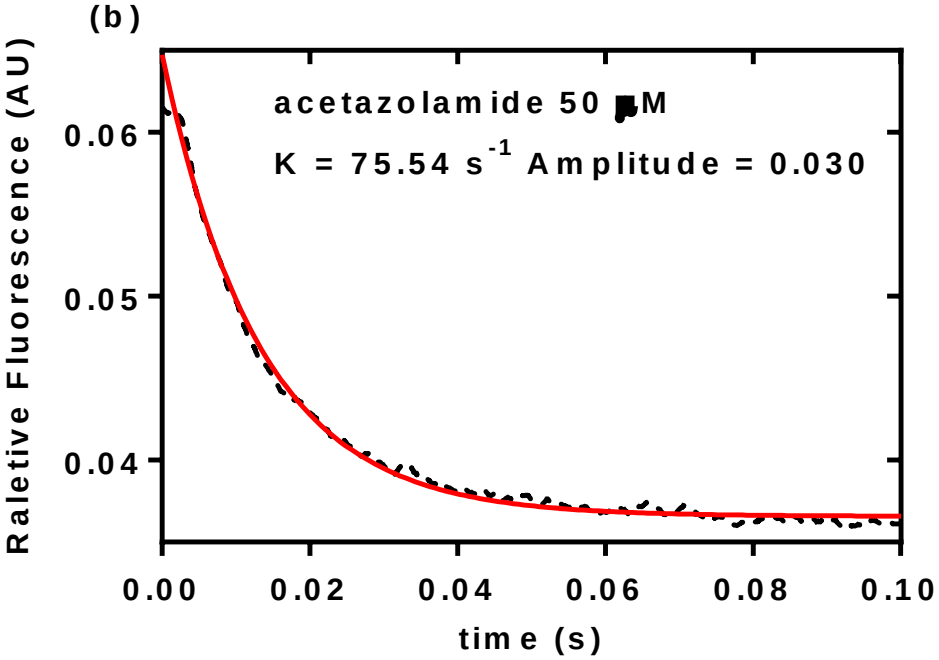
(b)
acetazolamide 50 μM
K = 75.54 s-1 Amplitude = 0.030
Raletive Fluorescence (AU)
0.06
0.05
0.04
0.00
0.02
0.04
0.06
0.08
0.10
time (s)

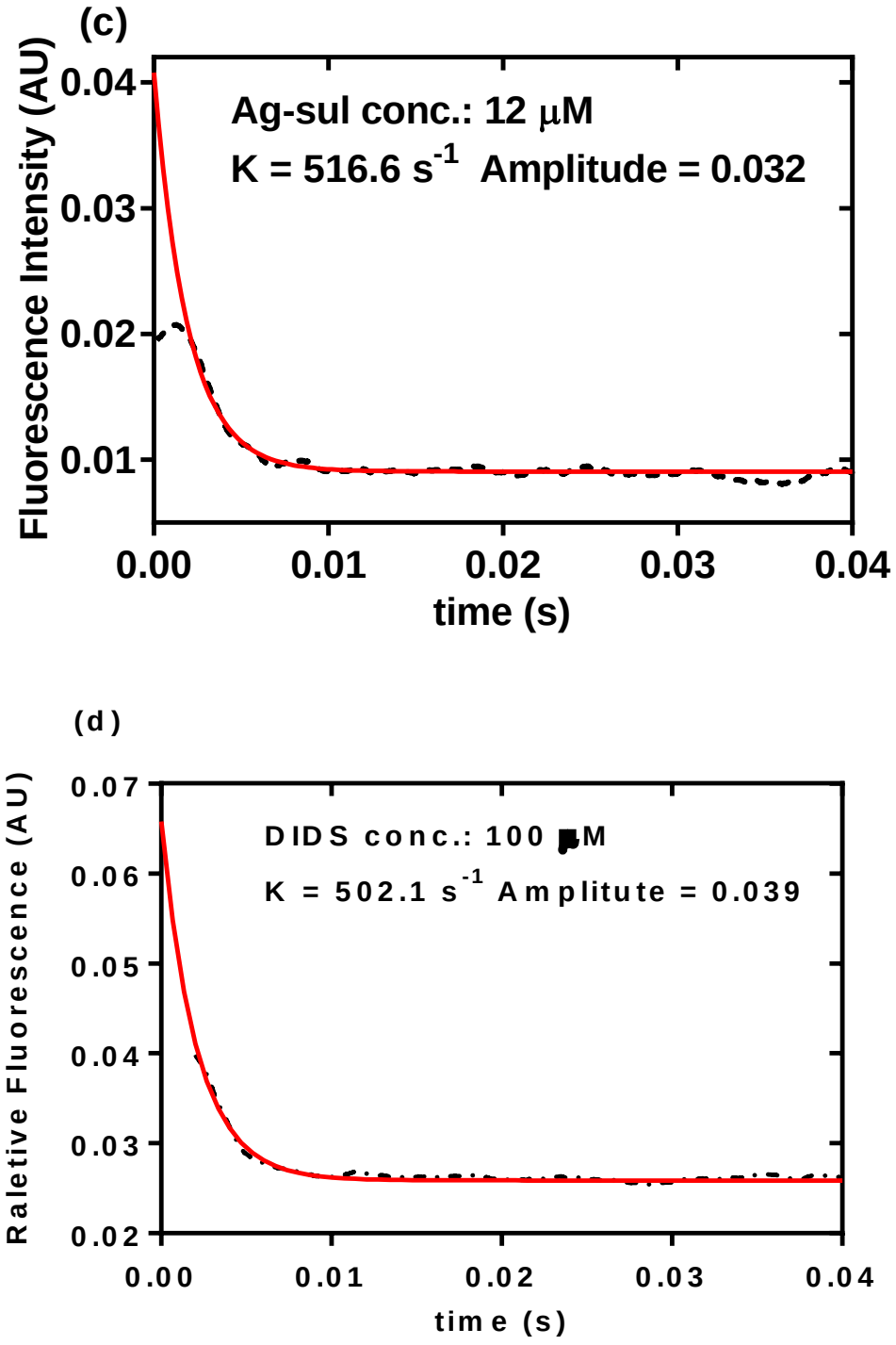

Figure 2-5. Time course of acidification in vesicles in response to CO_2 transport with and without inhibitors at 13.5 ℃. (a) Time course of acidification in plasma membrane vesicles in response to CO_2 transport. The data were fitted with exponential curves to obtain a rate constant. (b) With 50 μM acetazolamide. (c) With 12 μM Silver-sulfadiazine. (d) With 100 μM DIDS.

To test whether measured CO_2 permeability was affected by the amount of CA, vesicles were incubated with different concentrations of CA (final concentration inside the vesicles: 1.5, 4.5, 6, and 7.5 mg/ml). Thus, the acidification rates at different temperatures were compared (Figure 2-6a). The measured activation energy decreased as the CA concentration increased. Significant differences were observed between activation energies measured in the presence of 4.5 mg/ml CA and 6 mg/ml CA. However, with the presence of 6 mg/ml CA and 7.5 mg/ml CA, the activation energies did not vary significantly (Figure 2-6b). As CA concentration increases, the rate of CO_2 hydration increases until it is unlikely to limit the rate. For this reason, subsequent measurements were performed using CA concentrations greater than 6 mg/ml.

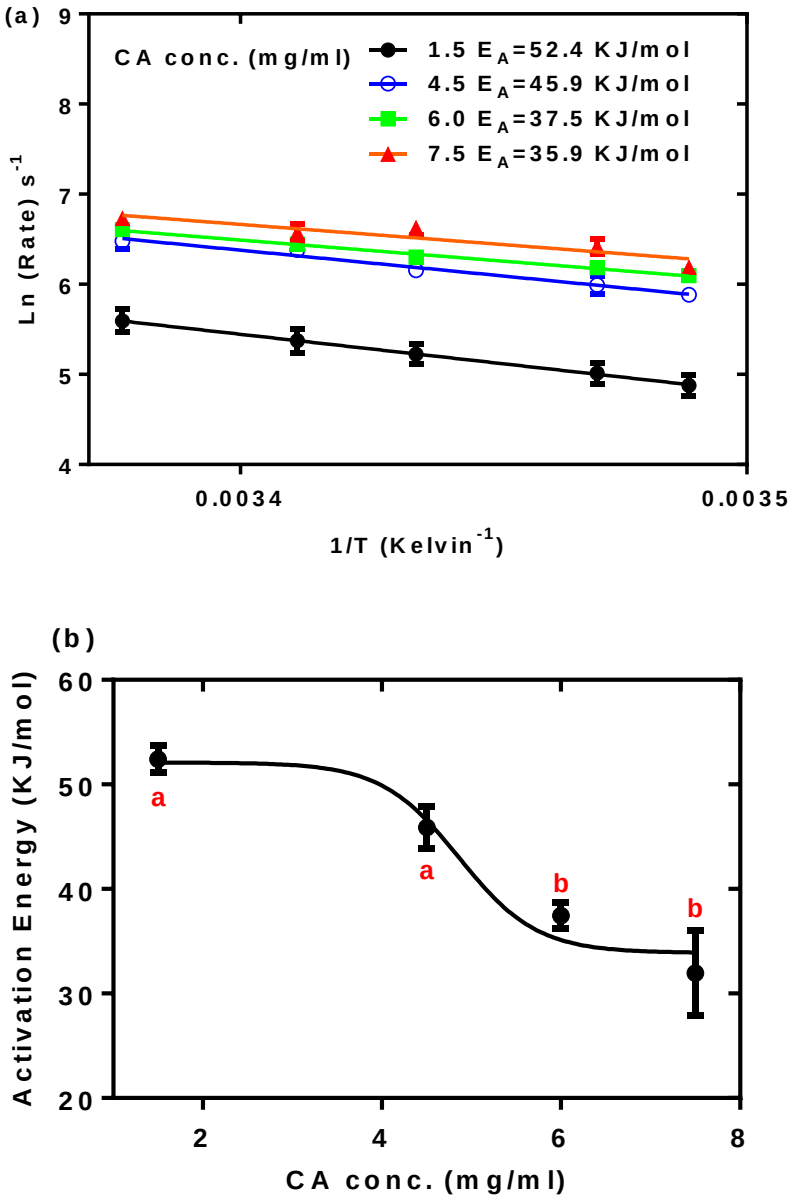

Figure 2-6. (a) CA and temperature dependence of vesicle acidification in response to CO_2 transport. Acidification rates were obtained for temperatures ranging from 13.5 ℃ to 23 ℃ with vesicles (UIII). Different CA concentrations were tested (● 1.5 mg/ml; ○ 4.5 mg/ml; ■ 6 mg/ml; ▲ 7.5 mg/ml). Activation energy was calculated using *Arrhenius* equation (● 52.411 KJ/mol; ○ 45.893 KJ/mol; ■ 37.463 KJ/mol; ▲ 35.900 KJ/mol). (b) The relationship between activation energy and CA concentration. Both error bars come from 4 replica of vesicles preparations. Different letters indicate significant differences (P = 0.05).

The temperature dependence of vesicle acidification in response to CO_2 transport was measured in the presence of various inhibitors (Figure 2-7). The measured activation energy in the presence of 12 μM Ag-sul is 20.4 KJ/mol, and in the presence of 100 μM DIDS is 27.7 KJ/mol. However, these values were slightly lower than the activation energy measured without aquaporin inhibitor (32.3 KJ/mol).

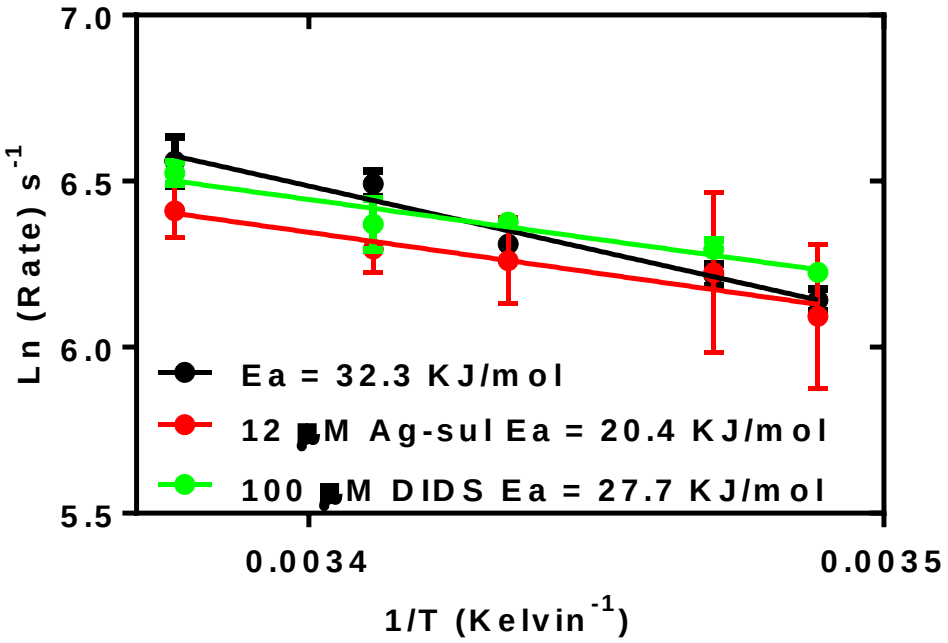

Figure 2-7. Temperature dependence of vesicle acidification in response to CO_2 transport with different kinds of treatment. Control (●); with 12 μM Ag-sul (●) and 100 μM DIDS (●). Acidification rates were obtained for temperatures ranging from 13.5 ℃ to 23 ℃ for vesicles (UIII). Activation energies were calculated using *Arrhenius* equation (● 32.3 KJ/mol; ● 20.4 KJ/mol; ● 27.7 KJ/mol). N = 3 independent vesicle preparations.

(3) Temperature and inhibition effect on CA

CA activity was temperature dependent at pH 7.5 (Figure 2-8). This could affect the measured CO_2 transport as CA catalysis may become the rate limiting step. 12 µM Ag-sul dissolved in 0.5% DMSO did not affect CA activity.

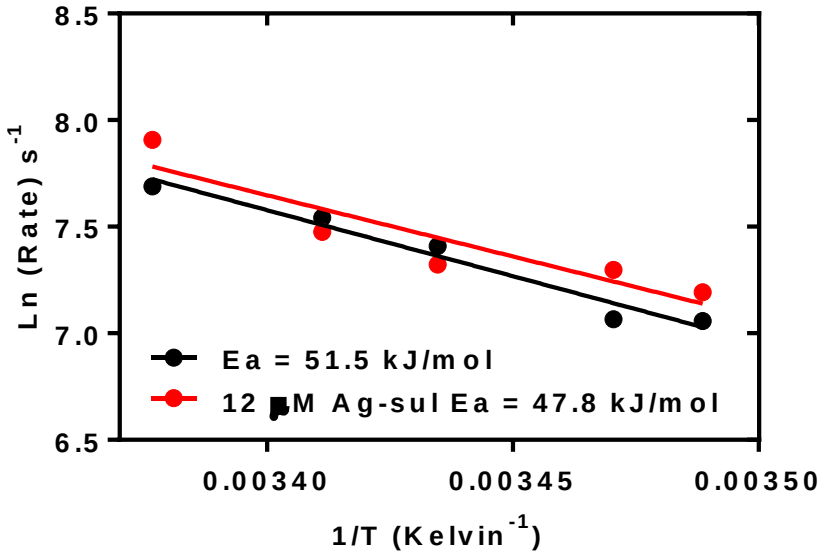

Figure 2-8. Temperature and 12 µM Ag-sul effect on CA. Solution (50 mM HEPES-NaOH) containing CA (6 mg/ml) and 0.15 mM dye injected against CO_2 saturated solution (50 mM HEPES-NaOH) with (●) and without (●) the presence of Ag-sul at different temperatures (13.5 to 23 ℃). Activation energies were calculated using *Arrhenius* equation (● 51.5 KJ/mol; ● 47.8 KJ/mol).

(4) Quencher efficiency test

To ensure that the fluorescence measured represented the fluorescence inside the vesicles, the quencher efficiency was tested. Without vesicles, with the dye concentration of 0.15 mM and pH 7.5, there is an extremely high fluorescence signal (Figure 2-9a, black continuous line). However, the addition of quencher (5 mM) abolished the signal (Figure 2-9a, red dashed line).

The same result was observed in the presence of 6 mg/ml CA (Figure 2-9b). The rate constant for CA catalysis was 1919 s^{-1} (Figure 2-9b continuous line). However, with 5 mM quencher in the solution, there is no fluorescence signal (Figure 2-9b red dashed line).

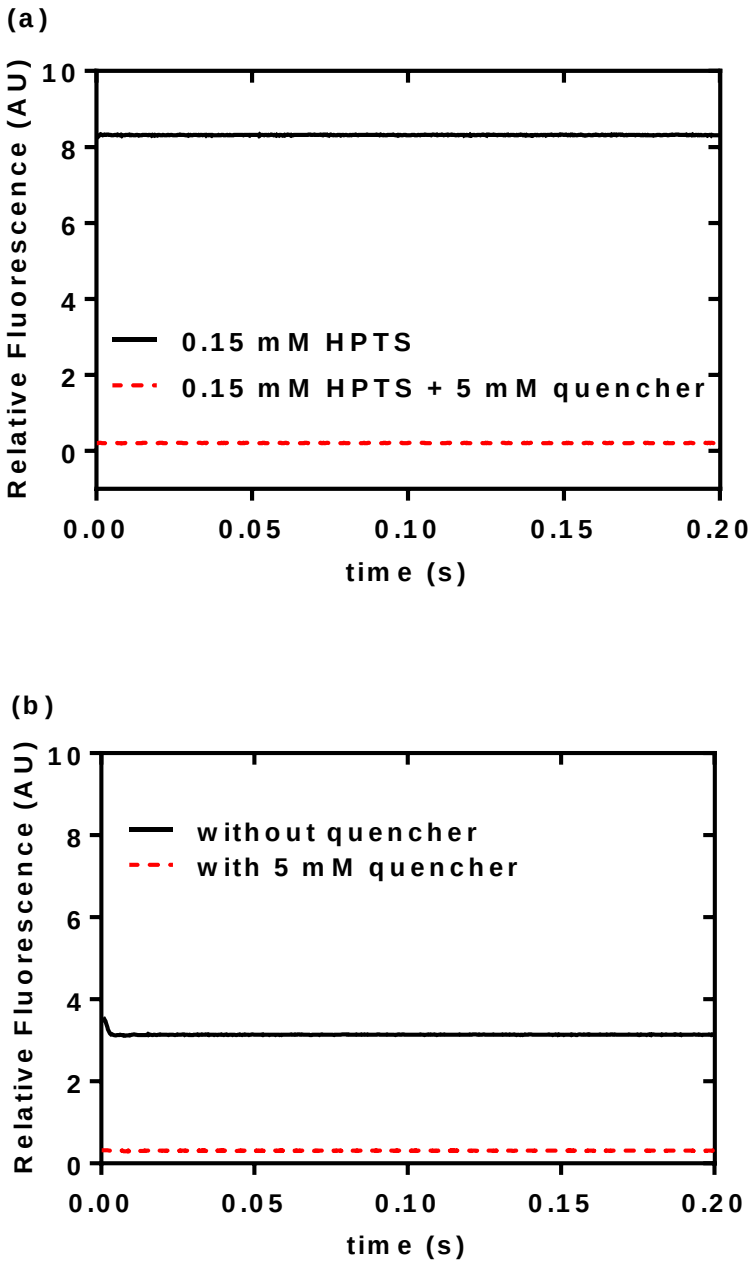

Figure 2-9. Quencher efficiency test. (a) 0.15 mM HPTS alone (black line), and injected against 10 mM quencher (dash line). (b) In the presence of CA.

(5) Amplitude

As described in Figure 2-5, after each injection, a single exponential curve was fit and amplitudes were collected. The responses to temperature of amplitudes obtained with and without 50 μM AZ at different temperatures were obtained (Figure 2-10). When CA was inhibited by AZ, the amplitude was independent of temperature (13.5 ℃: 0.026; 15 ℃: 0.027; 18 ℃: 0.028; 20 ℃: 0.028; 23 ℃: 0.028). At 13.5 ℃, there was no effect of AZ on the amplitude (without AZ: 0.025, with AZ 0.026). However, as temperature increased, the amplitude of the exponential curve without AZ treatment decreased (15 ℃: 0.024; 18 ℃: 0.022; 20 ℃: 0.022), being only half that of the AZ treated sample at 23 ℃ (0.013).

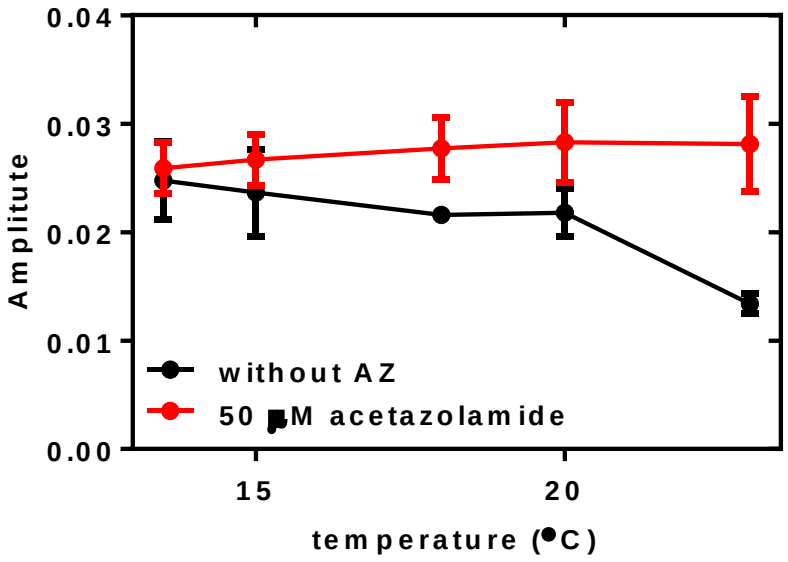

Figure 2-10 Temperature dependence of amplitude with / without the presence of 50 μM acetazolamide (●: with AZ; ●: without AZ) (n=3 vesicles prepations).

2.3.3 Stomatal conductance measurement

The stomatal conductances for peas without treatment (mean value: 345 $mmolm^{-2}s^{-1}$, 337 $mmolm^{-2}s^{-1}$, 300 $mmolm^{-2}s^{-1}$, 526 $mmolm^{-2}s^{-1}$, 434 $mmolm^{-2}s^{-1}$,) were significantly higher than the ones with treatments (mean value for 46 hours darkness treatment: 8 $mmolm^{-2}s^{-1}$; for 46 hours drought treatment: 18 $mmolm^{-2}s^{-1}$; for 3 hours darkness treatment: 183 $mmolm^{-2}s^{-1}$; for 2 hours treatment with 200 mM H_2O_2: 16 $mmolm^{-2}s^{-1}$) (Figure 2-11). The 200 mM H_2O_2 treatment was applied to roots through watering for two hours. Lower concentrations were also tried (2 mM, 5 mM and 100 mM) but there were no effects on the stomatal conductance. Spraying leaves with lower concentrations of H_2O_2 (2 mM or 5 mM) were tried with no obvious effect on stomatal conductance.

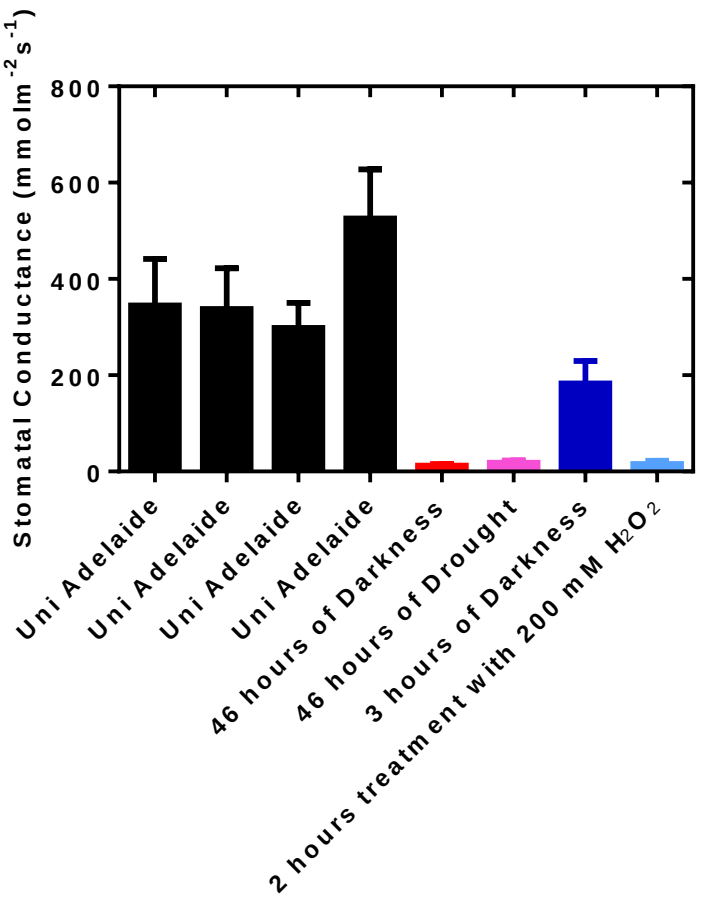

Figure 2-11. Stomatal conductances for peas grown in various conditions with and without treatments. The black bars are peas grown in University of Adelaide without any treatment. The coloured bars are with treatments (■: 46 hours of darkness; ■: 46 hours of drought; ■: 3 hours of darkness; ■: 2 hours treatment with 200 mM H_2O_2 during mid-day).

2.3.4 Water permeability of dark and drought treated peas

(1) Dark treatment

Vesicles isolated from plants that were put into darkness for 46 hours were tested for both water and CO_2 permeability. The testing condition was exactly the same with the vesicles

from the untreated pea plants. The results obtained in Figure 2-12a showed that the best fit for vesicle light scattering (shrinking) versus time was a double exponential rather than a single exponential. At 20 ℃, the rate constant for UIII vesicles were shown as two phases (described in the table below). In the presence of the Ag-sul, the fast phase of shrinking rate decreased over 5-fold to 37.12 s^{-1} (experiments of at least 3 replicate injections). CO_2 uptake kinetics are shown in Figure 2-12b.

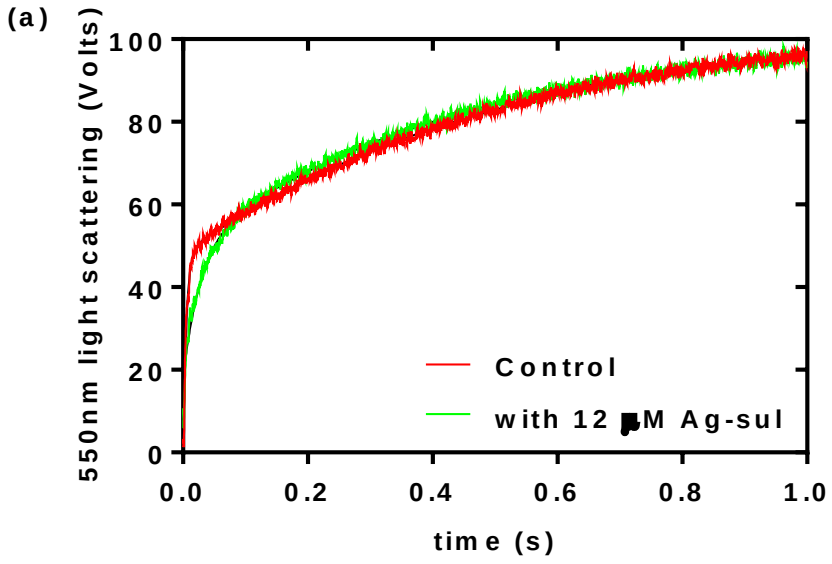

	Rate Constant (s^{-1})	Rate Constant with Ag-Sul (s^{-1})
Rate constant fast phase	181.6	37.12
Rate constant slow phase	1.989	1.912

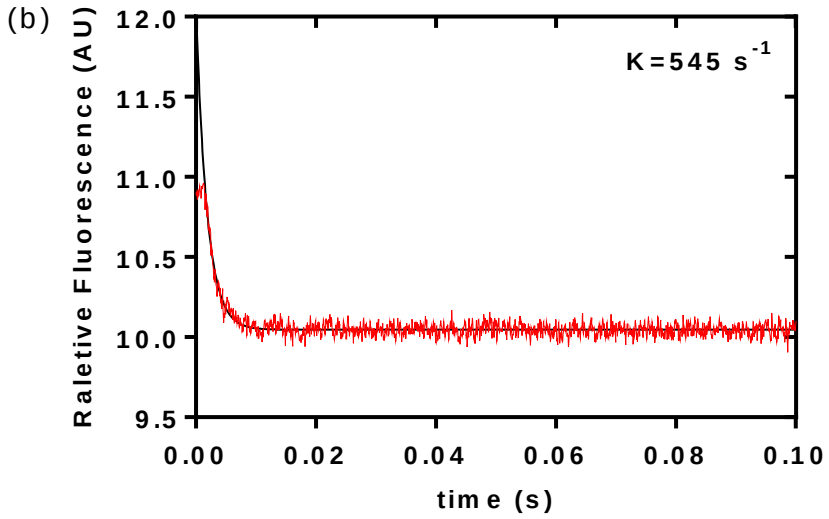

Figure 2-12. (a) Time course of 550-nm light scattering and activation energy for pea leaf vesicles from 46 hours of darkness treatment with (green) and without inhibitor (red). The data was fitted with double exponential. (b) Time course of acidification in vesicles in response to CO_2 transport. The data was fitted with single exponential curves to obtain a mean rate constant.

(2) Drought treatment

Similar results were obtained from vesicles isolated from drought treated pea (Figure 2-13).

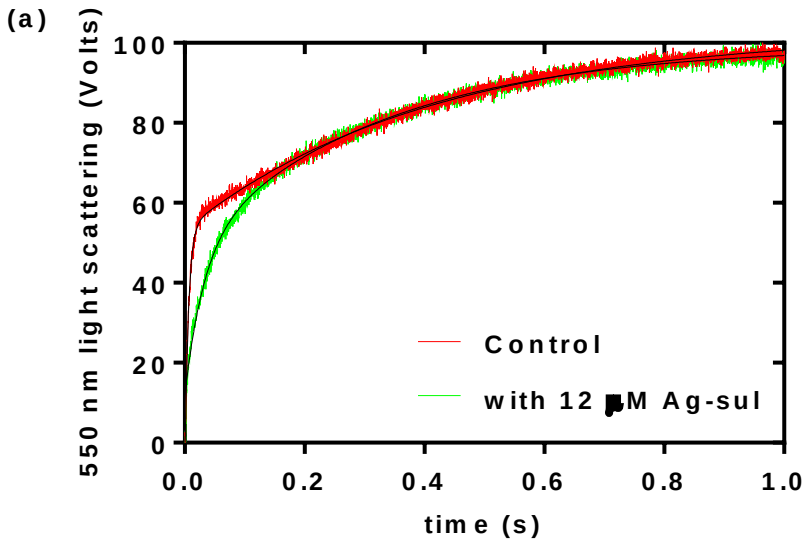

	Rate constant (s^{-1})	Rate constant with Ag-Sul (s^{-1})
Rate constant fast phase	169.9	31.33
Rate constant slow phase	2.428	3.064

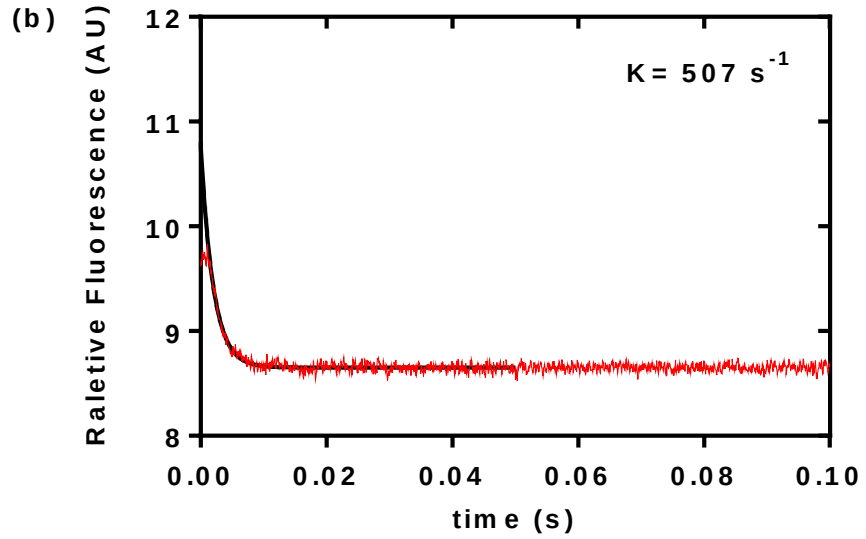

Figure 2-13. (a) Time course of 550-nm light scattering and activation energy for pea leaf vesicles from 46 hours of drought treatment with (green) and without (red) inhibitor. The data was fitted by double exponential. (b) Time course of acidification in vesicles in response to CO_2 transport. The data were fitted with single exponential curves to obtain a mean rate constant.

2.3.5 *Arabidopsis* vesicles

The water permeability of *Arabidopsis* vesicles tested was not as high as pea leaf vesicles. Interestingly, the curves for vesicles shrinking were better fit by a double exponential rather than a single exponential time course, which may indicate that the vesicles isolated from *Arabidopsis* do not have as high aquaporin activity compared to pea leaf vesicles. Figure 2-14a gives an example of the measured vesicle shrinking time course. The rate constant values are listed in the table below.

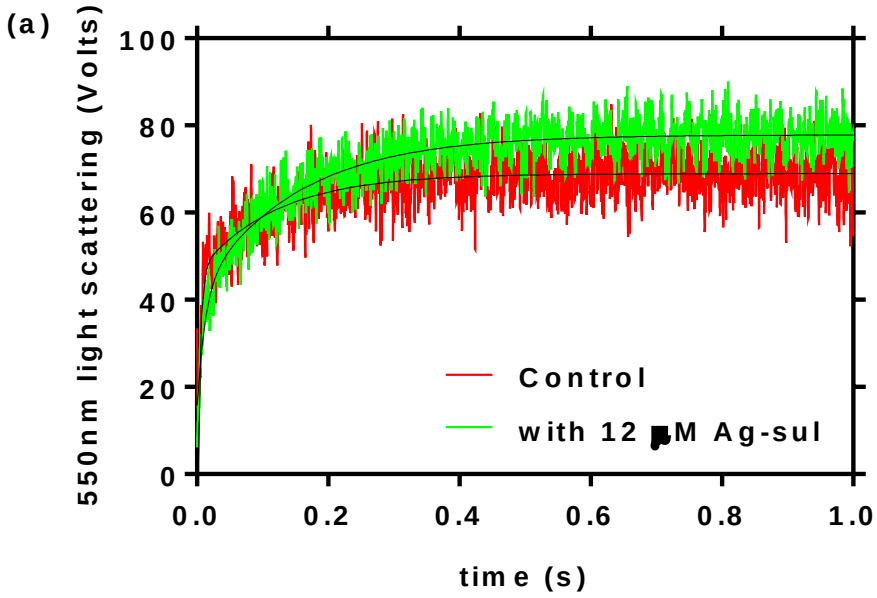

	Rate constant (s^{-1})	Rate constant with Ag-Sul (s^{-1})
Rate constant fast phase	257	83.6
Rate constant slow phase	8.43	6.68

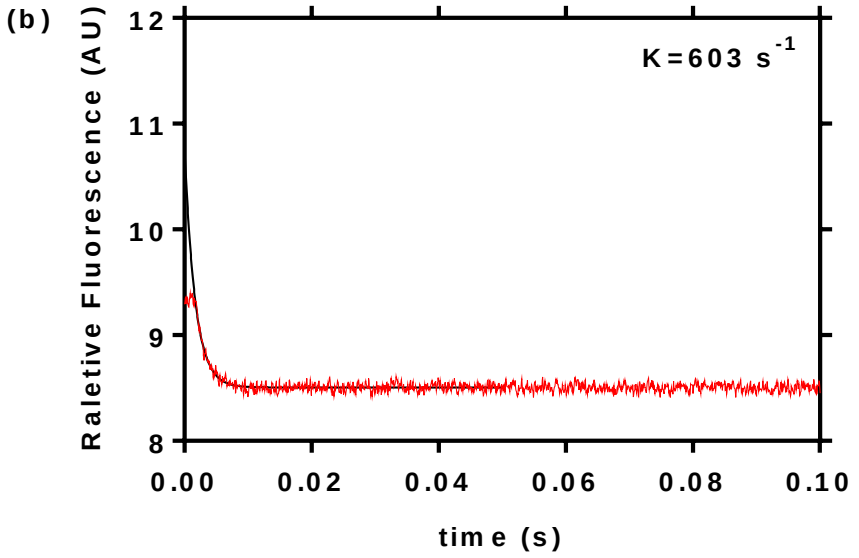

Figure 2-14. (a) Time course of 550-nm light scattering and activation energy for *Arabidopsis* leaf vesicles with (green) and without (red) inhibitor. The data was fitted by double exponential. (b) Time course of acidification in vesicles in response to CO_2 transport. The data were fitted with single exponential curves to obtain a mean rate constant.

2.3.6 The relationship between water permeability and CO_2 permeability

For each vesicle preparation, water and CO_2 permeabilities were calculated. The relationship between water and CO_2 permeability was compared between 19 replicates (Figure 2-15). Vesicles were isolated from pea plants grown under different conditions to promote variability in P_{os}. For example: different cities in Australia (Canberra: ▼, Adelaide:○), different weather conditions, different darkness treatment time (◆, ▲), 46 hours of drought treatment (□), or 2 hours of 200 mM H_2O_2 treatment (△). Meanwhile, *Arabidopsis* leaf vesicles were also plotted (■). Additionally, for most of the water transport experiments, the aquaporin inhibitor silver-sulfadiazine was tested (■).

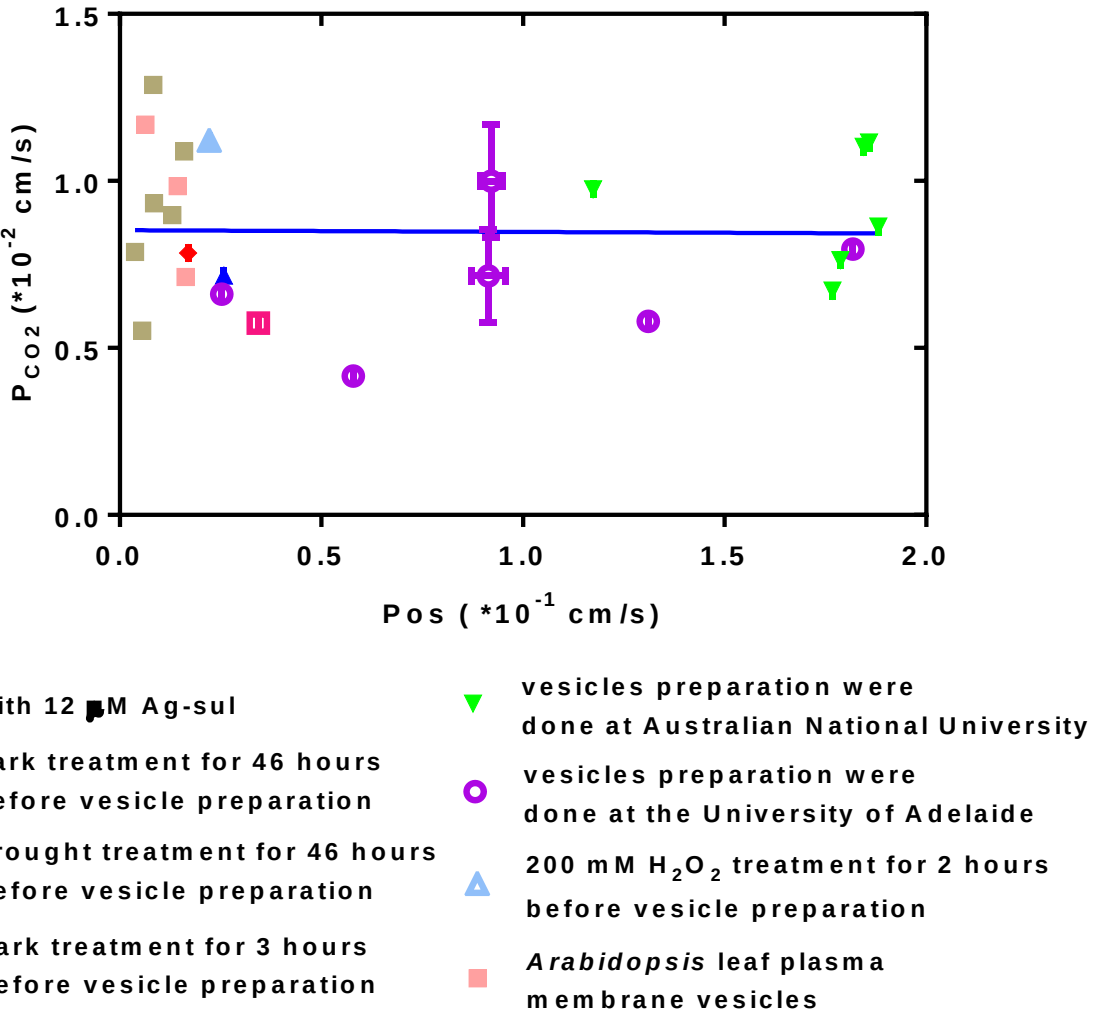

Figure 2-15. Relationship between water permeability and CO_2 permeability. Vesicle preparations were done at different places: Canberra (▼), Adelaide (○). Plants were treated with different conditions: darkness treatment (◆, ▲), 46 hours of drought treatment (□), or 2 hours of 200 mM H_2O_2 treatment (△). *Arabidopsis* leaf vesicles were also plotted (■). Additionally, 12 µM silver-sulfadiazine inhibition test (■).

2.4 Discussion

2.4.1 CO_2 pathway in plants and mesophyll conductance

In most C3-plant species, photosynthesis is rate limited by CO_2 availability (Morison et al., 2007). CO_2 has to overcome three resistances during the process of diffusion from the atmosphere to the site of carboxylation inside the chloroplast, as outlined previously. The reciprocal form of resistance, conductance, has generally been used in discussions (Evans et al., 1994; Evans et al., 2009). The mesophyll conductance can rate limit photosynthesis (Flexas et al., 2008), therefore, mesophyll conductance to CO_2 is an important photosynthetic trait that has been studied intensively in the past few decades. The mesophyll pathway comprises a series of "physical barriers" to CO_2 diffusion, including air, cell walls, lipid membranes and liquid cytoplasm and chloroplasts stroma (Terashima et al., 2011; Flexas et al., 2012). Membranes were shown to create significant resistance within mesophyll (Evans et al., 2009).

2.4.2 Do aquaporins facilitate CO_2 transport

Molecular evidence has accumulated that aquaporins can facilitate the diffusion of CO_2 and there is some evidence for the involvement of aquaporins in CO_2 diffusion across membranes (Nakhoul et al., 1998; Terashima and Ono, 2002; Katsuhara et al., 2003; Musa-Aziz et al., 2009; Otto et al., 2010; Heckwolf et al., 2011; Uehlein et al., 2012). Within plant membranes, Uehlein et al. (Uehlein et al., 2003) demonstrated that tobacco plasma membrane aquaporin NtAQP1 may facilitate CO_2 transport. The over-expression of NtAQP1 heightens

membrane permeability for both water and CO_2, and increases leaf growth. Heckwolf *et al.* showed that the *Arabidopsis thaliana* aquaporin AtPIP1;2 was probably a CO_2 transport facilitator (Heckwolf et al., 2011). They analyzed the effect of disruption to AtPIP1;2 by T-DNA insertion on CO_2 transport and photosynthesis using carbon isotope discrimination and CO_2 exchange during photosynthesis. Uehlein *et al.* (2012) studied the CO_2 flux into *Arabidopsis* mesophyll cells by using a scanning pH microelectrode and they suggested that cellular CO_2 transport was not limited by unstirred layers but rather depended on the expression of AtPIP1;2.

However, I found that there was no significant correlation between water permeability and CO_2 permeability indicating that aquaporins do not directly affect CO_2 diffusion. If changes in aquaporin density or activity as a result of different growing conditions affected water permeability, one would expect that parallel changes would be observed in CO_2 permeability. However, this argument assumes that both water and CO_2 permeate via the same aquaporin proteins. One cannot exclude the possibility that there is a particular class of aquaporin that functions to transport CO_2 which may make up a small proportion of the total population of aquaporins in the membrane. The treatments imposed here to alter the water permeability may be only affecting a broader class of aquaporins that only transport water, therefore it may not be the case that a correlation would be observed between the permeabilities to CO_2 and water. Another possibility is that the true membrane permeability to CO_2 was not measured and may reflect rate limitation caused by carbonic anhydrase or unstirred layers. These are discussed further below.

2.4.3 High water permeability indicating high aquaporins activity

As shown in Figure 2-2a the vesicles shrinking process was normally comprised of a single fast exponential. The fast phase was followed by a steady constant light scattering indicating that the vesicles were osmotically competent and that the solutes used did not permeate rapidly across the plasma membrane.

Maurel et al (1997) measured the water permeability of tobacco tonoplast membrane vesicles (690 μm s^{-1}) (Maurel et al., 1997). The water permeability for pea plasma membrane vesicles was two-fold higher (1478 μm s^{-1}). In the presence of the aquaporin inhibitor, silver sulfadiazine, the average rate for water transport obtained from pea plasma membrane vesicles decreased by over 17-fold. As it is also shown in Figure 2-2, E_a increased 4 times in the presence of silver sulfadiazine towards values expected for permeation through a lipid bilayer. This change in E_a with inhibition of water transport has previously been used to indicate involvement of aquaporins (Niemietz and Tyerman, 2002) since if the water pore was blocked the low E_a associated with water diffusion in a water filled pore would vanish. The combination of very high water permeability, low E_a, and strong inhibition with silver sulfadiazine, indicate very high activity of aquaporins in pea leaf plasma membrane vesicles.

2.4.4 The acidification rate inside vesicles

Because of the dead time of the stopped-flow spectrometer device, and the very fast rate of acidification, the reaction for the first 2 ms could not be caught. Only a small percentage of the acidification process could be monitored. Therefore, the single exponential fit was

extrapolated (Figure 2-4). In the presence of acetazolamide, a CA inhibitor, CO_2 would hydrate much slower than it is transported through the membrane (Gutknecht et al., 1977), that is, the reaction of CO_2 with water is the rate limiting step. Consequently, the change in the intravesicular acidification rate observed cannot be interpreted in terms of CO_2 diffusion, rather, it is the CO_2 hydrolysis reaction without CA catalysis. Interestingly, the amplitudes obtained from the reactions with and without acetazolamide were very similar (Figure 2-4 a~d). The fit for the reaction in the presence of acetazolamide (Figure 2-4 b) covered more than 98% of the acidification process and therefore can reflect the real reaction inside vesicles. Hence, having the similar amplitude indicates that the extrapolated single exponential fit was accurate and can represent the real CO_2 transport rate. It suggests that the measured kinetics are probably not missing a faster phase of acidification in the vesicle.

2.4.5 Carbonic anhydrase

Most of the previous research on CO_2 transport has not reported any effect of CA concentration or activity at different temperatures (Uehlein et al., 2008; Heckwolf et al., 2011; Uehlein et al., 2012). Prasad *et al.* (1998) reported the effect of CA concentration differences on the measured CO_2 permeability, however, they did not mention the temperature effect on CA activity (Prasad et al., 1998). Here it was shown that the CA concentration and changing the reaction temperature can significantly affect the measured CO_2 permeability. As shown in Figure 2-5, with increasing CA concentration, the E_a for acidification decreases. Varying the amount of entrapped CA revealed no significant difference in the rate of acidification and E_a, provided the CA concentration was above 6 mg/ml. Therefore, this concentration was used in all subsequent CO_2 transport measurements. Meanwhile, temperature also affects CA activity

(Figure 2-7). At lower temperature (13.5 ℃), CA catalysis reaction can rate limit the measured CO_2 permeability, as the temperature increases, it is less likely to be the rate limiting step, but the converse is that the transport rate and diffusion of CO_2 will increase with temperature. Here the CO_2 permeability was taken at 20 ℃. The reason will be addressed again in 2.4.8.

2.4.6 Pure biophysical point of view

Meyer and Overton established a simple rule to predict membrane permeabilities 110 years ago (Missner and Pohl, 2009). Membrane permeability for certain molecules depends on the molecule's oil-water partition coefficient. This rule does not account for transport processes that are facilitated by membrane proteins. The identification of several membrane-embedded "gas" channels which transport biological active gases such as carbon dioxide (Uehlein et al., 2012) and ammonia (Khademi et al., 2004) have challenged the Meyer-Overton rule. Missner and Pohl have argued that these results are not convincing and that the Meyer-Overton rule is robust (Missner et al., 2008; Missner and Pohl, 2009). Furthermore, in most studies on CO_2 transport the existence of both extracellular and intracellular unstirred layers have been ignored. Rapidly permeating substances could be rate-limited by unstirred layers rather than the membrane lipid bilayer (Pohl et al., 1998). Pohl concluded that large unstirred layers (1 μm) would rate limit CO_2 transport and may present much higher resistance than that of biological membranes. In the case of the pea plasma membrane vesicles that were of the order of 100 nm in diameter it would be expected that the unstirred layers would not exceed this diameter (Niemietz and Tyerman, 1997). Pohl et al. (1998) also expressed AQP1 in Madin-Darby canine kidney (MDCK) cells, where they observed a 3-fold increase in water

flux, however, the CO_2 fluxes across AQP1 expressing and none-expressing cells were identical. These results are similar to those reported here where P_{os} varied by nearly an order of magnitude due to different growth conditions and blocker effects, yet there was no significant change in CO_2 permeability.

With dark and drought treated pea plants, the water permeabilities were relatively low and the shrinking kinetics were more complex (double exponential kinetics). The explanation for this may be heterogeneity of vesicles, either in size or permeability (Alleva et al., 2009). There was no apparent difference in the distribution of vesicle size caused by the treatments suggesting that the difference was related to vesicle populations having different P_{os}. Interestingly the fast phase in the two phase exponential kinetics was decreased in rate with silver sulfadiazine treatment (Figure 2-12, 2-13). This supports the view that the heterogeneity was caused by vesicles with high and low aquaporin activity. The treatments (drought and dark) may reduce the amount of aquaporins in the membrane or their activity via post-translational modifications in a population of cells or membrane sites that then go on to form a large population of the vesicles. A similar phenomenon was observed for *Arabidopsis* vesicles (Figure 2-14). However, the differences in water permeability are not paralleled with differences in CO_2 permeability. This would indicate that water and CO_2 share different pathways, or that the true CO_2 permeability of the membrane was not measured.

Hub *et al.* (2008) studied the selectivity of AQP1 by using molecular dynamics simulations. They demonstrated that the energy barrier for CO_2 permeation through the lipid bilayer is much smaller than the energy barrier for diffusion through aquaporins (Hub and De Groot, 2008). E_a for CO_2 diffusion in water is 18.8 KJ/mol (Maharajh and Walkley, 1973; Jones et

al., 1995), and E_a that I measured for CO_2 transport was 37 KJ/mol. This result indicates that the unstirred layer of the vesicles isn't the only factor that rate limits CO_2 transport.

2.4.7 Aquaporin inhibitor effects

Silver sulfadiazine significantly inhibited the aquaporin activity (Figure 2-2); however, it did not have any inhibitory effect on the rate of acidification (Figure 2-4 a, c). Although, interestingly, both rate constant (Figure 2-4c) and E_a (Figure 2-6) obtained in the presence of silver sulfadiazine are slightly higher than that from control (Figure 2-4a and Figure 2-6). One hypothesis from these results is that CO_2 may go through either the central pore of aquaporin or the lipid bilayer and silver sulfadiazine inhibits the individual water pores of an aquaporin tetramer, and this may lead to the change of the structure of both the central cavity of aquaporin tetramer and bilayer membranes. Hub *et al.* (2006, 2008) used atomistic molecular dynamics simulations to address the pathway of CO_2 transport through AQP1. According to their calculation, the free energy barrier for CO_2 permeation through an empty central cavity is significantly smaller than for the monomeric channel. They concluded that significant aquaporin-1-mediated CO_2 permeation is to be expected only in membranes with a low intrinsic CO_2 permeability (Hub and de Groot, 2006, 2008). As mentioned before, DIDS is likely to be an inhibitor for the central pore of hsAQP1 (Endeward et al., 2006). However, considering the DIDS experiment (Figure 2-5b), DIDS did not inhibit the measured CO_2 permeability. Therefore, if DIDS works in the same way in plant aquaporins, it would indicate that CO_2 does no permeate via the central pore.

2.4.8 Selecting the most appropriate temperature to measure CO_2 permeability

According to Figure 2-10, the amplitudes obtained at different temperatures with the presence of acetazolamide were similar. By contrast, the amplitudes for control decreased with increasing temperature. The differences between the two amplitudes at temperatures of 13.5 ℃, 15 ℃, 18 ℃ and 20 ℃ are only slightly different, however, at higher temperature (23 ℃), the amplitude dropped to less than half of that with acetazolamide. This indicates that as the temperature increases the extrapolated single exponential regression curve becomes less accurate; because at higher temperature the kinetics of CO_2 diffusion would be much faster and therefore more of the decaying pH signal was missing due to the limitation of the stopped-flow device. It has been discussed in 2.4.5 that CA activity is also affected by temperature, and therefore, in order to measure the CO_2 permeability accurately, the temperature has to be as high as possible to make sure the CA catalysis reaction does not rate limit the measured CO_2 permeability. Meanwhile, the accuracy of the measurement has to be ensured. Hence, this is a double-edged sword. Taking all factors into consideration, data at 20 ℃ was selected to calculate the CO_2 permeability.

2.4.9 Correlation of water permeability and CO_2 permeability and conclusion

The pea plants with higher stomatal conductance correspond to the higher water permeability and *vice versa*. This indicates the high expression level or activity of aquaporins (Figure 2-11). The P value obtained from the plot of CO_2 permeability versus P_{os} (Deming regression,

where error occurs in both x and y) was 0.94, which means there is no significant relationship between water permeability and CO_2 permeability.

The average value of pea vesicle P_{CO_2} was 1.49 x 10^{-2} cm s^{-1} was in the medium range of measured values for plasma membrane (Uehlein et al., 2008; Evans et al., 2009) though much lower than the highest value measured for artificial lipid bilayers of 0.35 cm s^{-1} (Gutknecht et al., 1977). CA was affected by temperature and at lower temperature and lower concentrations of CA, it may become rate limiting, which will cause underestimation of P_{CO_2}. There was no significant correlation between water permeability and CO_2 permeability indicating that probably aquaporins do not directly affect CO_2 diffusion, assuming that P_{CO2} was accurately measured. The activation energy measured for CO_2 transport under conditions that would exclude the influence of CA would indicate more of a membrane diffusion process rather than diffusion in free solution as occurs in unstirred layers. Silver sulfadiazine does not have an effect on CO_2 transport whereas water transport was strongly inhibited. It remains unknown how aquaporins may affect CO_2 diffusion in leaves as has been observed in molecular studies of over expression and knock outs of particular aquaporin genes.

Chapter 3 Functional Characterisation of *Arabidopsis* aquaporins

3.1 Introduction

Generally, the aquaporin family seems to be a selective pathway for water or glycerol, and protons are strictly excluded (de Groot and Grubmuller, 2005). However, during the last decade, some aquaporins have been shown to conduct permeants such as gases (CO_2, NH_3, and NO), and non-charged solutes (silicic acid, boric acid and hydrogen peroxide etc.) (Dordas and Brown, 2001; Ma et al., 2006; Wu and Beitz, 2007; Maurel et al., 2008; Musa-Aziz et al., 2009). My project focuses on whether CO_2 can be facilitated by aquaporins. In Chapter 2, I have shown that water and CO_2 do not obviously share the same pathway when large variation is induced in water permeability of native pea leaf plasma membrane. In this chapter, I focus on specific aquaporin genes from *Arabidopsis* to ascertain their water permeation properties when expressed in *Xenopus* oocytes.

Water channel activity of aquaporins has generally been demonstrated by expression of the cRNA in *Xenopus laevis* oocytes. The *Xenopus* oocyte is a useful expression system for transport proteins in general because oocytes are large cells (1 mm diameter) that are easily manipulated, and for water transport they have low endogenous water permeability (Preston et al., 1992; Maurel et al., 1993). Other heterologous expression systems have also been used to examine aquaporins and include plant protoplasts (Kaldenhoff et al., 1998), pollen protoplasts (Sommer et al., 2008), the slime mold *Dictyostelium discoideum* (Chaumont et al., 1997) and *Saccharomyces cerevisiae* (Laize et al., 1995; Ishikawa et al., 2005; Verdoucq et al., 2008).

On the basis of their sequences similarity, the PIP sub-family in plants can be divided into two groups, PIP1 and PIP2 (Chaumont et al., 2000; Chaumont et al., 2001; Johanson et al., 2001; Fetter et al., 2004; Maurel et al., 2008). PIP2 proteins often present high water channel activity when expressed in *Xenopus* oocytes, however, PIP1 proteins are often inactive or show low water channel activity (Daniels et al., 1994; Kammerloher et al., 1994; Weig et al., 1997; Johansson et al., 1998; Biela et al., 1999).

High-resolution three-dimensional crystal structure of the mammalian aquaporins AQP0 (Gonen et al., 2004), AQP1 (Murata et al., 2000; Sui et al., 2001), AQP2 (Schenk et al., 2005) and AQP4 (Hiroaki et al., 2006), bacterial AQPZ (Ringler et al., 1999; Savage et al., 2003) and *Spinacia oleracea* plasma membrane intrinsic protein 2;1 (SoPIP2;1) (Kukulski et al., 2005) have been obtained and they demonstrate that aquaporins form homotetramers, with each monomer forming an independent water channel pore. In plants, it has been shown that aquaporins form both homo- and hetero-tetramers (Harvengt et al., 2000).

Fetter *et al.* (2004) showed that certain Maize ZmPIP1 proteins interact with ZmPIP2 proteins, and coexpression of the non-functional ZmPIP1s and the functional ZmPIP2s increased water permeability above that which was observed with the ZmPIP2 alone. This was also observed for grapevine PIP1 and PIP2 proteins (Vandeleur et al., 2009). The increase of water permeability is dependent on the amount of injected PIP1s. Using confocal analysis, oocytes coexpressing ZmPIP1;2-green fluorescent protein (GFP) and ZmPIP2;5 presented significantly greater ZmPIP1;2-GFP at the plasma membrane compared to oocytes expressing ZmPIP1;2-GFP alone. Heteromerization of both isoforms was demonstrated by nickel affinity chromatography purification of ZmPIP2;1 fused to a His tag co-eluted with ZmPIP1;2-GFP (Fetter et al., 2004). Temmei *et al.* (2005) heterologously expressed *Mimosa*

pudica (Mp) PIPs in oocytes and demonstrated that MpPIP1;1 facilitated the water channel activity of MpPIP2;1 in a phosphorylation-dependent manner. Phosphorylation of Ser-131 of MpPIP1;1 was essential for regulation of water channel activity of the MpPIP1;1 and MpPIP2;1 complex (Temmei et al., 2005).

Zelazny *et al.* (2007) first demonstrated protein-protein interaction between ZmPIP1 and ZmPIP2 in living plant cells using fluorescence resonance energy transfer (FRET). Their results indicated that ZmPIP1s were retained intracellularly and not targeted to the plasma membrane when expressed alone. However, ZmPIP1s and ZmPIP2s interacted when they were co-expressed, resulting in ZmPIP1 relocalization to the plasma membrane (Zelazny et al., 2007). Tetramer assembly is likely to be crucial for protein folding, stability and transport to target membranes (Chaumont et al., 2005). The formation of aquaporin heterotetramer increases the diversity of activity of water channels in the membrane and may provide cells with an additional mechanism for regulating membrane permeability (Zelazny et al., 2007).

While ZmPIP1;2 and ZmPIP2;5 interact, and result in an increase in water permeability, other PIP1 and PIP2 members may not interact. Even though ZmPIP1;1 shares 97% identity with ZmPIP1;2, it does not increase water permeability of oocytes when co-expressed with ZmPIP2;5 (Zelazny et al., 2007). Alexandersson *et al.* (2010) generated a network of co-expression in $C_{YTO\text{-}SCAPE}$ 2.2 by pearson's coefficients of all AtPIPs and four AtTIPs (Figure 3-1). Many AtPIPs and AtTIPs are highly co-expressed ($r > 0.6$), whereas AtPIP1;4, AtPIP2;5 and AtPIP2;6 do not co-express with other AtPIPs and AtTIPs ($r < 0.6$) (Alexandersson et al., 2010). The information provided by this analysis has been used here to target particular PIP combinations that are likely to interact in *planta*.

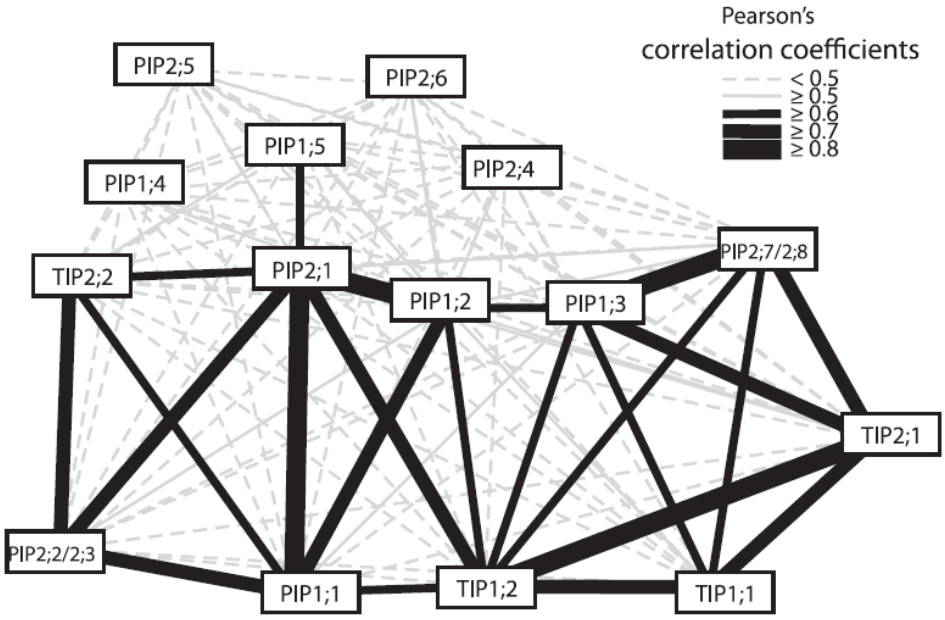

Figure 3 – 1 Co-expression analysis of all AtPIPs and four AtTIPs (Alexandersson et al., 2010).

Aquaporins present two filters: 1) the two NPA motifs fold to form a pore which is called Filter 1 (Figure 3-3 highlight in yellow). 2) the ar/R constriction forms Filter 2 (Figure 3-2). Hove *et al.* (2011) showed using bioinformatics and modeling approaches that NtAQP1, AtPIP1;2, HvPIP2;1 and PIPs from the moss *Physcomitrella patens* (Danielson and Johanson, 2008) exhibit highly conserved F-H-T-R in Filter 2, and this is also seen in some other PIPs (Figure 3-3 highlight in red). They demonstrated that this conserved pattern may be crucial for CO_2 transport. They also suggest that PIPs possessed the ability to facilitate CO_2 transport since their evolutionary origin. They concluded that there are four conserved amino acid sequences/patterns that a MIP should possess to enable CO_2 transport: 1) the two NPA motifs; 2) the F-H-T-R at Filter 2; 3) the S-A-F-W at Loop E and Transmembrane (TM) 6 region (position P2-P5 residues which were predicted to play a functional role in aquaporin (Froger et al., 1998)) (Figure 3-3 highlight in green); 4) a conserved AEF(M/I/V)AT at TM 1 region (Figure 3-2, Figure 3-3 highlight in blue) (Hove and Bhave, 2011).

In order to better understand the role that aquaporins play in photosynthesis (both water and CO_2 transport) (Chapter 2), the aquaporins that have higher expression levels in leaves were targeted. Expression analysis of the *Arabidopsis thaliana* aquaporin family has shown that *AtPIP1;2*, *AtPIP2;1* and *AtPIP2;6* are among the most highly expressed *PIP* genes in the *Arabidopsis* rosette, meanwhile *AtPIP1;4* and *AtPIP1;5* both have a medium expression in leaves (Alexandersson et al., 2005). AtPIP2;1 was demonstrated to transport H_2O_2 (Dynowski et al., 2008) and according to phylogenetic analysis, AtPIP2;1 clusters with those MIPs that transport molecules besides water (Hove and Bhave, 2011). Figure 3-1 shows that AtPIP1;2 and AtPIP1;5 are more likely to co-express with AtPIP2;1. Therefore testing water and CO_2 transport for these aquaporins and their interactions is important.

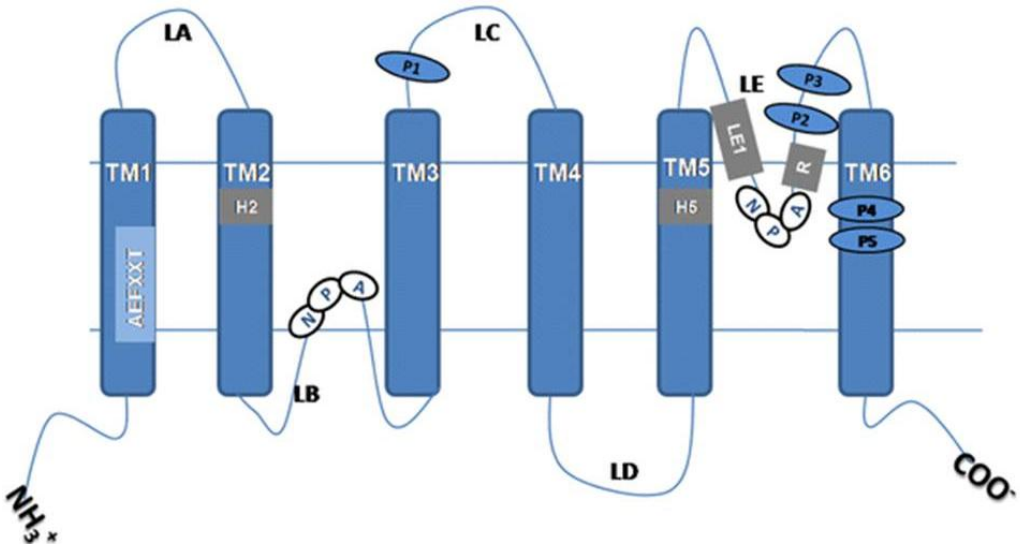

Figure 3-2 Aquaporin structure. Six transmembrane helices (TM1-TM6) were connected by 5 loops (LA-LE). Two conserved NPA motifs are in LB and LE, respectively. The grey rectangles consist Filter 2. The blue ovals show P1-P5 (Froger et al., 1998; Hove and Bhave, 2011).

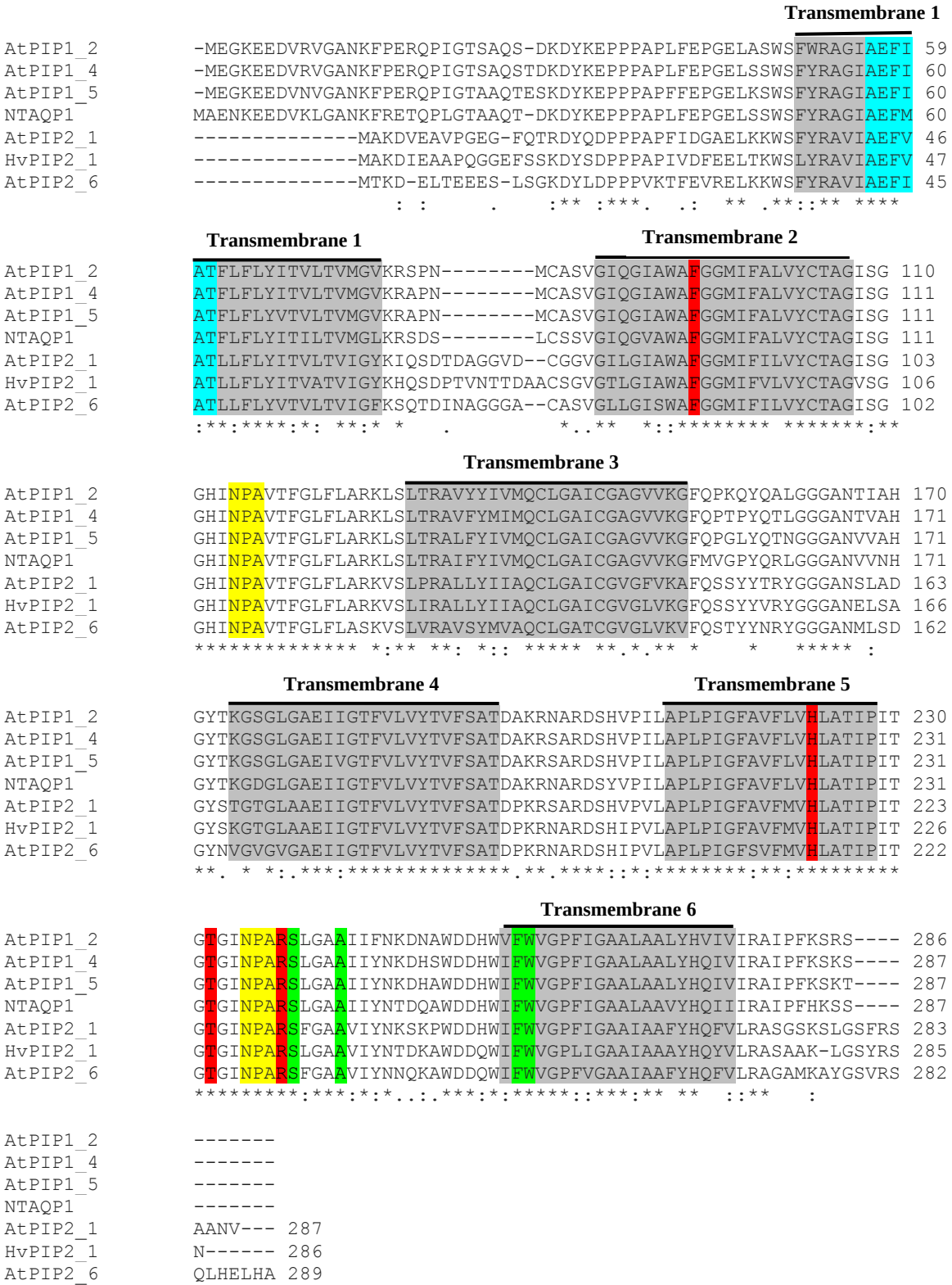

Figure 3-3 Alignments of putative amino acids sequences of some MIPs which have been shown to transport CO_2 (Hove and Bhave, 2011).

In this chapter, I focus on the water permeability of AtPIP1;2, AtPIP1;4, AtPIP1;5, AtPIP2;1 and AtPIP2;6. Water permeation via AtPIP1;2 has been previously shown using yeast protoplasts (Heckwolf et al., 2011), and AtPIP2;1 showed high water permeability when the purified protein was incorporated into liposomes (Verdoucq et al., 2008). In this chapter, I used gateway cloning techniques to clone *AtPIP1;2, AtPIP1;4, AtPIP1;5, AtPIP2;1* and *AtPIP2;6* into the pGEMHE-DEST *Xenopus* oocyte expression vector. The water channel functions of these aquaporins were tested by *Xenopus* oocyte swelling assays. The interaction of PIP1s and PIP2s was also investigated by both co-expression and site-direct mutagenesis. Finally, the aquaporin inhibitor, silver-sulfadiazine, was examined for its effect on water permeability through specific aquaporins.

3.2. Materials and Methods

3.2.1 Solutions, media and bacterial transformation

All components of solutions and media were analytical or molecular biology grade and purchased from Sigma-Aldrich unless indicated otherwise. All solutions and media were made with MilliQ water and when required, autoclaved at 121 ℃ for 20 min. The components of general solutions and media are listed in Table 3-1.

Table 3-1: General solutions and growth media.

Media/Solution	Components
Luria broth (LB)	1 % (w/v) yeast extract (Difco), 1 % (w/v) NaCl, 0.5 % (w/v) tryptone pH 7, + 2 % (w/v) agar for solid media
LB / Kan	LB + 50 µg ml^{-1} of kanamycin
LB / Amp	LB + 100 µg ml^{-1} of ampicillin
10 x TAE	0.4 M Tris, 0.01 M EDTA disodium salt, 0.2 M acetic acid
10 x TBE	0.89 M Tris, 0.02 M EDTA disodium salt, 0.89 M boric acid
agarose gels	1.0 – 1.2 % (w/v) agarose dissolved in 1 x TBE (or 1 x TAE) buffer

During gene cloning, chemically competent *Escherichia coli* One shot® TOPO10 cells (Invitrogen) were used for bacterial transformations unless indicated differently. These competent cells have very high transformation efficiency and are ideal for high efficiency cloning and plasmid propagation according to Invitrogen manual. 100 ~ 200 ng Plasmid DNA was transformed into 50 µl of chemically competent cells. Cells were incubated on ice for 30 min and then heat shocked at 42 ℃ for 30 s and placed on ice for another 2 min. 450 µl of LB was then added to cells and these were grown at 37 ℃, 200 rpm for 1 hour to allow recovery. 100 µl of transformation mix was spread onto LB agar plates with the appropriate antibiotic selection and grown at 37 ℃ overnight.

3.2.2 Cloning *Arabidopsis PIP1s* and *PIP2s* into pEntry TOPO® vector

Directional TOPO® cloning enables cloning of blunt-ended PCR products in a 5’ to 3’ orientation directly into an entry vector using a ligation reaction. Directional TOPO® cloning vectors contain a single-strand GTGG overhang on the 5’ end and a blunt end on the 3´end. Hence, gene specific forward primers with four extra bases of CACC at 5’ end were designed

to anneal to the GTGG sequence. Topoisomerase I then ligates the PCR product in the correct orientation (http://tools.invitrogen.com/content/sfs/manuals/pentr_dtopo_man.pdf).

Gene specific reverse primers were designed based on published sequences (NCBI database) of *Arabidopsis thaliana* aquaporins which are highly expressed in leaves (Alexandersson et al., 2005): the original clones of *AtPIP1;2, AtPIP1;4, AtPIP2;1* and *AtPIP2;6* (accession numbers: At2g45960, At4g00430, At3g53420, At2g39010) were bought from *Arabidopsis* Biological Resource Center (USA). Full-length *Arabidopsis* aquaporin *AtPIP1; 2*, *AtPIP1; 4*, *AtPIP2; 1* and *AtPIP2; 6* were amplified by PCR (Table 3-2). The PCR cycling conditions strictly followed the Phusion High-Fidelity DNA Polymerase F-530 instructions: initial denaturation: 98 ℃ for 30 s; denaturation: 98 ℃ for 10 sec; annealing for 30 sec (annealing temperature depends on the T_m of each gene); extension: 72 ℃ for 30 s; cycled 25-30 times; final extension: 72 ℃ for 10 min, 4 ℃ hold (Phusion, Finnzymes).

Table 3-2: Primers for amplification of *Arabidopsis* aquaporin genes products. The melting temperature (T_m) for each primer was calculated using the software on the website: https://www.finnzymes.fi/tm_determination.html

Arabidopsis Gene	Forward/Reverse 5'-3'	T_m (℃)
AtPIP1;2	F:5'CACCATGGAAGGTAAAGAAGAAGATGTTA3'	60.37 ℃
	R:5' TTAGCTTCTGGACTTGAATGG 3'	61.28 ℃
AtPIP1;4	F: 5' CACCATGGAAGGCAAAGAAG 3'	58.03 ℃
	R: 5' CTAACTCTTGCTCTTGAAAGGAATC 3'	58.57 ℃
AtPIP2;1	F: 5' CACCATGGCAAAGGATGTGGA 3'	60.62 ℃
	R: 5' TTAGACGTTGGCAGCAC 3'	61.51 ℃
AtPIP2;6	F: 5' CACCATGACGAAGGATGAGTTGAC 3'	59.67 ℃
	R: 5' TTAAGCATGGAGCTCATGA 3'	60.07 ℃

An agarose gel was ran after each PCR to check the size of the PCR products. Agarose gels were prepared by dissolving 1-1.2% (w/v) agarose in 1 x TBE buffer with the addition of 3.5 µL GelRed DNA stains (Biotium, USA) every 50 ml of dissolved gel. DNA samples were loaded in loading buffer and electrophoresed at ~ 80-100 V for 1~2 hours. Agarose gels were visualised under UV light using the Molecular Imager ChemiDoc XRS System (Biorad). The PCR products were then purified using ISOLATE II DNA and Gel Kit (Bioline, Australia), then the DNA concentration was identified by using a Nanodrop™ spectrophotometer, and then cloned into entry vector, pEntry TOPO® vector using the pEntr™ Directional TOPO® Cloning Kit (Invitrogen). The TOPO® cloning reaction was performed by adding 2.5 ng PCR products, 1 µl salt solution (provided in the kit), and 5 µl with sterile water. Finally, 1 µl of TOPO® vector was added to make a final volume of 6 µl. The reaction was mixed by pipetting up and down and then incubated at room temperature (22 ℃) for 30 min. The reaction was placed on ice before proceeding to the transformation. The most important factor for this cloning step to be successful is the amount of PCR product to use in the cloning reaction. Based on the instructions from Invitrogen, using 1~5 ng of a 1 kb PCR product or 5~10 ng of a 2 kb PCR product in a TOPO® Cloning reaction can achieve the best yield. Therefore, 2.5 ng purified PCR product was used.

The ligation products were then transformed into TOPO10 chemically competent cells using a heat shock method described above in the "transformation" section. The pEntry TOPO® vector contains the Kanamycin resistance gene allowing the selection of transformants on LB agar plates to grow with the presence of 50 µg/mL Kanamycin. Up to 10 single colonies were selected and were grown overnight in 5 mL LB plus 50 µg/mL Kanamycin at 37 ℃, rpm. Plasmid DNA was purified using the Sigma Genelute Plasmid Purification Kit (Sigma-Aldrich). The products were digested with *Not* I and *Asc* I restriction enzymes (BioLabs) at

37 ℃ for 90 min followed by running a gel to confirm that the correct sized product (~1kB) was present. Then, the products were sequenced at Australian Genome Research Facility Ltd (AGRF), South Australia. The primers used in two separate sequencing reactions were M13 forward (5'-GTAAAACGACGGCCAG-3') and M13 reverse (5'-CAGGAAACAGCTATGAC -3'). Approximately 300 ng DNA was used in each sequencing reaction mix. Alignment of the sequences was done by ApE.exe software: (http://biologylabs.utah.edu/jorgensen/wayned/ape/). (Sequence alignments see Appendix 1)

3.2.3 Cloning *Arabidopsis PIP1s* and *PIP2s* into oocyte expression vector

The oocyte expression vector, pGEMHE-DEST (Liman et al., 1992) was converted to a gateway vector using the Gateway Vector Conversion System (Invitrogen) by former lab member Megan Cherie Shelden (Figure 3-4). pGEMHE-DEST vector carries the 5' and 3' untranslated sequences of the ß-globin gene from *X. laevis*, that helps to promote translated sequences of the plant capped-RNA (cRNA) (Liman et al., 1992). Full length aquaporin genes were recombined into the pGEMHE-DEST vector using the LR recombination reaction kit (Invitrogen). The LR reaction allows the recombination of the *att*L in the entry clone vector with the *att*R in the destination vector (pGEMHE-DEST). *att*L and *att*R are the sites for site-specific recombination of the entry clone with a Gateway® destination vector. The LR reaction was set up strictly following the manufacturers' instructions (50-150 ng of *att*L entry clone and 150 ng destination vector, incubated with LR Clonase ™ II at 25℃ overnight). The LR recombination reaction was stopped by adding 1 µl proteinase K solution (2 µg/µl). Then, 2 µL of the LR reaction was transformed into TOPO10 chemically competent cells. The pGEMHE-DEST vector contains the Ampicillin resistance gene therefore allowing the selection of transformants on LB plates containing Ampicillin (100 µg/mL). Up to 4 single

colonies were then picked up and grown in liquid LB plus Ampicillin (100 µg/mL) at 37 ℃, 200 rpm overnight. A mini-prep of the plasmid DNA was performed and digested with the relevant restriction enzymes at 37 ℃ for 90 min, and followed by in gel confirmation of the correct sized product.

Plasmid DNA was purified using the Sigma Genelute Plasmid Purification Kit. The concentration of DNA was determined by a NanoDrop spectrophotometer 1000 (Thermo Scientific).

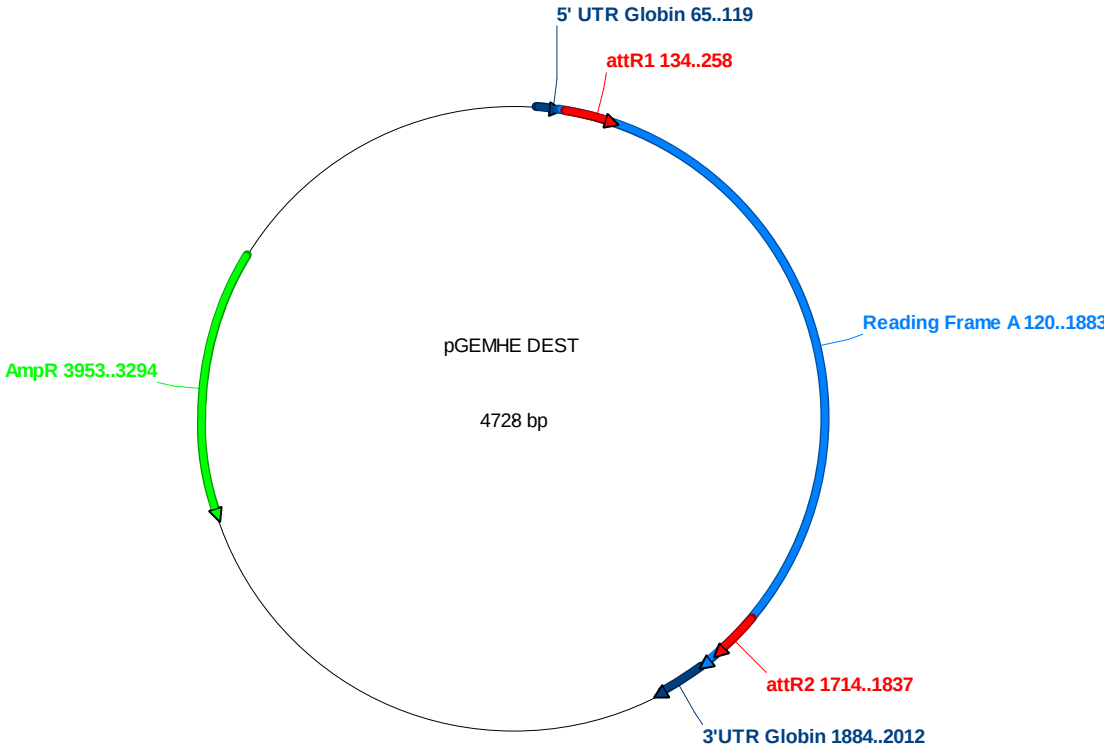

Figure 3-4. Expression vector pGEMHE-DEST. 5' and 3' UTRs from *Xenopus* ß-globin gene flank and polylinker (Krieg and Melton, 1984) enabling the recombination of the reading frame cassette A containing the *ccd*B gene and chlorophenical resistance gene.

3.2.4 Site-directed mutagenesis of *AtPIP2;1* (G100W)

(1) Primer design

The aim of the mutagenesis reaction was to substitute the Gly100 with Trp100 (G100W) in the highly conserved loop B region of *AtPIP2;1*. Previous research by Shelden *et al.* (2009) demonstrated that this amino acid is essential for water transport, and changing glycine to tryptophan can inhibit the water transport activity probably by blocking the water pore (Shelden et al., 2009). Site-directed mutagenesis was conducted by PCR. The mutagenic oligonucleotide primers for use in this reaction were designed according to the desired mutation by following the basic rules of the manual of QuikChange II Site-Directed Mutagenesis Kits (Agilent Technologies, USA):

Forward: 5'- CTACTGCACCGCCGGTATCTCTTGGGGTCACATTAAC-3'

Reverse: 5'- GTTAATGTGACCCCAAGAGATACCGGCGGTGCAGTAG-3'

The Tm for both primers is 80 ℃.

(2) Mutagenic strand synthesis reaction

Using *AtPIP2;1*-pGEMHE as a template, the following PCR was performed with Phusion High-Fidelity polymerase in a 50 µl system:

10 µl 5* Phusion High-Fidelity buffer (Finnzymes, Thermo Fisher Scientific Inc.)

10 ng double strand DNA (*AtPIP2;1*- pGEMHE)

125 ng Forward primer

125 ng Reverse primer

1 µl dNTP mix (QuikChange II Site-Directed Mutagenesis Kits)

ddH_2O top up to 50 µl

0.5 µl Phusion High-Fidelity (Finnzymes, Thermo Fisher Scientific Inc.)

10 ng double strands DNA was not included in the control reaction.

A gradient PCR was conducted to optimize the best annealing temperature with the following cycling protocol: denaturing: 98 ℃ for 30s; annealing: 15 cycles of 98 ℃ for 10s, 65 ℃~70 ℃ gradient for 30s; and extension: 72 ℃ for 2 min.

The expected product size was 3973 bp. Quality of the PCR was checked by running a small aliquot on a 1.2 % agarose gel in 1 * TBE buffer. The PCR product was transformed directly to TOP 10 competent cells. Positive colonies were selected on LB + Amp plates and grown overnight in liquid LB + Amp media to amplify plasmid DNA, mini-prepped and digested with *Nar* I (BioLab) at 37 ℃ for 90 min to confirm correct size. Once correct size was confirmed, the plasmid was sequenced with M13 forward (5'-GTAAAACGACGGCCAGT-3') and reverse primer (5'-AACAGCTATGACCATG-3') at AGRF to confirm the correct mutation (see Appendix 1).

3.2.5 cRNA transcription

The capped RNA (cRNA) mimics most eukaryotic mRNAs found *in vivo*. cRNA was synthesised using 1 µg of linearised DNA with the mMESSAGE mMachine Kit (Ambion) utilizing the T7 promoter of pGEMHE-DEST vector, according to the modified

manufacturers' instructions. The instructions were modified so as to achieve the maximum yield:

1) 3 μg of each pGEMHE-DEST vector with different aquaporin gene (*AtPIP1;2, AtPIP1;4, AtPIP1;5, AtPIP2;1, AtPIP2;6*) was digested with either the restriction enzyme *Nhe* I or *Sph* I (BioLabs) at 37 ℃ overnight to linearise the plasmid. All the plasmids were checked for complete digestion by running 120 ng on a 1% (w/v) agarose gel / 0.5 * TBE buffer.
2) After linearization the reaction was terminated with the addition of 0.5 % (w/v) sodium dodecyl sulphate (SDS) and 100 μg/ml proteinase K and heated at 55 ℃ for 50 min to 1 hour to get rid of all the RNases (Worthington, 2011).
3) Equal volume of Phenol: Chloroform: Isoamyl Alcohol (25:24:1 Saturated with 10 mM Tris, pH 8.0, 1 mM EDTA) was added to the reaction, vortexed vigorously and centrifuged 5 min at room temperature. The top liquid phase which contains DNA, was transferred to a new tube, followed by adding 1/10 th volume of 5 M NH_4OAc and 2 volume of ethanol into the tube. The DNA was therefore precipitated by incubating the tube at -80 ℃ overnight. Phenol: Chloroform extraction will remove all the proteins and achieve ultra-pure DNA to start the cRNA synthesis.
4) DNA was pelleted by centrifugation at maximum speed (14,000 rpm) for 20 min (Backman Coulter™ Mirofuge® 18 Centrifuge, USA), followed by washing with 70% ethanol to get rid of salt and pelleted again. Finally, the DNA was resuspended with nuclease-free water at a concentration of ~0.2-0.5 μg/μl. DNA concentration after recovery was confirmed by both running a gel and Nanodrop.
5) 20 μL cRNA synthesis reaction is prepared by adding 10 μL 2X NTP/CAP, 2 μL 10X reaction buffer, 1 μg linear template DNA, 2 μL enzyme mix and top up with nuclease-free water. The reaction was incubated at 37 ℃ for 6 hours.

6) 30 µl lithium chloride precipitation solution (7.5 M LiCl, 50 mM EDTA) and 20 µl nuclease-free water were added into the reaction to precipitate the synthesised cRNA at -80 ℃ overnight. The cRNA pellet was washed twice with 70% RNAse-free ethanol and resuspended with 10 µl RNAse-free water and stored in -80 ℃.

3.2.6 cRNA purity check and concentration quantification

Non-denaturing RNA agarose gels were run to check the cRNA quality. The following gel electrophoresis conditions were used:

1) Fresh gel (~1.2% agarose) and autoclaved buffer (1X TAE) were used as well as clean electrophoresis equipment (cleaned by Ambion® RNaseZap®) for RNA analysis. Clean gloves were used to protect RNA samples from degradation by nucleases.
2) For best resolution, running voltage up to 10 V/cm was used. Higher voltages are not recommended because they may lead to RNA degradation and poor resolution during electrophoresis (Sambrook J, 1989).
3) An aliquot of the RNA solution was heated at 85 ℃ for 1 min to denature the RNA and minimize its secondary structure, and placed on ice before loading on to the gel.
4) An RNA ladder was loaded alongside the RNA sample as a standard for determining the RNA size.
5) The sign of RNA degradation on the non-denaturing gel is a slight smear starting from the RNA bands and extending to the area of shorter fragments. In my experiment, only the samples that showed clear single bands were used.

cRNA was quantitated and checked by Quant-iT™ RiboGreen® RNA Reagent and Kit (Invitrogen). A high-range RNA standard curve (allows quantification of 20 ng/ml to 1 µg/ml)

was performed by mixing 1 ml 1x Quant-IT™ RiboGreen® reagent to 1 ml different concentrations of standard RNA (stock solution provided in the kit, final RNA concentration: 0 ng/ml, 20 ng/ml, 100 ng/ml, 500 ng/ml and 1 μg/ml), mixed well in cuvettes and incubated at room temperature for 5 min with the aluminium foil covered to protect the reaction from light. The fluorescence of each cuvette was then measured using a spectrofluorimetry (Bio-Rad) at an excitation wavelength of 480 nm-500 nm, and the emission maximum is ~520 nm. The blank was subtracted. An RNA concentration versus fluorescence intensity standard curve was generated by Prism 5 software and used to determine the unknown samples.

An aliquot of the unknown cRNA sample was first diluted to a final volume of 1 ml and mixed well with 1 ml 1×Quant-IT™ RiboGreen® reagent, the mixture was incubated for 5 minutes in the dark. The cRNA sample concentration was calculated from the equation for the standard curve. After the quantification of cRNA sample concentration by RiboGreen® RNA reagent, another electrophoresis was also run to confirm the accuracy of the method.

3.2.7 Harvesting oocytes

Oocytes were harvested from *Xenopus laevis* frogs by Dr. Sunita Ramesh and Ms Wendy Sullivan using the protocol described in (Hill et al., 2005). Following the harvest, oocytes were defolliculated at room temperature with 2 mg/ml collagenase in calcium-free ringers solution (96 mM NaCl, 2 mM KCl, 5 mM $MgCl_2$, 5 mM HEPES, pH 7.6) for 85 minutes with rotation. The oocytes were then defolliculated with a hypotonic buffer (100 mM KH_2PO_4-KOH, 0.1% BSA, pH 6.5). Then, the oocytes were washed three times with hypotonic buffer and two times with calcium-free ringers solution. The oocytes were transferred and stored in Ca-ringers solution plus antibiotics (100 μg/ml tetracycline, 100 μg/ml penicillin/streptomycin)

and horse serum (5 ml of horse serum liquid every 100 ml Ca-ringers solution) and kept at 18 ℃ until needed.

3.2.8 Expression of *Arabidopsis* aquaporins in *Xenopus* oocytes

Injection pipettes (Drummond Scientific, item # 3-000-203-G/X) were pulled in two stages with a capillary puller on heat setting 10.5 and 11 (Narishige Scientific Equipment Lab) and were bevelled by a micro grinder EG400 (Narishige Scientific Equipment Lab) to a tip diameter of 40 μm. Oocytes have two poles, the animal pole and the vegetal pole. The animal pole is dark brown in colour and the vegetal pole is creamy. Oocytes of uniform size (diameter ~ 1 mm) and colouring were selected and injected with 6 ng cRNA in 46 nl of nuclease-free water per oocyte at the border of the animal pole and vegetal pole. Genes were injected individually (*AtPIP1;2, AtPIP1;4, AtPIP1;5, AtPIP2;1, AtPIP2;6, hAQP*) or one *PIP1* and one *PIP2* co-injected together (*AtPIP1; 2* co *AtPIP2; 1*, *AtPIP1; 2* co *AtPIP2; 6*, *AtPIP1; 4* co *AtPIP2; 1* and *AtPIP1; 5* co *AtPIP2; 1*) to create a 1:1 ratio. The control oocytes were microinjected with 46 nl sterile nuclease-free water. After injection, the oocytes were incubated at 18 ℃ for 24 hours in Ca-ringers solution plus antibiotic and horse serum. The incubation solution was changed 1~2 times every 24 hours.

3.2.9 Oocytes swelling assay

After 24 hours incubation, the oocytes were transferred to another sterilized petri-dish with 5 ml hypo-osmotic solution (Ca-ringers solution diluted 5 fold with sterile water). The osmolarity of each solution was determined using a Fiske® 210 Micro-Sample freezing-point

osmometer (Advanced Instruments, Inc., USA). The oocytes were viewed with a Nikon SMZ800 light microscope (Nikon, Japan) with the 1.5x objective lens WD45 (Nikon, Japan). The changes in volume were captured with a Vicam colour camera (Pacific Communications, Australia) at 2 x magnification and the images were recorded with IC Capture 2.0 software (The imagine source, US) as AVI format video files. Images were acquired every 3 s for 1.5 min for each oocyte. Image J software (http://rsbweb.nih.gov/ij/, US Government) was utilised to calculate the change in the total area of the oocytes captured in the AVI video file, and assuming oocytes are spherical the change in volume was determined. For some tests, the aquaporin inhibitor silver-sulfadiazine (Niemietz and Tyerman, 2002) (final concentration: 12 μM) was added to the petri-dish. Osmotic permeability (P_{os}) was calculated for water injected and cRNA injected oocytes from the increase in volume with time (n = 5-10 ± SEM) using the following equation:

$$P_{os} = V_o\,(d(V/V_o)/dt) \,/\, S{*}V_w\,(Osm_{in}\text{-}Osm_{out}) \qquad \text{Equation 3-1}$$

where:

V_o is the initial oocyte volume (mm^3);

$d(V/V_o)/dt$ is the rate of initial relative cell volume change (mm^3/s);

S is the initial surface area (mm^2);

V_w is the partial molar volume of water, given as 18 cm^3/ mol;

Osm_{in}-Osm_{out} is the change in osmolarity (mol/cm^3).

3.3 Results

3.3.1 Transcription of cRNA and cRNA concentration quantification

Strong clear bands of the expected product sizes were transcribed from linearized pGEMHE-DEST plasmid DNA containing the coding sequence of the genes of interest (Figure 3-5): *AtPIP1;2* (906 bp); *AtPIP1;4* (864 bp); *AtPIP1;5* (864 bp); *AtPIP2;1* (864 bp) and *AtPIP2;6* (870 bp). Additional bands of larger sizes were observed for *AtPIP2;6* and *AtPIP1;2*. The cRNA transcription reaction was repeated several times and the additional bands were observed each time. The possible reasons of the presence of the larger bands are as follows: firstly, these larger bands may be additional unwanted transcribed products due to incomplete digestion of the original plasmid DNA, despite overnight digestion. Secondly, the formation of some of the larger bands is due to the secondary structure of cRNA. Because the secondary structure affects the rate of RNA movement through the agarose gel. Meanwhile, there is a possibility that some left over plasmid DNA may still present despite a DNAase treatment step. In future work, some steps could be undertaken to minimize contaminating bands, such as blunt the ends of the linearised plasmid DNA (Schenborn and Mierendorf, 1985; Hartje et al., 2000).

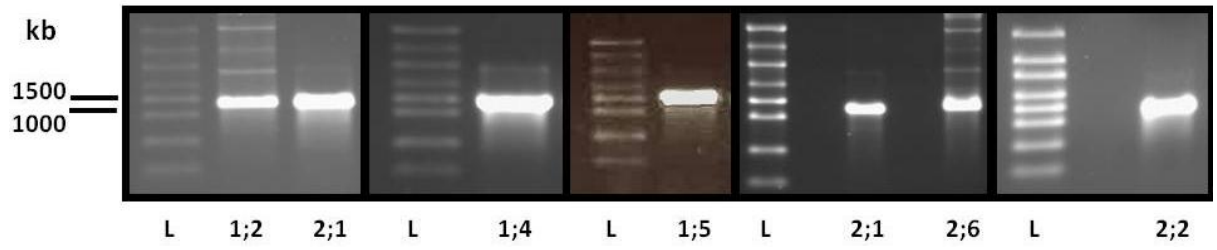

Figure 3-5. RNA products transcribed from the coding sequences of *AtPIP1;2; AtPIP1;4; AtPIP1;5; AtPIP2;1* and *AtPIP2;6*.

Figure 3-6 gives an example of the RNA standard curve of RNA concentration versus fluorescence intensity. The dash line represents the concentration of cRNA in the unknown sample. The electrophoresis results (Figure 3-7) with the same amount of cRNA for each sample, confirmed that the RiboGreen® method to quantify cRNA concentration was accurate and that the amount of each of the different cRNAs injected into the oocytes was the same.

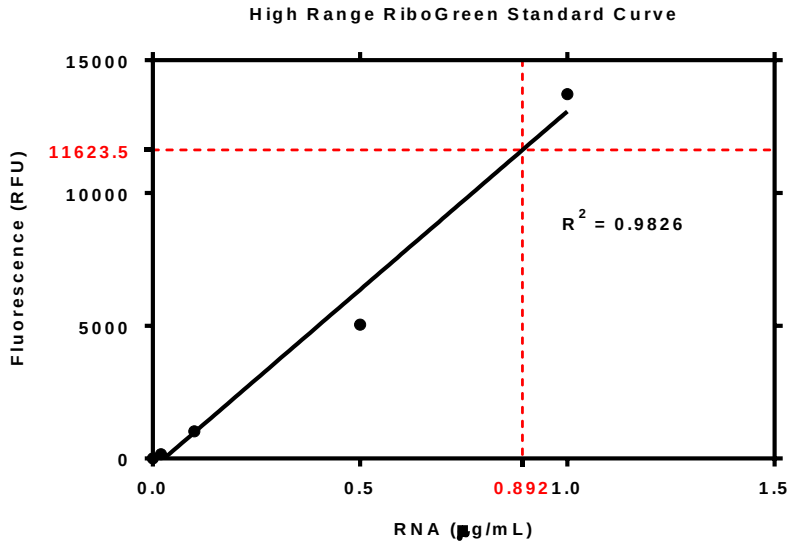

Figure 3-6. High range RNA standard curve. cRNA sample concentration was read through the standard curve.

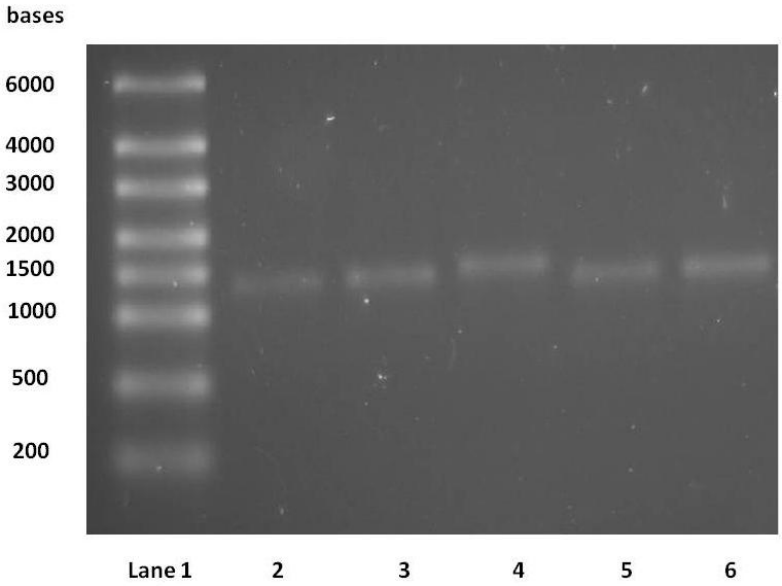

Figure 3-7. Electrophoresis of 62.5 ng per cRNA sample (based on the RiboGreen® method) (lane 1 to 6: *AtPIP1; 2, AtPIP1; 4, AtPIP1; 5, AtPIP2; 1* and *AtPIP2; 6*)

3.3.2 Aquaporin activity—the swelling assay

To identify the water channel activities of leaf-expressed aquaporins, the water permeability coefficient (P_{os}) was measured for *Xenopus* oocytes injected with 23 ng of each aquaporin cRNA. Human *AQP1* was used as a positive control since it is known to facilitate rapid water uptake (Laizé et al., 1995). Water injected oocytes served as negative controls. I focused on five aquaporin PIPs in this study, which was discussed in the introduction: *AtPIP1;4, AtPIP1;2, AtPIP1;5, AtPIP2;1, AtPIP2;6*. The water permeability was calculated from the rate of increase in the volume of the oocytes when exposed to the hypotonic solution (Figure 3-8).

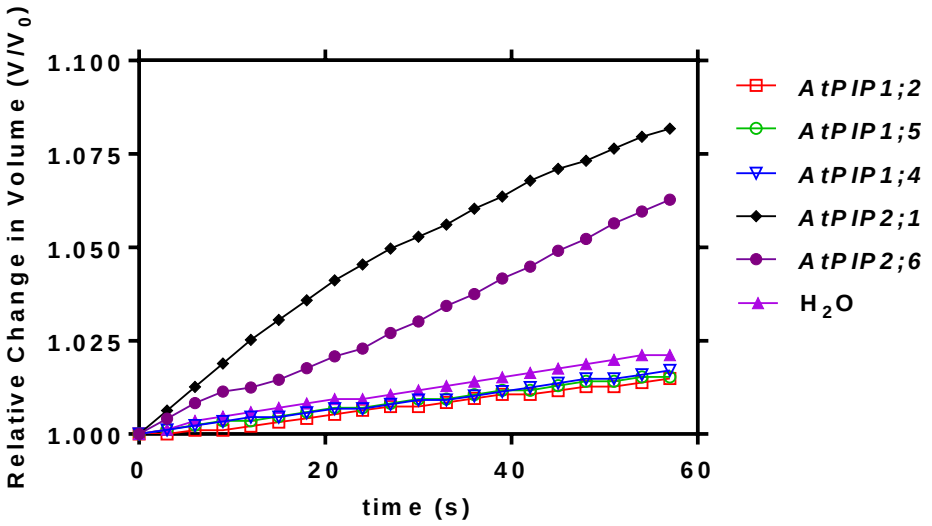

Figure 3-8. Relative change in volume (V/V_0) versus time (s) of oocytes injected with different cRNA respectively in hypotonic solution (*AtPIP1;2*: □; *AtPIP1;5*: ○; *AtPIP1;4*: ▽; *AtPIP2;1*: ◆; *AtPIP2;6*: ●; H_2O: ▲).

Figure 3-9 is an example of the pictures captured by camera every 3 seconds for a water injected oocyte (Figure 3-9a) and 23 ng *AtPIP2;1* injected oocyte (Figure 3-9b). It revealed dramatic explosion of oocytes when *AtPIP2;1* injected oocytes were placed in the hypotonic solution since swelling was very rapid (Figure 3-9b). Swelling could be measured accurately for up to 1 min before oocyte bursting. The water permeability of H_2O-injected negative controls had an average P_{os} of 1.14 x 10^{-3} cm s^{-1} (SEM 0.0002, N = 5). The P_{os} of oocytes injected with *AtPIP1;2, AtPIP1;5 or AtPIP1;4* showed that there was a slight increase of P_{os} (1.1-2.3 folds) compared with water control (not significant according to one-way ANOVA). By contrast, oocytes injected with *HsAQP1, AtPIP2;1 or AtPIP2;6* had a significant effect on P_{os} with increment up to 8.2-15 fold.

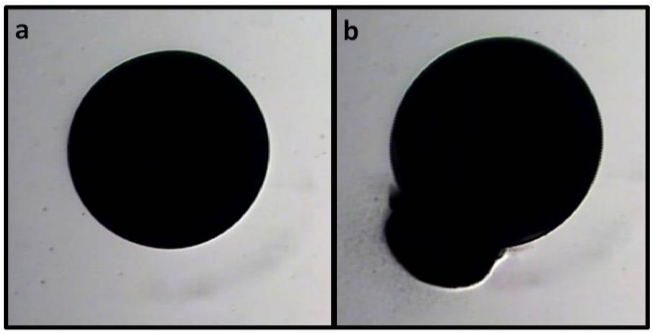

Figure 3-9. Functional expression of *AtPIP2;1* water channel in *Xenopus* oocytes. (a): incubation in hypotonic buffer fails to cause significant swelling of a water injected oocyte. (b): an oocyte injected with *AtPIP2;1* cRNA exhibits high water permeability and has exploded after 1 minute.

It was observed that many of the oocytes which were injected with 23 ng *AtPIP2;1* began to burst and die after 48 hours incubation. This phenomena may be caused by: 1) *AtPIP2;1* may transport other solutes and poisoned the oocytes; 2) Injection of 23 ng of *AtPIP2;1* cRNA may be intrinsically toxic to the eggs, either by high concentrations of the translated protein interacting with native proteins or by the RNA interacting with other components. Testing for the first possibility will be described in the next chapter.

In order to test the second possibility, different concentrations of cRNA (0 ng, 1 ng, 3 ng, 6 ng, 11.5 ng and 23 ng) were injected into the oocytes. Swelling assays were performed after 24 hours incubation. Even at the low cRNA concentration some oocytes still died after 24 hours of incubation. From Figure 3-10, it is obvious that the measured water permeability increases with the increasing amount of injected cRNA, however, it is not a linear relationship, and the measured water permeability began to be saturated when 11.5 ng *AtPIP2;1* cRNA was injected into the oocytes. Meanwhile, injection of 6 ng cRNA is definitely enough to give a large increase in oocyte water permeability. Therefore, in order to be consistent, subsequent measurements were performed by injecting 6 ng of each cRNA into the oocytes.

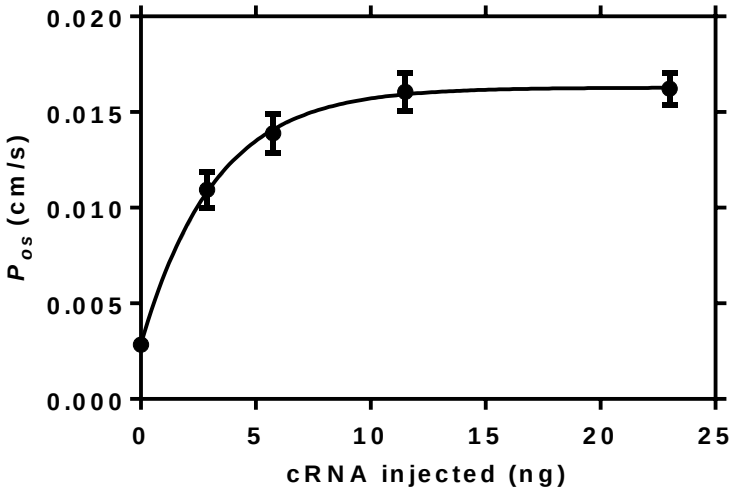

Figure 3-10. The relationship of cRNA of *AtPIP2;1* concentration versus water permeability.

3.3.3 Expression of PIPs alone or in PIP1-PIP2 combinations in *Xenopus* oocytes

To explore the effect on P_{os} of co-expression of *Arabidopsis* PIP1 and PIP2, one PIP1 and one PIP2 were co-injected together (6 ng co 6 ng) to create a 1:1 ratio. The water permeability of oocytes expressing 6 ng of *AtPIP1;2* (2.0 x 10^{-3} cm.s^{-1}, SEM 0.0002, N = 5), *AtPIP1;4* (2.91 x 10^{-3} cm.s^{-1}, SEM 0.001, N = 6) or *AtPIP1;5* (1.53 x 10^{-3} cm.s^{-1}, SEM 0.0003, N = 5) was not significantly greater than those injected with water (1.14 x 10^{-3} cm.s^{-1}, SEM 0.00015, N = 5) (Figure 3-11). Oocytes injected with 6 ng *AtPIP2;1* had a water permeability of 1.159 x 10^{-2} cm.s^{-1} (SEM 0.001, N = 12); injected with 6 ng *AtPIP2;6* had a water permeability of 4.27 x 10^{-3} cm.s^{-1} (SEM 0.001, N = 9). When equal amounts of PIP1 and PIP2 were injected there was an increase in water permeability above the level of PIP2 alone. Notably, when *AtPIP1;2* and *AtPIP2;6* were coexpressed, the water permeability of the oocytes approximately equals the addition of water permeability of *AtPIP1;2* and *AtPIP2;6* alone (7.4 x 10^{-3} cm.s^{-1}, SEM

0.001, N = 7 vs 6.3 x 10^{-3} cm.s^{-1}). The same phenomena were observed with *AtPIP1;4* and *AtPIP2;1* co-expression (1.450 x 10^{-2} cm.s^{-1}, SEM 0.001, N = 15 vs 1.482 x 10^{-2} cm.s^{-1}). However, with *AtPIP1;2* and *AtPIP2;1*, the water permeability of the oocytes was significantly greater than the additive water permeability of *AtPIP1;2* and *AtPIP2;1* alone (2.325 x 10^{-2} cm.s^{-1}, SEM 0.0011, N = 12 vs. 1.363 x 10^{-2} cm.s^{-1}). Similar results were obtained when coexpress *AtPIP1;5* and *AtPIP2;1* (2.926 x 10^{-2} cm.s^{-1}, SEM 0.001, N = 20 vs. 1.312 x 10^{-2} cm.s^{-1}).

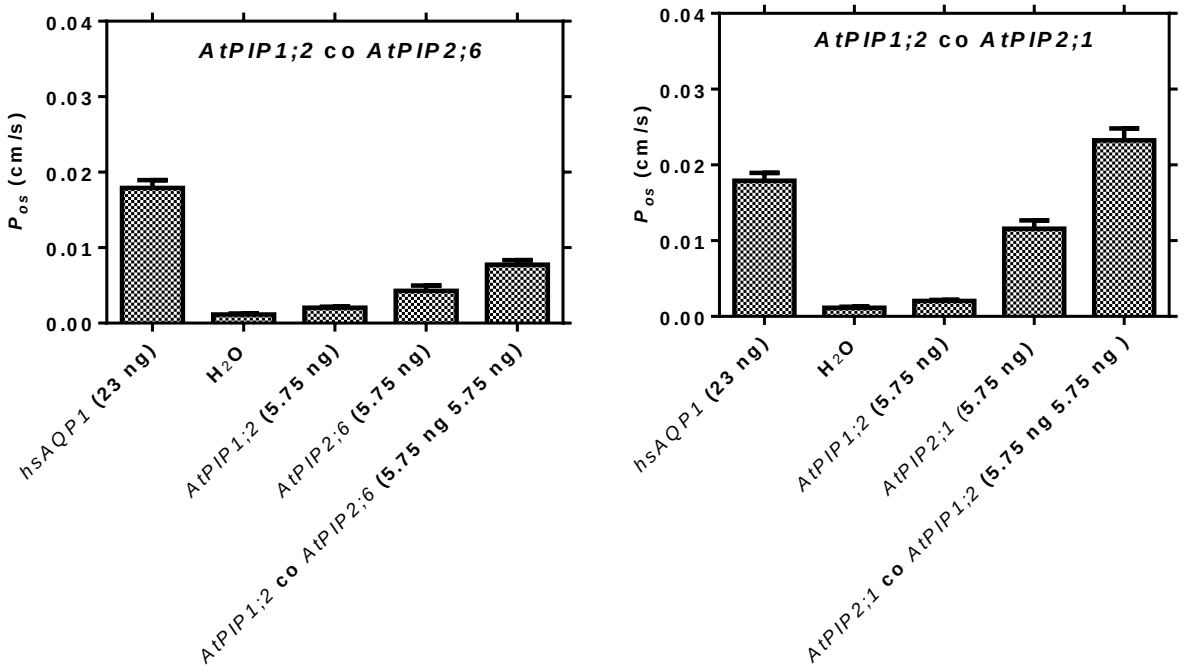

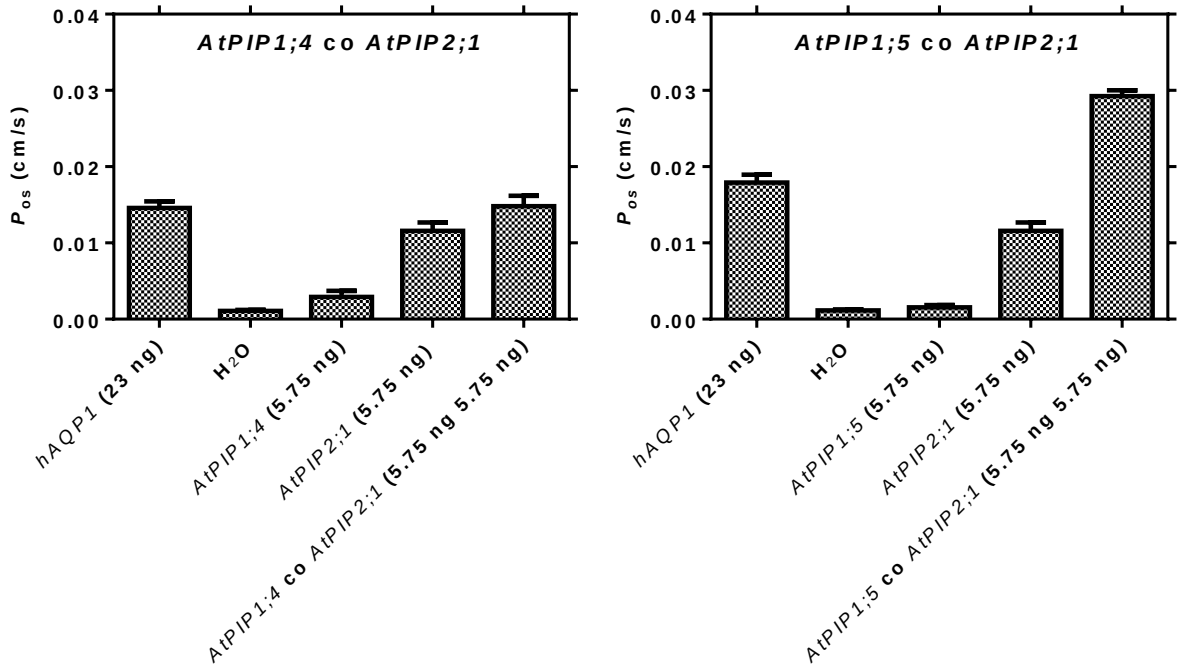

Figure 3-11. Water permeability of oocytes injected with H_2O, *AtPIP1s*, *AtPIP2s* and co-injected with *AtPIP1s* and *AtPIP2s* at a 1: 1 ratio.

3.3.4 Mutant *Atpip2;1*

(1) Site-directed mutagenesis

The gene, *AtPIP2;1*, was successfully mutated by PCR according to the sequencing results. The glycine 100 was substituted to tryptophan. 70 ℃ annealing temperature had the strongest band according to the gel analysis (Figure 3-12).

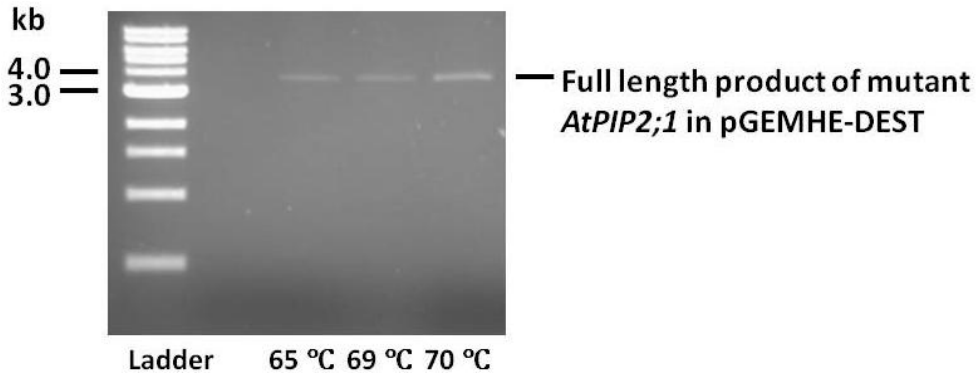

Figure 3-12. Electrophoresis of mutagenesis PCR product at different annealing temperatures (65 ℃, 69 ℃, 70 ℃).

The water permeability for *AtPIP1;2* injected oocytes was $2.31*10^{-3}$ cm/s, similar to that obtained for *Atpip2;1*-mutant (G100W) injected oocytes ($2.21*10^{-3}$ cm/s). This confirms the apparent blocking effect of the tryptophan in loop B in the water conducting channel as observed by Shelden *et al.* (Shelden et al., 2009). For co-expressed *AtPIP1;2* and *Atpip2;1*-mutant (G100W), the value for water permeability was increased dramatically relative to that of the mutant channel expressed alone $1.78 * 10^{-2}$ cm/s (Figure 3-13).

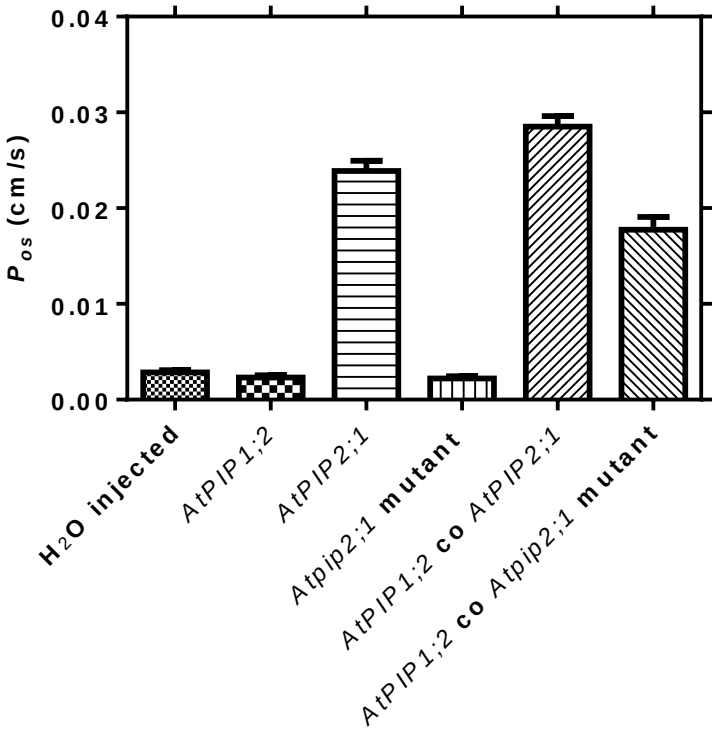

Figure 3-13 Water permeability for oocytes injected with: water, *AtPIP2;1*, mutant-*Atpip2;1* (G100W), *AtPIP1;2* co *AtPIP2;1* and *AtPIP1;2* co mutant-*Atpip2;1* (G100W).

3.3.5 Effect of silver-sulfadiazine on aquaporin water permeability

In 2002, Niemietz and Tyerman found that silver ions at low concentrations can block aquaporins *in vitro*. It is likely that silver reacts with the sulfhydryl group of a cysteine in the vicinity of the conserved NPA motif and thus blocks the constriction region of the water channel (Niemietz and Tyerman, 2002). Silver sulfadiazine (Ag-sul, 12 μM) strongly inhibits water permeability of oocytes expressing functional aquaporins. The water permeability of oocytes expressing *AtPIP2;1* was inhibited by 88.8%, while inhibition was 83.8% for *AtPIP2;6* injected oocytes, 77.8% for *hsAQP1* injected oocytes and 53.6% for water injected

oocytes. These results indicate aquaporin activity and the strong inhibition effect of Ag-Sul (Figure 3-14).

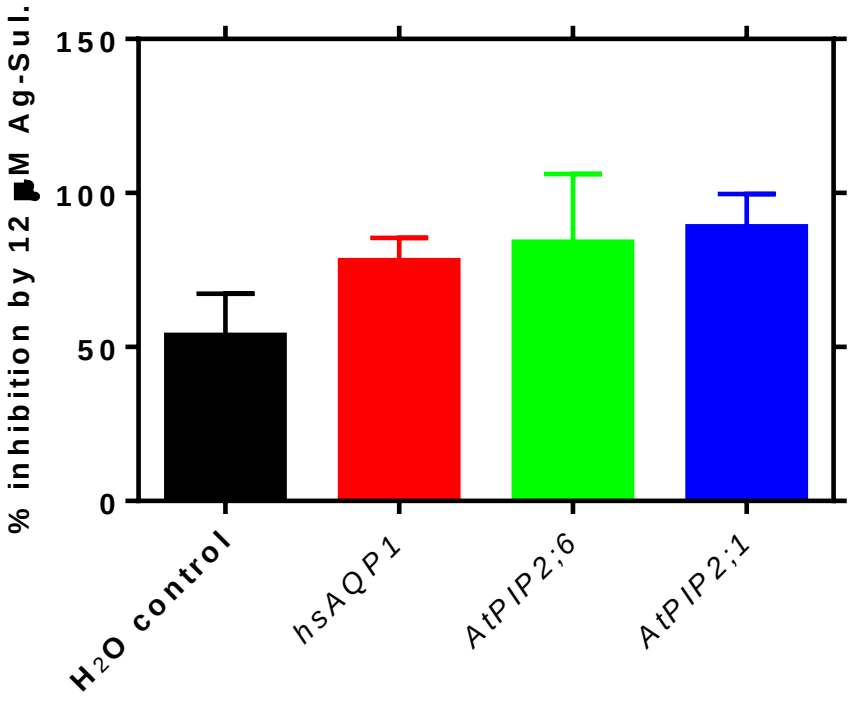

Figure 3-14. Ag-sul inhibition effect (inhibition percentage) for oocytes injected with water (●), *hsAQP1* (●), *AtPIP2;1* (●) and *AtPIP2;6* (●), respectively.

3.4 Discussion

3.4.1 Water permeability of AtPIP1s and AtPIP2s

Most PIP1s proteins identified in plants have no or very low aquaporin activity when expressed in oocytes. PIP2s have much higher water permeability in oocytes compared to PIP1s. For instance, NtAQP1, from the PIP1 group, showed higher water permeability

compared to water injected oocytes, but had significantly lower water permeability than PIP2s (Biela et al., 1999). ZmPIP1a and ZmPIP1b show no water channel activity when expressed in *Xenopus* oocytes, while ZmPIP2a has aquaporin activity (Chaumont et al., 2000). Moshelion *et al.* (2002) showed that oocytes expressing *Samanea saman* AQP1 (SsAQP1, a PIP1 member) were twice as permeable to water as water injected oocytes, by contrast, oocytes expressing SsAQP2 had a water permeability 10 times higher than that of SsAQP1 expressing oocytes (Moshelion et al., 2002). This has also been observed for *Vitis vinifera* PIP1 and PIP2 members (Vandeleur et al., 2009). Similarly, my results showed that both AtPIP2;1 and AtPIP2;6 caused an obvious increase in the rate of water transport through the membrane of *Xenopus* oocytes, whereas all PIP1s show extremely low or no aquaporin activity.

One possibility for the apparent inactivity or low activity of AtPIP1s aquaporins when expressed alone in *Xenopus* oocytes may be because of incorrect trafficking to the plasma membrane. Another possibility is that the AtPIP1s may need a positive regulator for functionality that is not present in oocytes (Chaumont et al., 2000; Zelazny et al., 2007).

Figure 3-10 showed that the water permeability and the injected *AtPIP2;1* cRNA concentration is not a linear relationship, rather, the measured water permeability saturated when the injected cRNA amount is above 11.5 ng. This result indicates that there might be a certain limitation of aquaporin density in the oocyte plasma membranes.

3.4.2 Interaction between AtPIP1s and AtPIP2s

Alexandersson *et al.* (2010) showed that MIP transcription in *Arabidopsis thaliana* is generally down regulated in leaves upon drought stress, however, *AtPIP1;4* and *AtPIP2;5* are up regulated and *AtPIP2;6* is unresponsive to drought stress (Alexandersson et al., 2005). Further study using promoter-GUS fusions for *AtPIP1;4, AtPIP2;5* and *AtPIP2;6* and using *Arabidopsis thaliana* trans-factor and cis-element prediction database (ATTED-II) showed that the MIPs that are down regulated upon drought stress are strongly co-expressed, whereas AtPIP1;4, AtPIP2;5 and AtPIP2;6 are less likely to co-express with this group (Alexandersson et al., 2010).

According to Figure 3-11, when AtPIP1;2 and AtPIP2;1 are co-expressed in oocytes, the water permeability was significantly higher compared to the additive water permeability for AtPIP2;1 and AtPIP1;2 alone. An even higher water permeability value was obtained when AtPIP1;5 and AtPIP2;1 were co-expressed. These results correspond with Figure 3-1, which indicates that AtPIP1;2 and AtPIP1;5 are more likely to interact with AtPIP2;1 ($r > 0.6$). However, when AtPIP1;4 and AtPIP2;1 were co-expressed, or AtPIP1;2 and AtPIP2;6 were co-expressed, the coexpressed water permeability value for the oocytes plasma membrane was almost equal to the additive water permeability value when expressed alone. These results indicate that AtPIP1;4 and AtPIP2;1 are less likely to interact; same with AtPIP1;2 and AtPIP2;6. These results also correspond with Figure 3-1.

Based on the work by Shelden *et al.* (2009), unlike other functional PIP2s, VvPIP2;5 does not have water transport activity. They concluded that the tryptophan in loop B was crucial for the loss of water transport activity of VvPIP2;5 (Figure 3-15) because it is hydrophobic and

blocks the centre of the water channel (Shelden et al., 2009). The mutant Atpip2;1 (G100W) displayed no apparent water permeability, which confirms the structural analysis by Shelden *et al.* (2009). Interestingly, when co-expressed with AtPIP1;2 in *Xenopus* oocytes, the oocytes restored their water permeability (Figure 3-13). This is important since it showed that the mutant channel still expressed and was interacting with AtPIP1;2. The water permeability of the co-expressed AtPIP1;2 and Atpip2;1 oocytes therefore probably represented the water permeability of AtPIP1;2 alone. This result also corresponds to previous conclusions by Fetter *et al.* (2004) indicating that PIP1s are not apparently functional because they are not trafficked and localized in the membrane when expressed alone (Fetter et al., 2004). Further experiments with GFP-fusion proteins are needed to confirm this for AtPIP1;2 and Atpip2;1 coexpression.

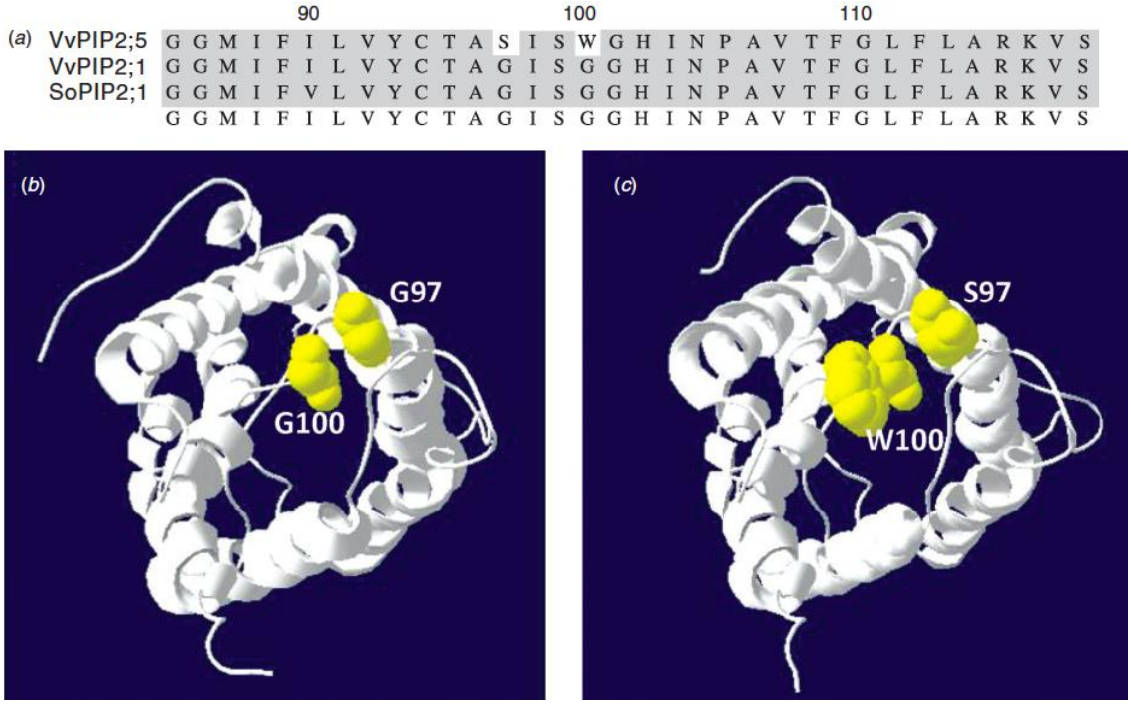

Figure 3-15 (a) Sequence alignment of aquaporin loop B of VvPIP2;5, VvPIP2;1 and SoPIP2;1. (b) The structure of SoPIP2;1. Yellow: Gly97 and Gly100. (c) The structure of VvPIP2;5. Yellow: Ser97 and Trp100 (Shelden et al., 2009).

3.4.3 Aquaporin inhibition

Niemietz *et al*. (2002) discovered some powerful aquaporin inhibitors such as silver and gold compounds. Silver, as silver nitrite and silver sulfadiazine and gold, as $HAuCl_4$, inhibit the water permeability of peribacteroid membrane from soybean with a very high potency. Mercurials have been used more often to block aquaporins, however, their high cell toxicity limits the interpretation of the effects. Silver is the most potent aquaporin inhibitor so far described. The inhibition effect is rapid and is not reversible with mercaptoethanol. The mechanism of silver and gold inhibition is likely due to their ability to interact with sulfhydryl groups of a cysteine in the vicinity of the conserved NPA motif and thus effectively blocks the constriction region of the water channel. The non-reversibility of inhibition by mercaptoethanol also suggests a inhibition mode that differs to that caused by mercury (Niemietz and Tyerman, 2002). As demonstrated here, silver sulfadiazine also blocked specific aquaporins when expressed in *Xenopus* oocytes, as opposed to the inhibition observed in native membranes (Chapter 2 and Niemietz and Tyerman, 2002).

In conclusion, five aquaporins with high or medium expression level in *Arabidopsis* leaves were cloned into oocyte expression vector. I have shown that when expressed in *Xenopus* oocytes, AtPIP2;1 and AtPIP2;6 aquaporins are highly permeable to water. AtPIP1;2, AtPIP1;4 and AtPIP1;5 aquaporins present no or low water permeability when expressed in *Xenopus* oocytes. This may be due to incorrect trafficking or incorrect assembly into the oocytes plasma membrane (Fetter et al., 2004). AtPIP1;2 and AtPIP2;1; AtPIP1;5 and AtPIP2;1 did interact in *Xenopus* oocytes to up-regulate the water permeability. AtPIP1;2 and AtPIP2;6; AtPIP1;4 and AtPIP2;1 are unlikely to interact. The oocytes expressing the mutant Atpip2;1 (G100W) lost their water transport activity but regain this when co-expressed with

AtPIP1;2. This is evidence indicating that AtPIP1;2 and AtPIP2;1 interact physically. It appears that PIP1s may be involved in regulation of water permeability of other aquaporins or increase the diversity of control of water channel activity in the membrane in addition to having a water transport role. Silver sulfadiazine is a powerful aquaporin inhibitor and can inhibit *Arabidopsis* aquaporins.

Chapter 4 Ion Currents Induced by *AtPIP2;1* in *Xenopus* Oocytes

4.1 Introduction

The aim of expressing aquaporins in *Xenopus* oocytes was to eventually test the CO_2 permeability across plasma membranes using an external pH microelectrode technique (Endeward et al., 2006; Geyer et al., 2013). The detail of the technique was discussed in Chapter 1. Before investigating the CO_2 permeability, experiments were performed to examine if an ion conductance was induced by the expression of aquaporins. An implicit assumption in the pH electrode technique is that there should not be any ion currents induced by the expression of the aquaporins of interest. If they conduct ions or protons then this would complicate the transients in pH that are measured upon supply of bicarbonate/CO_2 in the external solution. When CO_2 enters into the cells it will react with water immediately and release bicarbonate and carbonate plus protons as described in the previous chapters (Chapter 1, 2), this is a complicated reaction as it forms different products, therefore, it is essential to check that the particular aquaporins of interest do not induce any ionic currents in oocytes, which could potentially change external pH either directly or indirectly. In this Chapter, I describe how AtPIP2;1 induced an ionic current in oocytes. Interestingly, there is indeed some recent research that has demonstrated that several classes of MIPs can act as ion channels.

Aquaporin water channels are found in all cellular life forms (Reizer et al., 1993). There has been much research focusing on characterising aquaporins from different species and identifying their transport properties. During the last two decades, more evidence has

accumulated that some aquaporins are not only involved in water transport, but also in nutrient transport, and nitrogen and carbon fixation in plants (Hachez and Chaumont, 2010; Soto et al., 2010). Some aquaporins from mammals can act as ion channels (Yool and Stamer, 2004; Yool, 2007; Yool, 2007; Yool et al., 2010; Campbell et al., 2012; Yool and Campbell, 2012). Several approaches have been used to analyse aquaporin ion channel activity, mainly using two electrode voltage clamping (TEVC) in *Xenopus* oocytes expressing the aquaporin, and site-directed mutagenesis to identify amino acid residues that are responsible for ion selectivity (Yool and Campbell, 2012).

The most studied aquaporins for ion channel activity are mammalian aquaporins. Until now, there are 13 aquaporins that have been discovered in human, AQP0 - AQP12 (Agre, 2011). hsAQP1 is a well known water channel, and interestingly, electrophysiology of *Xenopus* oocytes expressing hsAQP1 has shown that it also functions as a non-selective monovalent cation channel when activated by intracellular cGMP (Yool et al., 1996; Yool and Weinstein, 2002). By mutation of lys 51 to cys (K51C) in the central pore of the cys-less hsAQP1 tetramer, a site for inhibition of ionic conductance by the mercuric ion was created. This suggested that the pathway for ion currents is the central pore of the homotetrameric hsAQP1 (Campbell et al., 2012). Holm *et al.* (2005) expressed hsAQP3, hsAQP8 and hsAQP9 in *Xenopus* oocytes and tested the transport of ammonia (NH_3) and ammonium (NH_4^+) using TEVC (Holm et al., 2005). They observed that hsAQP3, hsAQP8 and hsAQP9 showed NH_3 permeability by the acidification of a well stirred bath medium. Under voltage-clamp, they demonstrated that hsAQP3, hsAQP8 and hsAQP9 also support inward currents carried by NH_4^+ apparently gated by NH_3. The currents were affected by the pH in a manner indicating that NH_3 was involved and they were abolished when pH was below 6.8 while saturating when pH was above 7.8. They suggested a model that these ammonia permeable aquaporins

transport NH_3 and H^+ in the form of NH_4^+. NH_3 that is presented in an ammonia permeable aquaporin could act as a binding site for H^+, therefore, NH_4^+ is formed and proceeds across the channel. The problem with this hypothesis is that it seems to be inconsistent with the theory that the aquaporins can transport H_2O but no H_3O^+ (Murata et al., 2000). However, they argued that the property and structure of NH_3 and H_2O are different therefore they may behave differently in the NPA selectivity filter region of aquaporins (Holm et al., 2005).

Another human aquaporin that has been intensively studied for ion channel activity is hsAQP6. When expressed in *Xenopus* oocytes, hsAQP6 presented minimal water permeability (Liu et al., 2005). One early study showed that hsAQP6 was permeable to anions which was induced by either acidic pH or treatment with $HgCl_2$ (Hazama et al., 2002). AQP6 was localized to intracellular vesicles in renal epithelia (Yool and Campbell, 2012). Ikeda *et al.* (2002) tagged the N-terminus of rat *AQP6* with green fluorescence protein (GFP) which resulted in the redirection of AQP6 to the plasma membrane of mammalian renal cells (Ikeda et al., 2002). Employing the patch clamping technique, they observed that rat AQP6-GFP exhibited highly selective nitrate permeability even without activation by acidic pH and $HgCl_2$. Furthermore, they identified that the pore-lining residue of threonine at position 63 was crucial for anion channel selectivity. Site-direct mutation of threonine 63 to isoleucine reduced the nitrate permeability and the NO_3^-/Cl^- selectivity (Ikeda et al., 2002). By sequence alignments, Liu *at al.* identified the key amino acids for ion permeability in AQP6. These amino acids include: Asn-60, Thr-63, Trp-71 and Lys-72, and all of these amino acids locate in transmembrane domain 1 (TM1) and Loop B (Figure 4-29 high light in blue with bold underline). By mutation of asn-60 to gly, anion transport of AQP6 was abolished but retained water permeability (Liu et al., 2005).

Until now, only one or two plant aquaporins have been identified as being ion permeable: NOD26 and TaTIP2;1. NOD26 is located on the peribacteroid membrane of soybean root nodules which enclose symbiotic nitrogen-fixing bacteroids. By testing peribacteroid membrane vesicles, it was demonstrated that NOD26 played an essential role in ammonia transport and nitrogen fixation (Niemietz and Tyerman, 2000; Hwang et al., 2010). NOD26, when purified and inserted into artificial lipid bilayers, was also shown to act as a voltage sensitive ion channel that transported both cations and anions with a weak selectivity for anions (Weaver et al., 1994). By expression of TaTIP2;1 in *Xenopus* oocytes, Holm *et al.* (2005) observed that TaTIP2;1 can transport both NH_3 and NH_4^+ using TEVC and by monitoring the changes in the pH of the bath solution (Holm et al., 2005).

In this chapter, the TEVC technique was used to examine ion currents induced in *Xenopus* oocytes expressing AtPIP1;2, AtPIP2;1, and a mutant Atpip2;1 (G100W) (Chapter 3), AtPIP2;2 and the coexpression of AtPIP1;2 and AtPIP2;1.

4.2 Materials and Methods

4.2.1 Oocytes harvesting and cRNA injection

Oocytes were harvested from *Xenopus laevis* frogs by lab colleagues Dr. Sunita Ramesh and Ms Wendy Sullivan using the protocol described by (Hill et al., 2005). The methods of oocytes harvesting, processing and cRNA microinjection were described in Chapter 3.

4.2.2 cRNA synthesis

The cRNA of *AtPIP1;2* (accession number: AT2G45960), *AtPIP2;1* (accession number: AT3G53420) and *AtPIP2;2* (accession number: AT2G37170.1) were synthesized as described in Chapter 3. cRNA quality was checked using gel electrophoresis. The gel picture of *AtPIP1;2* and *AtPIP2;1* were shown in Chapter 3, and strong clear bands of *AtPIP2;2* (858 bp) cRNA is shown as Figure 4-1.

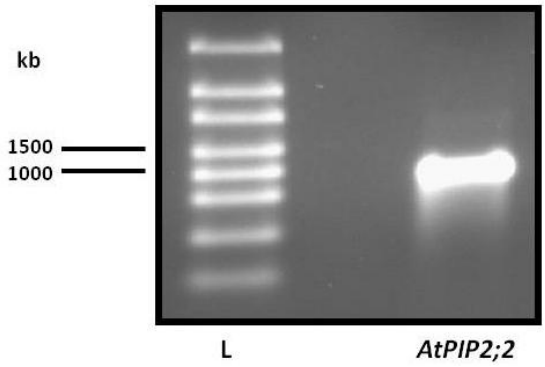

Figure 4-1 cRNA products transcribed from the coding sequences of *AtPIP2;2*.

4.2.3 Voltage-clamp pipettes

Borosilicate glass pipettes (Harvard Apparatus, GC150F-10, 1.5 mm O.D. x 0.86 mm I.D.) were fire polished to smooth the end of the pipettes to avoid damage to the AgCl layer on the silver electrode. Pipettes were pulled in two stages with a microelectrode puller on heat setting 11.0 and 9.0 (Narishige Scientific Equipment Lab). This gave suitable electrode tip openings as checked using the "bubble number" method described in (Schnorf et al., 1994). The pipettes typically had a bubble number between 6-7 giving resistances of between 0.5 to 1 MΩ with the standard filling solution which was 3M KCl, and are suitable for two electrode

voltage clamping of oocytes. The 3M KCl for filling voltage-clamp pipettes was filtered (Sartorius Stedim, Minisart 0.22 μm) before use. The pipettes contain a fused internal filament making electrolyte filling convenient. Borosilicate glass provides low noise and low capacitance, as well as good membrane-adhesive properties (Schnorf et al., 1994).

4.2.4 TEVC recording from *Xenopus* oocytes

Electrophysiological measurements were made 24 hours after cRNA injection with a two-microelectrode voltage clamp amplifier (Oocyte Clamp OC-725C, Warner Instruments) together with a Digidata 1440A data acquisition system interface (Axon Instruments) at room temperature (~ 20 ℃).

(1) Solutions

All components of solutions were analytical or molecular biology grade and purchased from Sigma-Aldrich unless indicated otherwise (Table 4-1).

Table 4-1 Recipe of solutions that were used in electrophysiology experiments

Solutions	Recipe
ND96 (96 NaCl)	96 mM NaCl, 2 mM KCl, 1 mM $MgCl_2$, 1.8 mM $CaCl_2$, 5 mM HEPES pH 6.5/7.5/8.5 with Tris-base
CO_2/HCO_3 solution	63 mM NaCl, 33 mM $NaHCO_3$, 2 mM KCl, 1 mM $MgCl_2$, 1.8 mM $CaCl_2$, 5 mM HEPES pH 7.5 with Tris-base
10 NaMES	10 mM NaMES, 2 mM KCl, 1 mM $MgCl_2$, 1.8 mM $CaCl_2$, 5 mM HEPES pH 7.5/8.5 with MES

ND10 (10 NaCl)	10 mM NaCl, 2 mM KCl, 1 mM $MgCl_2$, 1.8 mM $CaCl_2$, 5 mM HEPES pH 7.5/8.5 with Tris-base
ND50 (50 NaCl)	50 mM NaCl, 2 mM KCl, 1 mM $MgCl_2$, 1.8 mM $CaCl_2$, 5 mM HEPES pH 7.5/8.5 with Tris-base
10 $NaNO_3$	10 mM $NaNO_3$, 2 mM KCl, 1 mM $MgCl_2$, 1.8 mM $CaCl_2$, 5 mM HEPES pH 7.5/8.5 with Tris-base
10 $NaHCO_3$	10 mM $NaHCO_3$, 2 mM KCl, 1 mM $MgCl_2$, 1.8 mM $CaCl_2$, 5 mM HEPES pH 7.5 with Tris-base
Niflumic acid (NFA), $LaCl_3$, 5-Nitro-2-(3-phenylpropylamino)benzoic acid (NPPB)	Each chemical has a final concentration of 200 μM

Membrane currents were initially measured in base solution; base solution was either ND96 or ND10 depending on the experiment. Osmolarities of all the solutions were adjusted with mannitol to 230-240 mosmol/kg using a vapour pressure osmometer (Wescor 5500, Wescor). Bath solutions were modified with different concentrations of NaCl, $NaNO_3$ or $NaHCO_3$ as specified above.

(2) Electrophysiology

A bath clamp system was used to minimize the effect of series resistance in the bath solution. The current and voltage electrodes consist of a silver-silver chloride (Ag-AgCl) connected to the bath by 2% agar/3 M KCl bridges. The oocyte was placed in a perfusion chamber and continuously perfused with solutions. The perfusion rate of the bath solution past the oocytes was about 3-4 ml/min. Each oocyte was carefully stabbed with the voltage and current electrodes and membrane voltage allowed to stabilise. The normal criterion used to reject unhealthy oocytes was a membrane potential above (more negative than) -40 mV depending on the solution composition, (ie. some solutions induced membrane depolarisation because of the expressed genes). A voltage-pulse protocol was performed with Clampex 10.2 software

(Axon Instruments, CA, USA). The acquisition mode was set to episodic stimulation; the sampling rate per signal was set to 1000 Hz; the sweep duration was set to 3 s. To collect data for current-voltage (I-V) relationships, the voltage clamp protocol was set up as follows: -40 mV for 0.5 s, then the membrane potential was increased in 20 mV steps from 40 mV through to -100 mV, each voltage was held for 2 s, followed by -40 mV for 0.5 s (Figure 4-7 a). Water-injected oocytes as controls were included in all experiments. All experiments were performed at room temperature (~ 20 ℃). The I-V curves were obtained by plotting the steady-state (the last 0.2 ms) current response of the oocytes at each voltage step and analysed with Clampfit 10.2 software.

4.3 Results

4.3.1 AtPIP1;2

Fang *et al*. (2002) used CO_2/HCO_3^- solution (33 mM $NaHCO_3$) to test the CO_2 permeability of hsAQP1 (Fang et al., 2002), therefore this solution was used to characterize whether *AtPIP1;2* injected oocytes show ion conductivity. There were no significant differences (analysed using the unpaired t test by Prism5.0) in the ionic currents between water-injected oocytes and *AtPIP1;2* injected oocytes in response to either ND96 or CO_2/HCO_3^- over the voltage range of 40 mv to -100 mV (Figure 4-2 and 4-3).

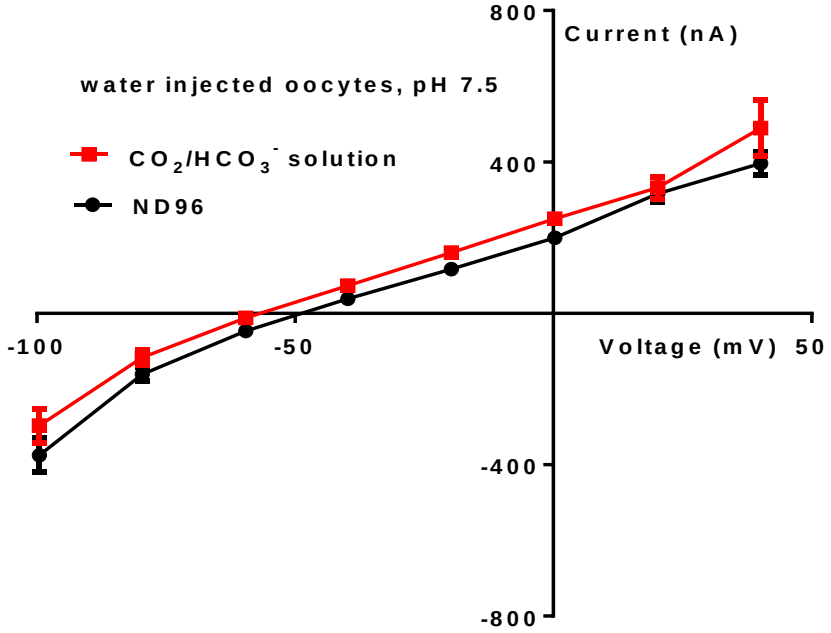

Figure 4-2 Current-voltage curves for oocytes injected with water in pH 7.5 solutions with different anions: ND96 solution (●) and CO_2/HCO_3^- solution (■). N=17 oocytes for each solution.

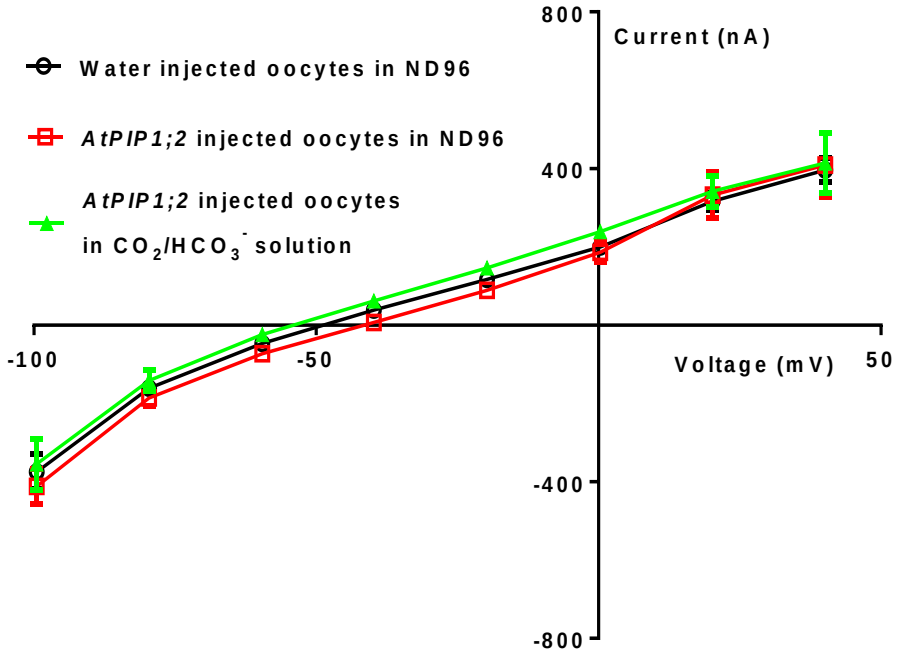

Figure 4-3 Current-voltage curves for *AtPIP1;2* expressing oocytes in solutions with different anions: ND96 (□) and CO_2/HCO_3^- (▲). Water injected oocytes in ND96 (○). N=17 oocytes for each solution.

4.3.2 AtPIP2;2

AtPIP2;2 shares 93% similarity with AtPIP2;1 according to the alignment result which will be discussed in detail in the discussion of this chapter. AtPIP2;2 showed obvious water permeability (Figure 4-4), however, no significant increase in ion currents compared with water-injected oocytes (Figure 4-5 and 4-6) for various bath solutions that were also tested on AtPIP2;1. The details of the currents induced by AtPIP2;1 will be discussed later.

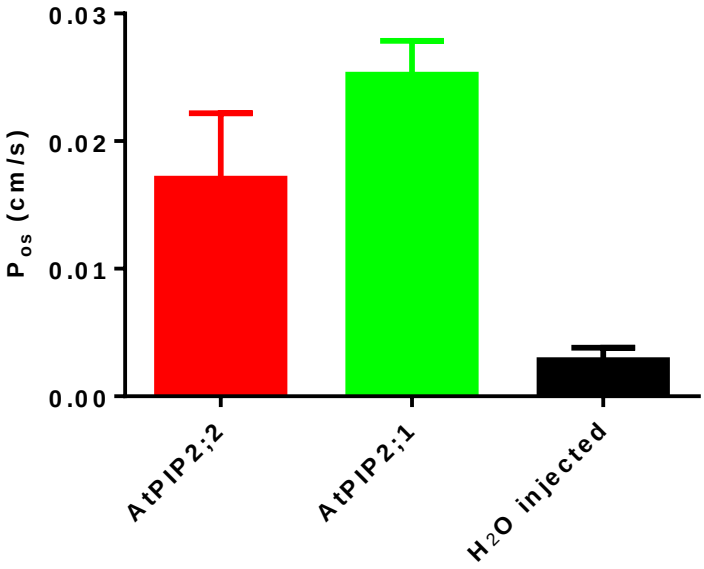

Figure 4-4 Water permeability of AtPIP2;1, AtPIP2;2 and water injected oocytes.

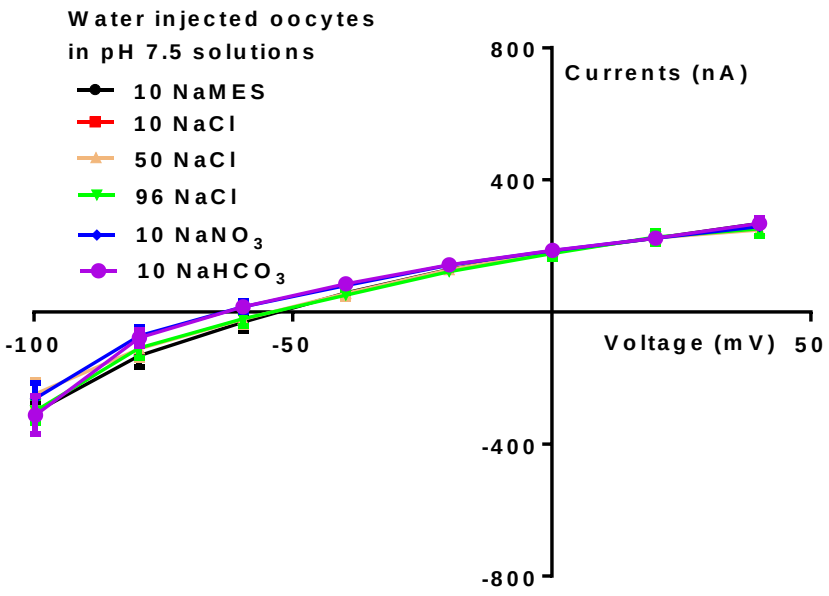

Figure 4-5 Current-voltage curves for oocytes injected with water in pH 7.5 solutions with different anions: 10 NaMES (●), ND10 (■), ND50 (▲), ND96 (▼), 10 $NaNO_3$ (♦) and 10 $NaHCO_3$ (●), respectively. N=6 oocytes for each solution.

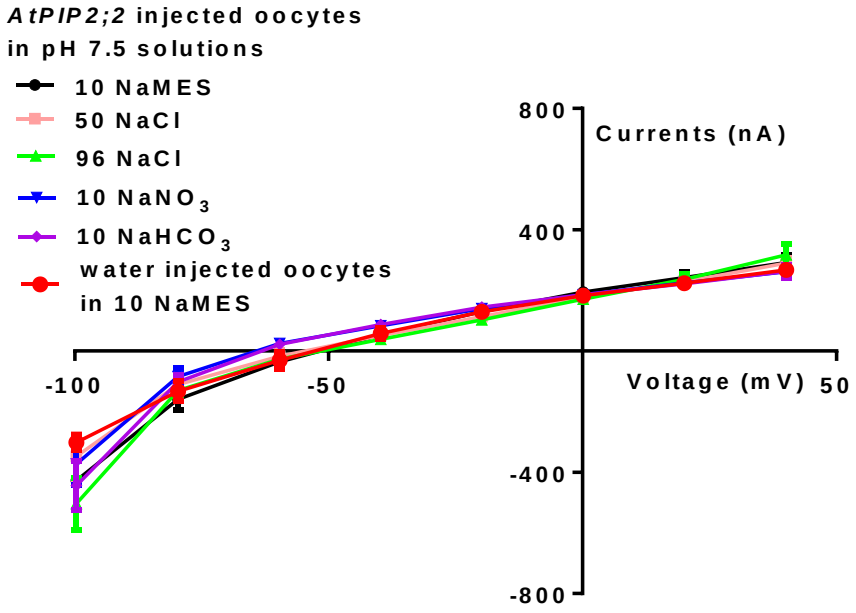

Figure 4-6 Current-voltage curves for oocytes injected with *AtPIP2;2* in pH 7.5 solutions with different anions: 10 NaMES (●), ND50 (▲), ND96 (▼), 10 $NaNO_3$ (♦), 10 $NaHCO_3$ (●), respectively. Water injected oocytes in ND50, pH 7.5 (●). N=5 oocytes for each solution.

4.3.3 AtPIP2;1

Figure 4-7 illustrates an example of currents observed with control which is water injected oocytes and *AtPIP2;1* injected oocytes bathed in ND96 solution upon a series of changes in voltage. *AtPIP2;1* injected oocytes showed significantly larger inward and outward currents compared to control water injected oocytes both in ND96 and CO_2/HCO_3^- solutions. The currents in the two solutions are almost the same.

The intercept of the current/voltage (I/V) curve on the voltage axis is the reversal potential, where all net ion currents are zero, and should be equal to the resting membrane voltage. Compared to water injected oocytes (control) (reversal potential: -41.52 mV in ND96), the reversal potentials of *AtPIP2;1* injected oocytes were more positive: – 30.55 mV (ND96) and -32.31 mV (CO_2/HCO_3^-). These reversal potentials were more positive than -40 mV because the expression of *AtPIP2;1* induced membrane depolarisation (Figure 4-8).

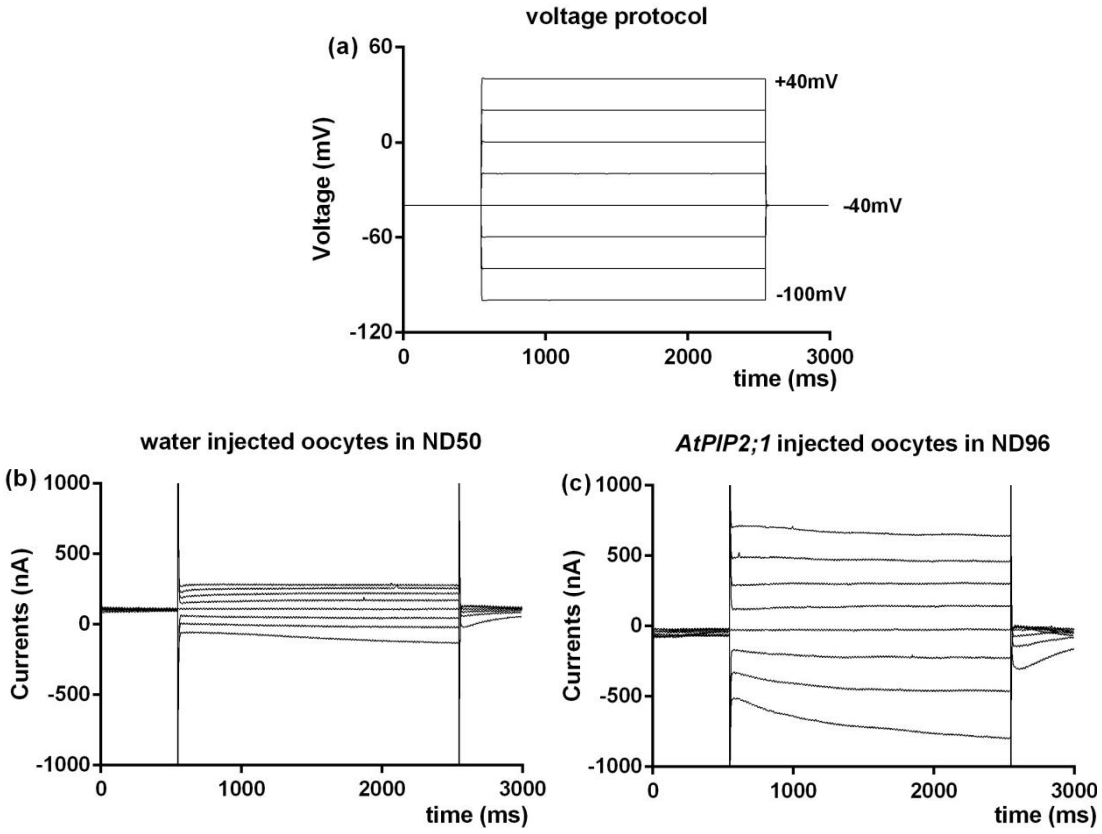

Figure 4-7 (a): Voltage protocol. An example of current versus time traces at each voltage of (b): water injected control oocytes, and (c): *AtPIP2;1* cRNA injected oocytes bathed in ND96.

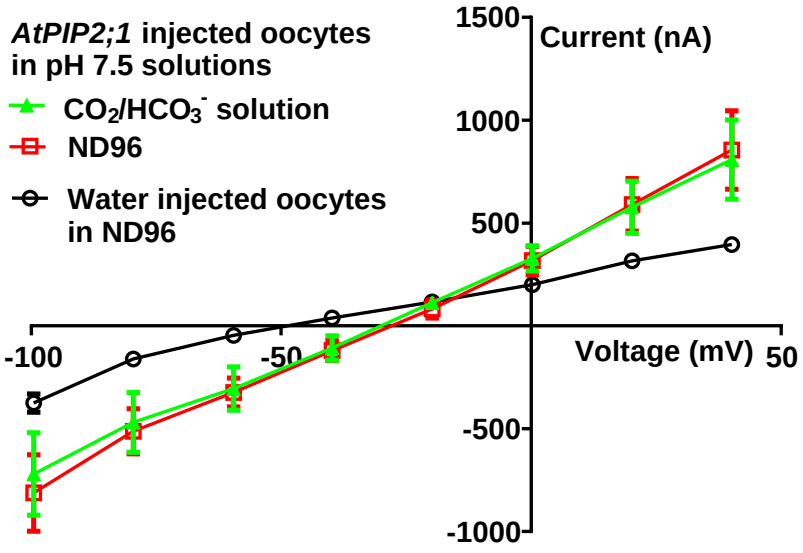

Figure 4-8 Current-voltage curves for AtPIP2;1 expressing oocytes in pH 7.5 solutions with different anion: ND96 (□) and CO_2/HCO_3^- (▲). Water injected oocytes in ND96 (o). N=7 oocytes for each solution.

Varying the concentration of NaCl did not significantly change ionic currents in water injected oocytes (Figure 4-9). By contrast, both inward (negative) and outward (positive) currents of *AtPIP2;1* injected oocytes gradually increased with increasing external NaCl concentration. An approximately 10-fold change in the external [Cl^-] concentration at constant external osmolarity adjusted by mannitol, from 10 NaMES (see components in "solutions" above, contained 7.6 mM Cl^-) to ND96, led to a two-fold increase of outward currents and 3.4-fold increase of inward current and the reversal potential shifting positively, from -44.7 mV to -26.6 mV (Figure 4-10). The outward currents at 40 mV and inward current at -100 mV were fitted using a Michaelis-Menten equation, the currents at both 40 mV and -100 mV appeared to saturate at 17.6 mM of [Cl^-] concentration (Figure 4-11).

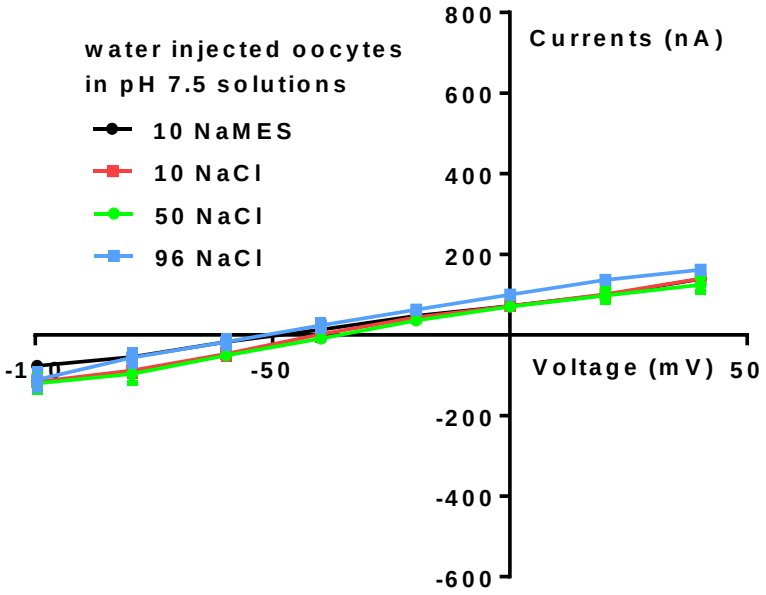

Figure 4-9 Current-voltage curves for oocytes injected with water, in pH 7.5 solutions with different NaCl concentrations: 10 NaMES (●), ND10 (■), ND50 (●), ND96 (■), respectively. N=4 oocytes for each solution.

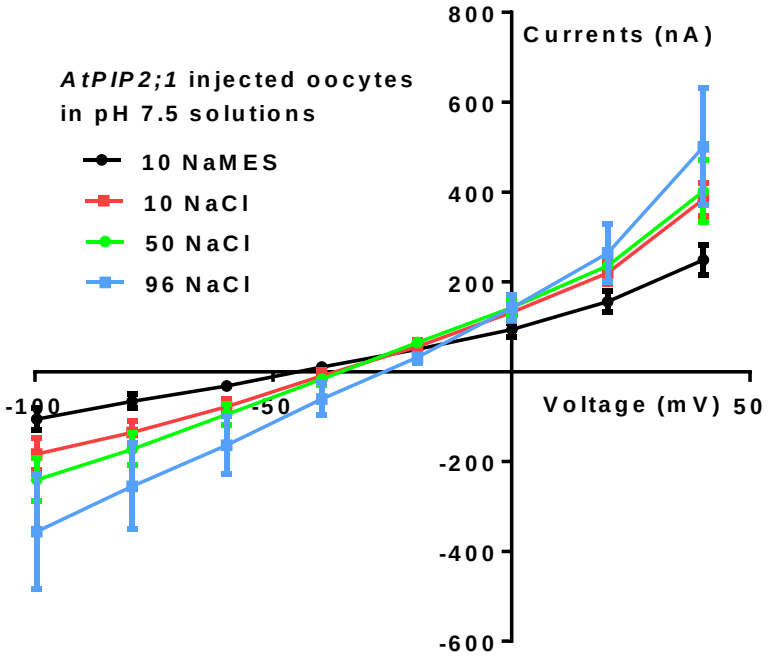

Figure 4-10 Current-voltage curves for oocytes injected with *AtPIP2;1* cRNA, in pH 7.5 solutions with different NaCl concentrations: 10 NaMES (●), ND10 (■), ND50 (●), and ND96 (■), respectively. N=8 oocytes for each solution.

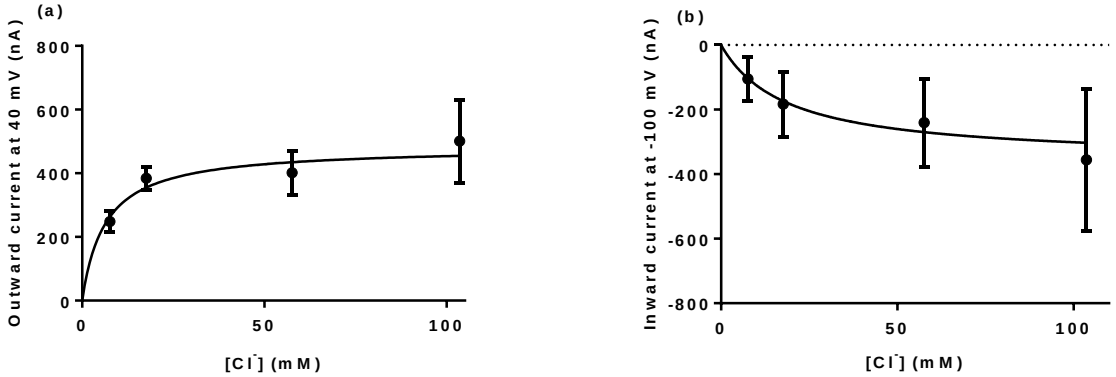

Figure 4-11 Concentration dependence of outward current at 40 mV (a) and -100 mV (b) for oocytes injected with *AtPIP2;1* cRNA in pH 7.5 solutions with different varying $[Cl^-]$ as shown in Figure 4-10. (a) R^2=0.2270 and (b) R^2=0.2920.

4.3.4 Co-expression of *AtPIP1;2* and *AtPIP2;1*

According to the results in Chapter 3, AtPIP1;2 and AtPIP2;1 strongly interact in terms of measured water permeability. The electrophysiology experiments above showed that when AtPIP2;1 was expressed alone in oocytes, significant ionic currents were observed. However, no significant ionic currents were observed in oocytes when equal amounts of AtPIP1;2 and AtPIP2;1 were co-expressed compared to water injected oocytes (Figure 4-12). Ordinary one-way ANOVA showed that *AtPIP2;1* injected oocytes showed significant difference (****) of the current at 40 mV compared to the water injected oocytes, whereas the co-injection oocytes showed no significant difference (ns). Lower pH (pH 6.5) of ND96 (Figure 4-13) and higher pH (pH 8.5) of ND96 (Figure 4-14) were also tested and similar results were observed. However, at higher pH, the intensity of both inward and outward currents is higher.

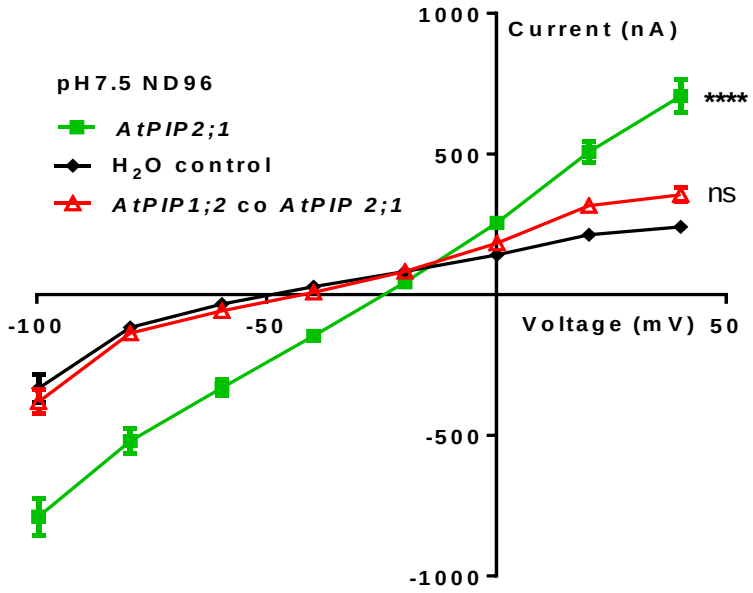

Figure 4-12 Current-voltage curves for H_2O injected oocytes (◆), *AtPIP2;1* injected oocytes (■) and equal amount of *AtPIP2;1* and *AtPIP1;2* co-injected oocytes (△) in pH 7.5 ND96 solution. N=15-21 oocytes for each solution.

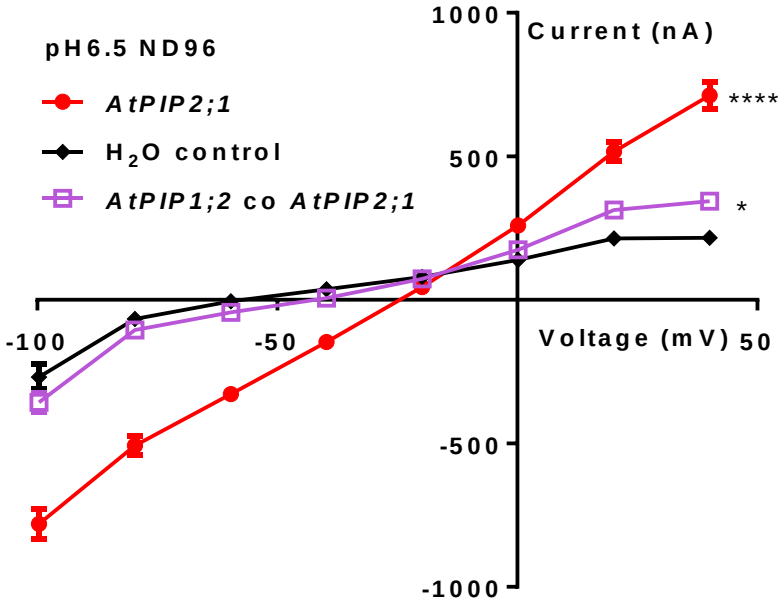

Figure 4-13 Current-voltage curves for H_2O injected oocytes (◆), *AtPIP2;1* injected oocytes (●) and equal amount of *AtPIP2;1* and *AtPIP1;2* co-injected oocytes (□) in pH 6.5 ND96 solution. N=15-21 oocytes for each solution.

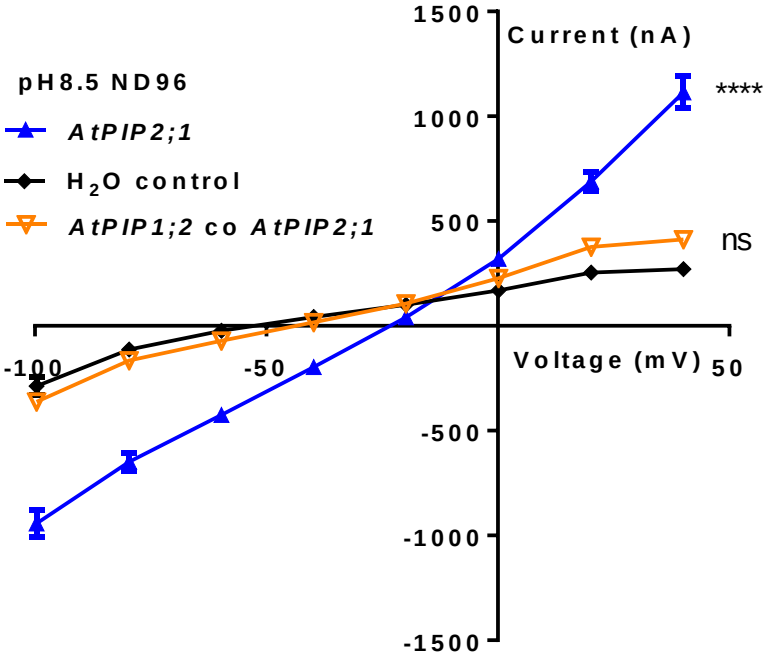

Figure 4-14 Current-voltage curves for H_2O injected oocytes (◆), *AtPIP2;1* injected oocytes (▲) and equal amount of *AtPIP2;1* and *AtPIP1;2* co-injected oocytes (▽) in pH 8.5 ND96 solution. N=15-21 oocytes for each solution.

4.3.5 Ionic selectivity of *AtPIP2;1*

Varying the concentration of Cl^- at a fixed Na^+ concentration did not induce change of ionic currents in water injected oocytes (Figure 4-15). By contrast, both inward and outward currents of *AtPIP2;1* injected oocytes gradually increased with increasing external Cl^- concentration. An approximately 7-fold change in the external Cl^- concentration, from 50 NaMES to 50 NaCl, leads to a 1.5-fold increase in outward current and 2.3-fold increase in inward current, with the reversal potential shifting positively, from -31.25 mV to -20.55 mV (Figure 4-16). Since Na^+ concentration was constant this increase in current indicates a Cl^- dependent conductance. The Cl^- equilibrium potential for *Xenopus* oocytes under these

conditions would be –7.36 mV in an external Cl^- concentration of 57.6 mM (The calculation is using Nernst Equation which will be discussed later).

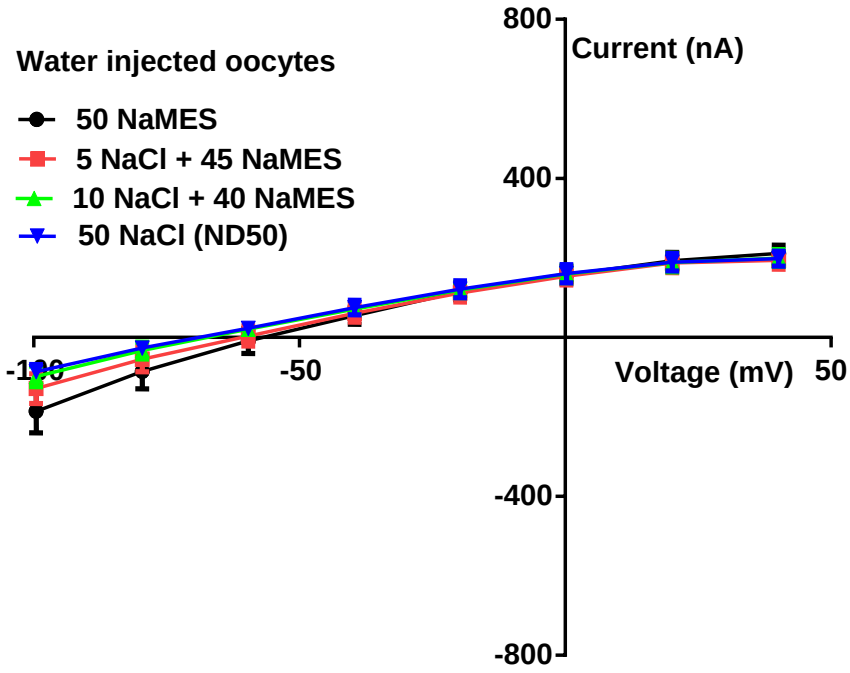

Figure 4-15 Current-voltage curves for oocytes injected with water, in pH 7.5 solutions with different Cl^- concentrations and constant Na^+ concentration: 50 mM NaMES, 7.6 mM Cl^- (●), 5 mM NaCl and 45 mM NaMES, 12.6 mM Cl^- (■),10 mM NaCl and 40 mM NaMES, 17.6 mM Cl^- (▲) and 50 mM NaCl, 57.6 mM Cl^- (▼), respectively. N=4 oocytes for each solution.

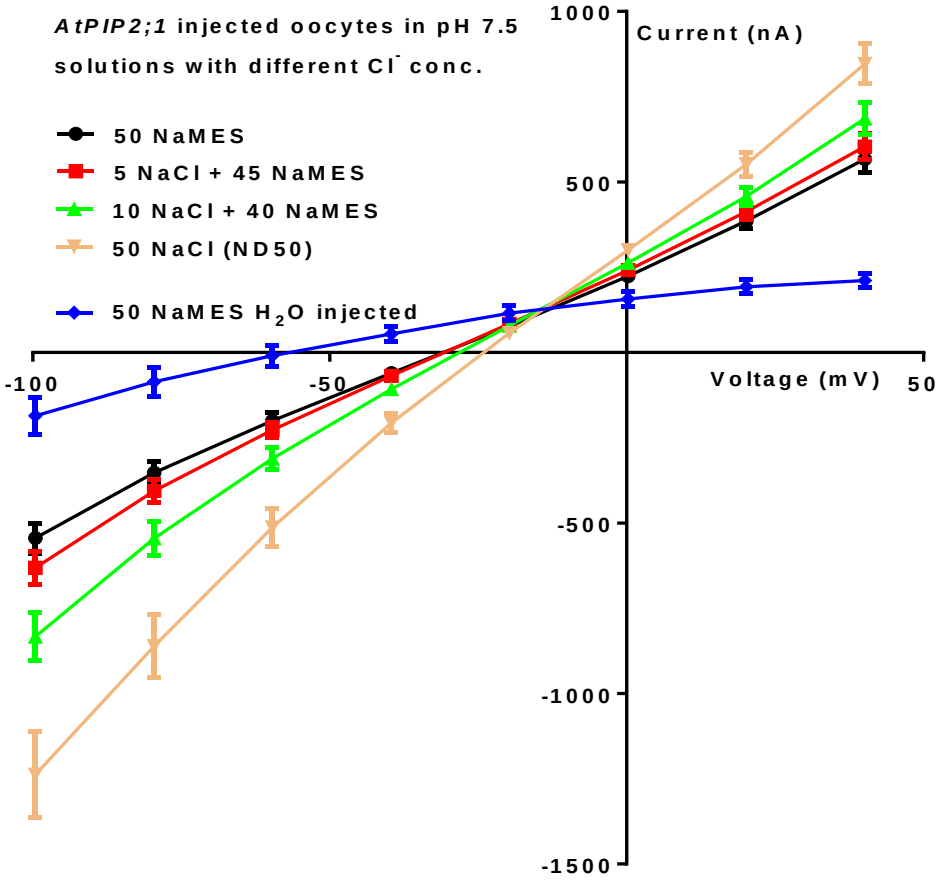

Figure 4-16 Current-voltage curves for oocytes injected with *AtPIP2;1* in pH 7.5 solutions with different Cl^- concentrations and constant Na^+ concentration: 50 mM NaMES, 7.6 mM Cl^- (●), 5 mM NaCl and 45 mM NaMES, 12.6 mM Cl^- (■),10 mM NaCl and 40 mM NaMES, 17.6 mM Cl^- (▲) and 50 mM NaCl, 57.6 mM Cl^- (▼), respectively. Water injected oocytes (◆). N=18 oocytes for each solution.

Ionic selectivity of the AtPIP2;1 induced currents was also tested with different anions and the effect of external pH was also examined. No significant ionic currents were observed for water-injected oocytes in different bath solutions examined at pH 7.5 and pH 8.5 (Figure 4-17). Currents induced by AtPIP2;1 in response to different anions was investigated with constant cation concentration. Similar outward current were observed from oocytes exposed to 10 NaCl or 10 $NaNO_3$, respectively. However, the outward currents obtained with 10

$NaHCO_3$ and 10 NaMES were lower (Figure 4-18a), but still higher than observed with the H_2O controls. Ordinary one-way ANOVA showed that *AtPIP2;1* injected oocytes showed significant difference (Significant results were marked with stars, and the number of stars indicates the significance level. **** for 10 NaCl, 10 $NaNO_3$ and 10 $NaHCO_3$ or *** for NaMES) of the current at 40 mV compared to the water injected oocytes in different solutions. The inward currents were also different in each solution, although, in 10 NaMES, 10 $NaNO_3$ and 10 $NaHCO_3$, the inward currents at -100 mV were similar (-105.3 nA, -93.3 nA and -78.7 nA, respectively). In 10 NaCl solution, the inward current was almost twice that observed with the other anions (-183.3 nA). Figure 4-18b shows more detail of the currents near the reversal potentials. There was an obvious positive shift in reversal potential (by 12 mV) with NaCl, while with NO_3^- and HCO_3^- the reversal potential shifted to more negative values by 10 mV. The same experiment was repeated at pH 8.5, except without 10 $NaHCO_3$ as it precipitates at pH 8.5 (Figure 4-19), the magnitude of the currents was slightly higher, however, a similar trend of the currents observed with the reversal potential for Cl more positive than NO_3^- (12.7 mV).

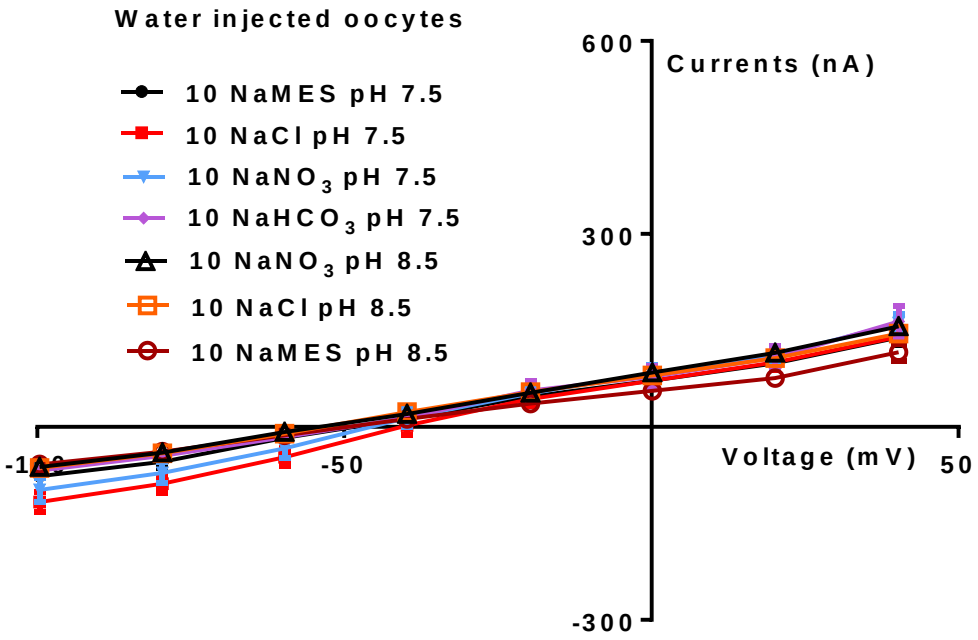

Figure 4-17 Current-voltage curves for oocytes injected with water in solutions with different anions and different pH. pH 7.5 solutions: 10 mM NaMES (●), 10 mM NaCl (■), 10 mM $NaNO_3$ (▼) and 10 mM $NaHCO_3$ (♦), respectively. pH 8.5 solutions: 10 mM NaCl (□), 10 mM $NaNO_3$ (△) and 10 mM NaMES (○), respectively. N= 4 oocytes for each solution.

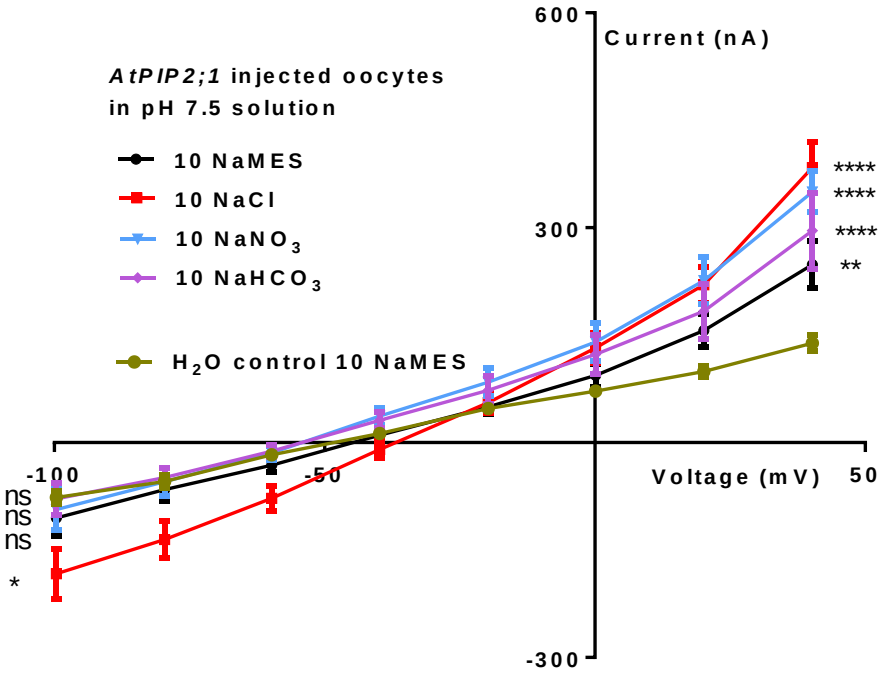

Figure 4-18a Current-voltage curves for oocytes injected with *AtPIP2;1* cRNA in pH 7.5 solutions with different anion concentrations: 10 mM NaMES (●),10 mM NaCl (■),50 mM NaCl (▲)10 mM $NaNO_3$ (▼) and 10 mM $NaHCO_3$ (♦), respectively. Water injected oocytes in pH 7.5, 10 mM NaMES (●). Significance was shown in the figure. N= 8 oocytes for each solution.

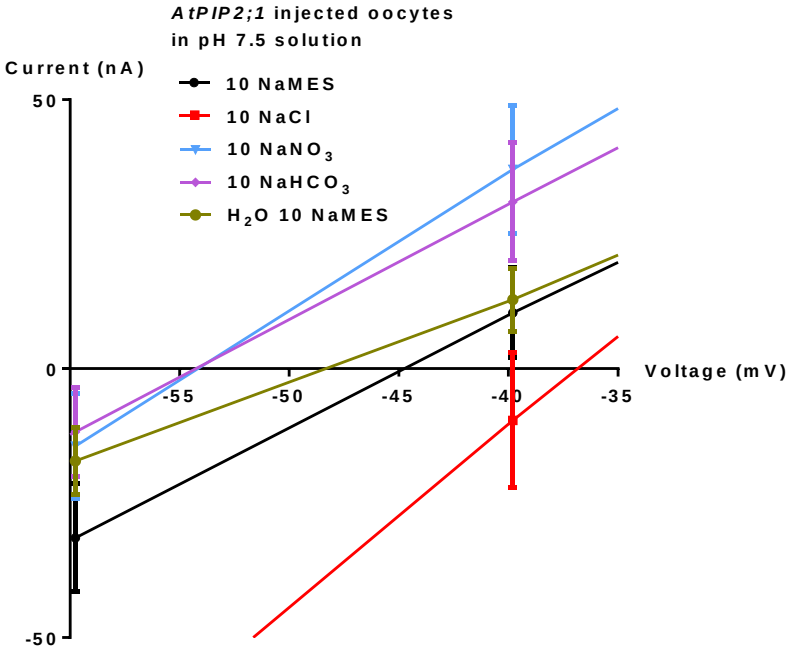

Figure 4-18b Detail of currents near the reversal potential from Figure 4-18a.

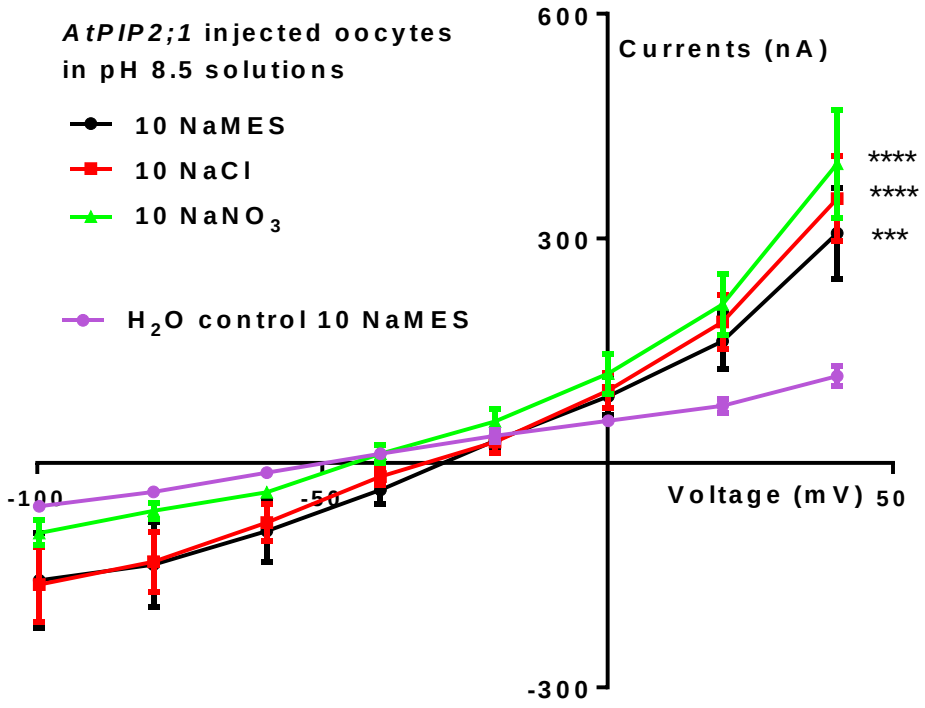

Figure 4-19 Current-voltage curves for oocytes injected with *AtPIP2;1* cRNA in pH 8.5 solutions with different anion concentrations: 10 mM NaMES (●), 10 mM NaCl (■) and 10 mM NaNO3 (▲), respectively. Water injected oocytes in pH 8.5, 10 mM NaMES (●). Significance was shown in the figure. N = 5 oocytes for each solution.

4.3.6 Increasing *AtPIP2;1* cRNA concentration

Increasing amounts of cRNA for *AtPIP2;1* were injected to examine the effect of cRNA content on the ionic currents induced by *AtPIP2;1*. In pH 7.5 ND50 solution, both inward and outward currents increased with increasing amount of cRNA. The expression of 3 ng *AtPIP2;1* in oocytes resulted in a significant increase of current from 226 nA to 674 nA in 50 NaCl solution at 40 mV, and from -57 nA to -513 nA at -100 mV (Figure 4-20a). However, with the increment of cRNA concentration, both the inward and outward currents were saturated at a cRNA concentration of about 6 ng (Figure 4-20b,c).

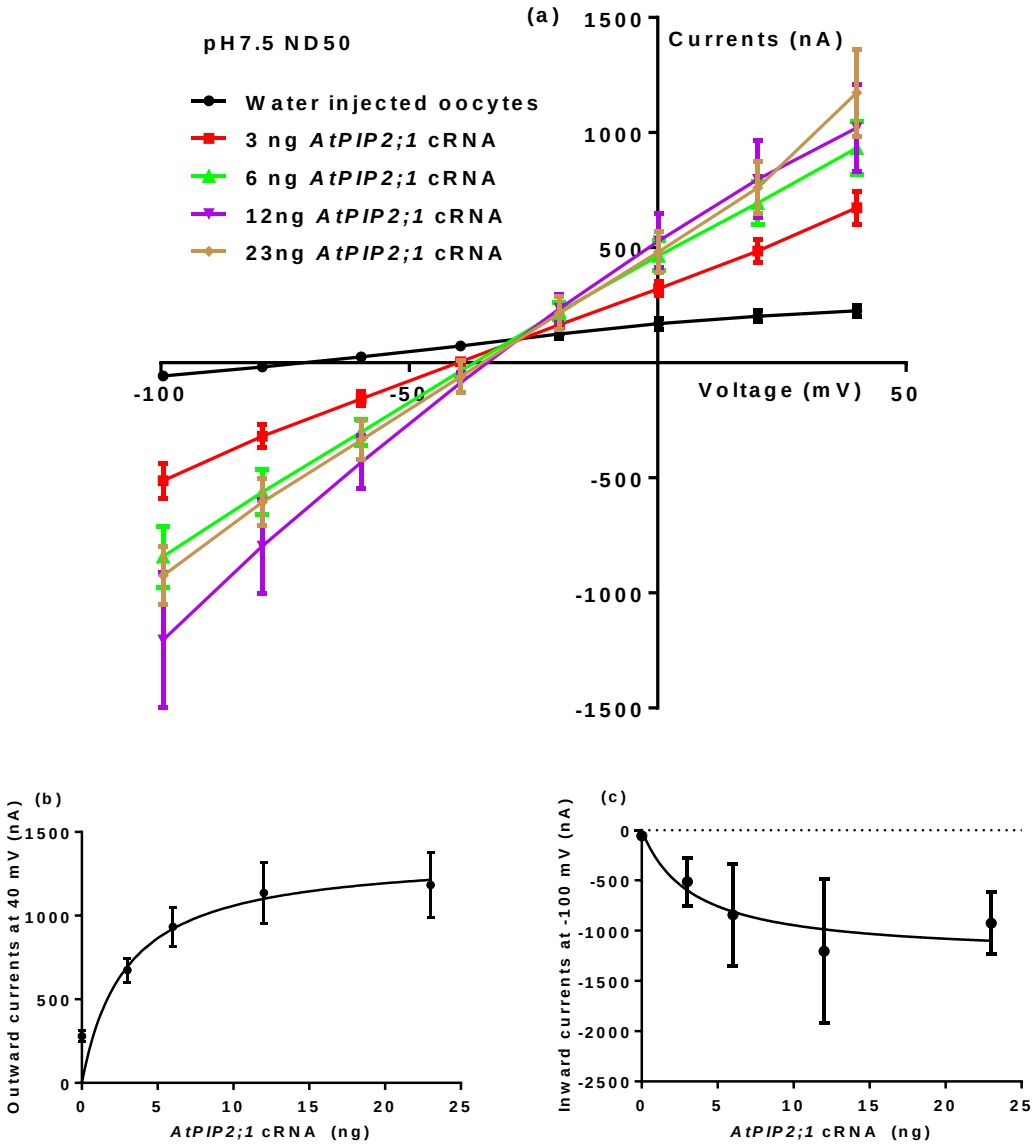

Figure 4-20 (a): Current-voltage curves for oocytes injected with different amount of *AtPIP2;1* cRNA, in pH 7.5 ND50 solution. Water-injected control (●), 3 ng *AtPIP2;1* cRNA (■), 6 ng *AtPIP2;1* (▲), 12 ng *AtPIP2;1* (▼) and 23 ng *AtPIP2;1* (●), respectively. Outward current (b) and inward current (c) verse cRNA concentration curves for oocytes injected with different amount of *AtPIP2;1* cRNA. For (b), V_{max} = 1367 K_m = 2.911 and (c) V_{max} = 1259 K_m = 3.316. N=4-15 oocytes for each solution.

4.3.7 Effect of ion channel blockers on AtPIP2;1 induced ion currents

Niflumic acid (NFA), a potent but relatively non-selective blocker of anion channels (Garrill et al., 1996; Souktani et al., 2000; Kucherenko et al., 2013), was tested. The AtPIP2;1 induced currents were significantly blocked (Figure 4-21). At lower Cl^- concentration (10 NaMES, 7.6 mM Cl^-), the blockage effect was not significant (Figure 4-21 a), however in ND10 solution (17.6 mM Cl^-), 200 μM NFA decreased the peak outward current at 40 mV from approximately 384 nA to 165 nA, and the inward current from -183 nA to -62 nA, which are similar to that of the current of water injected oocytes (Figure 4-21 b). NFA has the same inhibition effect in ND50 (57.6 mM Cl^-) solution and ND96 solution (103.6 mM Cl^-), respectively (Figure 4-21 c-d). The aquaporin blocker silver-sulfadizine (Niemietz and Tyerman, 2002) was also tested, however, when 10 μM final concentration of silver-sulfadizine was added, the currents were very large and the oocytes could not be clamped properly.

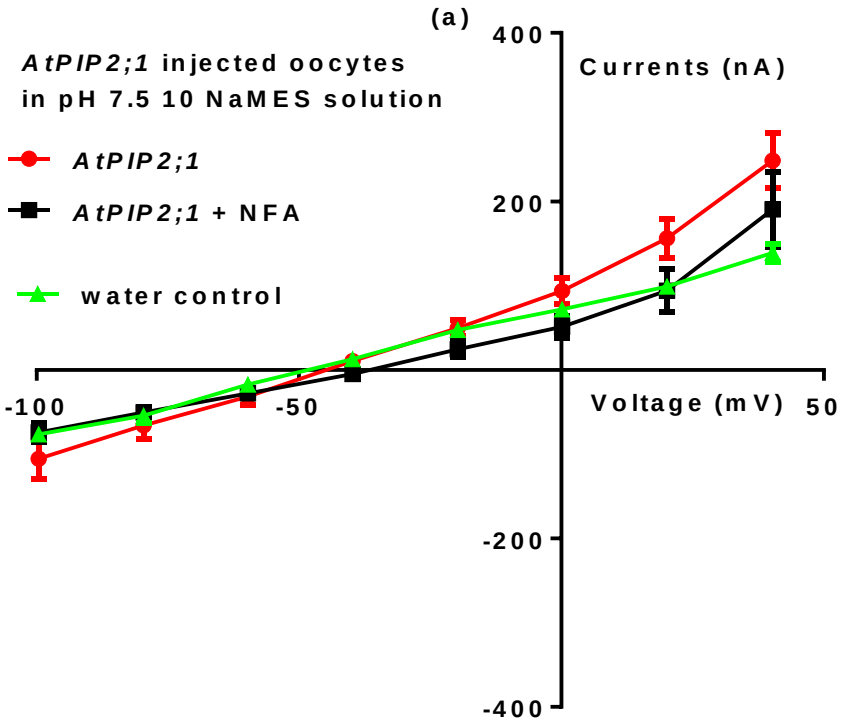
(a)
AtPIP2;1 injected oocytes
in pH 7.5 10 NaMES solution
AtPIP2;1
AtPIP2;1 + NFA
water control
400
200
-200
-400
Currents (nA)
Voltage (mV)
-100
-50
50

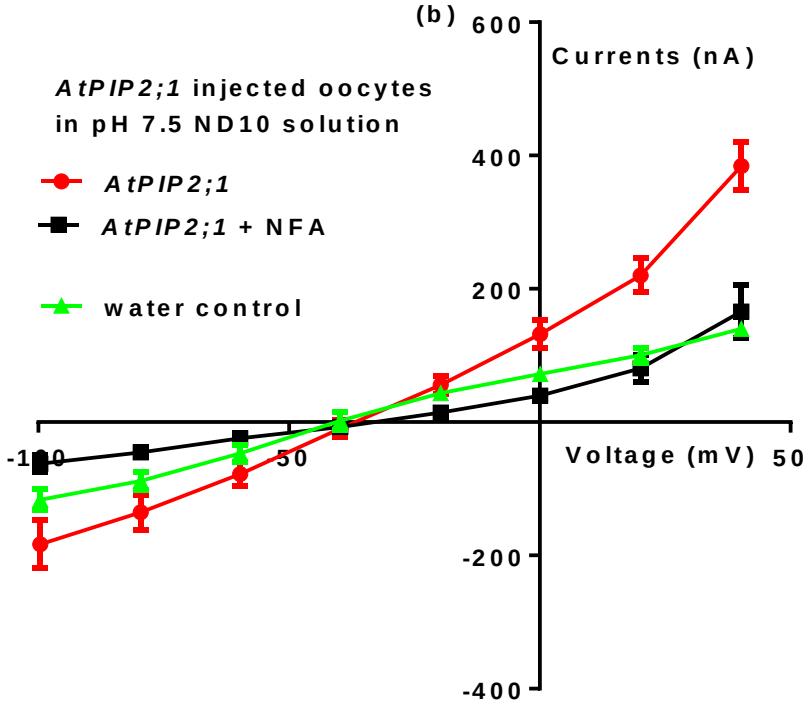
(b)
AtPIP2;1 injected oocytes
in pH 7.5 ND10 solution
AtPIP2;1
AtPIP2;1 + NFA
water control
600
400
200
-200
-400
Currents (nA)
Voltage (mV)
50

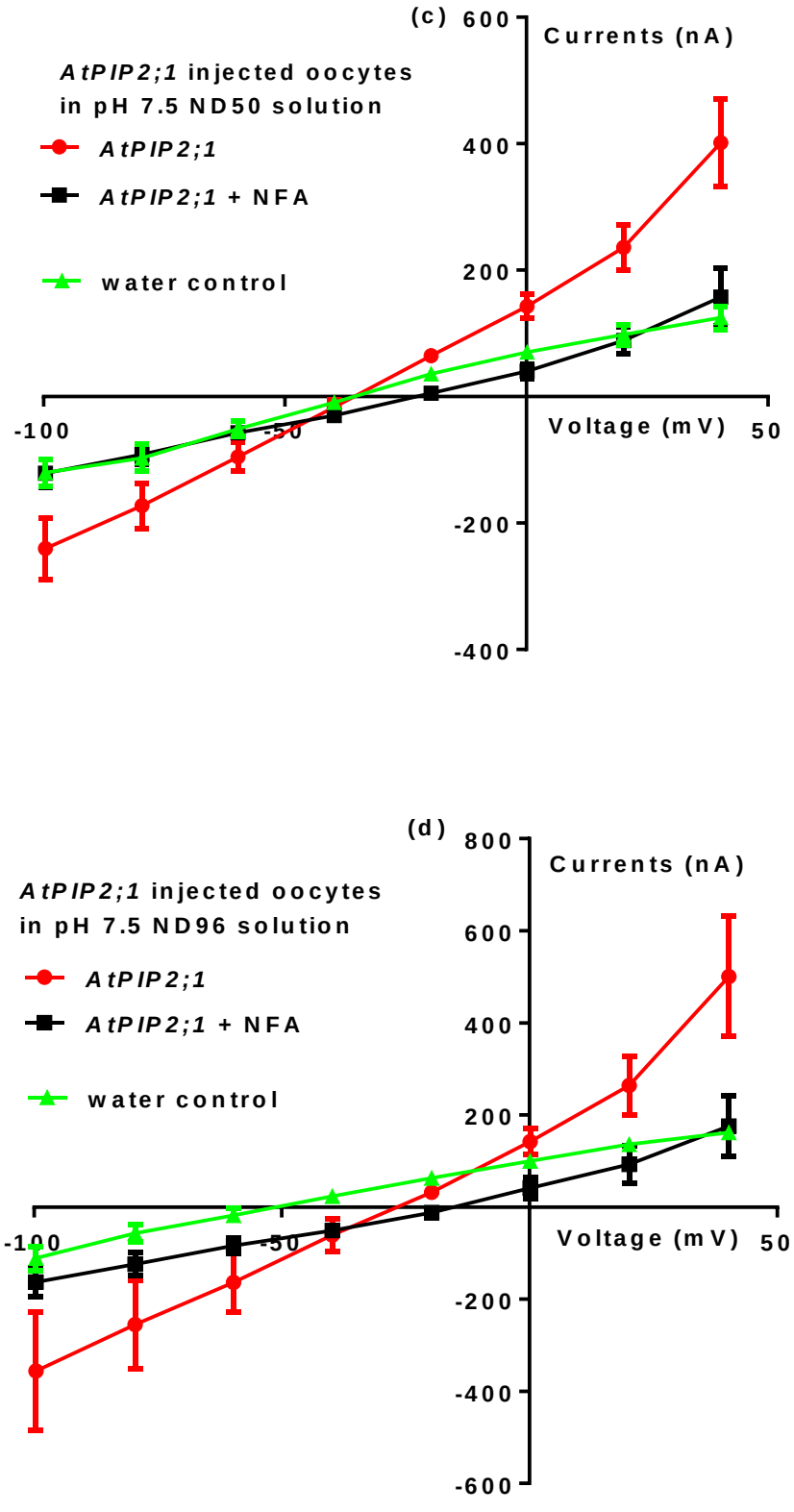

Figure 4-21 Current-voltage curves for oocytes injected with *AtPIP2;1* in pH 7.5 solutions with different [Cl^-] concentrations with (■) and without 200 μM NFA (●). (a): 10 NaMES; (b): ND10; (c): ND50; (d): ND96. Water-injected control (▲). N= 3-8 oocytes for each solution.

Two other ion channel blockers, NPPB (5-Nitro-2-(3-phenylpropylamino) benzoic acid) (200 μM) (Garrill et al., 1996; Aiken et al., 2012) and lanthanum chloride (200 μM) (Friedman et al., 1998) were also tested. These blockers had no significant effects on the currents in water injected control oocytes (Figure 4-22). No significant change of currents were observed with the oocytes that co-express AtPIP1;2 and AtPIP2;1 (Figure 4-23). For *AtPIP2;1* injected oocytes, all inhibitors can decrease the outward current as well as the inward currents as shown in Figure 4-24a. 200 μM NPPB decreased the outward current at 40 mV from 415 nA to 190 nA and the inward current from -283 nA to -104 nA, while 200 μM $LaCl_3$ decreased the outward current from 415 nA to 220 nA and the inward current from -283 nA to -59 nA. Among these three inhibitors, however, according to ordinary one-way ANOVA, NFA had the highest inhibitory effect as it brought both the inward (Figure 4-24c) and outward (Figure 4-24b) current level back to almost the same as the current from the water-injected controls.

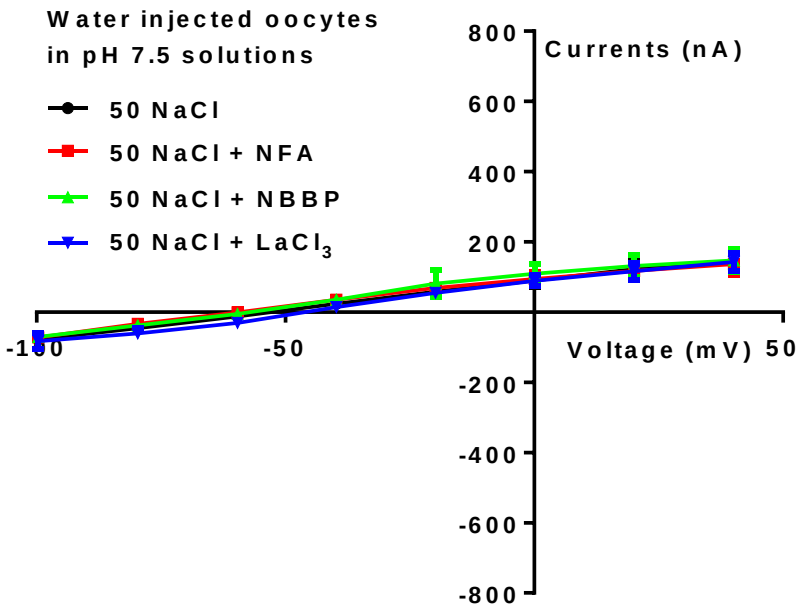

Figure 4-22 Current-voltage curves for oocytes injected with water, in pH 7.5 ND50 without inhibitors (●) or with 200 μM NFA (■), 200 μM NPPB (▲), and 200 μM $LaCl_3$ (▼), respectively. N=3 oocytes for each solution.

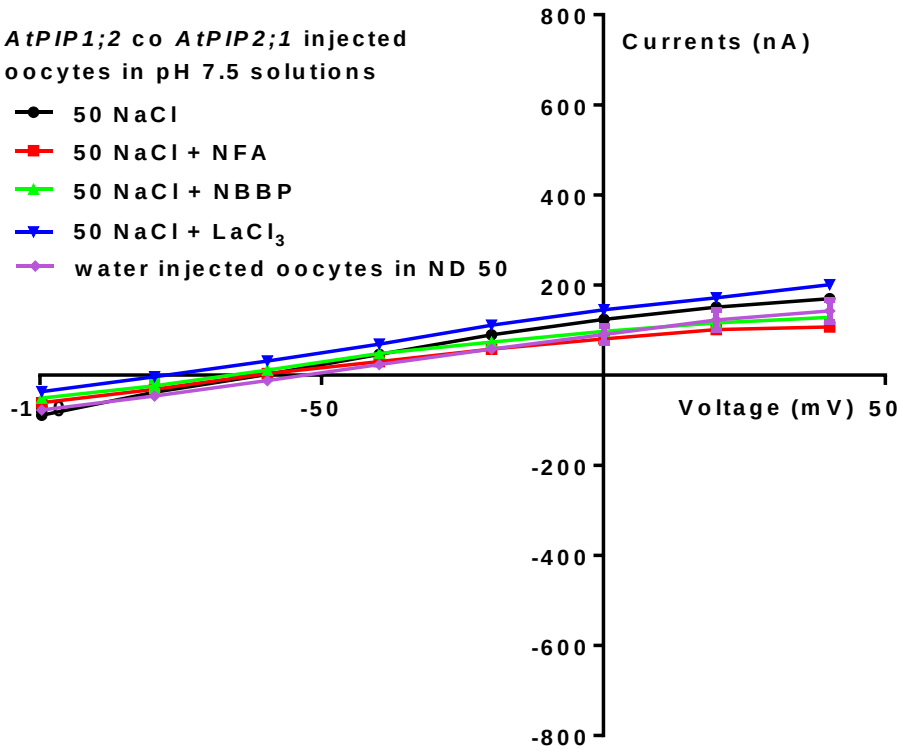

Figure 4-23 Current-voltage curves for oocytes injected with *AtPIP2;1* co *AtPIP1;2*, in pH 7.5 ND50 without inhibitors or (●) with 200 μM NFA (■), 200 μM NPPB (▲), and 200 μM $LaCl_3$ (▼), respectively. Water-injected control in pH 7.5 ND50 (♦). N=3-9 oocytes for each solution.

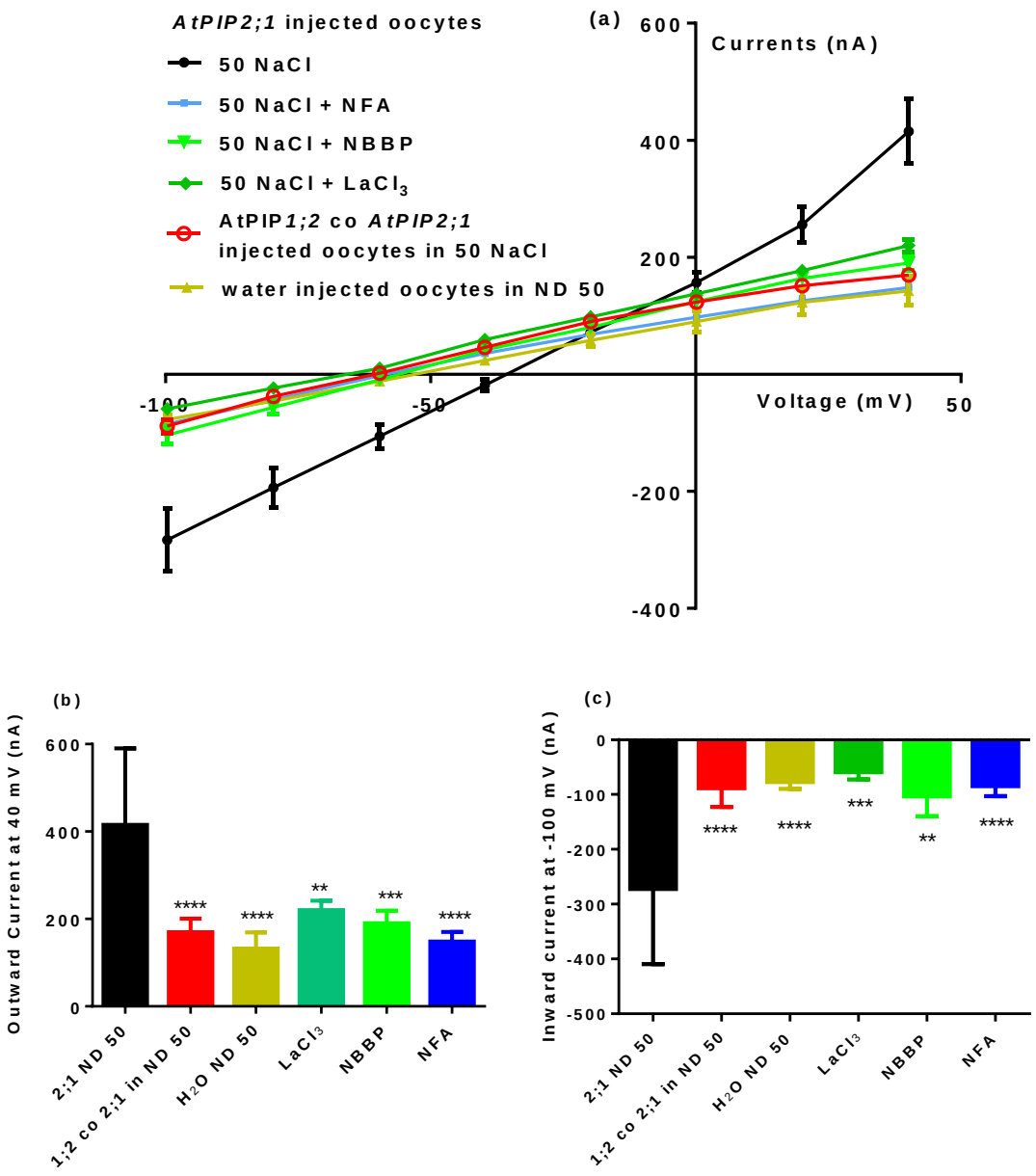

Figure 4-24 Current-voltage curves (a), outward current at 40 mV (b), and inward current at -100 mV (c), for oocytes injected with *AtPIP2;1* in pH 7.5 ND50 without inhibitors (●); with 200 μM NFA (■); 200 μM NPPB (▼) and 200 μM $LaCl_3$ (♦), respectively. *AtPIP2;1* co *AtPIP1;2* injected oocytes (O) and water control (▲) in pH7.5 ND50. N=4-10 oocytes for each solution.

4.3.8 Ion channel blocker effects on water permeability

Water permeability was not significantly inhibited by NFA or NPPB (Figure 4-25), although, however, according to ordinary one-way ANOVA, the oocytes injected with *AtPIP2;1* had a slightly lower water permeability in the presence of 200 μM $LaCl_3$.

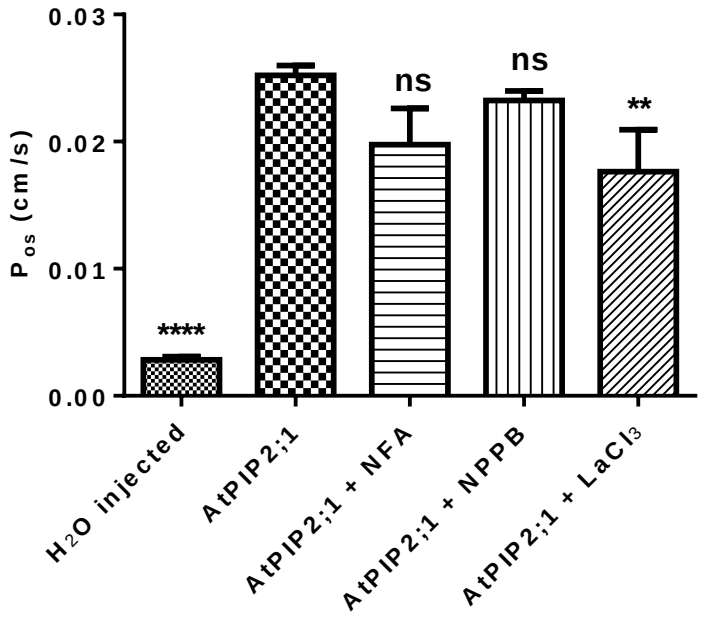

Figure 4-25 Water permeability for water control, *AtPIP2;1* injected oocytes, and *AtPIP2;1* injected oocytes in the presence of different inhibitors (200 μM NFA, 200 μM NPPB and 200 μM $LaCl_3$, respectively). N = average of more than 5 oocytes for each solution.

4.3.9 Mutant Atpip2;1 (G100W)

It was shown in Chapter 3 that the mutant G100W Atpip2;1 lost water transport function (Shelden et al., 2009), however, it can still interact with AtPIP1;2 and the co-expression of G100W Atpip2;1 and AtPIP1;2 restored water permeability. G100W Atpip2;1 was tested

with different ions. There was no difference in ion currents for different bath solutions at pH 7.5 for water-injected oocytes (Figure 4-26). For G100W Atpip2;1 no outward or inward currents were observed that were larger than the controls from oocytes exposed to 10 NaCl, 10 $NaNO_3$, 10 $NaHCO_3$ or 50 NaCl respectively (Figure 4-27), which contrasts to the results obtained with wild-type AtPIP2;1. The same result was obtained when AtPIP1;2 was co-injected with G100W Atpip2;1 (Figure 4-28) despite the fact that water permeability was significantly induced with this co-expression (Chapter 3).

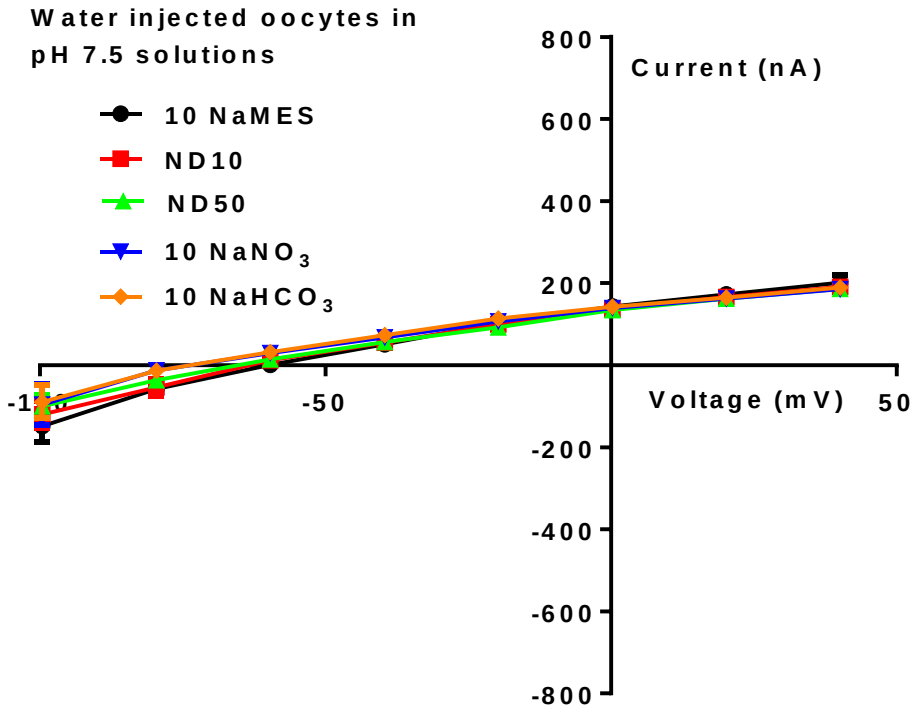

Figure 4-26 Current-voltage curves for oocytes injected with water. Oocytes were exposed to pH 7.5 solutions with 10 NaMES (●), ND10 (■), ND50 (▲), 10 $NaNO_3$ (▼), and 10 $NaHCO_3$ (◆), respectively. N=4 oocytes for each solution.

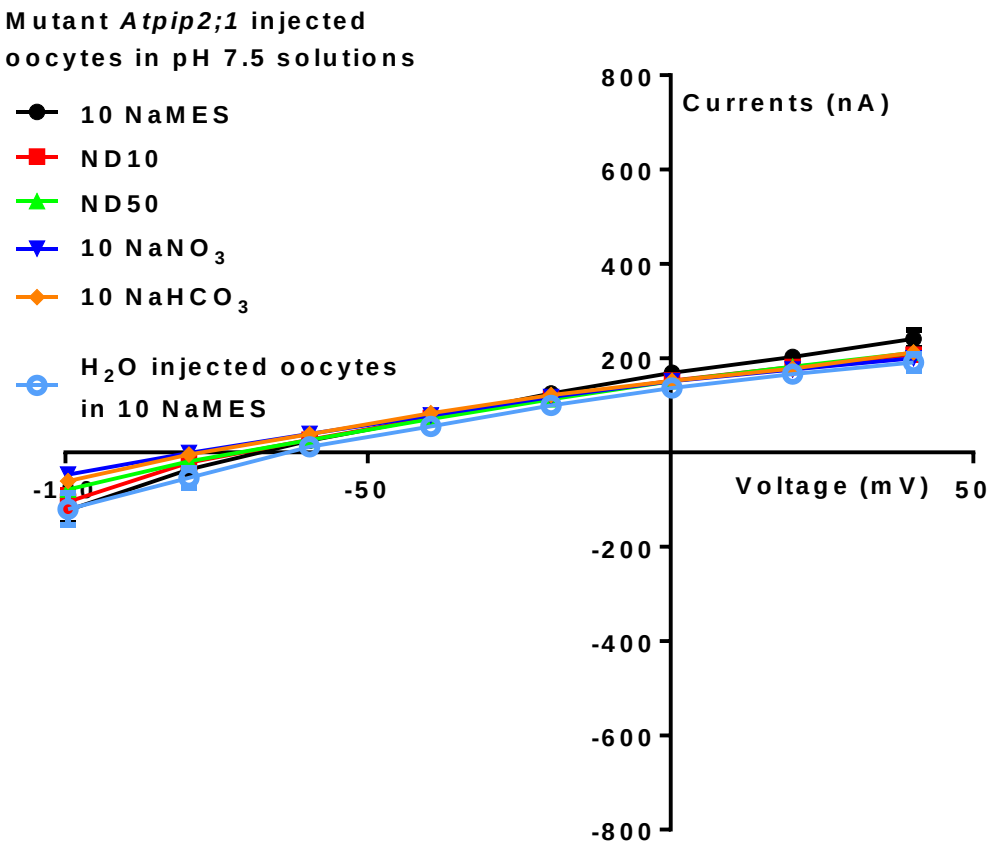

Figure 4-27 Current-voltage curves for oocytes injected with mutant *Atpip2;1*. Oocytes were exposed to pH 7.5 solutions with 10 NaMES (●), ND10 (■), ND50 (▲), 10 $NaNO_3$ (▼) and 10 $NaHCO_3$ (◆), respectively. Water control in 10 NaMES was also plotted (○). N=9 oocytes for each solution.

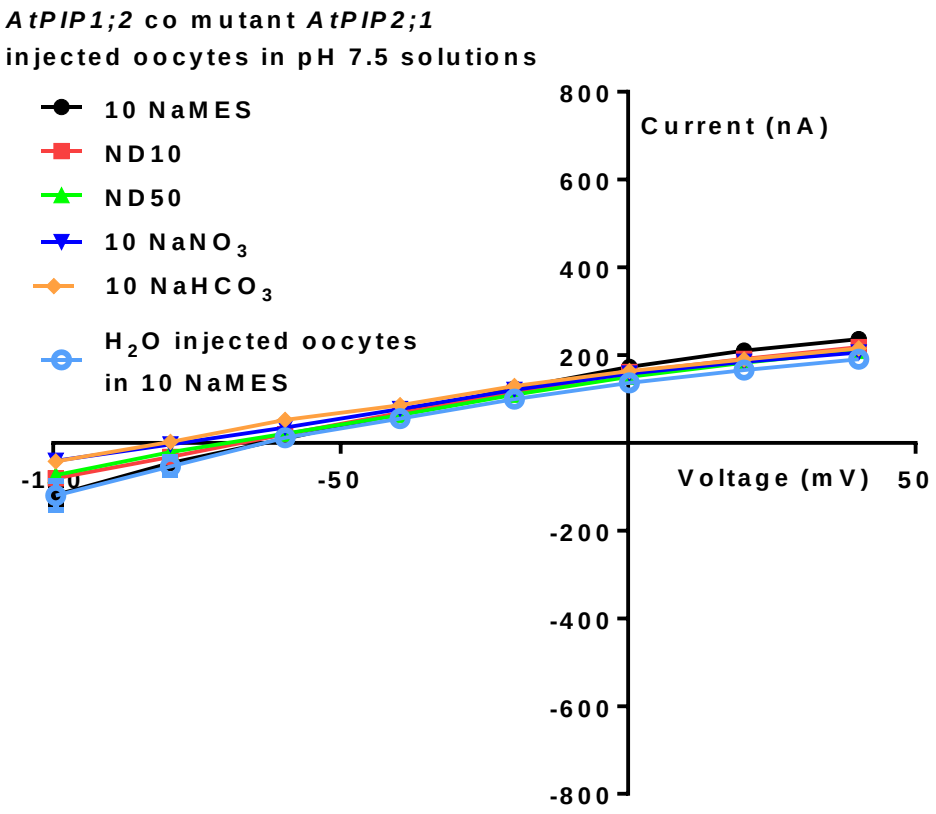

Figure 4-28 Current-voltage curves for oocytes co-injected with *AtPIP1;2* and mutant *Atpip2;1*. Oocytes were exposed to pH 7.5 solutions with 10 NaMES (●), ND10 (■), ND50 (▲), 10 $NaNO_3$ (▼) and 10 $NaHCO_3$ (◆), respectively. Water control in 10 NaMES was also plotted (○). N=5 oocytes for each solution.

4.4 Discussion

4.4.1 Aquaporin induced ion conductance

Some aquaporins can act as ion channels under certain conditions (Yool, 2006; Yool, 2007; Yool, 2007). For instance, the function of an aquaporin, Big Brain (BIB) from *Drosophila*, was characterised in *Xenopus* oocytes and it was observed that BIB does not present any water channel activity, however, it serves as a monovalent non-selective cation channel that

was activated by tyrosine kinase signalling (Yanochko and Yool, 2002). It was concluded that BIB may be essential in the neurogenic function of membrane depolarization in early development of the fly (Yool and Campbell, 2012). BIB is not the only aquaporin member that has shown ion channel activity. The human aquaporin channel 1 (hsAQP1) shows kinase A or cGMP gated non-selective ion channel activity when expressed in *Xenopus* oocytes (Yool et al., 1996; Boassa and Yool, 2003; Boassa et al., 2006). Taking a molecular modelling approach, it was shown that the ionic current carried by Na^+ probably goes through the central pore of the *AQP1* tetramer (Yu et al., 2006). In contrast, *AQP6*, when expressed in *Xenopus* oocytes, forms a pH or mercury gated anion channel where it is thought that the anion permeates through the water pore in the monomer (Ikeda et al., 2002). From my experiments, AtPIP2;1 also induced currents in *Xenopus* oocytes, whereby either AtPIP2;1 serves as an ion channel itself, or it induced ion currents through interaction with other proteins in *Xenopus* oocytes.

4.4.2 AtPIP2;1 induced currents

AtPIP1;2 and AtPIP2;2 did not induce ionic currents when expressed in *Xenopus* oocytes, even though AtPIP2;2 is water permeable and shares 93% similarity with AtPIP2;1 and only differs in certain AAs according to the alignment results (Figure 4-29, high light in yellow). Thus if there are differences in ion currents induced by either aquaporin it may be useful to probe the differences in the amino acids between the AtPIP2;1 and AtPIP2;2. The sequences of these two aquaporins (AtPIP2;2 and AtPIP2;1) were obtained from NCBI (http://www.ncbi.nlm.nih.gov/) and agree 100% with the sequence obtained for my cDNA (See Appendix for DNA sequence alignments). Sequence alignments were conducted by

using Clustal Omega (http://www.ebi.ac.uk/Tools/msa/clustalo/) with default settings (Figure 4-29). Interestingly, some of those different amino acids also have different charge: at the N-terminal, the gln19 in AtPIP2;1 is an uncharged AA whereas the glu17 is negatively charged; the asp69 in loop A of AtPIP2;1 is negatively charged, however the corresponding lys67 in AtPIP2;2 is positively charged; the thr152 in loop C of AtPIP2;1 has no charge, however the asp150 in AtPIP2;2 is negatively charged. These different charges may be relevant to the anion conductance in AtPIP2;1. Meanwhile, another difference is that with the loop C ser166 and loop D ser194 in AtPIP2;1, the correspondent AAs in AtPIP2;2 are: asn164 and asn193, this is very important because some reports demonstrated that aquaporin function and localization can be affected by phosphorylation of certain serine residues (Johansson et al., 1998; Procino et al., 2003; Prado et al., 2013). Therefore, if the two ser in AtPIP2;1 are phosphorylated, there may be an effect on AtPIP2;1 function.

The mammalian AQP6 (accession number: NP_071517) was demonstrated as an anion channel that is selective for nitrate as discussed above. Therefore alignment of AQP6 with AtPIP2;1 and AtPIP2;2 was also examined (Ikeda et al., 2002; Liu et al., 2005) (Figure 4-29). The underlined (bold) region is the loop D of AQP6 and this region was implicated as essential and relevant for ion channel function (Yool and Campbell, 2012). The residues identified on TM1 in AQP6 (asn60, thr63, trp71 and lys72) that are involved in anion permeability do not occur in AtPIP2;1, and furthermore there is no difference between AtPIP2;1 and AtPIP2;2 in this region. Considering the alignment results of AtPIP2;1 and AtPIP2;2, there is a serine in AtPIP2;1 which corresponds to an asparagine in AtPIP2;2, which is the only difference in Loop D. This is a potential phosphorylation site in AtPIP2;1 and it may be interesting to mutate this residue to asparagine (as in AtPIP2;2) or glutamic acid which may mimic phosphorylation (Maciejewski et al., 1995).

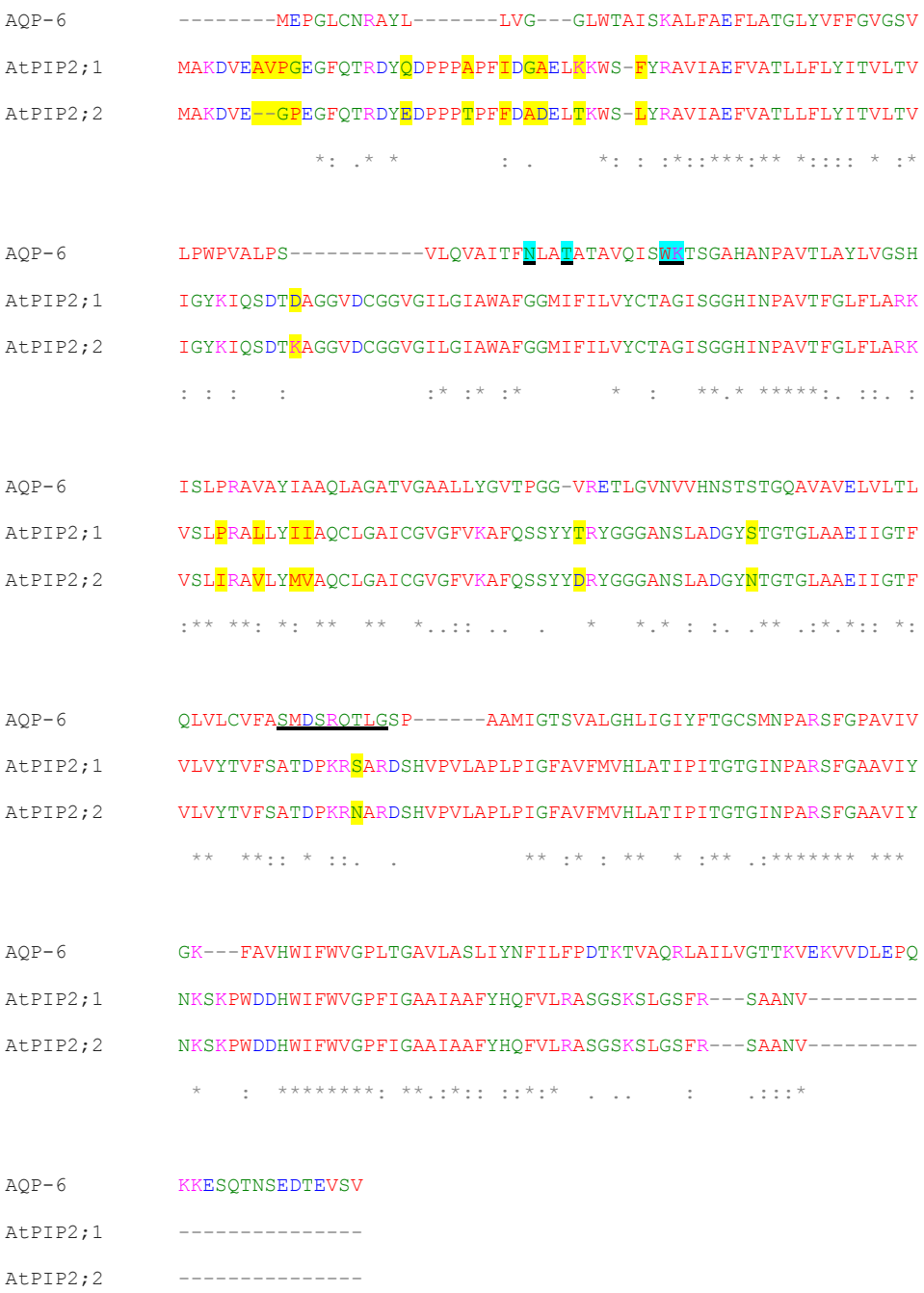

Figure 4-29 Alignments of amino acids sequences of rat AQP-6, AtPIP2;1 and AtPIP2;2. (underlined, bold) shows Loop D of aquaporins. Asterisks (*) show residues that are identical in all aligned sequences, colons (:) show conserved substitutions, and periods (.) show semi-conserved substitutions. Colours represent physiochemical properties of each amino acid residue; basic (magenta), acidic (blue), small + hydrophobic (red), and hydroxyl + sulfhydryl + amine groups (green). High light in yellow represents the different AAs between AtPIP2;1 and AtPIP2;2. High light in blue with bold underline represents the AAs of Asn-60, Thr-63, Trp-71 and Lys-72 in AQP6.

It is obvious that AtPIP2;1 induced an ionic current in *Xenopus* oocytes (Figure 4-8) and by increasing the concentration of NaCl (Figure 4-10), both outward and inward currents increase (Figure 4-11) indicating the possibility that the currents could be carried by either Na^+ or Cl^- or both. However, by fixing the concentration of Na^+ and only changing the Cl^- concentration (Figure 4-16), the same phenomena was observed. This would suggest that the currents are Cl^- dependent. More difficult to explain is that despite the Na^+ concentration being fixed, the inward current still increased with increasing concentration of Cl^-. This suggests that Cl^- efflux was stimulated by increasing external Cl^- concentration. Considering Figure 4-18 (selectivity test), it is apparent that at -100 mV, the currents with 10 NaMES, 10 $NaNO_3$ and 10 $NaHCO_3$ are almost the same as for water injected oocytes, and that $NaNO_3$ induced a significant outward current. This strongly suggests an anion permeability with higher selectivity towards NO_3^-. In contrast, 10 NaCl induced a larger conductance, and caused a significant increase in the inward current. The only change compared to NaMES was the anion, indicating that probably the inward currents are induced by Cl^- efflux and not Na^+ influx In the presence of 17.6 mM Cl^-, both the outward and inward currents appear to reach saturation of AtPIP2;1 (Figure 4-11). The activation of inward current in Figure 4-16 may be caused by trans-activation by Cl^-, that is, the Cl^- in the trans-side of the plasma membrane of oocytes can activate the efflux of Cl^- through the channel. The same explanation applies for Figure 4-18, where with the increase of Cl^- concentration in the bath solution, the inward current also increases. This behaviour is similar to that observed with the AtALMT9 anion channel. AtALMT9 is a malate-activated chloride channel located on the tonoplast. In the presence of cytosolic malate, an inward current carried by the efflux of Cl^- from the vacuoles is induced (De Angeli et al., 2013). From Figure 4-18, the selectivity of AtPIP2;1 can be described as: $Cl^- \approx NO_3^- > HCO_3^-$. It is difficult to conclude whether AtPIP2;1 can also transport MES^- as in 10 NaMES solution, as there is still 7.6 mM Cl^-

present, therefore the current might be caused by the Cl^- but not the MES^-. pH 7.5 and pH 8.5 do not seem to affect the ionic currents (Figure 4-18, 4-19).

The equilibrium potential for a particular ion is determined by the concentration of that ion on either side of the membrane. It can be calculated with the Nernst equation:

$$E_{rev} = (RT/zF) \ln(C_0/C_i) \quad \text{Equation 4-1}$$

Where E_{rev} is the reversal potential (mV);

R is the gas constant (8.31 J/K);

T is the absolute temperature (Kelvin);

z is the charge on the ion;

F is the Faraday constant (9.654 x 10^4 Coulombs/mol);

C is the concentration of the ion: inside (*C*i) or outside (*C*o) of the membrane.

At 25 ℃, the equation can be rearranged to:

$$E_{rev} = z*58 \log_{10}(C_0/C_i) \quad \text{Equation 4-2}$$

Considering Figure 4-18, with bath solution of 10 NaMES, the Cl^- concentration outside the oocyte is 7.6 mM. The intra-oocyte Cl^- concentration is within the range of 24 mM ~ 62 mM (Sobczak et al., 2010), using the average (43 mM) and the Nernst equation above (Equation 4-2), the calculated equilibrium potential for Cl^- (E_{cl-}) in the oocyte is +43.7 mV. Similarly, with 10 NaCl solution, the E_{cl-} in the oocyte is +22.5 mV (the measured reversal potential is -36.7 mV). Thus, the reversal potential from Figure 4-16 indicates that as the Cl^- concentration increases, the reversal potential is shifting more positive and more towards the E_{cl-} in each solution. However, the influx of anions such as Cl^- can only occur with the membrane potential being more positive than the equilibrium potential of Cl^- (Teakle and

Tyerman, 2010). For instance, the discovery of an anion channel in wheat root under saline conditions, using the whole-cell patch clamping technique, at an increase in Cl^- concentration, the outward ionic current increase significantly with the membrane reversal potential shifting from positive to negative (Skerrett and Tyerman, 1994). Although I also observe an increase in outward current with increasing Cl^- concentration the reversal potential does not shift negatively. The explanation for the positive shift in reversal potential that I observed is that as Cl^- increases the conductance through the channel increases and the reversal potential shifts more towards the equilibrium potential for Cl^-, which is positive. Contrasting to this, NO_3^- and HCO_3^- did not induce an inward current, but the reversal potential shifted negative compared to 10 NaMES solution and water injected controls. This can be explained by the fact that the equilibrium potential for both NO_3^- and HCO_3^- is *Xenopus* oocytes should be quite negative since there would be very low concentration of these ions in the cytoplasm.

4.4.3 The effect of increasing cRNA concentration

From Figure 4-20, as the injected cRNA concentration increases, the outward currents also increase until saturated at the highest injected cRNA concentration (23 ng injected cRNA). These results correlate to the cRNA concentration effect on water permeability in Chapter 3 (Figure 3-10). The similarity between the effect of cRNA concentration on water permeability and ion permeability indicates that the cRNA is probably not causing some form of toxic response in the oocytes to induce an ionic current (and water permeability), though I cannot exclude the possibility that the *AtPIP2;1* protein may be interacting with a native oocyte transport protein to induce ion currents (see below).

4.4.4 Inhibitor effects and cell apoptosis induced chloride current

An aquaporin inhibitor, silver sulfadiazine, was tested; however, as mentioned above, in the presence of silver sulfadiazine, the oocytes exhibit large currents that could not be properly voltage clamped. Previous research using *E.coli* showed that the silver can cause damage to cell membranes and lead to cell death (Pal et al., 2007; Coskun et al., 2012).

As indicated in Chapter 3 oocytes expressing AtPIP2;1 appeared to be more fragile and after 48 hours there was a higher mortality rate than for water injected controls. This observation therefore must be considered in terms of the ionic currents that are induced by AtPIP2;1. The issue is whether the cell death is caused by the ionic currents induced by AtPIP2;1, or if in the process of cell death, a native anion channel is activated which gives rise to the observed ionic currents.

Apoptosis has several characteristics; one of the most important traits is cell shrinkage, which happens before cell fragmentation. This process is induced by activation of ionic channels (Okada and Maeno, 2001). By using *Xenopus* oocytes, it was demonstrated that lowering the extracellular Cl^- concentration dramatically decreases the current during apoptosis. Anion channel inhibitors, NPPB (0.1 mM) and Lanthanum (1 mM), can eliminate the current, while NFA (0.05 mM) did not block the current (Souktani et al., 2000). In my experiments, NPPB, NFA, and Lanthanum were also used (Schmieder et al., 2002; Kucherenko et al., 2013). My results showed that in oocytes NFA, NPPB and lanthanum can inhibit the ionic current, but in contrast to the apoptosis induced channels, NFA has the best inhibitory affect. According to one-way ANOVA, Figure 4-21 to Figure 4-24 indicate the inhibition effect: NFA > NPPB >

Lanthanum. NFA and NPPB do not inhibit water permeability whereas Lanthanum inhibit only 30% of the water permeability of AtPIP2;1 (Figure 4-25). Therefore, the ionic currents that are induced by AtPIP2;1 are unlikely to be due to cell apoptosis.

4.4.5 Co-expression of AtPIP1;2 and AtPIP2;1

Interestingly, AtPIP1;2 can silence the current induced by AtPIP2;1 at different pHs according to Figure 4-12 to Figure 4-14. In the previous chapter (Chapter 3), it was demonstrated that AtPIP1;2 interacts with AtPIP2;1 and the water permeability of the oocytes that co-expressed AtPIP1;2 and AtPIP2;1 was higher than the additive water permeability of oocytes expressing AtPIP1;2 and AtPIP2;1 alone. When AtPIP2;1 is expressed alone in *Xenopus* oocytes, it probably forms homotetramers, however, when co-expressed with AtPIP1;2, it is likely that they form both homo- and heterotetramers (Fetter et al., 2004). This presents the possibility that the homotetrameric form of AtPIP2;1 can conduct ions, but not the heterotetrameric form with AtPIP1;2. Alternatively the AtPIP1;2 co-expression may prevent AtPIP2;1 from interacting with a native channel.

4.4.6 Mutant Atpip2;1 (G100W)

As described in Chapter 3, the *Atpip2;1* mutant construct, in which Gly100 was substituted with Try (G100W), eliminated the water permeability completely. A structural model indicated that the large Try may sterically block the water conducting pore in the monomer (Shelden et al., 2009). This mutation does not appear to alter targeting to the plasma membrane since co-expression with AtPIP1;2 induced additional water permeability,

indicating that G100W Atpip2;1 still allows AtPIP1;2 to traffic to the plasma membranes (Fetter et al., 2004). However, there was no visible ionic current induced in *Atpip2;1* (G100W) injected oocytes, nor in oocytes that co-express AtPIP1;2 and Atpip2;1 (G100W). This result is important since it would suggest that the AtPIP2;1 is not interacting with a native oocyte channel to induce the ionic current. It would not be expected that one amino acid change would abolish such an interaction when it still allows the interaction to occur with AtPIP1;2. Assuming that the Atpip2;1 (G100W) mutant is correctly targeted to the plasma membrane, then the anion and water may share the same conductance pore. However, there are also some other possibilities: the mutant Atpip2;1 may have a larger change in tertiary structure than has been modelled by Shelden *et al.* (2009), and this may lead to change of the structure of homotetramers which affects the ion transport.

4.4.7 Induction of endogenous channels in *Xenopus* oocytes

Some reports have indicated that high levels of heterologously expressed membrane proteins can induce endogenous channels of *Xenopus* oocytes (Tzounopoulos et al., 1995). For instance, human min K protein was suggested to be a potassium-selective channel, however, when high concentrations of min K cRNA (100 ng/µl) were injected into oocytes, hyperpolarization-activated chloride currents were induced in addition to the potassium current that was specifically induced by the min K protein itself. This chloride current can be inhibited by tetraethylammonium (TEA) and DIDS. High injection concentration results in high expression level of membrane protein (Attali et al., 1993; Tzounopoulos et al., 1995). For my experiments, I injected relatively small amounts (6 ng/µl) of cRNA, and the current induced by this reached saturation of the outward current (Figure 4-15). Therefore, even if it

is a very low amount of injected cRNA, it may still result in a high expression level of protein that could be too high and beyond the limitation of the oocytes.

In Conclusion, the microelectrode method for testing the CO_2 permeability cannot be used for *AtPIP2;1* injected *Xenopus* oocytes. The CO_2 hydrolysis equation described in chapter 2 reflects the principle of the microelectrode technique: with the influx of CO_2, the pH on the surface of the plasma membrane of oocytes increases and this increase is suppose to be purely induced by the transport of CO_2. However, since AtPIP2;1 protein shows anion transport activity as described in this chapter, and the transport of some anions such as HCO_3^- leads to the change of pH on both sides of the plasma membrane dramatically, therefore the pH change will be complicated. According to my results, the homotetramer form of AtPIP2;1 induces a non-selective anion current when expressed in *Xenopus* oocytes, and Cl^- trans-activates an inward current. It is likely that water and anions share the same pathway. It is also possible that AtPIP2;1 induces endogenous channels though this is considered as only a remote possibility for the reasons given above (blocker effects and co-expression effects).

Chapter 5 Expression of *AtPIP2;1* in Yeast and Examination of Yeast Anion Tolerance

5.1 Introduction

In Chapter 4, *Arabidopsis* aquaporins was heterologously expressed in *Xenopus* oocytes to check the ion channel activity. Because *AtPIP2;1* showed anion channel activity, in this chapter, yeast heterologous expression system was used to examine anion tolerance of yeast expressing AtPIP2;1.

Saccharomyces cerevisiae (baker's yeast) has been used for heterologous expression of plant aquaporins due to its low intrinsic plasma membrane water permeability (Jahn et al., 2004; Suga and Maeshima, 2004; Sakurai et al., 2005; Bienert et al., 2011; Navarro-Ródenas et al., 2012). By heterologous expression of a group of *Solanaceae* XIPs in yeast, using a yeast growth assay (spotting plate assay), it was demonstrated that XIPs facilitate the transport of a series of neutral molecules such as urea and boric acid (Bienert et al., 2011). A recent study reported the expression in yeast of VvTnPIP1;1, VvTnPIP2;2 and VvTnTIP2;1 from grapevine (*Vitis vinifera cv*. Touriga nacional). By tagging the protein with green fluorescence protein (GFP), it was observed that all three aquaporins were localized to the yeast plasma membrane. Water transport was tested by stopped-flow spectrofluorimetry (see Chapter 2) on intact yeast cells loaded with a volume sensitive dye. Only VvTnTIP2;1 showed water channel activity, and acidifying the cytosol in the yeast regulated VvTnTIP2;1 gating. Using a yeast growth assay, they observed that the yeast cells that express

VvTnTIP2;1 exhibit an inhibition of growth in high media osmolarity (above 0.5 M KCl) compared to the yeast cells that express VvTnPIP1;1 and VvTnPIP2;2 (Leitão et al., 2012). Another recent study reported the expression of the *Cyanobacteria* Aquaporin-Z (*SsAqpZ*) in yeast. By pre-treating the yeast cells with a pH sensitive dye of fluorescein diacetate (FDA), which will be quenched by acidic pH, the CO_2 permeability was measured from the rate of FDA quenching in stopped-flow spectrofluorimetry. The results indicated that SsAqpZ can transport CO_2 (Ding et al., 2013).

In this chapter, the water channel activity of AtPIP2;1 was first tested in yeast spheroplasts that express AtPIP2;1 to ascertain that AtPIP2;1 was targeted to the plasma membrane and increased water permeability as observed in *Xenopus* oocytes. Subsequently growth assays were performed to test tolerance of yeast expressing AtPIP2;1 to high concentrations of anions.

5.2 Materials and Methods

5.2.1 Molecular cloning of yeast destination vector

AtPIP2;1 was cloned into pENTR vector (Invitrogen) from pUNI51 vector as described in Chapter 3. Those clones were transformed into *Escherichia coli* strain TOPO 10 and transformants were sequenced. Gateway LR recombination reaction using LR Clonase™ (Invitrogen) was performed to transform the gene from the entry vector into the destination vector, pYES3-DEST by gateway cloning. pYES3-DEST is a modified version of pYES2 (Invitrogen), a yeast expression vector. It was converted to a Gateway vector using the

Gateway Vector Conversion System (Invitrogen) by former lab member Megan Cherie Shelden. pYES3-DEST has GAL1 promoter where galactose is used to activate the gene. The URA3 gene is to complement URA3 - minus strains. The Amp gene is used for selection in *E. coli*. The pUC origin of replication allows a high-copy replication and maintenance in *E. coli*. The presence of attR1 and attR2 sites allows the gene of interest in the entry construct to recombine with a Gateway® destination vector. The T7 promoter/priming site allows *in vitro* transcription, and sequencing of the insert. Upon recombination, the ccdB gene is replaced by the gene of interest (Figure 5-1).

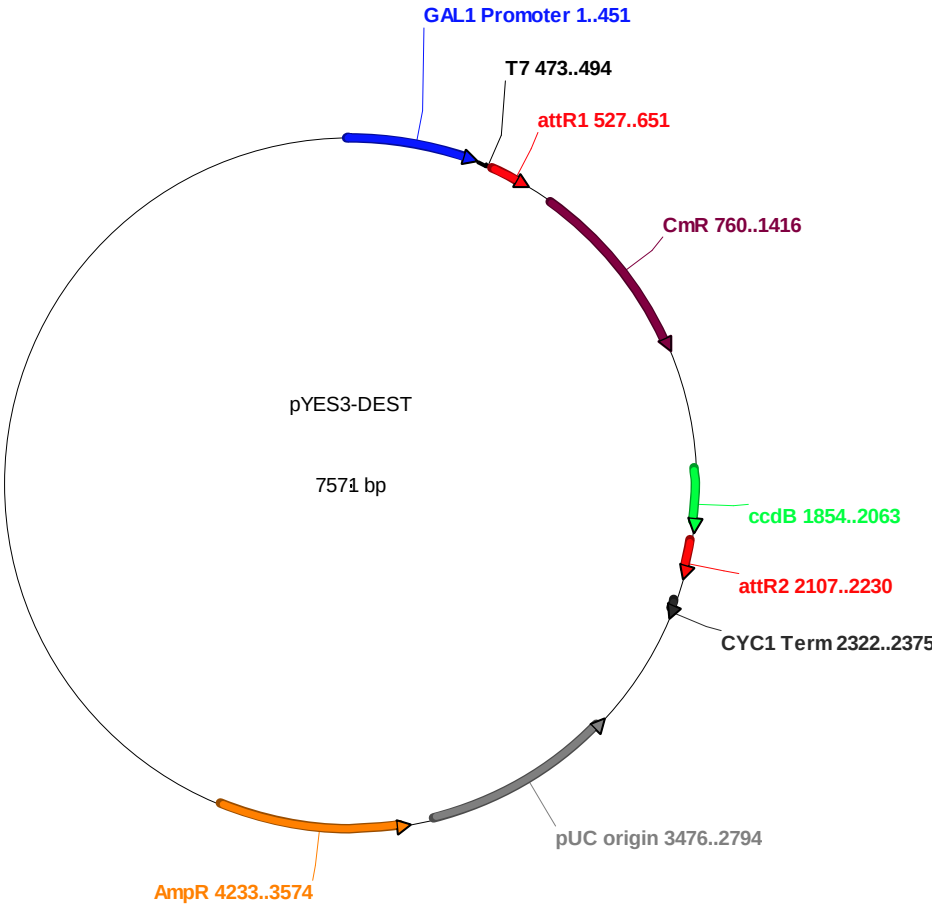

Figure 5-1 Yeast expression vector pYES3-DEST. The figure was generated by Ape.exe software (Chapter 3).

5.2.2 Yeast transformation

(1) Solutions and medium

All components of solutions and medium were analytical or molecular biology grade and purchased from Sigma-Aldrich unless indicated otherwise. All solutions and medium were made with MilliQ water and when required, autoclaved at 121 ℃ for 20 min. The components of general growth medium are listed in Table 5-1. The components of solutions for yeast transformation are listed in Table 5-2. Working solutions for yeast transformation were freshly prepared immediately prior to use.

Table 5-1: General growth medium.

Medium / Solution	Components
YPAD	1% (w/v) Yeast Extract (Difco), 2% (w/v) Bacto® peptone, 2% (w/v) Glucose, With/without 2% Agar (w/v) Autoclave
SD Dropout Medium (-URA)	0.67 % yeast nitrogen base (YNB) (Difco) without amino acids, 2% Glucose/Galactose, 0.14% amino acid dropout powder (-URA), pH 5.6 with 10 M NaOH. With/without 2% Agar. Autoclave
10 * 1L Grenson's Medium Solution 1	$MgSO_4 \cdot 7H_2O$ 7 g, KH_2PO_4 10 g, $CaCl_2 \cdot 2H_2O$ 4 g, NaCl 5 g, K_2SO_4 10 g, Citric-Acid ·H2O 105 g, 160 ml 10 M KOH, pH 6.1 with 10 M KOH. Autoclave
1L Grenson's Medium Solution 2	H_3BO_4 10 mg, $CuSO_4 \cdot 5H_2O$ 5 mg, KI 2 mg, $Na_2MoO_4 \cdot 2H_2O$ 4 mg, $ZnSO_4 \cdot 7H_2O$ 1 mg, Citric-Acid ·H_2O 10 g, $MnSO_4$ ·H2O 400 mg, $FeCl_3 \cdot 6H_2O$ 5 g. Autoclave
1L Grenson's Medium Solution 3	D-Biotin 250µg, thiamine ·HCl 100 mg, inositol 1g, Calcium D-pantothenate 200 mg, Pyridoxine ·HCl 100 mg. Autoclave
1L Grenson's	10 * Solution 1 98.9 ml, Solution 2 1 ml, Solution 3 10 ml,

Medium Final mix	0.1 % L-Proline, 2% Galactose. Top up with H_2O to 1L in Laminar flow.
YNB Minimal Medium	0.67 % yeast nitrogen base (YNB) without amino acids, 2% Glucose /Galactose, 2% Agar. Autoclave

Table 5-2: General solutions for yeast transformation.

Stock Solutions	Components
10 * Lithium Acetate	1 M LiAc, pH 7.5 with acetic acid. Autoclave
10 * TE	0.1 M Tris-HCl + 0.01 M EDTA (pH 7.5). Autoclave
50% PEG 4000	50 g PEG 4000 dissolved in 30 ml MilliQ water and top up with Milli Q water to 100 ml. Autoclave
Salmon Sperm DNA	10 mg/ml dissolved in 1 * TE buffer pH 8.0. Pipette up and down with a 5 ml pipette. Stand overnight at 4 ℃ to produce a homogeneous viscous solution. Aliquot 2 ml into falcon tubes and sonicate so that the majority of fragments are 7 kB to 15 kB long. Store at -20 ℃ for future use.

(2) Yeast transformation procedure

Yeast Strain *Saccharomyces cerevisiae* 31019b was selected for expression of AtPIP2;1. 31019b strain is defective in three endogenous NH_4^+ transporters (Mep1, Mep2, and Mep3), and thus unable to grow on a medium containing <5 mM NH_4^+ as the sole N source (Marini et al., 1997). However the main reason this strain was selected was because it has been previously successfully used to examine function of plant aquaporins (Besse et al., 2011). The 31019b yeast glycerol was plated out on YPAD-Agar medium to grow at 29 ℃ for approximately 48 hours to develop good-size colonies. Selected colonies were inoculated into 5~7 mls YPAD liquid medium and grown over night at 29 ℃, (300 rpm shaker) to make the starter culture for yeast transformation. The pYES3-DEST that contained the gene of interest

was then transformed into 31019b. The protocol used was lithium chloride (LiAc)/PEG method and was based on Gietz's protocol in 2007, with small modification on the yeast transformation reaction (Table 5-3) to achieve high efficiency (Gietz and Schiestl, 2007).

Table 5-3: Yeast transformation reaction

Component	Volume
PEG 4000 (50% w/v)	240 µl
1 M LiAc	36 µl
Salmon Sperm DNA (2 mg/ml)	25 µl
Plasmid DNA	~500 ng
H_2O	Top up to 50 µl

Once colonies (1-2 mm diameter transformants) have appeared on the SD-URA (glucose) plates, 8 single colonies were picked from each transformation and they were transferred to a fresh SD-URA (glucose) plate. When transferring the colonies, 2 cm x 2 cm patches were made to allow growth of a large amount of yeast cells. The plates were incubated in an incubator at 30 ℃ for two days for the yeast patches to grow. Glycerols were made for each colony. The plates can be stored at 4 ℃. The colonies have to be transfer to a fresh plate every fortnight.

5.2.3 Yeast spheroplast and swelling assay

Based on the uracil selection method, transformed yeast cells (*AtPIP2;1* and pYES3-DEST empty vector) were grown in 10 ml SD-URA medium supplemented with 2% glucose for 16 hours in 29 ℃ at 300 rpm. These yeast cells were then spiked into 50 ml Grenson's medium

(Dubois and Grenson, 1979) supplemented with 2% proline and 0.1 % galactose, cultured and induced for 16 hours to reach OD600 0.8~1. Then these yeast cells were spheroplasted based on modifying the protocol by Bienert in 2007 (Bienert et al., 2007). The solutions that were used for spheroplasting are as follows (Table 5-4):

Table 5-4: Solutions needed for yeast spheroplast reaction.

Solutions	Components
First wash solution	5 mM KH_2PO_4, pH 7.5 with KOH
Softening solution	Add 20 µl of ß-mercaptoethanol to every 10 ml of first wash solution
Enzyme solution	2.4 M Sorbitol, 5 mM KH_2PO_4, pH 7.5 with KOH, add ~100 units/ml lyticase
Resuspension solution	10 mM MES, 1 mM EDTA, 0.4 M K_2SO_4, 0.5 M Sorbitol, pH 6.0 with MES

(1) Yeast Spheroplast Procedure

1) Overnight yeast culture (Grenson's medium) was transferred into 50 mL Falcon tubes. The cells were pelleted at 4000 rpm for 2 min, and the supernatant was discarded.

2) The cells were washed with 50 ml of first wash solution, then, the cells were resuspended to OD600 1.0 in softening solution, and incubated at 28 ℃ (200 rpm) for 45 min.

3) The yeast cells were centrifuged at 4000 rpm for 2 min, and then resuspended in enzyme solution. The cells were incubated at 28 ℃ for 1 h (200 rpm).

4) The yeast spheroplasts were centrifuged at 4000 rpm for 5 min. The supernatant was carefully removed and the spheroplasts washed once in resuspension solution.

5) The spheroplasts were resuspended with resuspension buffer and diluted to a uniform OD 475 of 1.0. They were subsequently placed on ice.

6) 10 µl of yeast cells was carefully pipetted onto a glass slide and covered with a coverslip, checked under light microscopy (40x, A40-PL, Olympus CH-2, U. S) to monitor the conversion to spheroplasts.

(2) Yeast swelling assay

Water transport of spheroplasts was conducted using stopped-flow spectrofluorimetry (Applied Photophysics) as described in Chapter 2. The kinetics of swelling was measured at 16 ℃ using light scattering (wavelength = 475 nm) (Sloot et al., 1988). The reaction was monitored for 6 s and 5000 points were collected. The yeast spheroplasts in the resuspension solution were injected against a series dilution of the resuspension solutions, the dilution factors of which are 1/2, 3/4 and 7/8, respectively. When the yeast spheroplast in the resuspension solution was injected against these hypoosmotic solutions, 1/2 diluted resuspension solution for instance, the starting osmolarity was 1472 mosmol, and the final (after mixing) osmolarity was 1104 mosmol. All data presented were average of at least 10 injections. The rate constants were obtained by fitting the curve using non-linear regression. The kinetics of light scattering were best fit to a single-exponential function (control spheroplasts that harboured empty vector) and a double-exponential function was required for AtPIP2;1 expressing spheroplasts due to a fast phase that was present (Liu et al., 2006; Bienert et al., 2007; Besse et al., 2011). The rate constant is proportional to the water permeability coefficient (Kozono et al., 2003; Calamita et al., 2005). Data analysis was done using Graph Pad Prism 5.

5.2.4 Growth assay for yeast

Growth assays (spot-plate) were conducted to detect effects of expression of *AtPIP2;1* on anion tolerance. The assay was based on the following steps:

1) Yeast cells with different constructs (empty vector: pYES3-URA DEST vector and *AtPIP2;1*) were grown in YNB-Glucose minimal liquid medium in conical flasks with cotton stoppers wrapped in aluminium foil at 29 ℃ at constant rotation of 300 rpm overnight.

2) On the following day, the yeast cells were washed twice with water to remove glucose, then, resuspended in 10 ml sterile water.

3) To determine their OD600, 20 µl of each culture was transferred to a new Eppendoff tube containing 200 µl sterile water and mixed by pipetting. The OD600 was measured with a plate reader. The OD600 of the initial cultures was calculated by multiplying the OD600 of the cultures in the plate by a dilution factor of 11.

4) Based on the OD600 of initial yeast cultures, the yeast cells were then resuspended to OD600 of 1.0 with sterile water. Serial dilution was carried out to dilute the yeast cell from OD600 of 1.0 to 0.1, 0.01, 0.001, and 0.0001.

5) YNB-Galactose agar minimal medium was prepared. 2% glucose was supplied to one plate, and 2% galactose and the desired salt was supplied to all of the other plates. The plates were dried in a sterile laminar flow hood at room temperature for 20 min and placed on a gird.

6) For each culture, 10 µl from the six dilutions were spotted in a row on both repressing and inducing medium. Two replicates were conducted. After spotting all plates, the plates were left open in a laminar flow hood for several minutes to dry completely. Then, they were covered, and sealed with parafilm and placed in a 30 ℃ yeast incubator for certain times.

7) The yeast growth was analysed by taking pictures with Gel Doc™ (Bio Rad) in trans-white mode on day 1, 3, 5, 7. Firstly, this confirmed that there were growing colonies on day 1 on the YNB-glucose medium and that cell densities and growth of the two replicates were similar. Comparison was made of the growth of the culture expressing the gene of interest (*AtPIP2;1*) with the culture carrying an empty vector (pYES3-DEST-URA) on the plate containing galactose.

5.3 Results

5.3.1 Water transport by yeast spheroplasts expressing AtPIP2;1

A simple swelling assay was carried out by dilution of the resuspension solution to test the osmotic integrity of 31019b. 31019b expressing AtPIP2;1 transported water faster than empty vector as shown in Figure 5-2 (a - c). The water permeability (P_{os}) values for different diluted solutions were also calculated. It showed that when injected against 1/2 diluted resuspension solution, 31019b spheroplasts expressing AtPIP2;1 had a rate constant of the faster phase of the double-exponential of 9.865 s^{-1}, (P_{os}: 0.01034 cm/s), 60 times higher compared to the 31019b spheroplasts with empty vector (pYES3-DEST), which had a rate constant of 0.1643 s^{-1} (P_{os}: 0.000172 cm/s). Similar results were obtained with the spheroplasts injected with 3/4 diluted resuspension solution (AtPIP2;1: 8.771 s^{-1}, P_{os}: 0.0079 cm/s; empty vector: 0.1489 s^{-1}, P_{os}: 0.000134 cm/s). When injected against 7/8 diluted solution, the rate constant for AtPIP2;1 was 13.61 s^{-1}, P_{os}: 0.0114 cm/s, however, the rate for spheroplasts with empty vector was extremely small: 0.08908 s^{-1}, P_{os}: $7.47*10^{-5}$ cm/s. This experiment was repeated and the results were similar.

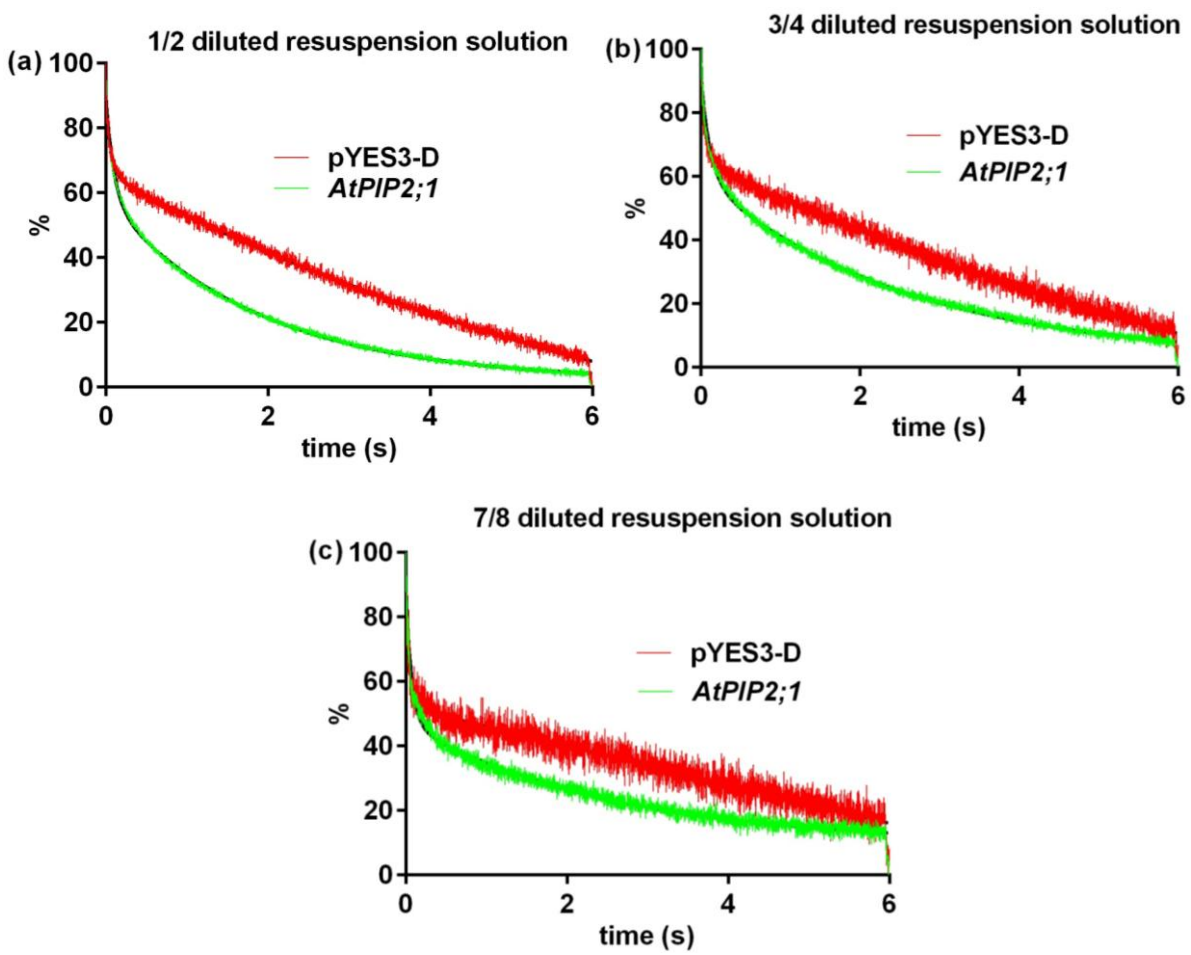

Figure 5-2 Analysed results from stopped flow spectrometry. Yeast spheroplasts were injected against different diluted resuspension solutions (a - c). The spheroplasts swelled as the percentage was decreasing across time. The solid line is the fitting of the curve using non-linear regression, double exponential.

5.3.2 Yeast growth assay

To examine the anion tolerance to bromine survival and growth of 31019b expressing *AtPIP2;1* were grown in high concentration of KBr and YNB without uracil. 31019b are grown either on glucose (where gene expression was suppressed) or galactose (where gene expression was induced) to serve as a positive control. The 31019b that were spotted on

glucose medium was expected to grow. Regardless of whether the gene was induced or not, yeast grew, however, they grew better on suppressed medium than induced medium (Figure 5-3 a, b). This is because yeast prefers glucose as their carbon source. When grown in the induced medium, the yeast with empty vector grew better compare to the yeast expressing *AtPIP2;1* (Figure 5-3 b-e). The presence of KBr (200 mM) was also tested and it showed that the growth of the yeast was significantly inhibited (Figure 5-3 f). Lower concentrations of NaBr (50 mM) was also tested and the growth of the yeast with either empty vector or *AtPIP2;1* were similar and both of them were strongly inhibited (Figure 5-3 g). Interestingly, with 100 mM NaBr, even though growth was strongly inhibited, there appeared to be greater reduction in growth for yeast expressing *AtPIP2;1* (Figure 5-3 h). The explanation for these results is that both sodium (Munns et al., 2012) and bromide are toxic for yeast, hence, yeast expressing AtPIP2;1 may have a greater growth reduction due to anion transport. This experiment was repeated and similar results were observed.

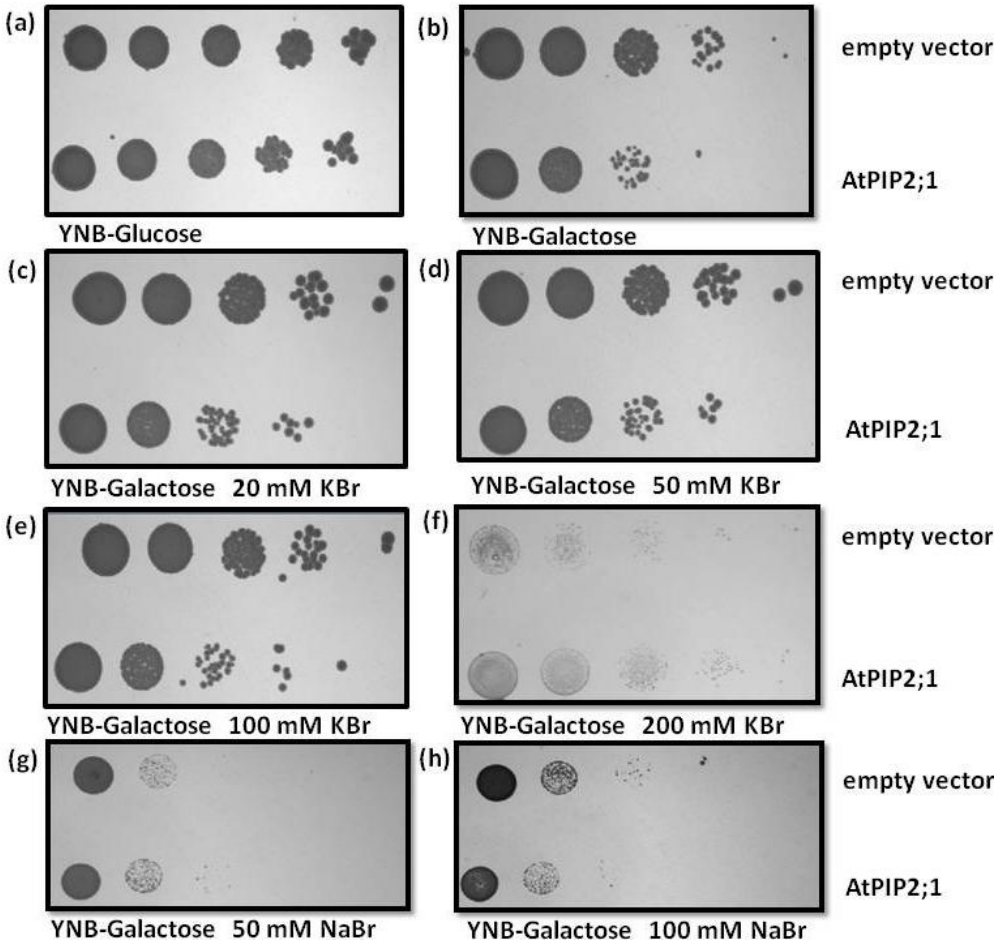

Figure 5-3 10 µl of 31019b with various constructs (empty vector, AtPIP2;1) were spotted on YNB plates as positive control (a, b); with different concentration of KBr (c-f); and with different concentrations of NaBr (g-f). Row 1 is yeast with empty vector and row 2 is yeast with AtPIP2;1. The spot with the highest OD600 is on the left. All plates were YNB-Gal minimal medium without uracil. The plates above showed the growth of the all 31019b constructs at day 7.

In addition, medium with some other salts and different concentrations were also tested, although the results were not conclusive. The growth of the empty vector control on the medium with 200 mM KCl or 200 mM NaCl was strongly inhibited, presumably due to the high concentration of the salt. Medium with lower concentration of KCl (50 mM) was also tested, and the results were inconclusive because yeast appears to be quite tolerant to this

concentration of chloride. 200 mM NaBr medium was tried, however this prevented any growth. Chapter 4 showed that 200 µM niflumic acid (NFA) inhibits the anion current induced by AtPIP2;1 in *Xenopus* oocytes, therefore, mediums with NFA (200 µM) were also tested. However, the yeast did not grow in the presence of this concentration of NFA.

5.4 Discussion

5.4.1 Water permeability of yeast cells expressing AtPIP2;1

It was shown in Chapter 3 that the *Xenopus* oocytes expressing AtPIP2;1 have significantly higher water permeability. From Figure 5-2 and the calculation for P_{os}, it is obvious that in yeast expression system, AtPIP2;1 induced higher water permeability. The water permeability values are similar to those recorded previously (Besse et al., 2011). They expressed HvPIP2;2 in 31019b yeast strain and had a water permeability of 0.0083 cm/s when yeast were injected against 1/2 diluted resuspension solution (Besse et al., 2011).

5.4.2 Salt tolerance of yeast cells expressing *AtPIP2;1*

The yeast on YNB-Glucose grew healthily regardless of harbouring empty vector or *AtPIP2;1* (Figure 5-3 a). However, when the media changed to YNB-galactose (Figure 5-3 b), yeast with AtPIP2;1 expression did not grow as well as empty vector controls indicating that the expression of the gene inhibits growth. Bromide is often used as an analog of Cl, but it can be highly toxic (Pavelka, 2004). Therefore, if AtPIP2;1 acts as a non-selective anion channel with a high selectivity to Cl^-, Br^- may also permeate faster across the yeast plasma membrane.

According to Figure 5-3 c-f, the medium with KBr showed significant inhibition to the growth of yeast expressing AtPIP2;1; similar phenomena were observed with 100 mM NaBr (Figure 5-3 h). The inhibition of growth might be caused by Br^-. However, if comparison is made between Figure 5-3 b (YNB-galactose media without KBr) with c-f, g (YNB-galactose media with KBr/NaBr), there is no apparent difference. Thus, in induced media, the yeast cells that express AtPIP2;1 are compromised compared with the empty vector. One explanation for this result is that there are already some anions in the basal medium (YNB-minimal medium) that are transported by AtPIP2;1 causing growth inhibition. Alternatively, anion efflux would be facilitated by AtPIP2;1 from yeast cells by virtue of the large negative membrane potential. Also it should be noted that the maximal currents observed in oocytes were already saturated at 17 mM Cl^- (Chapter 4). The main component in the basal medium is Difco™ Yeast Nitrogen Base (YNB), the formulae of which includes salts such as 1.7 mM NaCl, 1.8 mM $CaCl_2$, 4.2 mM $MgSO_4$ and 7.3 mM KH_2PO_4, and trace elements. Therefore yeast expressing AtPIP2;1 may already have compromised growth because of anion transport through AtPIP2;1 regardless of whether KBr was present or not.

To conclude, according to stopped-flow experiments, significant water permeability was observed with yeast that express AtPIP2;1 indicating strong aquaporin activity. According to the yeast growth assay experiments, it is still not clear whether the phenotype is caused by actual transport of Br^- or AtPIP2;1 was affecting transport of other anions in the cell or in the basal medium. What is clear is that AtPIP2;1 has similar effects in yeast as it has in *Xenopus* oocytes, though the ion channel function has not been resolved conclusively in yeast. Further experiments such as manipulating the composition of the basal medium or using lower concentrations of anion channel blockers are needed to investigate this question.

Chapter 6 General Discussion

The pathway of CO_2 transport across biological membranes is still unclear. During the last two decades, much research has been done to investigate this long unsolved issue, for which there are the following possibilities: 1) CO_2 diffuses via the lipid bilayer (Missner and Pohl, 2009); 2) CO_2 diffuses via the aquaporin monomer water channel (Uehlein et al., 2008; Boron et al., 2011; Uehlein et al., 2012); 3) CO_2 diffuses via the central pore of the tetrameric aquaporin protein (Endeward et al., 2006; Hub and de Groot, 2006). These possibilities may be purely academic, if *in vivo* or in experimental systems, the unstirred layers are rate limiting.

CO_2 pathway across membranes

In Chapter 2, the relationship between P_{os} and CO_2 permeability was studied in native plasma membrane vesicles isolated form leaves. Despite a large and variable P_{os}, which certainly reflected high aquaporin activity, there appeared to be no variation in the apparent CO_2 permeability. This would indicate that the aquaporins that determine water permeability were not strongly influencing the transport of CO_2. In addition, Ag-sul, which inhibited water transport, did not inhibit CO_2 transport. Also, the putative central pore inhibitor of human aquaporin 1 (hsAQP1), DIDS (Endeward et al., 2006), did not inhibit plasma membrane vesicle CO_2 permeability.

The fact that CO_2 permeability was relatively stable may indicate that in the vesicle system unstirred layers may have been rate limiting. Indeed if this were the case and unstirred layer effects could be abolished (hypothetically), the faster kinetics of vesicular pH change would

have been difficult to measure with the dead-time of the stopped flow instrument. This puts an upper limit on the maximum CO_2 permeability that could be measured with this technique and size of vesicles, of the order of 6×10^{-2} cm s^{-1} or about 4-fold higher than the measured value of 1.5×10^{-2} cm s^{-1} since faster rate constants would largely be invisible during the 2 ms dead-time depending on the sensitivity of the instrument. This value is still much lower than the maximum permeability measured for a lipid bilayer of 1.6 cm s^{-1} (Missner et al., 2008).

It has previously been suggested unstirred layers rate limit CO_2 transport through membranes (Missner and Pohl, 2009). Therefore, the diffusion process of CO_2 into the cytosol actually can be divided into three parts: firstly, diffusion through the unstirred layer outside the membrane, diffusion through the membrane, and finally, diffusion through the unstirred layer inside the cell. Because CO_2 is more lipophilic, theoretically, the diffusion rate of CO_2 in the membrane should be much faster than the rate of diffusion through the unstirred water layers. So the measured value of CO_2 permeability may be a combination of these three processes. Whether unstirred layers present more resistance to CO_2 transport than the lipid bilayer is still controversial and unclear, although previous research demonstrated that for human red blood cell, the unstirred layer effect is minimal (Endeward and Gros, 2009). For leaf plasma membrane vesicles the activation energy for CO_2 transport was twice that expected for CO_2 diffusion in water, suggesting diffusion in water was not rate limiting. However, as was shown from the temperature dependence of CA in Chapter 2 the activation energy measured for CO_2 uptake could be due to the temperature dependence of CA, which would imply that CA was rate limiting vesicle acidification. However, the rate constants for acidification were saturated at increasing concentration of CA suggesting that this was not the case.

It is also important to note that previous research on CO_2 permeability was mostly focused on one specific aquaporin (Heckwolf et al., 2011; Navarro-Ródenas et al., 2012; Uehlein et al., 2012; Ding et al., 2013; Geyer et al., 2013). In the leaf plasma membrane vesicles there would be a "mix" of different PIP aquaporin isoforms. Thus there is the possibility that one isoform permeable to CO_2 was not contributing to water transport. In this case there would be no apparent relationship between P_{os} and CO_2 permeability if the different conditions and blockers did not impact on this isoform. The counter argument to this is that one would expect a high CO_2 permeability if the presence of aquaporins was to facilitate more rapid diffusion of CO_2 across the plasma membrane to the sites of fixation in the chloroplast. Also the most widely studied CO_2 permeable plant aquaporin, NtAQP1 is also water permeable (Siefritz et al., 2002).

Some previous studies have shown involvement of aquaporins in CO_2 transport. Significant reduction of measured CO_2 permeability was observed in the presence of mercury (Uehlein et al., 2008; Boron et al., 2011; Terashima et al., 2011). However, care has to be taken when interpreting these results since mercury may inhibit the carbonic anhydrase (CA) relied upon in the pH change techniques. This was clearly demonstrated in the present work by the large effect of the CA inhibitor, acetazolamide on the kinetics while Ag-Sul did not inhibit CA. Hence, the role of CA in determining the kinetics must be carefully evaluated. The results obtained in Chapter 2 provide the first detailed examination of the important role of CA in the technique. The measured CO_2 permeability was influenced by the temperature dependence of CA and the CA concentration entrapped in the vesicle. Only at very high concentration was it apparent that CA was no longer rate limiting to the kinetics. The temperature effect was CA dependent which matches perfectly to one early work (Downton and Slatyer, 1972).

Taking into consideration the discussion above, the overall conclusion from my experiments is that CO_2 permeability is extremely difficult to measure accurately, but on balance it would appear that aquaporins are not strongly influencing the transport of CO_2 across the plasma membranes isolated from pea, despite an extremely high water permeability measured for these membranes. In some special cases, for instance, if the native lipid bilayer has a very low CO_2 permeability, then aquaporins may act as the major way for CO_2 transport provided they offer a relatively low resistance pathway compared to the lipid bilayers. The magnitude of the CO_2 permeability measured for pea leaf plasma membranes (1.5×10^{-2} cm s^{-1}) would appear to be one of the highest measured so far for plant membranes (Evans et al., 2009).

Problems with measuring CO_2 permeability using the pH microelectrode method

Specific aquaporins that may transport CO_2, and which have relative high expression levels in mesophyll cells of *Arabidopsis* were selected and expressed in *Xenopus* oocytes. Water permeability of PIPs was studied first (Chapter 3 and discussed below). One of the well-established techniques to study CO_2 permeability is the external micro-electrode technique (Geyer et al., 2013). The original aim was to use this technique to test the CO_2 permeability of specific aquaporins that were described in Chapter 3. However, before the test, a series of checks by electrophysiology were done to make sure the aquaporins of interest do not induce any ion conductance (Chapter 4). This is very important because the transport of ions can potentially affect the measured external pH, particularly if the ion transported is a product of CO_2 hydration, i.e. HCO_3^-. The results obtained from Chapter 4 showed that AtPIP2;1 induced an anion current in *Xenopus* oocytes that included a selectivity to HCO_3^-. It was

reasoned in Chapter 4 (Discussion) that this is more likely to be via the aquaporin itself rather than through induction of an endogenous ionic current. However, further work to identify key amino acid residues that differ from the close relative, AtPIP2;2, which does not induce anion transport are required. The ion transport via AtPIP2;1 is discussed further after the water transport is examined.

Water permeability of *Arabidopsis* PIP aquaporins

When aquaporins were expressed in *Xenopus* oocytes, PIP1s did not show water transport activity while PIP2s showed significant water transport activity confirming many previous studies (Fetter et al., 2004; Shelden et al., 2007; Vandeleur et al., 2009). However, when PIP1s and PIP2s were co-expressed, some PIP1s interacted with PIP2s while others did not. The ones that were interacting included: AtPIP1;2 and AtPIP2;1, AtPIP1;5 and AtPIP2;1. These results match with previous research showing that specific interactions occur (Fetter et al., 2004; Alexandersson et al., 2010). *Xenopus* oocytes that express functional PIP2 aquaporins and interacting PIP1:PIP2 showed higher water permeability compared to control oocytes, and silver-sulfadiazine inhibited the water permeability. Interestingly, in agreement with previous research by Shelden *et al.* (2009), the mutant *Atpip2;1* (G100W) injected oocytes completely lost water transport activity (Shelden et al., 2009), but this was not apparently due to lack of targeting to the membrane since when co-expressed with AtPIP1;2 the aquaporins physically interact to give a high water permeability. The water permeability value observed from this co-expression probably indicated the water permeability of AtPIP1;2 alone (Fetter et al., 2004).

AtPIP2;1 induce ionic current when express in *Xenopus* oocytes

There are some aquaporins that have been demonstrated to be ion transporters, for instance the mammalian aquaporin 1 and aquaporin 6 (AQP1 and AQP6) (Hazama et al., 2002; Yool and Weinstein, 2002; Campbell et al., 2012), aquaporin related protein in *Drosophila*, Big Brain (BIB) (Yanochko and Yool, 2002) and some plant aquaporins such as NOD26 and TaTIP2;1 (Holm et al., 2005; Yool and Campbell, 2012).

The external pH micro-electrode technique would not be suitable for the measurement of CO_2 permeability of AtPIP2;1 when expressed in oocytes because of the ion currents that it induced. It was likely that the homotetramers of AtPIP2;1 function as an anion channel. The reasons for this are: 1) AtPIP2;1 induced a non-selective anion current; 2) the ion channel blockers (NFA, NPPB and lanthanum) could block this ionic current; 3) the co-expression of AtPIP1;2 and AtPIP2;1 silenced this ionic current; 4) The mutant *Atpip2;1* (G100W) injected *Xenopus* oocytes lost both water and ion transport properties.

Until now, the only two reported plant aquaporins that transport ions are NOD26 and TaTIP2;1 (Holm et al., 2005; Hwang et al., 2010; Yool and Campbell, 2012). There has not been any report about PIPs that act as ion transporters. Thus, it is very important that an endogenous current induced by expression of AtPIP2;1 in *Xenopus* oocytes can be categorically excluded, and further experiments are required to confirm this. In this respect, oocytes that co-express AtPIP1;2 and AtPIP2;1 lost the ionic current, indicating that the ionic current may have some relationship with the AtPIP2;1 homo-tetramer structure. It is not clear to what extent AtPIP2;1 forms homotetramers *in vivo.* In this respect it is interesting to note

that this aquaporin is rapidly withdrawn from root plasma membrane upon salinity stress that involves phosphorylation on the C-terminus (Prak et al., 2008) perhaps giving a clue to the possibility that it may also transport ions *in vivo*.

AtPIP2;1 induced ionic channels in yeast?

Yeast is also a well-established system to express aquaporin water channels in order to study their water transport properties via stopped-flow (Suga and Maeshima, 2004; Ishikawa et al., 2005), or to express ion transport proteins to study their role in salt tolerance or ion toxicities using growth assays (Schnurbusch et al., 2010; Munns et al., 2012; Schmidt et al., 2012). To further explore the function of AtPIP2;1, yeast expression system was used to determine the anion tolerance of AtPIP2;1 (Chapter 5). AtPIP2;1 clearly increased water permeability of yeast by many folds and in growth assays there was a growth depressing phenotype when AtPIP2;1 expression was induced, suggesting a toxicity was induced in the yeast. It is possible that this toxicity is due to leakage of anions from the cell, but further experiments are required to determine this. For example, the efflux of $^{15}NO_3^-$ could be examined for AtPIP2;1 induced and empty vector controls to test this hypothesis. Expression of another plant aquaporin (VvTIP2;1) has been shown to induce intolerance to high osmotic pressure (Leitão et al., 2012) but this did not appear to be the case for AtPIP2;1.

Conclusion

The data obtained in this thesis provides a comprehensive examination of factors that may influence the movement of CO_2 through aquaporins using different techniques. The main

findings are: CO_2 most probably moves across pea leaf plasma membranes by diffusion through the lipid bilayer pathway with little apparent effect of the activity of water conducting aquaporins. AtPIP2;1 induced a non-selective anion current in *Xenopus* oocytes that included the ability to allow HCO_3^- transport. AtPIP2;1 physically interacts with AtPIP1;2 to increase the water permeability of oocytes, but this interaction abolishes the anion current induced by AtPIP2;1.

Appendix

(1) *AtPIP2;1* (pEntry clone) sequence alignment results by APE software.

Upper sequence: *AtPIP2;1* sequence from NCBI (accession# AT3G53420)

Lower sequence: *AtPIP2;1* in pEntry clone.

Primer: M13 forward primer (perfectly aligned from 1-474 bp)

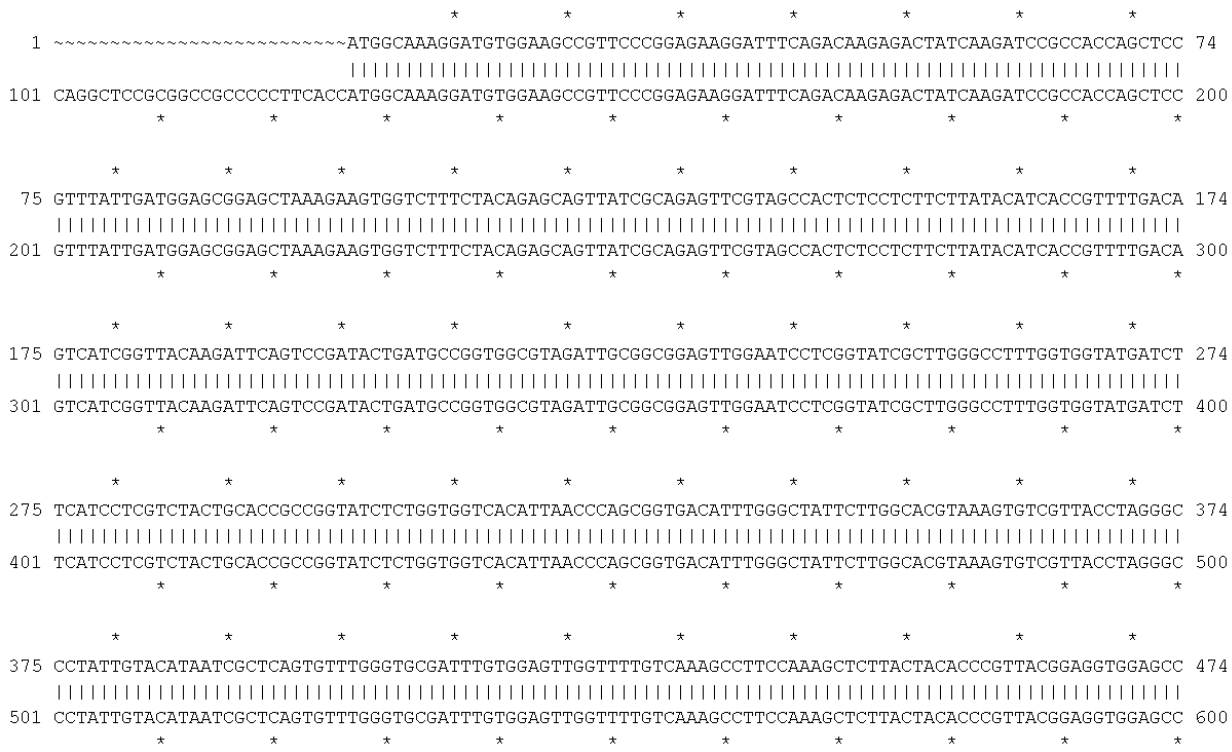

Primer: M13 reverse primer (perfectly aligned from 451-864 bp)

```
             *         *         *         *         *         *         *         *         *         *
401 TGGGTGCGATTTGTGGAGTTGGTTTTGTCAAAGCCTTCCAAAGCTCTTACTACACCCGTTACGGAGGTGGAGCCAACTCTCTAGCCGATGGCTACAGCAC 500
                                                      ||||||||||||||||||||||||||||||||||||||||||||||||||
562 ~~~~~~~~~~~~~~~~~~~~~~~~~~~~~~~~~~~~~~~~~~~~~~~~~~TACACCCGTTACGGAGGTGGAGCCAACTCTCTAGCCGATGGCTACAGCAC 513
                                                          *         *         *         *         *

             *         *         *         *         *         *         *         *         *         *
501 AGGGACCGGTCTAGCCGCAGAGATCATTGGTACTTTCGTTCTTGTCTACACCGTCTTCTCTGCCACTGACCCCAAACGTAGTGCCAGAGACTCCCACGTT 600
    ||||||||||||||||||||||||||||||||||||||||||||||||||||||||||||||||||||||||||||||||||||||||||||||||||||
512 AGGGACCGGTCTAGCCGCAGAGATCATTGGTACTTTCGTTCTTGTCTACACCGTCTTCTCTGCCACTGACCCCAAACGTAGTGCCAGAGACTCCCACGTT 413
        *         *         *         *         *         *         *         *         *         *

             *         *         *         *         *         *         *         *         *         *
601 CCGGTGTTGGCGCCACTTCCAATCGGATTTGCCGTGTTCATGGTACATTTGGCTACCATTCCCATTACCGGAACCGGAATTAACCCGGCAAGGAGTTTCG 700
    ||||||||||||||||||||||||||||||||||||||||||||||||||||||||||||||||||||||||||||||||||||||||||||||||||||
412 CCGGTGTTGGCGCCACTTCCAATCGGATTTGCCGTGTTCATGGTACATTTGGCTACCATTCCCATTACCGGAACCGGAATTAACCCGGCAAGGAGTTTCG 313
        *         *         *         *         *         *         *         *         *         *

             *         *         *         *         *         *         *         *         *         *
701 GAGCTGCCGTAATCTACAACAAGAGCAAGCCATGGGATGACCACTGGATATTTTGGGTTGGACCATTCATTGGAGCTGCGATAGCTGCATTCTACCACCA 800
    ||||||||||||||||||||||||||||||||||||||||||||||||||||||||||||||||||||||||||||||||||||||||||||||||||||
312 GAGCTGCCGTAATCTACAACAAGAGCAAGCCATGGGATGACCACTGGATATTTTGGGTTGGACCATTCATTGGAGCTGCGATAGCTGCATTCTACCACCA 213
        *         *         *         *         *         *         *         *         *         *

             *         *         *         *         *         *
801 ATTCGTTCTGAGAGCTTCAGGTTCTAAGTCTCTTGGATCATTCAGAAGTGCTGCCAACGTCTAA~~~~~~~~~~~~~~~~~~~~~~~~~~~~~~~~~~~~ 864
    ||||||||||||||||||||||||||||||||||||||||||||||||||||||||||||||||
212 ATTCGTTCTGAGAGCTTCAGGTTCTAAGTCTCTTGGATCATTCAGAAGTGCTGCCAACGTCTAAAAGGGTGGGCGCGCCGACCCAGCTTTCTTGTACAAA 113
        *         *         *         *         *         *         *         *         *         *
```

(2) *AtPIP2;6* (pEntry clone) sequence alignment results by APE software.

Upper sequence: *AtPIP2;6* sequence from NCBI (accession# AT2G39010)

Lower sequence: *AtPIP2;6* in pEntry clone.

Primer: M13 forward primer (perfectly aligned from 1-549 bp)

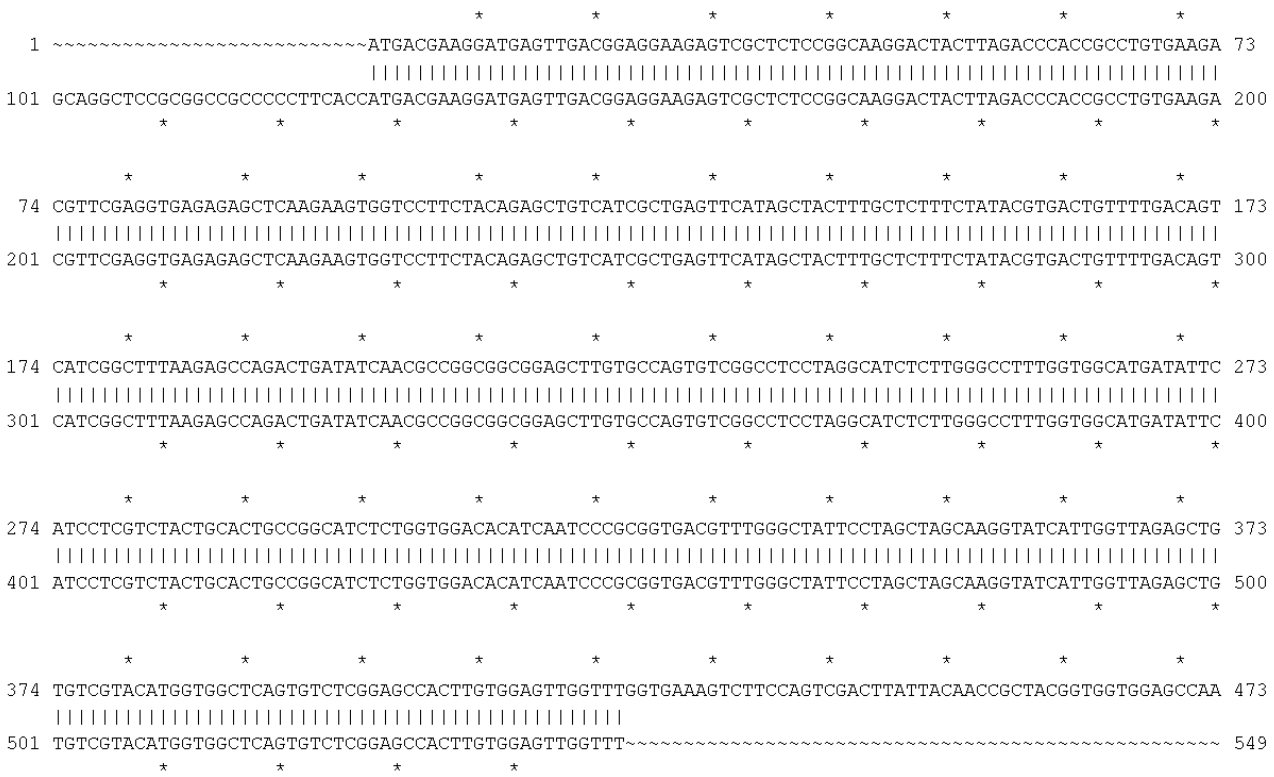

Primer: M13 reverse primer (perfectly aligned from 300-870 bp)

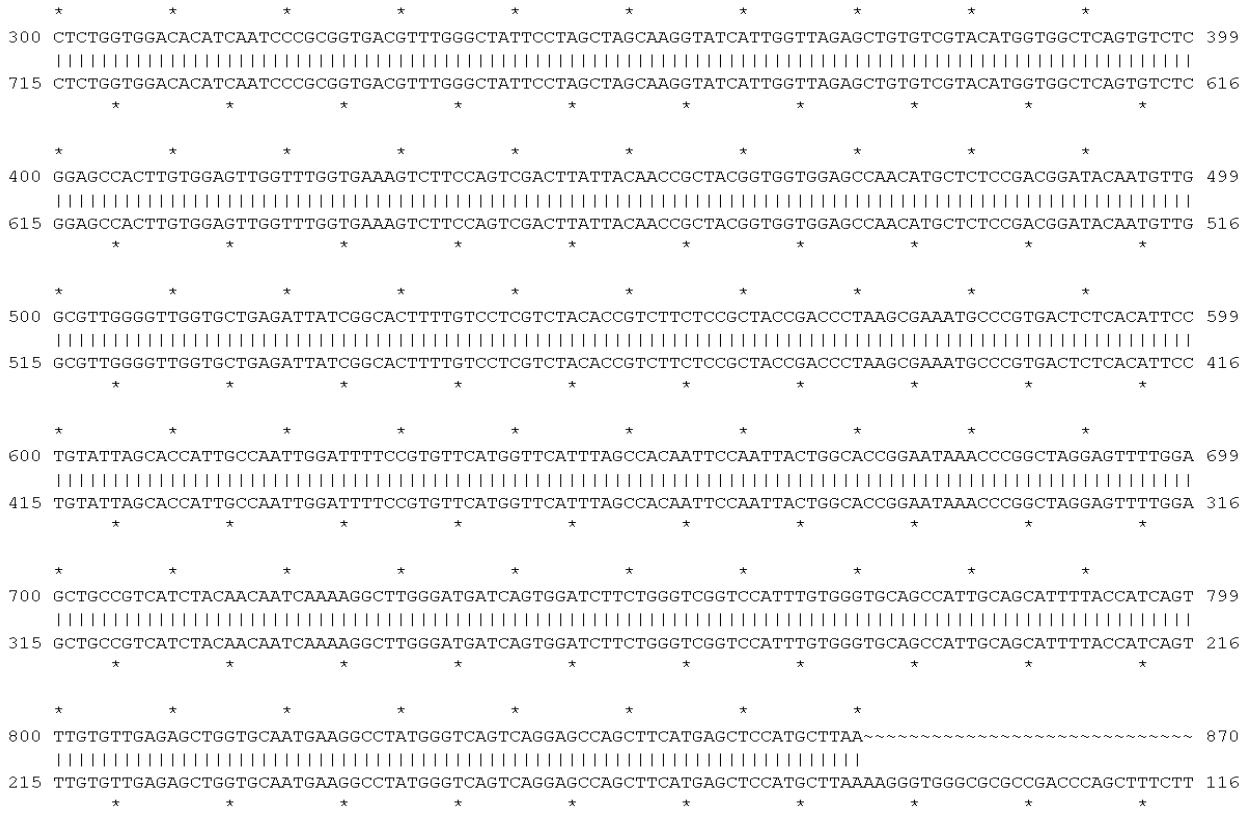

(3) *AtPIP1;4* (pGEMHE clone) sequence alignment results by APE software.

Upper sequence: *AtPIP1;4* sequence from NCBI (accession# AT4G00430)

Lower sequence: *AtPIP1;4* in pGEMHE clone.

Primer: M13 forward primer. There are two silent mutations, therefore the sequence is correct as the *AtPIP1;4* protein is not affected (274 T mutants to G, UCT ↔ GCG = Ala; and 423T mutants to C, UGU ↔ UGC = Cys).

```
  1 ~~~~~~~~~~~~~~~~~~~~~~~~~~~~~~~~~~~~~~~~~~~~~~~~~~~~~~~~~~~ATGGAAGGCAAAGAAGAAGATGTACGAGTGGGAGCTAACAAGTTCCCGGAG 51
                                                                |||||||||||||||||||||||||||||||||||||||||||||||||||
111 CACAAGTTTGTACAAAAAAGCAGGCTCCGCGGCCGCCCCCTTCGCGCCCACCCTTCACCATGGAAGGCAAAGAAGAAGATGTACGAGTGGGAGCTAACAAGTTCCCGGAG 220

 52 AGGCAACCCATCGGTACATCGGCTCAGTCCACCGACAAGGACTACAAAGAGCCACCTCCTGCGCCACTGTTCGAGCCCGGCGAGCTCAGCTCATGGTCTTTCTACAGAGC 161
    ||||||||||||||||||||||||||||||||||||||||||||||||||||||||||||||||||||||||||||||||||||||||||||||||||||||||||||||
221 AGGCAACCCATCGGTACATCGGCTCAGTCCACCGACAAGGACTACAAAGAGCCACCTCCTGCGCCACTGTTCGAGCCCGGCGAGCTCAGCTCATGGTCTTTCTACAGAGC 330

162 CGGAATAGCTGAGTTTATCGCTACTTTCTTGTTTCTCTACATCACTGTTTTGACTGTAATGGGAGTTAAGAGAGCACCAAACATGTGTGCTTCTGTTGGAATCCAAGGTA 271
    ||||||||||||||||||||||||||||||||||||||||||||||||||||||||||||||||||||||||||||||||||||||||||||||||||||||||||||||
331 CGGAATAGCTGAGTTTATCGCTACTTTCTTGTTTCTCTACATCACTGTTTTGACTGTAATGGGAGTTAAGAGAGCACCAAACATGTGTGCTTCTGTTGGAATCCAAGGTA 440

272 TCGCTTGGGCTTTTGGTGGCATGATCTTTGCTCTTGTCTACTGTACTGCTGGAATTTCAGGTGGACACATCAACCCTGCTGTAACATTCGGTCTGTTCTTGGCTCGGAAG 381
    ||||#|||||||||||||||||||||||||||||||||||||||||||||||||||||||||||||||||||||||||||||||||||||||||||||||||||||||||
441 TCGCGTGGGCTTTTGGTGGCATGATCTTTGCTCTTGTCTACTGTACTGCTGGAATTTCAGGTGGACACATCAACCCTGCTGTAACATTCGGTCTGTTCTTGGCTCGGAAG 550

382 TTATCTCTGACCAGAGCAGTGTTCTACATGATTATGCAATGTCTTGGAGCCATCTGTGGTGCCGGAGTCGTCAAAGGTTTCCAGCCAACGCCGTACCAGACTCTCGGTGG 491
    |||||||||||||||||||||||||||||||||||||||||#||||||||||||||||||||||||||||||||||||||||||||||||||||||||||||||||||||
551 TTATCTCTGACCAGAGCAGTGTTCTACATGATTATGCAATGCCTTGGAGCCATCTGTGGTGCCGGAGTCGTCAAAGGTTTCCAGCCAACGCCGTACCAGACTCTCGGTGG 660

492 TGGTGCTAACACCGTTGCTCATGGCTACACCAAAGGTTCTGGCCTTGGTGCTGAAATCATCGGAACATTCGTTCTCGTCTACACTGTCTTCTCCGCCACCGACGCCAAGA 601
    ||||||||||||||||||||||||||||||||||||||||||||||||||||||||||||||||||||||||||||||||||||||||||||||||||||||||||||||
661 TGGTGCTAACACCGTTGCTCATGGCTACACCAAAGGTTCTGGCCTTGGTGCTGAAATCATCGGAACATTCGTTCTCGTCTACACTGTCTTCTCCGCCACCGACGCCAAGA 770

602 GAAGCGCCCGTGACTCACACGTCCCGATTTTGGCGCCGCTCCCAATCGGATTTGCAGTGTTCTTGGTACACTTGGCAACAATACCGATCACCGGGACCGGAATCAACCCA 711
    ||||||||||||||||||||||||||||||||||||||||||||||||||||||||||||||||||||||||||||||||||||||||||||||||||||||||||||||
771 GAAGCGCCCGTGACTCACACGTCCCGATTTTGGCGCCGCTCCCAATCGGATTTGCAGTGTTCTTGGTACACTTGGCAACAATACCGATCACCGGGACCGGAATCAACCCA 880

712 GCTAGAAGTCTTGGAGCCGCAATTATCTACAACAAGGACCACTCTTGGGATGACCATTGGATTTTCTGGGTTGGACCATTCATTGGAGCAGCTCTAGCAGCACTATATCA 821
    ||||||||||||||||||||||||||||||||||||||||||||||||||||||||||||||||||||||||||||||||||||||||||||||||||||||||||||||
881 GCTAGAAGTCTTGGAGCCGCAATTATCTACAACAAGGACCACTCTTGGGATGACCATTGGATTTTCTGGGTTGGACCATTCATTGGAGCAGCTCTAGCAGCACTATATCA 990

822 CCAGATTGTCATCAGAGCGATTCCTTTCAAGAGCAAGAGTTAG~~~~~~~~~~~~~~~~~~~~~~~~~~~~~~~~~~~~~~~~~~~~~~~~~~~~~~~~~~~~~~~~~~~ 864
    |||||||||||||||||||||||||||||||||||||||||||
991 CCAGATTGTCATCAGAGCGATTCCTTTCAAGAGCAAGAGTTAGAAGGTGGGCGCGCCGACCCAGCCTTTCTTGTACAAAGTGTGATGATCCGAAATCCTCTAGAGCAAGC 110
```

(4) *AtPIP1;5* (pGEMHE clone) sequence alignment results by APE software.

Upper sequence: *AtPIP1;5* sequence from NCBI (accession# AT4G23400)

Lower sequence: *AtPIP1;5* in pGEMHE clone.

Primer: M13 forward primer (perfectly aligned from 1-864 bp)

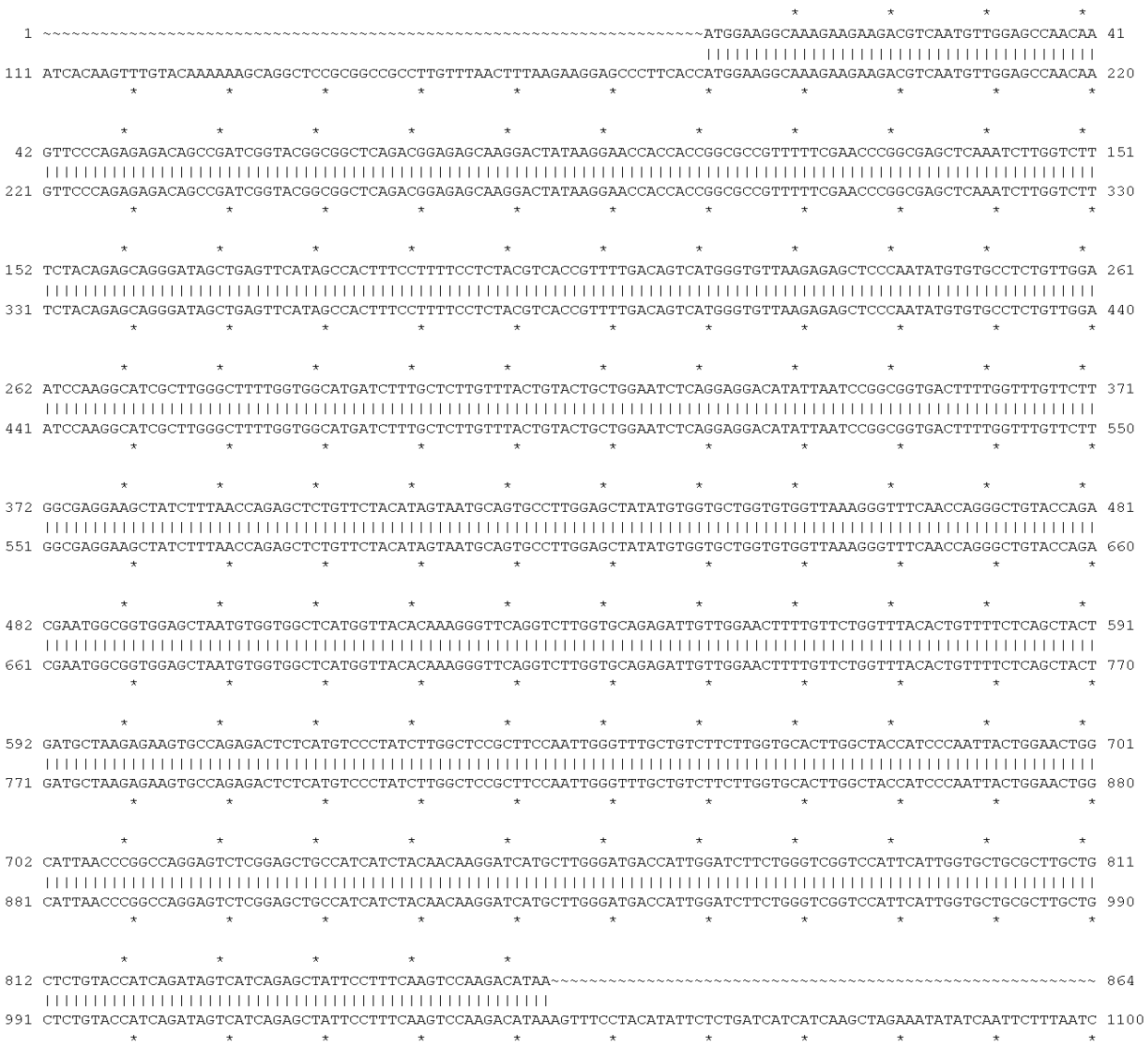

(5) *AtPIP1;2* (pEntry clone) sequence alignment results by APE software.

Upper sequence: *AtPIP1;2* sequence from NCBI (accession# AT2G45960.3**)**

Lower sequence: *AtPIP1;2* in pGEMHE clone.

Primer: M13 forward primer (perfectly aligned from 1-861 bp)

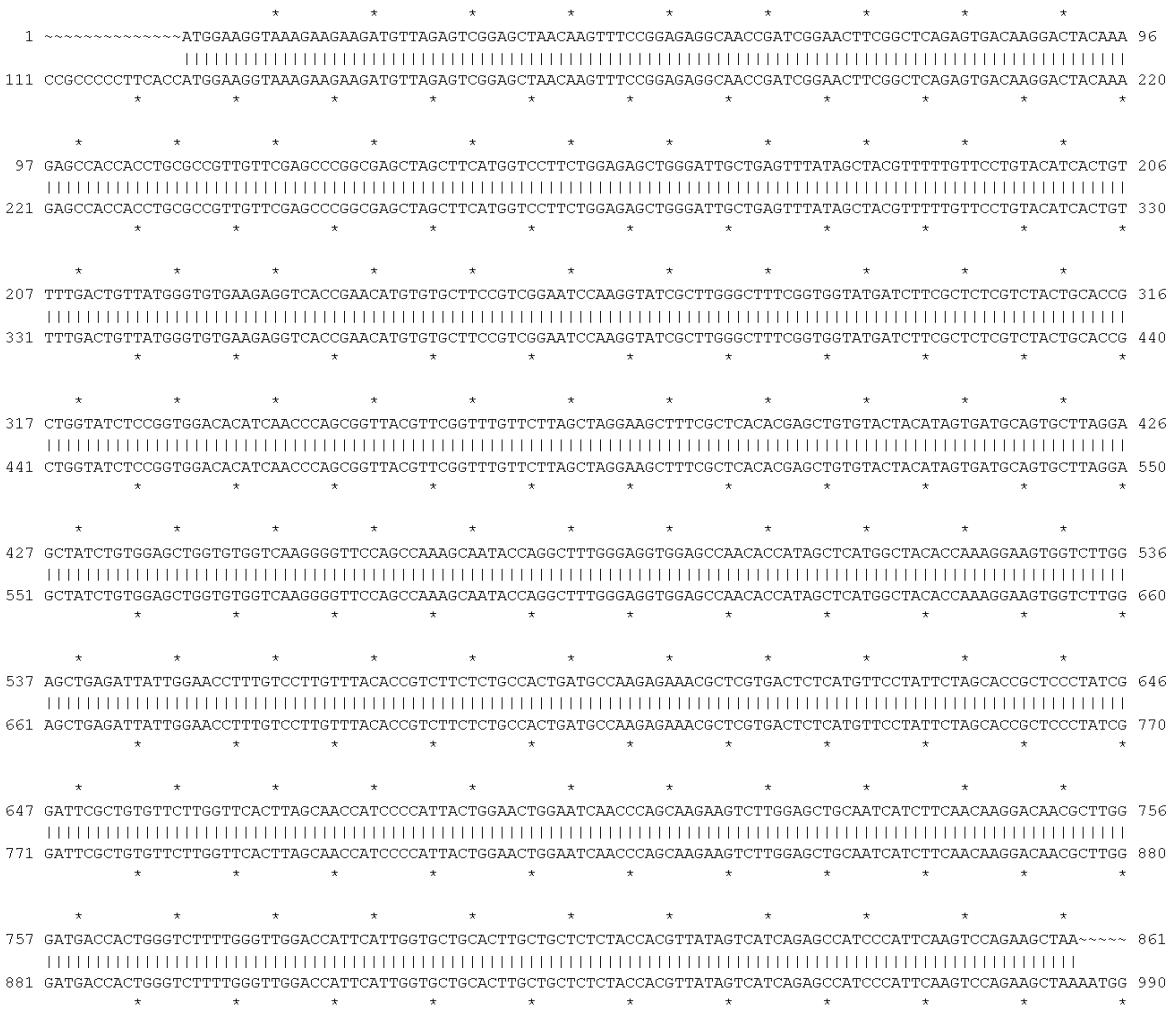

(6) *AtPIP2;2* (pGEMHE clone) sequence alignment results by APE software.

Upper sequence: *AtPIP2;2* sequence from NCBI (accession# AT2G37170.1)

Lower sequence: *AtPIP2;2* in pGEMHE clone.

Primer: M13 forward primer. There is a silent mutations, therefore the sequence is correct as the *AtPIP2;2* protein is not affected (231 A mutants to G, GGA ↔ GGG = Gly)

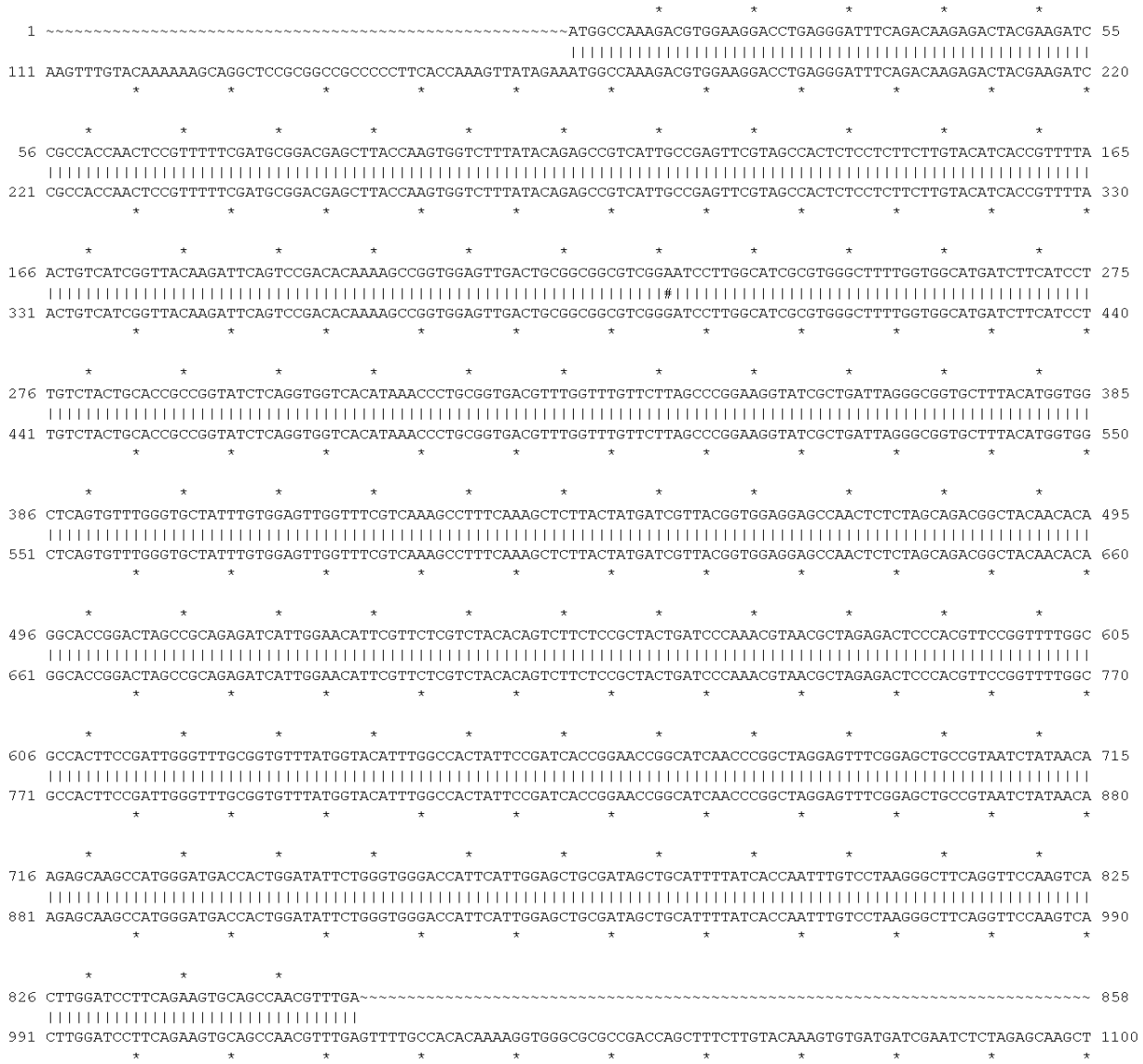

(7) *Atpip2;1* mutant G100W (pGEMHE clone) sequence alignment results by APE software.

Upper sequence: *AtPIP2;1* sequence from NCBI (accession# AT3G53420)

Lower sequence: *Atpip2;1* in pGEMHE clone (after the site-directed mutagenesis).

Primer: M13 forward primer (GGT, Gly, was mutant to TGG, Trp as shown in the box below)

```
                                                         *         *         *         *         *         *
  1 ~~~~~~~~~~~~~~~~~~~~~~~~~~~~~~~~~~~~~~~~~~~~~ATGGCAAAGGATGTGGAAGCCGTTCCCGGAGAAGGATTTCAGACAAGAGACTATCAAGATCCGCC 65
                                                 |||||||||||||||||||||||||||||||||||||||||||||||||||||||||||||||||
111 ACAAGTTTGTACAAAAAAGCAGGCTCCGCGGCCGCCCCCTTCACCATGGCAAAGGATGTGGAAGCCGTTCCCGGAGAAGGATTTCAGACAAGAGACTATCAAGATCCGCC 220
              *         *         *         *         *         *         *         *         *         *         *

        *         *         *         *         *         *         *         *         *         *         *
 66 ACCAGCTCCGTTTATTGATGGAGCGGAGCTAAAGAAGTGGTCTTTCTACAGAGCAGTTATCGCAGAGTTCGTAGCCACTCTCCTCTTCTTATACATCACCGTTTTGACAG 175
    ||||||||||||||||||||||||||||||||||||||||||||||||||||||||||||||||||||||||||||||||||||||||||||||||||||||||||||||
221 ACCAGCTCCGTTTATTGATGGAGCGGAGCTAAAGAAGTGGTCTTTCTACAGAGCAGTTATCGCAGAGTTCGTAGCCACTCTCCTCTTCTTATACATCACCGTTTTGACAG 330
              *         *         *         *         *         *         *         *         *         *         *

        *         *         *         *         *         *         *         *         *         *         *
176 TCATCGGTTACAAGATTCAGTCCGATACTGATGCCGGTGGCGTAGATTGCGGCGGAGTTGGAATCCTCGGTATCGCTTGGGCCTTTGGTGGTATGATCTTCATCCTCGTC 285
    ||||||||||||||||||||||||||||||||||||||||||||||||||||||||||||||||||||||||||||||||||||||||||||||||||||||||||||||
331 TCATCGGTTACAAGATTCAGTCCGATACTGATGCCGGTGGCGTAGATTGCGGCGGAGTTGGAATCCTCGGTATCGCTTGGGCCTTTGGTGGTATGATCTTCATCCTCGTC 440
              *         *         *         *         *         *         *         *         *         *         *

        *         *          *         *         *         *         *         *         *         *         *
286 TACTGCACCGCCGGTATCTCT-GGTGGTCACATTAACCCAGCGGTGACATTTGGGCTATTCTTGGCACGTAAAGTGTCGTTACCTAGGGCCCTATTGTACATAATCGCTC 394
    ||||||||||||||||||||| || |||||||||||||||||||||||||||||||||||||||||||||||||||||||||||||||||||||||||||||||||||||
441 TACTGCACCGCCGGTATCTCTTGG-GGTCACATTAACCCAGCGGTGACATTTGGGCTATTCTTGGCACGTAAAGTGTCGTTACCTAGGGCCCTATTGTACATAATCGCTC 549
              *         *           *         *         *         *         *         *         *         *

         *         *          *         *         *         *         *         *         *         *         *
395 AGTGTTTGGGTGCGATTTGTGGAGTTGGTTTTGTCAAAGCCTTCCAAAGCTCTTACTACACCCGTTACGGAGGTGGAGCCAACTCTCTAGCCGATGGCTACAGCACAGGG 504
    ||||||||||||||||||||||||||||||||||||||||||||||||||||||||||||||||||||||||||||||||||||||||||||||||||||||||||||||
550 AGTGTTTGGGTGCGATTTGTGGAGTTGGTTTTGTCAAAGCCTTCCAAAGCTCTTACTACACCCGTTACGGAGGTGGAGCCAACTCTCTAGCCGATGGCTACAGCACAGGG 659
    *          *         *          *         *         *         *         *         *         *         *

         *         *          *         *         *         *         *         *         *         *         *
505 ACCGGTCTAGCCGCAGAGATCATTGGTACTTTCGTTCTTGTCTACACCGTCTTCTCTGCCACTGACCCCAAACGTAGTGCCAGAGACTCCCACGTTCCGGTGTTGGCGCC 614
    ||||||||||||||||||||||||||||||||||||||||||||||||||||||||||||||||||||||||||||||||||||||||||||||||||||||||||||||
660 ACCGGTCTAGCCGCAGAGATCATTGGTACTTTCGTTCTTGTCTACACCGTCTTCTCTGCCACTGACCCCAAACGTAGTGCCAGAGACTCCCACGTTCCGGTGTTGGCGCC 769
    *          *         *          *         *         *         *         *         *         *         *

         *         *          *         *         *         *         *         *         *         *         *
615 ACTTCCAATCGGATTTGCCGTGTTCATGGTACATTTGGCTACCATTCCCATTACCGGAACCGGAATTAACCCGGCAAGGAGTTTCGGAGCTGCCGTAATCTACAACAAGA 724
    ||||||||||||||||||||||||||||||||||||||||||||||||||||||||||||||||||||||||||||||||||||||||||||||||||||||||||||||
770 ACTTCCAATCGGATTTGCCGTGTTCATGGTACATTTGGCTACCATTCCCATTACCGGAACCGGAATTAACCCGGCAAGGAGTTTCGGAGCTGCCGTAATCTACAACAAGA 879
    *          *         *          *         *         *         *         *         *         *         *
```

Primer: M13 reverse primer (perfectly aligned from 660-864 bp)

```
    *          *         *          *         *         *         *         *         *         *         *
660 TCCCATTACCGGAACCGGAATTAACCCGGCAAGGAGTTTCGGAGCTGCCGTAATCTACAACAAGAGCAAGCCATGGGATGACCACTGGATATTTTGGGTTGGACCATTCA 769
    ||||||||||||||||||||||||||||||||||||||||||||||||||||||||||||||||||||||||||||||||||||||||||||||||||||||||||||||
634 TCCCATTACCGGAACCGGAATTAACCCGGCAAGGAGTTTCGGAGCTGCCGTAATCTACAACAAGAGCAAGCCATGGGATGACCACTGGATATTTTGGGTTGGACCATTCA 743
          *         *          *         *         *         *         *         *         *         *         *

    *          *         *          *         *         *         *         *         *         *
770 TTGGAGCTGCGATAGCTGCATTCTACCACCAATTCGTTCTGAGAGCTTCAGGTTCTAAGTCTCTTGGATCATTCAGAAGTGCTGCCAACGTCTAA~~~~~~~~~~~~~~~ 864
    |||||||||||||||||||||||||||||||||||||||||||||||||||||||||||||||||||||||||||||||||||||||||||||||
744 TTGGAGCTGCGATAGCTGCATTCTACCACCAATTCGTTCTGAGAGCTTCAGGTTCTAAGTCTCTTGGATCATTCAGAAGTGCTGCCAACGTCTAAAAGGGTGGGCGCGCC 853
          *         *          *         *         *         *         *         *         *         *         *
```

References

Agre P (2011) Aquaporin water channels: from atomic structure to clinical medicine. Journal of Pharmacological Sciences **115:** 2P-2P

Aharon R, Shahak Y, Wininger S, Bendov R, Kapulnik Y, Galili G (2003) Overexpression of a plasma membrane aquaporin in transgenic tobacco improves plant vigor under favorable growth conditions but not under drought or salt stress. Plant Cell **15:** 439-447

Aiken ML, Painter RG, Zhou Y, Wang G (2012) Chloride transport in functionally active phagosomes isolated from human neutrophils. Free Radical Biology and Medicine **53:** 2308-2317

Alexandersson E, Danielson JAH, Rade J, Moparthi VK, Fontes M, Kjellbom P, Johanson U (2010) Transcriptional regulation of aquaporins in accessions of *Arabidopsis* in response to drought stress. Plant Journal **61:** 650-660

Alexandersson E, Fraysse L, Sjövall-Larsen S, Gustavsson S, Fellert M, Karlsson M, Johanson U, Kjellbom P (2005) Whole gene family expression and drought stress regulation of aquaporins. Plant Molecular Biology **59:** 469-484

Alexandersson E, Saalbach G, Larsson C, Kjellbom P (2004) *Arabidopsis* plasma membrane proteomics identifies components of transport, signal transduction and membrane trafficking. Plant and Cell Physiology **45:** 1543-1556

Alleva K, Chara O, Amodeo G (2012) Aquaporins: Another piece in the osmotic puzzle. FEBS Letters **586:** 2991-2999

Alleva K, Chara O, Sutka MR, Amodeo G (2009) Analysis of the source of heterogeneity in the osmotic response of plant membrane vesicles. European Biophysics Journal **38:** 175-184

Ampilogova YN, Zhestkova I, Trofimova M (2006) Redox modulation of osmotic water permeability in plasma membranes isolated from roots and shoots of pea seedlings. Russian Journal of Plant Physiology **53:** 622-628

Anderberg H, Danielson J, Johanson U (2011) Algal MIPs, high diversity and conserved motifs. BMC Evolutionary Biology **11:** 1-15

Attali B, Guillemare E, Lesage F, Honore E, Romey G, Lazdunski M, Barhanin J (1993) The protein isk is a dual activator of K^+ and Cl^- channels. Nature **365:** 850-852

Azad AK, Katsuhara M, Sawa Y, Ishikawa T, Shibata H (2008) Characterization of four plasma membrane aquaporins in tulip petals: a putative homolog is regulated by phosphorylation. Plant and Cell Physiology **49:** 1196-1208

Barkla BJ, Vera-Estrella R, Pantoja O, Kirch HH, Bohnert HJ (1999) Aquaporin localization - how valid are the TIP and PIP labels? Trends in Plant Science **4:** 86-88

Barrieu F, Chaumont F, Chrispeels MJ (1998) High expression of the tonoplast aquaporin ZmTIP1 in epidermal and conducting tissues of maize. Plant Physiology **117:** 1153-1163

Beaudette PC, Chlup M, Yee J, Emery RN (2007) Relationships of root conductivity and aquaporin gene expression in Pisum sativum: diurnal patterns and the response to $HgCl_2$ and ABA. Journal of Experimental Botany **58:** 1291-1300

Beebo A, Mathai JC, Schoefs B, Spetea C (2013) Assessment of the requirement for aquaporins in the thylakoid membrane of plant chloroplasts to sustain photosynthetic water oxidation. FEBS Letters **587:** 2083-2089

Benga G, Popescu O, Pop VI, Hodor P, Borza T (1992) Effects on water diffusion of inhibitors affecting various transport processes in human red-blood-cells. European Journal of Cell Biology **59:** 219-223

Bertl A, Kaldenhoff R (2007) Function of a separate NH_3-pore in Aquaporin TIP2;2 from wheat. FEBS Letters **581:** 5413-5417

Besse M, Knipfer T, Miller AJ, Verdeil J-L, Jahn TP, Fricke W (2011) Developmental pattern of aquaporin expression in barley (*Hordeum vulgare L.*) leaves. Journal of Experimental Botany **62:** 4127-4142

Biela A, Grote K, Otto B, Hoth S, Hedrich R, Kaldenhoff R (1999) The *Nicotiana* tabacum plasma membrane aquaporin NtAQP1 is mercury-insensitive and permeable for glycerol. Plant Journal **18:** 565-570

Bienert GP, Bienert MD, Jahn TP, Boutry M, Chaumont F (2011) Solanaceae XIPs are plasma membrane aquaporins that facilitate the transport of many uncharged substrates. The Plant Journal **66:** 306-317

Bienert GP, Moller ALB, Kristiansen KA, Schulz A, Moller IM, Schjoerring JK, Jahn TP (2007) Specific aquaporins facilitate the diffusion of hydrogen peroxide across membranes. Journal of Biological Chemistry **282:** 1183-1192

Bing M, XIANG Y, Sheng-mei M, Tao L, He-ming Y, Xue-jun L (2004) Effects of acetazolamide and anordiol on osmotic water permeability in AQP1-cRNA injected *Xenopus* oocyte. Acta Pharmacol. Sin **25:** 90-97

Blank ME, Ehmke H (2003) Aquaporin-1 and HCO_3^-–Cl^- transporter-mediated transport of CO_2 across the human erythrocyte membrane. The Journal of Physiology **550:** 419-429

Block MA, Dorne AJ, Joyard J, Douce R (1983) Preparation and characterization of membrane-fractions enriched in outer and inner envelope membranes from spinach-chloroplasts .1. electrophoretic and immunochemical analyses. Journal of Biological Chemistry **258:** 3273-3280

Boassa D, Stamer WD, Yool AJ (2006) Ion channel function of aquaporin-1 natively expressed in choroid plexus. The Journal of Neuroscience **26:** 7811-7819

Boassa D, Yool AJ (2003) Single amino acids in the carboxyl terminal domain of aquaporin-1 contribute to cGMP-dependent ion channel activation. BMC Physiology **3:** 12-12

Bolter B, Soll J (2001) Ion channels in the outer membranes of chloroplasts and mitochondria: open doors or regulated gates? EMBO Journal **20:** 935-940

Bolter B, Soll J, Hill K, Hemmler R, Wagner R (1999) A rectifying ATP-regulated solute channel in the chloroplastic outer envelope from pea. EMBO Journal **18:** 5505-5516

Boron WF, Deweer P (1976) Intracellular pH transients in squid giant-axons caused by CO_2, NH_3, and metabolic-inhibitors. Journal of General Physiology **67:** 91-112

Boron WF, Endeward V, Gros G, Musa-Aziz R, Pohl P (2011) Intrinsic CO_2 permeability of cell membranes and potential biological relevance of CO_2 channels. ChemPhysChem **12:** 1017-1019

Brooks HL, Regan JW, Yool AJ (2000) Inhibition of aquaporin-1 water permeability by tetraethylammonium: involvement of the loop E pore region. Molecular Pharmacology **57:** 1021-1026

Calamita G, Ferri D, Gena P, Liquori GE, Cavalier A, Thomas D, Svelto M (2005) The inner mitochondrial membrane has aquaporin-8 water channels and is highly permeable to water. Journal of Biological Chemistry **280:** 17149-17153

Campbell EM, Birdsell DN, Yool AJ (2012) The Activity of Human Aquaporin 1 as a cGMP-Gated Cation Channel Is Regulated by Tyrosine Phosphorylation in the Carboxyl-Terminal Domain. Molecular Pharmacology **81:** 97-105

Catala A (2012) Lipid peroxidation modifies the picture of membranes from the "Fluid Mosaic Model" to the "Lipid Whisker Model". Biochimie **94:** 101-109

Chaumont F, Barrieu F, Jung R, Chrispeels MJ (2000) Plasma membrane intrinsic proteins from maize cluster in two sequence subgroups with differential aquaporin activity. Plant Physiology **122:** 1025-1034

Chaumont F, Barrieu F, Wojcik E, Chrispeels MJ, Jung R (2001) Aquaporins constitute a large and highly divergent protein family in maize. Plant Physiology **125:** 1206-1215

Chaumont F, Loomis WF, Chrispeels MJ (1997) Expression of an *Arabidopsis* plasma membrane aquaporin in *Dictyostelium* results in hypoosmotic sensitivity and developmental abnormalities. Proceedings of the National Academy of Sciences of the United States of America **94:** 6202-6209

Chaumont F, Moshelion M, Daniels MJ (2005) Regulation of plant aquaporin activity. Biology of the Cell **97:** 749-764

Cheng AC, vanHoek AN, Yeager M, Verkman AS, Mitra AK (1997) Three-dimensional organization of a human water channel. Nature **387:** 627-630

Choi W-G, Roberts DM (2007) *Arabidopsis* NIP2;1, a major intrinsic protein transporter of lactic acid induced by anoxic stress. Journal of Biological Chemistry **282:** 24209-24218

Chrispeels MJ, Agre P (1994) Aquaporins - water channel proteins of plant and animal-cells. Trends in Biochemical Sciences **19:** 421-425

Chrispeels MJ, Maurel C (1994) Aquaporins - the molecular-basis of facilitated water-movement through living plant-cells. Plant Physiology **105:** 9-13

Clement NR, Gould JM (1981) Pyranine (8-hydroxy-1, 3, 6-pyrenetrisulfonate) as a probe of internal aqueous hydrogen ion concentration in phospholipid vesicles. Biochemistry **20:** 1534-1538

Cooper GJ, Boron WF (1998) Effect of PCMBS on CO_2 permeability of *Xenopus* oocytes expressing aquaporin 1 or its C189S mutant. American Journal of Physiology-Cell Physiology **275:** C1481-C1486

Coskun D, Britto DT, Jean Y-K, Schulze LM, Becker A, Kronzucker HJ (2012) Silver ions disrupt K^+ homeostasis and cellular integrity in intact barley (*Hordeum vulgare L.*) roots. Journal of Experimental Botany **63:** 151-162

Daleke DL, Hong K, Papahadjopoulos D (1990) Endocytosis of liposomes by macrophages: binding, acidification and leakage of liposomes monitored by a new fluorescence assay. Biochimica et Biophysica Acta (BBA) - Biomembranes **1024:** 352-366

Damiano E, Bassilana M, Rigaud J-L, Leblanc G (1984) Use of the pH sensitive fluorescence probe pyranine to monitor internal pH changes in *Escherichia coli* membrane vesicles. FEBS Letters **166:** 120-124

Daniels MJ, Chrispeels MJ, Yeager M (1999) Projection structure of a plant vacuole membrane aquaporin by electron cryo-crystallography. Journal of Molecular Biology **294:** 1337-1349

Daniels MJ, Mirkov TE, Chrispeels MJ (1994) The plasma-membrane of *Arabidopsis thaliana* contains a mercury-insensitive aquaporin that is a homolog of the tonoplast water channel protein tip. Plant Physiology **106:** 1325-1333

Danielson J, Johanson U (2008) Unexpected complexity of the Aquaporin gene family in the moss *Physcomitrella* patens. BMC Plant Biology **8:** 45

De Angeli A, Zhang J, Meyer S, Martinoia E (2013) AtALMT9 is a malate-activated vacuolar chloride channel required for stomatal opening in *Arabidopsis*. Nature Communications **4:** 1804

de Groot BL, Grubmuller H (2005) The dynamics and energetics of water permeation and proton exclusion in aquaporins. Current Opinion in Structural Biology **15:** 176-183

de Groot BL, Hub JS (2011) A decade of debate: significance of CO_2 permeation through membrane channels still controversial. Chemphyschem **12:** 1021-1022

Dean RM, Rivers RL, Zeidel ML, Roberts DM (1999) Purification and functional reconstitution of soybean nodulin 26. An aquaporin with water and glycerol transport properties. Biochemistry **38:** 347-353

Denker BM, Smith BL, Kuhajda FP, Agre P (1988) Identification, purification, and partial characterization of a novel Mr 28,000 integral membrane protein from erythrocytes and renal tubules. Journal of Biological Chemistry **263:** 15634-15642

Ding X, Matsumoto T, Gena P, Liu C, Pellegrini-Calace M, Zhong S, Sun X, Zhu Y, Katsuhara M, Iwasaki I, Kitagawa Y, Calamita G (2013) Water and CO_2 permeability of SsAqpZ, the cyanobacterium Synechococcus sp PCC7942 aquaporin. Biology of the Cell **105:** 118-128

Dordas C, Brown PH (2001) Evidence for channel mediated transport of boric acid in squash (*Cucurbita pepo*). Plant and Soil **235:** 95-103

Downton J, Slatyer R (1972) Temperature dependence of photosynthesis in cotton. Plant Physiology **50:** 518-522

Dubois E, Grenson M (1979) Methylamine-ammonia uptake systems in *saccharomyces-cerevisiae* - multiplicity and regulation. Molecular & General Genetics **175:** 67-76

Dynowski M, Schaaf G, Loque D, Moran O, Ludewig U (2008) Plant plasma membrane water channels conduct the signalling molecule H_2O_2. Biochemical Journal **414:** 53-61

Eckert M, Biela A, Siefritz F, Kaldenhoff R (1999) New aspects of plant aquaporin regulation and specificity. Journal of Experimental Botany **50:** 1541-1545

Endeward V, Cartron J-P, Ripoche P, Gros G (2008) RhAG protein of the Rhesus complex is a CO_2 channel in the human red cell membrane. The FASEB Journal **22:** 64-73

Endeward V, Gros G (2005) Low carbon dioxide permeability of the apical epithelial membrane of guinea-pig colon. The Journal of Physiology **567:** 253-265

Endeward V, Gros G (2009) Extra- and intracellular unstirred layer effects in measurements of CO_2 diffusion across membranes - a novel approach applied to the mass spectrometric O-18 technique for red blood cells. Journal of Physiology-London **587:** 1153-1167

Endeward V, Musa-Aziz R, Cooper GJ, Chen L-M, Pelletier MF, Virkki LV, Supuran CT, King LS, Boron WF, Gros G (2006) Evidence that aquaporin 1 is a major pathway for CO_2 transport across the human erythrocyte membrane. The FASEB Journal **20:** 1974-1981

Engel A, Fijiyoshi Y, Agre P (2000) The importance of aquaporin water channel protein structures. Embo Journal **19:** 800-806

Engelman DM (2005) Membranes are more mosaic than fluid. Nature **438:** 578-580

Eriksson UK, Fischer G, Friemann R, Enkavi G, Tajkhorshid E, Neutze R (2013) Subangstrom Resolution X-Ray Structure Details Aquaporin-Water Interactions. Science **340:** 1346-1349

Evans JR, Kaldenhoff R, Genty B, Terashima I (2009) Resistances along the CO_2 diffusion pathway inside leaves. Journal of Experimental Botany **60:** 2235-2248

Evans JR, Voncaemmerer S, Setchell BA, Hudson GS (1994) The relationship between CO_2 transfer conductance and leaf anatomy in transgenic tobacco with a reduced content of rubisco. Australian Journal of Plant Physiology **21:** 475-495

Fang X, Yang B, Matthay MA, Verkman AS (2002) Evidence against aquaporin-1-dependent CO_2 permeability in lung and kidney. The Journal of Physiology **542:** 63-69

Fetter K, Van Wilder V, Moshelion M, Chaumont F (2004) Interactions between plasma membrane aquaporins modulate their water channel activity. Plant Cell **16:** 215-228

Flexas J, Barbour MM, Brendel O, Cabrera HM, Carriqui M, Diaz-Espejo A, Douthe C, Dreyerc E, Ferrio JP, Gago J, Galle A, Galmes J, Kodama N, Medrano H, Niinemets U, Peguero-Pina JJ, Poua A, Ribas-Carbo M, Tomas M, Tosens T, Warren CR (2012) Mesophyll diffusion conductance to CO_2: An unappreciated central player in photosynthesis Plant Science **196:** 31-31

Flexas J, Ribas-Carbo M, Diaz-Espejo A, Galmes J, Medrano H (2008) Mesophyll conductance to CO_2: current knowledge and future prospects. Plant Cell and Environment **31:** 602-621

Flugge UI, Benz R (1984) Pore-forming activity in the outer-membrane of the chloroplast envelope. FEBS Letters **169:** 85-89

Forrest KL, Bhave M (2008) The PIP and TIP aquaporins in wheat form a large and diverse family with unique gene structures and functionally important features. Functional & Integrative Genomics **8:** 115-133

Fortin MG, Morrison NA, Verma DPS (1987) Nodulin-26, a peribacteroid membrane nodulin is expressed independently of the development of the peribacteroid compartment. Nucleic Acids Research **15:** 813-824

Fotiadis D, Jeno P, Mini T, Wirtz S, Muller SA, Fraysse L, Kjellbom P, Engel A (2001) Structural characterization of two aquaporins isolated from native spinach leaf plasma membranes. Journal of Biological Chemistry **276:** 1707-1714

Franks PJ, Adams MA, Amthor JS, Barbour MM, Berry JA, Ellsworth DS, Farquhar GD, Ghannoum O, Lloyd J, McDowell N, Norby RJ, Tissue DT, von Caemmerer S (2013) Sensitivity of plants to changing atmospheric CO_2 concentration: from the geological past to the next century. New Phytologist **197:** 1077-1094

Friedman H, Meir S, Rosenberger I, Halevy AH, Kaufman PB, Philosoph-Hadas S (1998) Inhibition of the gravitropic response of snapdragon spikes by the calcium-channel blocker lanthanum chloride. Plant Physiology **118:** 483-492

Froger A, Thomas D, Delamarche C, Tallur B (1998) Prediction of functional residues in water channels and related proteins. Protein Science **7:** 1458-1468

Fu D, Libson A, Miercke LJW, Weitzman C, Nollert P, Krucinski J, Stroud RM (2000) Structure of a glycerol-conducting channel and the basis for its selectivity. Science **290:** 481-486

Fu D, Lu M (2007) The structural basis of water permeation and proton exclusion in aquaporins. Molecular Membrane Biology **24:** 366-374

Fujiyoshi Y (2007) Structure and function of channels. Journal of Biomolecular Structure & Dynamics **24:** 730-731

Garrill A, Tyerman SD, Findlay GP, Ryan PR (1996) Effects of NPPB and niflumic acid on outward K^+ and Cl^- currents across the plasma membrane of wheat root protoplasts. Australian Journal of Plant Physiology **23:** 527-534

Gerbeau P, Guclu J, Ripoche P, Maurel C (1999) Aquaporin Nt-TIPa can account for the high permeability of tobacco cell vacuolar membrane to small neutral solutes. Plant Journal **18:** 577-587

Geyer RR, Musa-Aziz R, Qin X, Boron WF (2013) Relative CO_2/NH_3 selectivities of mammalian aquaporins 0-9. American journal of physiology. Cell physiology **304:** C985-994

Gietz RD, Schiestl RH (2007) High-efficiency yeast transformation using the LiAc/SS carrier DNA/PEG method. Nature Protocols **2:** 31-34

Gonen T, Sliz P, Kistler J, Cheng YF, Walz T (2004) Aquaporin-0 membrane junctions reveal the structure of a closed water pore. Nature **429:** 193-197

Gonen T, Walz T (2006) The structure of aquaporins. Quarterly Reviews of Biophysics **39:** 361-396

Gregoire C, Remus-Borel W, Vivancos J, Labbe C, Belzile F, Belanger RR (2012) Discovery of a multigene family of aquaporin silicon transporters in the primitive plant Equisetum arvense. Plant Journal **72:** 320-330

Gu R, Chen X, Zhou Y, Yuan L (2012) Isolation and characterization of three maize aquaporin genes, ZmNIP2;1, ZmNIP2;4 and ZmTIP4;4 involved in urea transport. Bmb Reports **45:** 96-101

Gustavsson S, Lebrun AS, Norden K, Chaumont F, Johanson U (2005) A novel plant major intrinsic protein in Physcomitrella patens most similar to bacterial glycerol channels. Plant Physiology **139:** 287-295

Gutknecht J, Bisson MA, Tosteson FC (1977) Diffusion of carbon-dioxide through lipid bilayer membranes - effects of carbonic-anhydrase, bicarbonate, and unstirred layers. Journal of General Physiology **69:** 779-794

Hachez C, Chaumont F (2010) Aquaporins: a family of highly regulated multifunctional channels. *In* TP Jahn, GP Bienert, eds, Mips and Their Role in the Exchange of Metalloids, Vol 679, pp 1-18

Hanba YT, Miyazawa SI, Terashima I (1999) The influence of leaf thickness on the CO_2 transfer conductance and leaf stable carbon isotope ratio for some evergreen tree species in Japanese warm-temperate forests. Functional Ecology **13:** 632-639

Hanba YT, Shibasaka M, Hayashi Y, Hayakawa T, Kasamo K, Terashima I, Katsuhara M (2004) Overexpression of the barley aquaporin HvPIP2;1 increases internal CO_2 conductance and CO_2 assimillation in the leaves of transgenic rice plants. Plant and Cell Physiology **45:** 521-529

Hartje S, Zimmermann S, Klonus D, Mueller-Roeber B (2000) Functional characterisation of LKT1, a K^+ uptake channel from tomato root hairs, and comparison with the closely related potato inwardly rectifying K^+ channel SKT1 after expression in *Xenopus* oocytes. Planta **210:** 723-731

Harvengt P, Vlerick A, Fuks B, Wattiez R, Ruysschaert JM, Homble F (2000) Lentil seed aquaporins form a hetero-oligomer which is phosphorylated by a Mg^{2+}-dependent and Ca^{2+}-regulated kinase. Biochemical Journal **352:** 183-190

Hazama A, Kozono D, Guggino WB, Agre P, Yasui M (2002) Ion permeation of AQP6 water channel protein - Single-channel recordings after Hg^{2+} activation. Journal of Biological Chemistry **277:** 29224-29230

Heckwolf M, Pater D, Hanson DT, Kaldenhoff R (2011) The *Arabidopsis thaliana* aquaporin AtPIP1;2 is a physiologically relevant CO_2 transport facilitator. The Plant Journal **67:** 795-804

Heibert T, Steinkamp T, Hinnah S, Schwarz M, Flueggel U-I, Weber A, Wagner R (1995) Ion channels in the chloroplast envelope membrane. Biochemistry **34:** 15906-15917

Heinen RB, Ye Q, Chaumont F (2009) Role of aquaporins in leaf physiology. Journal of Experimental Botany **60:** 2971-2985

Hempleman SC, Rodriguez TA, Bhagat YA, Begay RS (2000) Benzolamide, acetazolamide, and signal transduction in avian intrapulmonary chemoreceptors. American Journal of Physiology - Regulatory, Integrative and Comparative Physiology **279:** R1988-R1995

Heymann JB, Engel A (1999) Aquaporins: Phylogeny, structure, and physiology of water channels. News in Physiological Sciences **14:** 187-193

Hill WG, Southern NM, MacIver B, Potter E, Apodaca G, Smith CP, Zeidel ML (2005) Isolation and characterization of the *Xenopus* oocyte plasma membrane: a new method for studying activity of water and solute transporters. American Journal of Physiology - Renal Physiology **289:** F217-F224

Hiroaki Y, Tani K, Kamegawa A, Gyobu N, Nishikawa K, Suzuki H, Walz T, Sasaki S, Mitsuoka K, Kimura K, Mizoguchi A, Fujiyoshi Y (2006) Implications of the aquaporin-4 structure on array formation and cell adhesion. Journal of Molecular Biology **355:** 628-639

Holm LM, Jahn TP, Moller ALB, Schjoerring JK, Ferri D, Klaerke DA, Zeuthen T (2005) NH_3 and NH_4^+ permeability in aquaporin-expressing *Xenopus* oocytes. Pflugers Archiv-European Journal of Physiology **450:** 415-428

Hove RM, Bhave M (2011) Plant aquaporins with non-aqua functions: deciphering the signature sequences. Plant Molecular Biology **75:** 413-430

Hub JS, de Groot BL (2006) Does CO_2 permeate through aquaporin-1? Biophysical Journal **91:** 842-848

Hub JS, De Groot BL (2008) Mechanism of selectivity in aquaporins and aquaglyceroporins. Proceedings of the National Academy of Sciences of the United States of America **105:** 1198-1203

Hwang JH, Ellingson SR, Roberts DM (2010) Ammonia permeability of the soybean nodulin 26 channel. Febs Letters **584:** 4339-4343

Ikeda M, Beitz E, Kozono D, Guggino WB, Agre P, Yasui M (2002) Characterization of aquaporin-6 as a nitrate channel in mammalian cells - Requirement of pore-lining residue threonine 63. Journal of Biological Chemistry **277:** 39873-39879

Ilan B, Tajkhorshid E, Schulten K, Voth GA (2004) The mechanism of proton exclusion in aquaporin channels. Proteins: Structure, Function, and Bioinformatics **55:** 223-228

Ishibashi K (2006) Aquaporin subfamily with unusual NPA boxes. Biochimica Et Biophysica Acta-Biomembranes **1758:** 989-993

Ishikawa F, Suga S, Uemura T, Sato MH, Maeshima M (2005) Novel type aquaporin SIPs are mainly localized to the ER membrane and show cell-specific expression in Arabidopsis thaliana. FEBS Letters **579:** 5814-5820

Itel F, Al-Samir S, Öberg F, Chami M, Kumar M, Supuran CT, Deen PMT, Meier W, Hedfalk K, Gros G, Endeward V (2012) CO_2 permeability of cell membranes is regulated by membrane cholesterol and protein gas channels. The FASEB Journal **26:** 5182-5191

Jahn TP, Moller ALB, Zeuthen T, Holm LM, Klaerke DA, Mohsin B, Kuhlbrandt W, Schjoerring JK (2004) Aquaporin homologues in plants and mammals transport ammonia. FEBS Letters **574:** 31-36

Jang JY, Lee SH, Rhee JY, Chung GC, Ahn SJ, Kang H (2007) Transgenic *Arabidopsis* and tobacco plants overexpressing an aquaporin respond differently to various abiotic stresses. Plant Molecular Biology **64:** 621-632

Johanson U, Karlsson M, Johansson I, Gustavsson S, Sjovall S, Fraysse L, Weig AR, Kjellbom P (2001) The complete set of genes encoding major intrinsic proteins in arabidopsis provides a framework for a new nomenclature for major intrinsic proteins in plants. Plant Physiology **126:** 1358-1369

Johansson I, Karlsson M, Johanson U, Larsson C, Kjellbom P (2000) The role of aquaporins in cellular and whole plant water balance. Biochimica et Biophysica Acta (BBA) - Biomembranes **1465:** 324-342

Johansson I, Karlsson M, Shukla VK, Chrispeels MJ, Larsson C, Kjellbom P (1998) Water transport activity of the plasma membrane aquaporin PM28A is regulated by phosphorylation. Plant Cell **10:** 451-459

Jones TG, Walker JCF, Langrish TAG (1995) Dissolved carbon-dioxide gas-diffusion in green nothofagus-fusca heartwood. Wood Science and Technology **29:** 171-176

Jozefkowicz C, Rosi P, Sigaut L, Soto G, Pietrasanta LI, Amodeo G, Alleva K (2013) Loop A is critical for the functional interaction of two beta vulgaris PIP aquaporins. Plos One **8:** e57993

Jung JS, Preston GM, Smith BL, Guggino WB, Agre P (1994) Molecular-structure of the water channel through aquaporin chip - the hourglass model. Journal of Biological Chemistry **269:** 14648-14654

Kaldenhoff R (2012) Mechanisms underlying CO_2 diffusion in leaves. Current Opinion in Plant Biology **15:** 276-281

Kaldenhoff R, Fischer M (2006) Functional aquaporin diversity in plants. Biochimica Et Biophysica Acta-Biomembranes **1758:** 1134-1141

Kaldenhoff R, Grote K, Zhu JJ, Zimmermann U (1998) Significance of plasmalemma aquaporins for water-transport in *Arabidopsis thaliana*. Plant Journal **14:** 121-128

Kammerloher W, Fischer U, Piechottka GP, Schaffner AR (1994) Water channels in the plant plasma-membrane cloned by immunoselection from a mammalian expression system. Plant Journal **6:** 187-199

Kano K, Fendler JH (1978) Pyranine as a sensitive pH probe for liposome interiors and surfaces. pH gradients across phospholipid vesicles. Biochimica et Biophysica Acta (BBA)-Biomembranes **509:** 289-299

Karlsson M, Johansson I, Bush M, McCann MC, Maurel C, Larsson C, Kjellbom P (2000) An abundant TIP expressed in mature highly vacuolated cells. Plant Journal **21:** 83-90

Katsuhara M, Hanba Y, Shibasaka M, Hayashi Y, Hayakawa T, Kasamo K (2003) Increase in CO_2 permeability (diffusion conductance) in leaves of transgenic rice plant over-expressing barley aquaporin. Plant and Cell Physiology **44:** S86-S86

Khademi S, O'Connell J, Remis J, Robles-Colmenares Y, Miericke LJW, Stroud RM (2004) Mechanism of ammonia transport by Amt/MEP/Rh: Structure of AmtB at 1.3.5 angstrom. Science **305:** 1587-1594

Knipfer T, Besse M, Verdeil J-L, Fricke W (2011) Aquaporin-facilitated water uptake in barley (*Hordeum vulgare L*.) roots. Journal of Experimental Botany **62:** 4115-4126

Kozono D, Ding XD, Iwasaki I, Meng XY, Kamagata Y, Agre P, Kitagawa Y (2003) Functional expression and characterization of an archaeal aquaporin - AqpM from Methanothermobacter marburgensis. Journal of Biological Chemistry **278:** 10649-10656

Krieg PA, Melton DA (1984) Functional messenger-rnas are produced by sp6 invitro transcription of cloned cdnas. Nucleic Acids Research **12:** 7057-7070

Kucherenko YV, Wagner-Britz L, Bernhardt I, Lang F (2013) Effect of Chloride Channel Inhibitors on Cytosolic Ca^{2+} Levels and Ca^{2+}-Activated K^+ (Gardos) Channel Activity in Human Red Blood Cells. Journal of Membrane Biology **246:** 315-326

Kukulski W, Schenk AD, Johanson U, Braun T, de Groot BL, Fotiadis D, Kjellbom P, Engel A (2005) The 5 angstrom structure of heterologously expressed plant aquaporin SoPIP2;1. Journal of Molecular Biology **350:** 611-616

Laizé V, Rousselet G, Verbavatz J-M, Berthonaud V, Gobin R, Roudier N, Abrami L, Ripoche P, Tacnet F (1995) Functional expression of the human CHIP28 water channel in a yeast secretory mutant. FEBS Letters **373:** 269-274

Larsson C, Kjellbom P, Widell S, Lundborg T (1984) Sidedness of plant plasma-membrane vesicles purified by partitioning in aqueous 2-phase systems. FEBS Letters **171:** 271-276

Larsson C, Sommarin M, Widell S (1994) [44] Isolation of highly purified plant plasma membranes and separation of inside-out and right-side-out vesicles. *In* GJ Harry Walter, ed, Methods in Enzymology, Vol Volume 228. Academic Press, pp 451-469

Larsson C, Widell S, Kjellbom P (1987) [52] Preparation of high-purity plasma membranes. *In* RD Lester Packer, ed, Methods in Enzymology, Vol Volume 148. Academic Press, pp 558-568

Leitão L, Prista C, Moura TF, Loureiro-Dias MC, Soveral G (2012) Grapevine aquaporins: gating of a tonoplast intrinsic protein (TIP2; 1) by cytosolic pH. Plos One **7:** e33219

Li G-W, Zhang M-H, Cai W-M, Sun W-N, Su W-A (2008) Characterization of OsPIP2;7, a Water Channel Protein in Rice. Plant and Cell Physiology **49:** 1851-1858

Li T, Choi W-G, Wallace IS, Baudry J, Roberts DM (2011) *Arabidopsis thaliana* NIP7;1: an anther-specific boric acid transporter of the aquaporin superfamily regulated by an unusual tyrosine in helix 2 of the transport pore. Biochemistry **50:** 6633-6641

Liman ER, Tytgat J, Hess P (1992) Subunit stoichiometry of a mammalian K^+ channel determined by construction of multimeric cDNAs. Neuron **9:** 861-871

Liu K, Kozono D, Kato Y, Agre P, Hazama A, Yasui M (2005) Conversion of aquaporin 6 from an anion channel to a water-selective channel by a single amino acid substitution. Proceedings of the National Academy of Sciences of the United States of America **102:** 2192-2197

Liu K, Nagase H, Huang CG, Calamita G, Agre P (2006) Purification and functional characterization of aquaporin-8. Biology of the Cell **98:** 153-161

Liu LH, Ludewig U, Gassert B, Frommer WB, von Wiren N (2003) Urea transport by nitrogen-regulated tonoplast intrinsic proteins in *Arabidopsis*. Plant Physiology **133:** 1220-1228

Loo DDF, Zeuthen T, Chandy G, Wright EM (1996) Cotransport of water by the Na^+/glucose cotransporter. Proceedings of the National Academy of Sciences of the United States of America **93:** 13367-13370

Lopez D, Bronner G, Brunel N, Auguin D, Bourgerie S, Brignolas F, Carpin S, Tournaire-Roux C, Maurel C, Fumanal B, Martin F, Sakr S, Label P, Julien JL, Gousset-Dupont A, Venisse JS (2012) Insights into Populus XIP aquaporins: evolutionary expansion, protein functionality, and environmental regulation. Journal of Experimental Botany **63:** 2217-2230

Loque D, Ludewig U, Yuan LX, von Wiren N (2005) Tonoplast intrinsic proteins AtTIP2;1 and AtTIP2;3 facilitate NH_3 transport into the vacuole. Plant Physiology **137:** 671-680

Lowry OH, Rosebrough NJ, Farr AL, Randall RJ (1951) Protein measurement with the folin phenol reagent. Journal of Biological Chemistry **193:** 265-275

Luu D-T, Maurel C (2013) Aquaporin trafficking in plant cells: an emerging membrane-protein model. Traffic **14:** 629-635

Ma JF, Tamai K, Yamaji N, Mitani N, Konishi S, Katsuhara M, Ishiguro M, Murata Y, Yano M (2006) A silicon transporter in rice. Nature **440:** 688-691

Maciejewski PM, Peterson FC, Anderson PJ, Brooks CL (1995) Mutation of serine 90 to glutamic acid mimics phosphorylation of bovine prolactin. Journal of Biological Chemistry **270:** 27661-27665

Maharajh DM, Walkley J (1973) Temperature-dependence of diffusion-coefficients of Ar, CO_2, CH_4, CH_3Cl, CH_3Br, and $CHCl_2F$ in water. Canadian Journal of Chemistry-Revue Canadienne De Chimie **51:** 944-952

Marini A-M, Soussi-Boudekou S, Vissers S, André B (1997) A family of ammonium transporters in *Saccharomyces cerevisiae*. Molecular and Cellular Biology **17:** 4282-4293

Marrink SJ, Berendsen HJC (1994) Simulation of water transport through a lipid-membrane. Journal of Physical Chemistry **98:** 4155-4168

Martinière A, Li X, Runions J, Lin J, Maurel C, Luu D-T (2012) Salt stress triggers enhanced cycling of *Arabidopsis* root plasma-membrane aquaporins. Plant Signaling & Behavior **7:** 529-532

Martre P, Morillon R, Barrieu F, North GB, Nobel PS, Chrispeels MJ (2002) Plasma membrane aquaporins play a significant role during recovery from water deficit. Plant Physiology **130:** 2101-2110

Masalkar P, Wallace IS, Hwang JH, Roberts DM (2010) Interaction of cytosolic glutamine synthetase of soybean root nodules with the C-terminal domain of the symbiosome membrane Nodulin 26 Aquaglyceroporin. Journal of Biological Chemistry **285:** 23880-23888

Maurel C (2007) Plant aquaporins: Novel functions and regulation properties. FEBS Letters **581:** 2227-2236

Maurel C, Chrispeels MJ (2001) Aquaporins. A molecular entry into plant water relations. Plant Physiology **125:** 135-138

Maurel C, Kado RT, Guern J, Chrispeels MJ (1995) Phosphorylation regulates the water channel activity of the seed-specific aquaporin alpha-tip. Embo Journal **14:** 3028-3035

Maurel C, Reizer J, Schroeder JI, Chrispeels MJ (1993) The vacuolar membrane-protein gamma-tip creates water specific channels in xenopus-oocytes. Embo Journal **12:** 2241-2247

Maurel C, Tacnet F, Güclü J, Guern J, Ripoche P (1997) Purified vesicles of tobacco cell vacuolar and plasma membranes exhibit dramatically different water permeability and water channel activity. Proceedings of the National Academy of Sciences of the United States of America **94:** 7103-7108

Maurel C, Verdoucq L, Luu D-T, Santoni V (2008) Plant aquaporins: Membrane channels with multiple integrated functions. *In* Annual Review of Plant Biology, Vol 59, pp 595-624

Missner A, Kuegler P, Saparov SM, Sommer K, Mathai JC, Zeidel ML, Pohl P (2008) Carbon dioxide transport through membranes. Journal of Biological Chemistry **283:** 25340-25347

Missner A, Pohl P (2009) 110 years of the Meyer–Overton rule: predicting membrane permeability of gases and other small compounds. ChemPhysChem **10:** 1405-1414

Montpetit J, Vivancos J, Mitani-Ueno N, Yamaji N, Remus-Borel W, Belzile F, Ma JF, Belanger RR (2012) Cloning, functional characterization and heterologous expression of TaLsi1, a wheat silicon transporter gene. Plant Molecular Biology **79:** 35-46

Morison JIL, Lawson T, Cornic G (2007) Lateral CO_2 diffusion inside dicotyledonous leaves can be substantial: quantification in different light intensities. Plant Physiology **145:** 680-690

Moshelion M, Becker D, Biela A, Uehlein N, Hedrich R, Otto B, Levi H, Moran N, Kaldenhoff R (2002) Plasma membrane aquaporins in the motor cells of Samanea saman: Diurnal and circadian regulation. Plant Cell **14:** 727-739

Munns R, James RA, Xu B, Athman A, Conn SJ, Jordans C, Byrt CS, Hare RA, Tyerman SD, Tester M (2012) Wheat grain yield on saline soils is improved by an ancestral Na^+ transporter gene. Nature Biotechnology **30:** 360-364

Murata K, Mitsuoka K, Hirai T, Walz T, Agre P, Heymann JB, Engel A, Fujiyoshi Y (2000) Structural determinants of water permeation through aquaporin-1. Nature **407:** 599-605

Musa-Aziz R, Chen L-M, Pelletier MF, Boron WF (2009) Relative CO_2/NH_3 selectivities of AQP1, AQP4, AQP5, AmtB, and RhAG. Proceedings of the National Academy of Sciences of the United States of America **106:** 5406-5411

Naccache P, Shaafi RI (1974) Effect of pcmbs on water transfer across biological-membranes. Journal of Cellular Physiology **83:** 449-456

Nakhoul NL, Davis BA, Romero MF, Boron WF (1998) Effect of expressing the water channel aquaporin-1 on the CO_2 permeability of *Xenopus* oocytes. American Journal of Physiology-Cell Physiology **274:** C543-C548

Nakhoul NL, Hering-Smith KS, Abdulnour-Nakhoul SM, Hamm LL (2001) Transport of NH_3/NH_4^+ in oocytes expressing aquaporin-1. American Journal of Physiology-Renal Physiology **281:** F255-F263

Navarro-Ródenas A, Ruíz-Lozano JM, Kaldenhoff R, Morte A (2012) The aquaporin TcAQP1 of the desert truffle terfezia claveryi is a membrane pore for water and CO_2 transport. Molecular Plant-Microbe Interactions **25:** 259-266

Negrete HO, Lavelle JP, Berg J, Lewis SA, Zeidel ML (1996) Permeability properties of the intact mammalian bladder epithelium. American Journal of Physiology - Renal Physiology **271:** F886-F894

Niemietz CM, Tyerman SD (1997) Characterization of water channels in wheat root membrane vesicles. Plant Physiology **115:** 561-567

Niemietz CM, Tyerman SD (2000) Channel-mediated permeation of ammonia gas through the peribacteroid membrane of soybean nodules. FEBS Letters **465:** 110-114

Niemietz CM, Tyerman SD (2002) New potent inhibitors of aquaporins: silver and gold compounds inhibit aquaporins of plant and human origin. FEBS Letters **531:** 443-447

Niinemets O, Reichstein M (2003) Controls on the emission of plant volatiles through stomata: A sensitivity analysis. Journal of Geophysical Research **108:** ACH3-1-10

Nobel PS (1977) Internal leaf area and cellular CO_2 resistance - photosynthetic implications of variations with growth-conditions and plant species. Physiologia Plantarum **40:** 137-144

Okada Y, Maeno E (2001) Apoptosis, cell volume regulation and volume-regulatory chloride channels. Comparative Biochemistry and Physiology Part A: Molecular & Integrative Physiology **130:** 377-383

Otto B, Uehlein N, Sdorra S, Fischer M, Ayaz M, Belastegui-Macadam X, Heckwolf M, Lachnit M, Pede N, Priem N, Reinhard A, Siegfart S, Urban M, Kaldenhoff R (2010) Aquaporin tetramer composition modifies the function of tobacco aquaporins. Journal of Biological Chemistry **285:** 31253-31260

Pal S, Tak YK, Song JM (2007) Does the antibacterial activity of silver nanoparticles depend on the shape of the nanoparticle? A study of the gram-negative bacterium *Escherichia coli*. Applied and Environmental Microbiology **73:** 1712-1720

Pamgren MG, Askerlund P, Fredrikson K, Widell S, Sommarin M, Larsson C (1990) Sealed inside-out and right-side-out plasma membrane vesicles. Plant Physiology **92:** 871-880

Park JH, Saier MH (1996) Phylogenetic characterization of the MIP family of transmembrane channel proteins. Journal of Membrane Biology **153:** 171-180

Pavelka S (2004) Metabolism of bromide and its interference with the metabolism of iodine. Physiological Research **53:** S81-90

Pohl P, Saparov SM, Antonenko YN (1998) The size of the unstirred layer as a function of the solute diffusion coefficient. Biophysical Journal **75:** 1403-1409

Pohlmeyer K, Soll J, Grimm R, Hill K, Wagner R (1998) A high-conductance solute channel in the chloroplastic outer envelope from pea. Plant Cell **10:** 1207-1216

Pohlmeyer K, Soll J, Steinkamp T, Hinnah S, Wagner R (1997) Isolation and characterization of an amino acid-selective channel protein present in the chloroplastic outer envelope membrane. Proceedings of the National Academy of Sciences of the United States of America **94:** 9504-9509

Poorter H (1993) Interspecific variation in the growth response of plants to an elevated ambient CO_2 concentration. Vegetatio **104:** 77-97

Pottosin II (1992) Single channel recording in the chloroplast envelope. FEBS Letters **308:** 87-90

Pou A, Medrano H, Flexas J, Tyerman SD (2013) A putative role for TIP and PIP aquaporins in dynamics of leaf hydraulic and stomatal conductances in grapevine under water stress and re-watering. Plant, Cell & Environment **36:** 828-843

Prado K, Boursiac Y, Tournaire-Roux C, Monneuse J-M, Postaire O, Da Ines O, Schaeffner AR, Hem S, Santoni V, Maurel C (2013) Regulation of *Arabidopsis* leaf hydraulics involves light-dependent phosphorylation of Aquaporins in veins. Plant Cell **25:** 1029-1039

Prak S, Hem S, Boudet J, Viennois G, Sommerer N, Rossignol M, Maurel C, Santoni V (2008) Multiple phosphorylations in the C-terminal tail of plant plasma membrane Aquaporins role in subcellular trafficking of AtPIP2; 1 in response to salt stress. Molecular & Cellular Proteomics **7:** 1019-1030

Prasad GVR, Coury LA, Finn F, Zeidel ML (1998) Reconstituted aquaporin 1 water channels transport CO_2 across membranes. Journal of Biological Chemistry **273:** 33123-33126

Preston GM, Carroll TP, Guggino WB, Agre P (1992) Appearance of water channels in *Xenopus* oocytes expressing red cell CHIP28 protein. Science **256:** 385-387

Procino G, Carmosino M, Marin O, BRUNATI AM, Contri A, Pinna LA, Mannucci R, Nielsen S, Kwon T-H, Svelto M (2003) Ser-256 phosphorylation dynamics of Aquaporin 2 during maturation from the ER to the vesicular compartment in renal cells. The FASEB Journal **17:** 1886-1888

Quigley F, Rosenberg JM, Shachar-Hill Y, Bohnert HJ (2002) From genome to function: the *Arabidopsis* aquaporins. Genome Biology **3:** 0001

Reizer J, Reizer A, Saier MH (1993) The mip family of integral membrane channel proteins - sequence comparisons, evolutionary relationships, reconstructed pathway of evolution, and proposed functional-differentiation of the 2 repeated halves of the proteins. Critical Reviews in Biochemistry and Molecular Biology **28:** 235-257

Ringler P, Borgnia MJ, Stahlberg H, Maloney PC, Agre P, Engel A (1999) Structure of the water channel AqpZ from *Escherichia coli* revealed by electron crystallography. Journal of Molecular Biology **291:** 1181-1190

Rivers RL, Dean RM, Chandy G, Hall JE, Roberts DM, Zeidel ML (1997) Functional analysis of nodulin 26, an aquaporin in soybean root nodule symbiosomes. Journal of Biological Chemistry **272:** 16256-16261

Søgaard R, Zeuthen T (2008) Test of blockers of AQP1 water permeability by a high-resolution method: no effects of tetraethylammonium ions or acetazolamide. Pflugers Archiv-European Journal of Physiology **456:** 285-292

Sade N, Vinocur BJ, Diber A, Shatil A, Ronen G, Nissan H, Wallach R, Karchi H, Moshelion M (2009) Improving plant stress tolerance and yield production: is the tonoplast aquaporin SlTIP2;2 a key to isohydric to anisohydric conversion? New Phytologist **181:** 651-661

Sakr S, Alves G, Morillon RL, Maurel K, Decourteix M, Guilliot A, Fleurat-Lessard P, Julien JL, Chrispeels MJ (2003) Plasma membrane aquaporins are involved in winter embolism recovery in walnut tree. Plant Physiology **133:** 630-641

Sakurai J, Ishikawa F, Yamaguchi T, Uemura M, Maeshima M (2005) Identification of 33 rice aquaporin genes and analysis of their expression and function. Plant and Cell Physiology **46:** 1568-1577

Sambrook J FE, Maniatis T (1989) Molecular Cloning, A Laboratory Manual, Ed Second Edition. Cold Spring Harbour Laboratory Press

Savage DF, Egea PF, Robles-Colmenares Y, O'Connell JD, Stroud RM (2003) Architecture and selectivity in aquaporins: 2.5 angstrom X-ray structure of aquaporin Z. Plos Biology **1:** 334-340

Schütz K, Tyerman SD (1997) Water channels in *Chara corallina*. Journal of Experimental Botany **48:** 1511-1518

Schenborn ET, Mierendorf RC (1985) A novel transcription property of sp6 and t7 rna-polymerases - dependence on template structure. Nucleic Acids Research **13:** 6223-6236

Schenk AD, Werten PJL, Scheuring S, de Groot BL, Muller SA, Stahlberg H, Philippsen A, Engel A (2005) The 4.5 angstrom structure of human AQP2. Journal of Molecular Biology **350:** 278-289

Schmidt M, Akasaka K, Messerly JT, Boyer MP (2012) Role of Hog1, Tps1 and Sod1 in boric acid tolerance of *Saccharomyces cerevisiae*. Microbiology **158:** 2667-2678

Schmieder S, Lindenthal S, Ehrenfeld J (2002) Cloning and characterisation of amphibian ClC-3 and ClC-5 chloride channels. Biochimica et Biophysica Acta (BBA) - Biomembranes **1566:** 55-66

Schnorf M, Potrykus I, Neuhaus G (1994) Microinjection technique - routine system for characterization of microcapillaries by bubble pressure measurement. Experimental Cell Research **210:** 260-267

Schnurbusch T, Hayes J, Hrmova M, Baumann U, Ramesh SA, Tyerman SD, Langridge P, Sutton T (2010) Boron toxicity tolerance in barley through reduced expression of the multifunctional Aquaporin HvNIP2;1. Plant Physiology **153:** 1706-1715

Secchi F, Lovisolo C, Uehlein N, Kaldenhoff R, Schubert A (2007) Isolation and functional characterization of three aquaporins from olive (*Olea europaea L.*). Planta **225:** 381-392

Serra IA, Nicastro S, Mazzuca S, Natali L, Cavallini A, Innocenti AM (2013) Response to salt stress in seagrasses: PIP1;1 aquaporin antibody localization in *Posidonia oceanica* leaves. Aquatic Botany **104:** 213-219

Shao H-B, Chu L-Y, Shao M-A, Zhao C-X (2008) Advances in functional regulation mechanisms of plant aquaporins: Their diversity, gene expression, localization, structure and roles in plant soil-water relations (review). Molecular Membrane Biology **25:** 179-191

Shelden M, Kaiser B, Tyerman S (2007) Identification and characterisation of aquaporins in the grapevine, *Vitis vinifera*. Photosynthesis Research **91:** 301-301

Shelden MC, Howitt SM, Kaiser BN, Tyerman SD (2009) Identification and functional characterisation of aquaporins in the grapevine, *Vitis vinifera*. Functional Plant Biology **36:** 1065-1078

Siefritz F, Tyree MT, Lovisolo C, Schubert A, Kaldenhoff R (2002) PIP1 plasma membrane aquaporins in tobacco from cellular effects to function in plants. The Plant Cell **14:** 869-876

Singh SK, Binder HJ, Geibel JP, Boron WF (1995) An apical permeability barrier to NH_3/NH_4^+ in isolated, perfused colonic crypts. Proceedings of the National Academy of Sciences of the United States of America **92:** 11573-11577

Skerrett M, Tyerman SD (1994) A channel that allows inwardly directed fluxes of anions in protoplasts derived from wheat roots. Planta **192:** 295-305

Sloot P, Hoekstra AG, Figdor CG (1988) Osmotic response of lymphocytes measured by means of forward light scattering: theoretical considerations. Cytometry **9:** 636-641

Sobczak K, Bangel-Ruland N, Leier G, Weber W-M (2010) Endogenous transport systems in the *Xenopus laevis* oocyte plasma membrane. Methods **51:** 183-189

Sommer A, Geist B, Da Ines O, Gehwolf R, Schaeffner AR, Obermeyer G (2008) Ectopic expression of *Arabidopsis thaliana* plasma membrane intrinsic protein 2 aquaporins in lily pollen increases the plasma membrane water permeability of grain but not of tube protoplasts. New Phytologist **180:** 787-797

Soto G, Fox R, Ayub N, Alleva K, Guaimas F, Erijman EJ, Mazzella A, Amodeo G, Muschietti J (2010) TIP5; 1 is an aquaporin specifically targeted to pollen mitochondria and is probably involved in nitrogen remobilization in *Arabidopsis thaliana*. The Plant Journal **64:** 1038-1047

Souktani R, Berdeaux A, Ghaleb B, Giudicelli JF, Guize L, Le Heuzey JY, Henry P (2000) Induction of apoptosis using sphingolipids activates a chloride current in *Xenopus laevis* oocytes. American Journal of Physiology-Cell Physiology **279:** C158-C165

Steudle E (1992) The biophysics of plant water: compartmentation, coupling with metabolic processes, and flow of water in plant roots. *In* G Somero, C Osmond, C Bolis, eds, Water and Life. Springer Berlin Heidelberg, pp 173-204

Suga S, Maeshima M (2004) Water channel activity of radish plasma membrane aquaporins heterologously expressed in yeast and their modification by site-directed mutagenesis. Plant and Cell Physiology **45:** 823-830

Sui HX, Han BG, Lee JK, Walian P, Jap BK (2001) Structural basis of water-specific transport through the AQP1 water channel. Nature **414:** 872-878

Sweet G, Gandor C, Voegele R, Wittekindt N, Beuerle J, Truniger V, Lin ECC, Boos W (1990) Glycerol facilitator of escherichia-coli - cloning of glpf and identification of the glpf product. Journal of Bacteriology **172:** 424-430

Takano J, Wada M, Ludewig U, Schaaf G, von Wiren N, Fujiwara T (2006) The *Arabidopsis* major intrinsic protein NIP5;1 is essential for efficient boron uptake and plant development under boron limitation. Plant Cell **18:** 1498-1509

Teakle NL, Tyerman SD (2010) Mechanisms of Cl^- transport contributing to salt tolerance. Plant, Cell & Environment **33:** 566-589

Temmei Y, Uchida S, Hoshino D, Kanzawa N, Kuwahara M, Sasaki S, Tsuchiya T (2005) Water channel activities of *Mimosa pudica* plasma membrane intrinsic proteins are regulated by direct interaction and phosphorylation. FEBS Letters **579:** 4417-4422

Terashima I, Hanba YT, Tazoe Y, Vyas P, Yano S (2006) Irradiance and phenotype: comparative eco-development of sun and shade leaves in relation to photosynthetic CO_2 diffusion. Journal of Experimental Botany **57:** 343-354

Terashima I, Hanba YT, Tholen D, Niinemets U (2011) Leaf functional anatomy in relation to photosynthesis. Plant Physiology **155:** 108-116

Terashima I, Ono K (2002) Effects of $HgCl_2$ on CO_2 dependence of leaf photosynthesis: evidence indicating involvement of aquaporins in CO_2 diffusion across the plasma membrane. Plant and Cell Physiology **43:** 70-78

Tornroth-Horsefield S, Wang Y, Hedfalk K, Johanson U, Karlsson M, Tajkhorshid E, Neutze R, Kjellbom P (2006) Structural mechanism of plant aquaporin gating. Nature **439:** 688-694

Tyerman SD, Bohnert HJ, Maurel C, Steudle E, Smith JAC (1999) Plant aquaporins: their molecular biology, biophysics and significance for plant water relations. Journal of Experimental Botany **50:** 1055-1071

Tzounopoulos T, Maylie J, Adelman J (1995) Induction of endogenous channels by high levels of heterologous membrane proteins in *Xenopus* oocytes. Biophysical Journal **69:** 904-908

Uehlein N, Lovisolo C, Siefritz F, Kaldenhoff R (2003) The tobacco aquaporin NtAQP1 is a membrane CO_2 pore with physiological functions. Nature **425:** 734-737

Uehlein N, Otto B, Hanson DT, Fischer M, McDowell N, Kaldenhoff R (2008) Function of *Nicotiana tabacum* aquaporins as chloroplast gas pores challenges the concept of membrane CO_2 permeability. The Plant Cell **20:** 648-657

Uehlein N, Sperling H, Heckwolf M, Kaldenhoff R (2012) The *Arabidopsis* aquaporin PIP1;2 rules cellular CO_2 uptake. Plant Cell and Environment **35:** 1077-1083

van Heeswijk MPE, van Os CH (1986) Osmotic water permeabilities of brush border and basolateral membrane vesicles from rat renal cortex and small intestine. Journal of Membrane Biology **92:** 183-193

Vandeleur RK, Mayo G, Shelden MC, Gilliham M, Kaiser BN, Tyerman SD (2009) The role of plasma membrane intrinsic protein aquaporins in water transport through roots: diurnal and

drought stress responses reveal different strategies between Isohydric and anisohydric cultivars of grapevine. Plant Physiology **149:** 445-460

Verdoucq L, Grondin A, Maurel C (2008) Structure-function analysis of plant aquaporin AtPIP2;1 gating by divalent cations and protons. Biochemical Journal **415:** 409-416

Waisbren SJ, Geibel JP, Modlin IM, Boron WF (1994) Unusual permeability properties of gastric gland cells. Nature **368:** 332-335

Wallace IS, Roberts DM (2004) Homology modeling of representative subfamilies of *Arabidopsis* major intrinsic proteins. Classification based on the aromatic/arginine selectivity filter. Plant Physiology **135:** 1059-1068

Wang Y, Cohen J, Boron WF, Schulten K, Tajkhorshid E (2007) Exploring gas permeability of cellular membranes and membrane channels with molecular dynamics. Journal of Structural Biology **157:** 534-544

Wayne R, Tazawa M (1990) Nature of the water channels in the internodal cells of nitellopsis. Journal of Membrane Biology **116:** 31-39

Weaver CD, Shomer NH, Louis CF, Roberts DM (1994) Nodulin 26, a nodule-specific symbiosome membrane protein from soybean, is an ion channel. Journal of Biological Chemistry **269:** 17858-17862

Weig A, Deswarte C, Chrispeels MJ (1997) The major intrinsic protein family of *Arabidopsis* has 23 members that form three distinct groups with functional aquaporins in each group. Plant Physiology **114:** 1347-1357

Whiteman S-A, Nuhse TS, Ashford DA, Sanders D, Maathuis FJM (2008) A proteomic and phosphoproteomic analysis of Oryza sativa plasma membrane and vacuolar membrane. Plant Journal **56:** 146-156

Worthington K, and Worthington, V. (2011) Worthington Enzyme Manual. Worthington Biochemical Corporation http://www.worthington-biochem.com/PROK/default.html

Wu B, Beitz E (2007) Aquaporins with selectivity for unconventional permeants. Cellular and Molecular Life Sciences **64:** 2413-2421

Yang B, Fukuda N, van Hoek A, Matthay MA, Ma T, Verkman AS (2000) Carbon dioxide permeability of Aquaporin-1 measured in erythrocytes and lung of *Aquaporin-1 null* mice and in reconstituted proteoliposomes. Journal of Biological Chemistry **275:** 2686-2692

Yanochko GM, Yool AJ (2002) Regulated cationic channel function in *Xenopus* oocytes expressing *Drosophila* big brain. The Journal of Neuroscience **22:** 2530-2540

Yool AJ (2006) Dominant-negative suppression of big brain ion channel activity by mutation of a conserved glutamate in the first transmembrane domain. Gene Expression **13:** 329-337

Yool AJ (2007) Aquaporins: multiple roles in the central nervous system. The Neuroscientist **13:** 470-485

Yool AJ (2007) Functional domains of aquaporin-1: keys to physiology, and targets for drug discovery. Current pharmaceutical design **13:** 3212-3221

Yool AJ, Brown EA, Flynn GA (2010) Roles for novel pharmacological blockers of aquaporins in the treatment of brain oedema and cancer. Clinical and Experimental Pharmacology and Physiology **37:** 403-409

Yool AJ, Campbell EM (2012) Structure, function and translational relevance of aquaporin dual water and ion channels. Molecular Aspects of Medicine **33:** 553-561

Yool AJ, Stamer WD (2004) Novel roles for aquaporins as gated ion channels. Molecular and Cellular Insights to Ion Channel Biology **32:** 351-379

Yool AJ, Stamer WD, Regan JW (1996) Forskolin stimulation of water and cation permeability in aquaporin1 water channels. Science **273:** 1216-1218

Yool AJ, Weinstein AM (2002) New roles for old holes: Ion channel function in aquaporin-1. News in Physiological Sciences **17:** 68-72

Yu J, Yool AJ, Schulten K, Tajkhorshid E (2006) Mechanism of gating and ion conductivity of a possible tetrameric pore in aquaporin-1. Structure **14:** 1411-1423

Yu Q, Hu Y, Li J, Wu Q, Lin Z (2005) Sense and antisense expression of plasma membrane aquaporin BnPIP1 from *Brassica napus* in tobacco and its effects on plant drought resistance. Plant Science **169:** 647-656

Zelazny E, Borst JW, Muylaert M, Batoko H, Hemminga MA, Chaumont F (2007) FRET imaging in living maize cells reveals that plasma membrane aquaporins interact to regulate their subcellular localization. Proceedings of the National Academy of Sciences of the United States of America **104:** 12359-12364

Zhang DY, Ali Z, Wang CB, Xu L, Yi JX, Xu ZL, Liu XQ, He XL, Huang YH, Khan IA, Trethowan RM, Ma HX (2013) Genome-wide sequence characterization and expression analysis of major intrinsic proteins in soybean (Glycine max L.). Plos One **8:** e56312-e56312

Zhang WH, Tyerman SD (1999) Inhibition of water channels by $HgCl_2$ in intact wheat root cells. Plant Physiology **120:** 849-857